



University of Kentucky
UKnowledge

Theses and Dissertations--Mechanical
Engineering

Mechanical Engineering


2017

ADVANCES IN MULTI-AGENT FLOCKING: CONTINUOUS-TIME AND DISCRETE-TIME ALGORITHMS

Brandon Wellman

University of Kentucky, bjwell3@g.uky.edu

Author ORCID Identifier:

 <https://orcid.org/0000-0001-5643-5466>

Digital Object Identifier: <https://doi.org/10.13023/ETD.2017.400>

[Right click to open a feedback form in a new tab to let us know how this document benefits you.](#)

Recommended Citation

Wellman, Brandon, "ADVANCES IN MULTI-AGENT FLOCKING: CONTINUOUS-TIME AND DISCRETE-TIME ALGORITHMS" (2017). *Theses and Dissertations--Mechanical Engineering*. 99.

https://uknowledge.uky.edu/me_etds/99

This Doctoral Dissertation is brought to you for free and open access by the Mechanical Engineering at UKnowledge. It has been accepted for inclusion in Theses and Dissertations--Mechanical Engineering by an authorized administrator of UKnowledge. For more information, please contact UKnowledge@lsv.uky.edu.

STUDENT AGREEMENT:

I represent that my thesis or dissertation and abstract are my original work. Proper attribution has been given to all outside sources. I understand that I am solely responsible for obtaining any needed copyright permissions. I have obtained needed written permission statement(s) from the owner(s) of each third-party copyrighted matter to be included in my work, allowing electronic distribution (if such use is not permitted by the fair use doctrine) which will be submitted to UKnowledge as Additional File.

I hereby grant to The University of Kentucky and its agents the irrevocable, non-exclusive, and royalty-free license to archive and make accessible my work in whole or in part in all forms of media, now or hereafter known. I agree that the document mentioned above may be made available immediately for worldwide access unless an embargo applies.

I retain all other ownership rights to the copyright of my work. I also retain the right to use in future works (such as articles or books) all or part of my work. I understand that I am free to register the copyright to my work.

REVIEW, APPROVAL AND ACCEPTANCE

The document mentioned above has been reviewed and accepted by the student's advisor, on behalf of the advisory committee, and by the Director of Graduate Studies (DGS), on behalf of the program; we verify that this is the final, approved version of the student's thesis including all changes required by the advisory committee. The undersigned agree to abide by the statements above.

Brandon Wellman, Student

Dr. Jesse B. Hoagg, Major Professor

Dr. Haluk E. Karaca, Director of Graduate Studies

ADVANCES IN MULTI-AGENT FLOCKING:
CONTINUOUS-TIME AND DISCRETE-TIME ALGORITHMS

DISSERTATION

A dissertation submitted in partial
fulfillment of the requirements for the
degree of Doctor of Philosophy in the
College of Engineering at the
University of Kentucky

By
Brandon J. Wellman
Lexington, Kentucky

Director: Dr. Jesse B. Hoagg, Professor of Mechanical Engineering
Lexington, Kentucky 2017

Copyright© Brandon J. Wellman 2017

ABSTRACT OF DISSERTATION

ADVANCES IN MULTI-AGENT FLOCKING: CONTINUOUS-TIME AND DISCRETE-TIME ALGORITHMS

We present multi-agent control methods that address flocking in continuous-time and discrete-time settings. The method is decentralized, that is, each agent's controller relies on local sensing to determine the relative positions and velocities of nearby agents. In the continuous-time setting, each agent has double-integrator dynamics. In the discrete-time setting, each agent has the discrete-time double-integrator dynamics obtained by sampling the continuous-time double integrator and applying a zero-order hold on the control input. We demonstrate using analysis, numerical simulations, and experimental demonstrations that agents using the flocking methods converge to flocking formations and follow the centralized leader (if applicable).

KEYWORDS: flocking, multi-agent system, consensus algorithm, formation control, sampled-data control, motion-capture system

Author's signature: Brandon J. Wellman

Date: September 21, 2017

ADVANCES IN MULTI-AGENT FLOCKING:
CONTINUOUS-TIME AND DISCRETE-TIME ALGORITHMS

By
Brandon J. Wellman

Director of Dissertation: Jesse B. Hoagg

Director of Graduate Studies: Haluk E. Karaca

Date: September 21, 2017

ACKNOWLEDGMENTS

Difficult projects cannot be done alone, and my work is no exception. In order to accomplish this, I have relied heavily on friends, family, and colleagues to help me along the way. I first thank God for blessing me with the mind, strength, and perseverance to earn this degree. I also want to thank my parents for their love and support, particularly in providing me so many opportunities to succeed. My sister has encouraged and helped me as only she can, and my grandmother has been a rock to lean on when I was discouraged.

In addition to my family, my friends have also supported me. My friends have been there to soothe my wounds and encourage me to achieve greatness. I thank them for what they have taught me and hope it was mutual.

Finally, I would like to thank my colleagues and advisors. I have benefitted greatly from conversations with my lab mates, notably Shaoqian Wang, Xingye Zhang, Daniel Poston, Thomas Kirven, Zack Lippay, Chris Heinz, Alireza Moosavi, Mohammadreza Kamaldar, Zahra Abbasi, and Roshan Chavan. I also appreciate the advice and guidance from my committee members Michael Seigler, Suzanne Smith, and James Lumpp. Even more so, I'm thankful for my advisor Jesse Hoagg for the many hours he has dedicated to mold me into a professional researcher.

TABLE OF CONTENTS

Acknowledgments	iii
Table of Contents	iv
List of Figures	vi
List of Tables	ix
Chapter 1 Introduction and Motivation	1
1.1 Literature Review	3
1.2 Introduction to Consensus Algorithms	6
1.3 Flocking Problem Formulation	8
1.4 Summary of Contributions	10
Chapter 2 Continuous-Time Flocking and Destination Seeking	12
2.1 Introduction	12
2.2 Problem Formulation	14
2.3 Review of Algorithm 1 from [1]	15
2.4 Flocking and Destination Seeking	16
2.5 Flocking Analysis	21
2.6 Destination-Seeking Analysis	24
2.7 Numerical Examples	27
2.8 Conclusions	30
2.9 Proof of Proposition 2	32
2.10 Proof of Theorem 1	33
2.11 Proof of Lemma 1	39
2.12 Proof of Theorems 2 and 3	39
Chapter 3 Discrete-Time Flocking	43
3.1 Introduction	43
3.2 Problem Formulation	45
3.3 Motivation	46
3.4 Discrete-Time Flocking	49
3.5 Flocking Analysis	52
3.6 Motivating Example Revisited	55
3.7 Numerical Examples	56
3.8 Conclusions	59
3.9 Proof of Proposition 3	60
3.10 Proof of Lemmas 2 and 3	61
3.11 Proof of Theorems 4 and 5	66
3.12 Propositions 4 and 5 used in the proof of Proposition 3	71

Chapter 4	Experimental Demonstrations of Discrete-Time Flocking Using Rotorcraft	76
4.1	Introduction	76
4.2	Approximate Dynamics for an Attitude-Stabilized Quadcopter	76
4.3	Discrete-Time Flocking	79
4.4	Description of Experimental Setup	83
4.5	Results and Discussion	87
	Demonstration 1: Rotorcraft Flock Without a Leader	88
	Demonstration 2: Rotorcraft Flock and Approach a Stationary Leader	89
	Demonstration 3: Rotorcraft Follow a Leader With a Helical Trajectory	92
	Demonstration 4: Rotorcraft Follow a Mouse-Driven Leader	95
	Summary of Results and Discussion	97
4.6	Conclusion	101
Chapter 5	Conclusions and Future Work	103
	Bibliography	105
	Vita	112

LIST OF FIGURES

1.1	A configuration of 7 agents based on a position-formation cohesion method	4
1.2	A configuration of 7 agents based on a distance-formation cohesion method	5
1.3	The graph $\mathcal{G}(\mathcal{I}, \mathcal{E}_1)$ has 7 vertices and 8 edges.	6
2.1	An example $\mu : [0, \infty) \rightarrow [0, 1]$ that satisfies (M1)–(M3).	18
2.2	A plot of ν , which is in the destination-seeking control	19
2.3	A plot of κ , which is in the damping control	19
2.4	Four types of equilibria for $n = 2$	25
2.5	Trajectories of $n = 3$ agents for $\gamma = 2 \text{ m/s}^2$ and 9 m/s^2	28
2.6	Speed and magnitude of control for the trajectory shown in Figure 2.5	28
2.7	A group of $n = 6$ agents that flock before they reach their destinations	29
2.8	The minimum interagent distance and maximum control magnitude for the trajectory shown in Figure 2.7	29
2.9	A group of $n = 20$ agents that flock before they reach their destinations	30
2.10	The minimum interagent distance and maximum control magnitude for the trajectory shown in Figure 2.9	31
2.11	A group of $n = 20$ agents that flock before they reach their destinations	31
2.12	The minimum interagent distance and maximum control magnitude for the trajectory shown in Figure 2.11	32
3.1	A trajectory of the closed-loop dynamics (3.1), (3.2), and (3.5). The agents asymptotically oscillate towards and away from each other.	48
3.2	The distance $\ q_2 - q_1\ $ between agents and the magnitude of the relative velocity $\ p_2 - p_1\ $ for a trajectory of the closed-loop dynamics (3.1), (3.2), and (3.5). The distance between agents oscillates about d asymptotically, and the relative velocity oscillates asymptotically.	49
3.3	The distance $\ q_2 - q_1\ $ between agents and the magnitude of the relative velocity $\ p_2 - p_1\ $ for a trajectory of the closed-loop dynamics (3.1), (3.2), and (3.5). The agents start near a flocking configuration; however, the agents do not stay in a flocking configuration.	50
3.4	A trajectory of the closed-loop system (3.1), (3.2), and (3.15) overlaid on the trajectory from Figure 3.1, which uses the control [1, Alg. 1]. The agents using (3.15) flock asymptotically.	56
3.5	The distance $\ q_2 - q_1\ $ between agents and the magnitude of the relative velocity $\ p_2 - p_1\ $ for a trajectory of the closed-loop system (3.1), (3.2), and (3.15) overlaid on the plot from Figure 3.2, which uses the control [1, Alg. 1]. Using (3.15), the distance between the agents converges to d , and the relative velocity converges to 0.	57

3.6	Trajectories of $n = 3$ agents that follow a leader whose position and velocity are $q_g(k) \equiv 0$ and $p_g(k) \equiv 0$. In one trajectory, agents use the control (3.15), which contains the FCTG term; in the other, agents use the control (3.15), where the FCTG term is omitted. The step $k_f \in \mathbb{N}$ is such that $q_i(k_f + 1) \approx q_i(k_f)$	58
3.7	The distances between $n = 3$ agents that follow the leader agent whose position is $q_g(k) \equiv 0$ and whose velocity is $p_g(k) \equiv 0$. In one trajectory, agents use the control (3.15), which contains the FCTG term; in the other, agents use the control (3.15), where the FCTG term is omitted. The agents using the FCTG term converge to d apart, whereas the agents that do not use the FCTG term converge to a distance less than d apart.	59
3.8	A group of $n = 3$ agents with no leader that flock. The agents form a flock, where all agents have the same velocity and are d apart from one another. The line between agents shows that agents are approximately d apart.	60
3.9	A group of $n = 3$ agents that flock and follow a leader. The line between agents shows that agents are approximately d apart.	61
3.10	A group of $n = 10$ agents that flock and follow a leader. The line between agents shows that agents are approximately d apart.	62
4.1	The position of the i th quadcopter's center of mass o_i relative to o_E is \vec{r}_i . The orientation of F_i relative to F_E is $\mathcal{O}(\psi_i)$, where ψ_i is the yaw angle, which is the angle from \hat{i}_e to \hat{i}_i	77
4.2	The Parrot Rolling Spider quadcopter is attitude-stabilized by Parrot's proprietary inner-loop controller.	78
4.3	A picture of the Rolling Spider quadcopter with 4 attached markers for motion capture.	83
4.4	The 6 OptiTrack Prime 13 cameras are mounted on tripods, arranged in a circular configuration, pointed towards the test-flight volume, and angled slightly downward.	84
4.5	The Rolling Spider uses onboard sensing with input v_i for inner-loop control and the motion-capture system's sensing with input q_g and p_g for outer-loop control.	86
4.6	Setup of discrete-time flocking control demonstration for $n = 3$ rotorcraft.	87
4.7	The trajectory of $n = 3$ rotorcraft that flock without a leader.	89
4.8	The distance and norm of the velocity difference between each pair of rotorcraft.	90
4.9	The rotorcraft-averaged velocity is approximately constant.	91
4.10	The trajectory of $n = 3$ rotorcraft that flock and follow a stationary leader.	92
4.11	The distance and norm of the velocity difference between pairs of rotorcraft.	93
4.12	The rotorcraft-averaged position and velocity approximately follow the leader's position and velocity.	94
4.13	The trajectory of $n = 3$ rotorcraft that flock and follow a leader with a helical trajectory.	96
4.14	The distance and norm of the velocity difference between pairs of rotorcraft.	97

4.15	The rotorcraft-averaged position and velocity approximately follow the leader's position and velocity.	98
4.16	The trajectory of $n = 3$ rotorcraft that flock and follow a leader that follows a mouse's position.	99
4.17	The distance and norm of the velocity difference between each pair of rotorcraft.	99
4.18	The rotorcraft-averaged position and velocity approximately follow the leader's position and velocity.	100

LIST OF TABLES

4.1	Summary of the steady-state results from Demonstrations 1–4 compared to the theoretical results in Chapter 3.	101
-----	---	-----

Chapter 1 Introduction and Motivation

A simple look around the world demonstrates that there is a multitude of life interacting with one another from the smallest bacteria to the largest whale. No animal lives in isolation from one another, and in fact, all life is interconnected. In the sciences, much attention has been paid to the study of a single animal. From this important work we have gleaned major insights into the anatomy, physiology, and psychology of all living beings. By studying how animals move and work, biology has given us not only insight into how nature does things but also inspiration to do it for ourselves. We watch flying birds and swimming fish, coveting the abilities ourselves. While all this knowledge is beautiful and worth studying, there comes a point when a single fish becomes humdrum and a single bird mundane.

At this point, we become keenly aware, however, that animals do not live in isolation. Indeed, animals depend on one another, whether predator or prey, big or small. Humans also depend on one another as well as machines to perform tasks. And why do we depend on each other? Because our ambitions are bigger than any one person. Thus, we need to study how animals, humans, machines, satellites, and other single agents can work together.

Example multi-agent systems include animal behavior [2], economic markets [3], reputation systems on websites such as Amazon or Ebay [4], biological systems [5], and computer networks [6]. With reputation systems, people read others' experiences buying from a seller and determine whether a seller is trustworthy or not. Other examples of multi-agents systems include sports teams designing game plans that accentuate their teams' strengths while exploiting the opponent's weaknesses, dancers and performers performing dangerous stunts and expecting their partners to help them land safely, employees obeying their boss' decisions, and solving a distributed consensus problem efficiently [7].

Multi-agent systems for vehicles have many exciting applications related such as distributed sensing, formation flying, cooperative surveillance, and point-to-point mail delivery. For example, autonomous aircraft or spacecraft can fly in formations for distributed sensing [8–10]. Coordinated aircraft could be used in a forest-fire scenario to measure wind velocities and thus, predict fire movement. In the agricultural industry, coordinated aircraft could conduct crop surveys. All of these applications require decentralized methods for coordinating and controlling groups of autonomous agents [11].

Problems in multi-agent systems utilize multiple decision-making agents that may either cooperate or compete with one another. A didactic multi-agent example is the prisoner's dilemma in which 2 criminals commit a crime together but are caught soon

after [12]. The police put the criminals into 2 separate rooms, where they attempt to elicit information from each criminal about the other. Three outcomes can occur: (1) if neither criminal incriminates the other, then they both serve 1 year; (2) if only one criminal incriminates the other, then that criminal receives no penalty while the other serves 3 years; and (3) if both criminals incriminate the other, then they both serve 2 years. Neither criminal is allowed to know what the other chooses before making their own decision. Thus, each criminal decides what's in their best interest with limited information.

The prisoner's dilemma illustrates several pivotal aspects of multi-agent systems. Each agent (criminal) makes its own decision independent of the other. However, the consequence of that decision affects both. In addition, each agent bases their decision on limited information, which means that agents may make a bad choice from the viewpoint of someone with more knowledge.

The focus of this dissertation is cooperative control, which is a subset of multi-agent systems, where agents work together to achieve goals that may be difficult or impossible for a single agent to achieve. Three examples of cooperative control systems are RoboCup, complex structures, and the point-to-point passenger transport problem. RoboCup competitors design teams of robots that play one another in soccer [13]. In this case, the environment is dynamic, states change in real time, agents do not have incomplete information, robots sense the environment, and each robot uses its own control, that is, this is a distributed control problem [13].

Building complex structures is another application of cooperative control. For example, a group of robots build a house together. Each robot uses a master set of instructions and determine its own list of tasks, which could include grabbing more materials, helping another robot carry a heavy beam, or holding a beam while another robot secures it. Because robots do not require an atmosphere and other harsh environments, such as those with high solar radiation, humans can rely on robots to help us colonize Mars or other planets. For example, robots can prepare sites on Mars before humans arrive or perform maintenance and repairs on equipment that may be difficult for a human to reach or fix [14].

In point-to-point passenger-transport problems, a large number of people in distributed locations need to be transported to a set of distributed destinations. We consider 2 approaches: a single large bus, and multiple smaller buses. Using a single bus big enough to transport all the passengers, the bus has to visit every passenger and every destination, which takes a long time even with an efficient route plan. Moreover, if the bus breaks down, then nobody gets to their destination. Using multiple smaller buses, each bus picks up fewer people at a time and transports them to their destinations in a timely manner. Moreover, if one bus breaks down, then the remaining buses can pick up the slack. Thus, by using multiple, smaller vehicles, people reach their destination quicker, and the transportation system does not stop when a vehicle breaks down.

In this dissertation, we focus on formation-control algorithms, which induce configurations of agents that are beneficial to the group in some way. For example, one car may draft off the car ahead of it to reduce wind resistance and save energy, and additional cars drafting in a line leads to platoons of vehicles [15]. Flocking algorithms

derive their name from groups of birds that fly together in a giant cluster or a specific formation such as a “V”. Flocking algorithms generalize birds to a broad range of vehicles such as cars, rotorcraft, aircraft, underwater vehicles, and spacecraft, and force vehicles to move into a desired configuration. The three characteristics of flocking are collision avoidance, velocity consensus, and cohesion [16]. Collision avoidance prevents birds colliding with one another. Velocity consensus causes the birds to fly at the same velocity as one another, and cohesion causes birds to be close to another. Flocking algorithms induce formations of vehicles in which the vehicles do not collide, maintain desired inter-agent distance, and have the same velocity.

1.1 Literature Review

Two papers in particular sparked the revolution in multi-agent formation control. In [17], agents have discrete-time dynamics with position-like and velocity-like states. Furthermore, the velocity-like state has constant magnitude, and the heading is updated using the average heading of nearby agents. In this case, agents approach the same heading angle using feedback of neighboring agents’ heading angles. In [16], agents follow the rules of flocking: collision avoidance, velocity matching, and flock centering (staying near other agents).

For coordinated control, each agent relies on sensing to determine the relative positions and velocities of nearby agents. Then, each agent uses these measurements combined with other information to accomplish tasks, which can include: cohesion, collision avoidance, velocity matching, and guidance. Cohesion attracts an agent to nearby agents, whereas collision avoidance repels an agent from nearby agents or obstacles. Velocity matching causes nearby agents to approach a consensus velocity, and guidance causes an agent or agents to follow a leader agent or approach a desired destination.

Cohesion and collision avoidance are often addressed simultaneously. Two common cohesion methods are position-formation methods [18–20] and distance-formation methods [1, 21–28]. A survey of formation methods is presented in [29]. Position-formation approaches force agents into a configuration by designing desired relative positions between pairs of agents. These approaches require prescribing the desired formation *a priori* and may be implemented using a linear control. Figure 1.1 demonstrates a configuration based on a position-formation cohesion method.

In contrast, distance-formation methods induce a configuration using only a desired distance between adjacent agents. In this case, the agents autonomously determine their configuration based on the desired interagent distance and initial conditions. Distance-formation approaches do not require prescribing the configuration *a priori* and are typically implemented with nonlinear controls. Figure 1.2 demonstrates a configuration based on a distance-formation cohesion method. The distance between all pairs of adjacent agents, that is, agents that are connected by a line, is the same. Note that in contrast to the position-formation configuration in Figure 1.1, the agents in Figure 1.2 are not labeled because the configuration depends on initial conditions.

A common approach for distance formation is to use potential functions that create attractive forces when nearby agents are too far away and repulsive forces when nearby

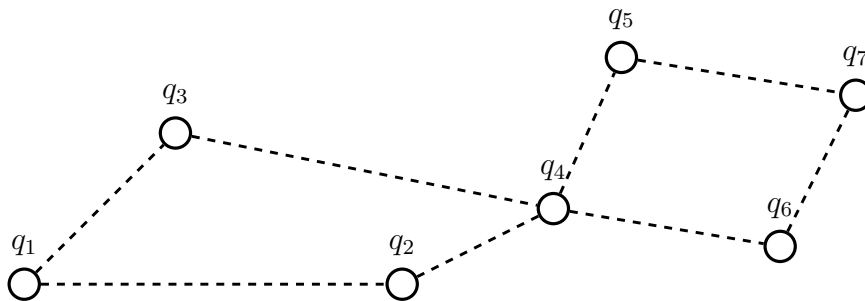


Figure 1.1: A configuration of 7 agents based on a position-formation cohesion method. The i th agent's position is q_i , and the dashed line denotes that agents can sense one another.

agents are too close [1, 21–27]. Potential functions are typically designed so that the potential decreases with respect to time and so that the minimum values of the potential have desired properties. For example, in formation control the minimum value often corresponds to the desired formation. Potential functions can also be designed for destination seeking [30], collision avoidance [1, 8, 22, 24–27, 30–32], and maintaining communication [26]. In [26], if agents are less than a certain distance apart, then the potential function is infinity. In this case, since the potential function is designed to be nonincreasing, it follows that for any initial condition such that the potential function is finite, the distance between agents is always lower bounded, which prevents collisions. Similarly, if agents are greater than a certain distance apart, then the potential function is infinity, which ensures cohesion. However, in this case, the gradient of the potential function, which is often in the control, may be unbounded so implementing this control may not be practical.

Potential functions that create attractive and repulsion forces are similar to artificial potential functions that are used for navigation (e.g., [33]). However, eliminating undesired local minima is an open problem [33]. In the context of formation control, undesired local minima may correspond to undesired formations. For example, when flocking and following a leader, agents may form a compressed formation around the leader.

Consensus algorithms [17, 34–56] can be used for multiple purposes in formation-control algorithms. The next section addresses consensus algorithms in depth. Formation-control algorithms often use consensus-like algorithms to achieve velocity matching [9, 18, 34, 45, 57–59]. In addition, some consensus algorithms can be extended to address formation control [46–48, 57, 58, 60]. However, these approaches are position-formation methods that force agents into a configuration using desired relative-position vectors between pairs of agents. Approaches that use distance-formation methods for cohesion and collision avoidance, and consensus for velocity matching lead to formations called *flocks* [1, 24–28, 61].

In addition to flocking, agents may also use guidance to accomplish external objectives such as following a leader agent, destination seeking, locating targets, and avoiding obstacles. Combining flocking with external objectives increases the com-

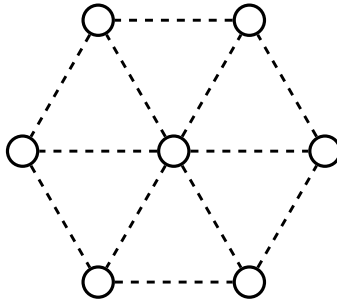


Figure 1.2: A configuration of 7 agents based on a distance-formation cohesion method. The distance between each pair of adjacent agents, that is, agents that are connected by a line, is the same. Each circle represents an agent’s position, and the dashed line denotes that agents are adjacent to and can sense one another.

plexity of the problem. For example, if agents are flocking and see an obstacle on the horizon, an agent who overprioritizes flocking may not be able to safely avoid an obstacle, whereas an agent who overprioritizes avoiding the obstacle may leave the flock. Thus, flocking with obstacle avoidance, and more generally flocking with any external objective(s), is difficult.

Two common forms of guidance are leader-follower methods [1, 9, 19, 21–26, 58, 60, 62] and destination-seeking methods [20, 63–65]. Leader-follower approaches, which are known as formation-tracking problems in [29], rely on a centralized leader, who can be an actual or virtual member of the formation and whose real-time position and velocity are known by all agents [1, 22–26] or at least by some [9, 19, 21]. Each agent uses knowledge of the centralized leader and measurements of nearby agents to induce a formation and follow the leader. In contrast, destination-seeking methods (e.g., [20, 63–65]) cause agents to approach desired destinations.

Agent dynamics affect both the analysis and implementation of formation-control algorithms. Formation-control algorithms are commonly implemented using single-integrator dynamics [8, 42, 66, 67], double-integrator dynamics [1, 24, 25, 27, 28, 30–32, 36, 42, 66–68], unicycle-like dynamics [9, 22, 69], and linear dynamics [18, 34, 35, 45, 57–59, 70, 71]. In particular, some algorithms for linear dynamics apply to heterogeneous vehicles [35, 45, 58], that is, vehicles with non-identical dynamics. In addition, the approaches in [1, 6, 9, 19, 20, 22, 24–27, 30, 58, 66, 68, 72, 73] consider continuous-time dynamics, whereas [34, 35, 37–42, 44, 46, 49, 57, 60, 62, 74–76] consider discrete-time dynamics. Formation-control algorithms may be designed using continuous-time dynamics, but implementing these algorithms requires sampled data. The results in [77] demonstrate several examples, where a control designed for continuous-time dynamics and implemented in a sampled-data setting fails.

In this dissertation, we provide experimental demonstration of the discrete-time flocking algorithm. Experimental demonstrations of formation-control algorithms are in [22, 23, 78–80]. Of these, only [79, 80] consider quadcopters, but [79, 80] use a position-formation algorithm for cohesion, whereas the experimental demonstrations in this dissertation use a distance-formation approach.

1.2 Introduction to Consensus Algorithms

Consensus algorithms cause agents to agree upon a value and are the basis of many formation-control algorithms. In this section, we present graph-theoretic material related to consensus algorithms, specifically the Laplacian matrix. Furthermore, we demonstrate how consensus algorithms use the Laplacian matrix.

Let n be a positive integer and define $\mathcal{I} \triangleq \{1, 2, \dots, n\}$. The elements of \mathcal{I} are called *vertices*, and \mathcal{I} is the *vertex set*. Define $\mathcal{E} \triangleq \{\{i, j\}: i, j \in \mathcal{I} \text{ and } i \neq j\}$. The elements of \mathcal{E} are called *edges* and \mathcal{E} is called the *edge set*. Consider the graph $\mathcal{G}(\mathcal{I}, \mathcal{E}_1)$, where $\mathcal{E}_1 \subseteq \mathcal{E}$. Since the elements of \mathcal{E} are distinct and $\{i, j\} \in \mathcal{E}$ implies $i \neq j$, the graph $\mathcal{G}(\mathcal{I}, \mathcal{E}_1)$ does not contain any self loops or multiple edges between any 2 nodes. For all $\{i, j\} \in \mathcal{E}$, we call $w_{i,j} = w_{j,i} \geq 0$ the *weight of $\{i, j\}$* . Furthermore, for all $\{i, j\} \in \mathcal{E}_1$, $w_{i,j} > 0$; and for all $\{i, j\} \notin \mathcal{E}_1$, $w_{i,j} = 0$. Thus, $w_{i,j} = 0$ is equivalent to $\{i, j\}$ not being an edge in the graph $\mathcal{G}(\mathcal{I}, \mathcal{E}_1)$. We say that the graph $\mathcal{G}(\mathcal{I}, \mathcal{E}_1)$ is *connected* if for all $i, j \in \mathcal{I}$ such that $i \neq j$, there exists a potentially null sequence $i_1, \dots, i_l \in \mathcal{I}$ such that $\{i, i_1\}, \{i_1, i_2\}, \{i_2, i_3\}, \dots, \{i_{l-1}, i_l\}, \{i_l, j\} \in \mathcal{E}_1$.

Graphs may be represented visually. The following example provides a visual representation of a graph.

Example 1. Let $n = 7$, and let

$$\mathcal{E}_1 = \{\{1, 2\}, \{1, 3\}, \{2, 4\}, \{3, 4\}, \{4, 5\}, \{4, 6\}, \{5, 7\}, \{6, 7\}\}.$$

Figure 1.3 is a visual representation of the graph $\mathcal{G}(\mathcal{I}, \mathcal{E}_1)$. △

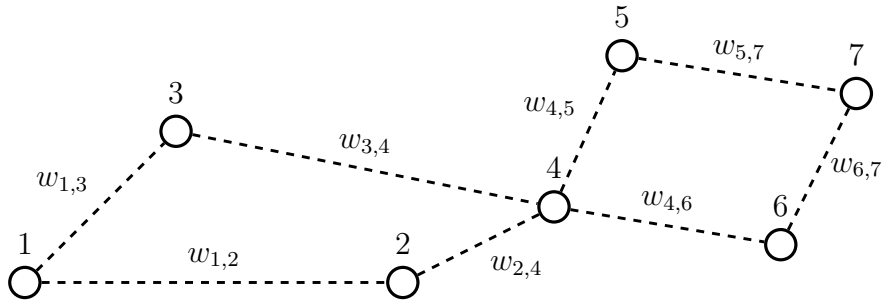


Figure 1.3: The graph $\mathcal{G}(\mathcal{I}, \mathcal{E}_1)$ has 7 vertices and 8 edges.

The *adjacency matrix* of the graph $\mathcal{G}(\mathcal{I}, \mathcal{E}_1)$ is

$$A(\mathcal{G}) \triangleq \begin{bmatrix} 0 & w_{1,2} & \cdots & w_{1,n} \\ w_{2,1} & 0 & & \vdots \\ \vdots & & \ddots & w_{n-1,n} \\ w_{n,1} & \cdots & w_{n,n-1} & 0 \end{bmatrix} \in \mathbb{R}^{n \times n};$$

the *degree matrix* of the graph $\mathcal{G}(\mathcal{I}, \mathcal{E}_1)$ is

$$D(\mathcal{G}) \triangleq \begin{bmatrix} \sum_{j \in \mathcal{I} \setminus \{1\}} w_{1,j} & 0 & \cdots & 0 \\ 0 & \sum_{j \in \mathcal{I} \setminus \{2\}} w_{2,j} & & \vdots \\ \vdots & & \ddots & 0 \\ 0 & \cdots & 0 & \sum_{j \in \mathcal{I} \setminus \{n\}} w_{n,j} \end{bmatrix} \in \mathbb{R}^{n \times n};$$

and the *Laplacian matrix* of the graph $\mathcal{G}(\mathcal{I}, \mathcal{E}_1)$ is

$$L(\mathcal{G}) \triangleq D(\mathcal{G}) - A(\mathcal{G}).$$

It follows from [81] that $L(\mathcal{G})$ is positive semidefinite. Furthermore, $L(\mathcal{G})$ has exactly 1 eigenvalue at 0 if and only if $\mathcal{G}(\mathcal{I}, \mathcal{E}_1)$ is connected.

To develop consensus algorithms, we define the states of n agents. For all $i \in \mathcal{I}$, let $x_i(\ell) \in \mathbb{R}$ be the i th agent's state at time ℓ . In this dissertation, we consider both continuous-time and discrete-time algorithms. For continuous time, we use $\ell = t \in [0, \infty)$. For discrete time, we use $\ell = k \in \{0, 1, 2, \dots\}$. We say that the agents in \mathcal{I} reach *consensus* if for all $\{i, j\} \in \mathcal{E}$,

$$\lim_{\ell \rightarrow \infty} [x_j(\ell) - x_i(\ell)] = 0.$$

For all $i \in \mathcal{I}$, define the *neighbor set*

$$\mathcal{N}_i \triangleq \{j \in \mathcal{I} : \{i, j\} \in \mathcal{E}_1\},$$

which is the set of vertices with an edge that is connected to the i th vertex. In the following examples, we demonstrate continuous-time and discrete-time consensus algorithms.

Example 2. For all $i \in \mathcal{I}$, consider the continuous-time dynamics given by

$$\dot{x}_i(t) = u_i(t), \tag{1.1}$$

where $t \geq 0$, and $x_i(t) \in \mathbb{R}$ and $u_i(t) \in \mathbb{R}$ are the i th agent's state and control. For all $i \in \mathcal{I}$, consider the control $u_i : \mathbb{R} \times \cdots \times \mathbb{R} \rightarrow \mathbb{R}$ defined by

$$u_i(x_1, \dots, x_n) \triangleq \sum_{j \in \mathcal{N}_i} w_{i,j} [x_j - x_i]. \tag{1.2}$$

Then, it follows from (1.1) and (1.2) that the closed-loop dynamics are

$$\begin{bmatrix} \dot{x}_1(t) \\ \vdots \\ \dot{x}_n(t) \end{bmatrix} = -L(\mathcal{G}) \begin{bmatrix} x_1(t) \\ \vdots \\ x_n(t) \end{bmatrix}.$$

If $\mathcal{G}(\mathcal{I}, \mathcal{E}_1)$ is connected, then [6, Lemma 1] implies that the agents in \mathcal{I} reach consensus. \triangle

Example 3. For all $i \in \mathcal{I}$, consider the discrete-time dynamics given by

$$x_i(k+1) = x_i(k) + u_i(k), \quad (1.3)$$

where $k \in \{0, 1, \dots\}$, and $x_i(k) \in \mathbb{R}$ and $u_i(k) \in \mathbb{R}$ are the i th agent's state and control. For all $i \in \mathcal{I}$, consider the control $u_i : \mathbb{R} \times \dots \times \mathbb{R} \rightarrow \mathbb{R}$ defined by

$$u_i(x_1, \dots, x_n) \triangleq \sum_{j \in \mathcal{N}_i} w_{i,j} [x_j - x_i]. \quad (1.4)$$

Then, it follows from (1.3) and (1.4) that the closed-loop dynamics are

$$\begin{bmatrix} x_1(k+1) \\ \vdots \\ x_n(k+1) \end{bmatrix} = [I - L(\mathcal{G})] \begin{bmatrix} x_1(k) \\ \vdots \\ x_n(k) \end{bmatrix}.$$

If for all $i \in \mathcal{I}$, $\sum_{j \in \mathcal{N}_i} w_{i,j} < 1$, then [6, Theorem 2] implies that the agents in \mathcal{I} reach consensus. \triangle

The above introduction considers the consensus problem for n agents in one dimension. Extensions of the above the results to arbitrary dimension is possible, for example in [18]. Consensus algorithms are also designed using directed graphs, where the edge set is defined using ordered pairs of elements [67]. Other research in consensus includes time-varying communication topologies [36, 71, 82] and time delays [35, 67, 70, 82]. Results for time-varying communication topologies and time delays rely on having a connected communication topology at all times and a bounded delay.

1.3 Flocking Problem Formulation

Let the positive integer n be the number of agents, and let $\mathcal{I} \triangleq \{1, 2, \dots, n\}$ be the agent index set. Let the positive integer m be the spatial dimension. Let $q_i(\ell) \in \mathbb{R}^m$ and $p_i(\ell) \in \mathbb{R}^m$ be the i th agent's position and velocity at time ℓ , respectively. In this dissertation, we consider both continuous-time and discrete-time algorithms. For continuous time, we use $\ell = t \in [0, \infty)$. For discrete time, we use $\ell = k \in \{0, 1, 2, \dots\}$.

Let $\mathcal{P} \triangleq \{(i, j) \in \mathcal{I} \times \mathcal{I} : i \neq j\}$ be the set of ordered pairs, and let $\delta_c > 0$ be the the minimum acceptable distance between agents. Let $\|\cdot\|$ be the 2-norm. If $\|q_j(\ell) - q_i(\ell)\| \leq \delta_c$, then the agents collide. The rules of flocking based on [16] are:

- (F1) [Collision avoidance] For all $(i, j) \in \mathcal{P}$ and all ℓ , $\|q_j(\ell) - q_i(\ell)\| > \delta_c$.
- (F2) [Velocity consensus] For all $(i, j) \in \mathcal{P}$, $\lim_{k \rightarrow \infty} [p_j(k) - p_i(k)] = 0$.
- (F3) [Cohesion] There exists $b > 0$ and exists $\ell_0 \in [0, \infty)$ such that for all $\ell \geq \ell_0$, $\max_{(i,j) \in \mathcal{P}} \|q_j(\ell) - q_i(\ell)\| \leq b$.

Condition (F1) states that there are no collisions. Condition (F2) states that agents asymptotically have the same velocity. Condition (F3) states that the maximum distance between agents is bounded asymptotically.

In addition to flocking, agents may have external objectives such as approaching a set of destinations, following a leader, and avoiding obstacles, which are accomplished with guidance. The additional objectives from guidance may conflict with flocking. For example, if each agent has a unique destination, then agents must decide whether it's better to stay in a flocking configuration or to leave the configuration and approach the destination. The combined problem of flocking and guidance, specifically following a leader, is considered more difficult than flocking by itself [29].

To address flocking and guidance, let $r_c > \delta_c$ be the communication radius. If $\|q_j(\ell) - q_i(\ell)\| < r_c$, then the i th agent can detect the j th agent's relative position and relative velocity at time ℓ and use the relative position and relative velocity in feedback, and vice versa. Define the *neighbor set*

$$\mathcal{N}_i(\ell) \triangleq \{j \in \mathcal{I} \setminus \{i\} : \|q_j(\ell) - q_i(\ell)\| < r_c\},$$

which is the set of agents that the i th agent can detect.

We address cohesion and collision avoidance together. Both position-formation and distance-formation methods induce configurations of agents that achieve cohesion and collision avoidance. Position-formation methods specify the desired configuration *a priori* by choosing the desired relative position between pairs of agents. For each $(i, j) \in \mathcal{P}$, let $\delta_{ji} \in \mathbb{R}^m$ be the desired relative position from the i th to the j th agent. Consider the i th agent's position-formation control $P_i : \mathbb{R}^{mn} \rightarrow \mathbb{R}^m$ defined by

$$P_i(q) \triangleq \sum_{j \in \mathcal{N}_i} \alpha [q_j - q_i - \delta_{ji}], \quad (1.5)$$

where $\alpha > 0$ is the position-formation gain and

$$q(\ell) \triangleq \begin{bmatrix} q_1(\ell) \\ \vdots \\ q_n(\ell) \end{bmatrix}.$$

Note that $P_i(q)$ is an affine function of position.

In contrast to position-formation methods, distance-formation methods specify the desired distance between pairs of agents. The following example demonstrates a distance-formation method for cohesion. Let $d \in (\delta_c, r_c)$ be the desired distance between pairs of agents. Let $\phi : [0, \infty) \rightarrow \mathbb{R}$ be a continuous function such that: for all $\eta \in [0, d)$, $\phi(\eta) < 0$; for all $\eta \in (d, \infty)$, $\phi(\eta) > 0$; and $\phi(d) = 0$. Consider the i th agent's distance-formation control $D_i : \mathbb{R}^{mn} \rightarrow \mathbb{R}^m$ defined by

$$D_i(q) \triangleq \sum_{j \in \mathcal{N}_i} \phi(\|q_j - q_i\|) [q_j - q_i], \quad (1.6)$$

which is nonlinear.

To achieve velocity consensus, consider the i th agent's velocity-consensus control $V_i : \mathbb{R}^{mn} \rightarrow \mathbb{R}^m$ defined by

$$V_i(p) \triangleq \sum_{j \in \mathcal{N}_i} \beta [p_j - p_i], \quad (1.7)$$

where $\beta > 0$ is the velocity-consensus gain and

$$p(\ell) \triangleq \begin{bmatrix} p_1(\ell) \\ \vdots \\ p_n(\ell) \end{bmatrix}.$$

The velocity-consensus control uses a consensus algorithm to cause the i th agent to approach a weighted average of its own and its neighbors' velocities.

To follow a leader agent, let $q_g \in \mathbb{R}^m$ and $p_g \in \mathbb{R}^m$ be the leader's position and velocity. Consider the i th agent's guidance control $L_i: \mathbb{R}^m \times \mathbb{R}^m \times \mathbb{R}^m \times \mathbb{R}^m \rightarrow \mathbb{R}^m$ defined by

$$G_i(q_i, p_i, q_g, p_g) \triangleq \gamma_1[q_g - q_i] + \gamma_2[p_g - p_i], \quad (1.8)$$

where $\gamma_1 > 0$ and $\gamma_2 > 0$.

To achieve (F1)–(F3) and guidance, flocking controls typically contain a summation of collision-avoidance, velocity consensus, cohesion, and guidance terms; and the collision-avoidance and cohesion terms are often combined. More specifically, the i th agent's flocking control typically has the form

$$u_i(\ell) \triangleq C_i(\ell) + V_i(\ell) + G_i(\ell), \quad (1.9)$$

where $C_i(\ell)$ is the collision-avoidance and cohesion term, $V_i(\ell)$ is the velocity-consensus term, and $G_i(\ell)$ is the guidance term. The flocking algorithms in [46–48, 57, 58, 60] use $C_i(\ell) \equiv P_i(q(\ell))$ to achieve (F3). If for all $(i, j) \in \mathcal{P}$, $\delta_{ji} = 0$, then (1.5) is a consensus algorithm that causes all agents to converge to the same position. The flocking algorithms in [1, 21–27] use $C_i(\ell) \equiv D_i(q(\ell))$ to achieve (F3).

In this dissertation, we develop and analyze flocking algorithms that cause agents to approach a set of destinations and follow a leader using distance-formation methods. The flocking algorithms we design have provable properties related to the configuration of agents, such as collision-free trajectories and bounded flock size. We also provide sufficient conditions such that agents reach their destinations and follow a leader.

1.4 Summary of Contributions

Chapter 2 presents a new multi-agent control method that addresses the combined problem of flocking and destination seeking. The method is completely decentralized, that is, each agent's controller relies on local sensing to determine the relative positions and velocities of nearby agents but does not rely on a centralized flock leader. Each agent has double-integrator dynamics and a potentially unique destination (i.e., position) that the agent must reach. We demonstrate that the flocking-and-destination-seeking control method accomplishes 2 objectives: if an agent is far from its destination, then that agent flocks with nearby agents, and if an agent is close to its destination, then that agent approaches its destination. The flocking-and-destination-seeking algorithm is demonstrated with several numerical examples. The novelty of the algorithm in this chapter is the combination of competing objectives, that is, flocking and destination seeking. Flocking algorithms typically consider only a centralized

leader that the agents follow, but in practical applications agents may have other objectives that are independent of other agents. The algorithm in this chapter allows agents to have an objective of which other agents do not have knowledge. The results of this research are published in [61].

Chapter 3 presents a new multi-agent control method that addresses flocking in discrete time. The method is decentralized. Each agent has the discrete-time double-integrator dynamics obtained by sampling the continuous-time double integrator and applying a zero-order hold on the control input. The method can use a centralized flock leader for guidance. We use a novel flock-correction-to-guidance term that prevents formations from collapsing around the leader. We demonstrate with analysis that agents using the discrete-time flocking method converge to a set of flocking formations. Notably, the flocking analysis relies on logarithmic potential functions. We also provide simulations demonstrating that agents using the discrete-time flocking method converge to a set of flocking formations and follow the centralized leader (if applicable). The results of this research are published in [83].

Chapter 4 validates the discrete-time flocking control method by implementing the control on rotorcraft. We present several experimental demonstrations of flocking with and without a leader. We compare the experimental demonstrations with applicable results in Chapter 3. The results demonstrate that in every case, the rotorcraft tend to a flocking configuration and do not collide with one another. In addition, the velocity difference between rotorcraft is bounded, and the rotorcraft approximately follow the leader with delay.

Chapter 2 Continuous-Time Flocking and Destination Seeking

We present a multi-agent control method that addresses the combined problem of flocking and destination seeking. The method is completely decentralized, that is, each agent’s controller relies on local sensing to determine the relative positions and velocities of nearby agents but does not rely on a centralized flock leader. Each agent has double-integrator dynamics and a potentially unique destination (i.e., position) that the agent must reach. We demonstrate that the flocking-and-destination-seeking control method accomplishes 2 objectives: (i) if an agent is far from its destination, then that agent flocks with nearby agents, and (ii) if an agent is close to its destination, then that agent approaches its destination. The flocking-and-destination-seeking algorithm is demonstrated with several numerical examples.

2.1 Introduction

Multi-agent systems have many exciting applications such as distributed sensing, formation flying, cooperative surveillance, and point-to-point mail delivery. For example, autonomous aircraft or spacecraft can fly in formations for distributed sensing [8,9]. Coordinated aircraft could be used in a forest-fire scenario to measure wind velocities and thus, predict fire movement. In the agricultural industry, coordinated aircraft could conduct crop surveys. All of these applications require decentralized methods for coordinating and controlling groups of autonomous agents [11].

For coordinated control, each agent relies on sensing to determine the relative positions and velocities of nearby agents. Then, each agent uses these measurements combined with other information such as mission objectives to accomplish tasks, which can include: cohesion, collision avoidance, velocity matching, and guidance. Cohesion attracts an agent to nearby agents, whereas collision avoidance repels an agent from nearby agents (or obstacles). Velocity matching causes nearby agents to approach a consensus velocity, and guidance causes an agent or agents to follow a leader agent or approach a desired destination.

Cohesion and collision avoidance can be addressed using position-formation methods [18–20] or distance-formation methods [1,21–28]. Position-formation approaches force agents into a configuration using desired relative-position vectors between pairs of agents. In contrast, distance-formation methods induce a configuration using only a desired distance between adjacent agents. In this case, the agents autonomously determine their configuration based on the desired interagent distance and initial conditions. A common approach for distance formation is to use potential functions that create attractive forces when nearby agents are too far away and repulsive

forces when nearby agents are too close [1, 21–27]. A survey of multi-agent formation methods is presented in [29]. Consensus algorithms [42, 67, 68, 71] are used to achieve velocity matching. Approaches that use distance-formation methods for cohesion and collision avoidance, and consensus for velocity matching lead to formations called *flocks* [1, 24–28].

Agent guidance is often addressed using leader-follower methods [1, 9, 19, 21–26] or destination-seeking methods [20, 63–65]. Leader-follower approaches rely on a centralized leader, who can be an actual or virtual member of the formation and whose real-time position and velocity are known by all agents [1, 22–26] or at least by some [9, 19, 21]. Each agent uses knowledge of the centralized leader and measurements of nearby agents to induce a formation and follow the leader. In contrast, destination-seeking methods (e.g., [20, 63–65]) cause agents to approach desired destinations. The flocking algorithms with leader-follower guidance in [1, 19, 21–26] do not address destination seeking, and the destination-seeking methods in [20, 63–65] do not address flocking. In contrast to [1, 9, 18–29, 63–65], this chapter addresses the combined problem of flocking and destination seeking.

The flocking-and-destination-seeking control objective is twofold—if an agent is far from its destination, then it flocks with nearby agents, but ultimately each agent approaches its destination. The flocking-and-destination-seeking algorithm in this paper uses a distance-formation approach for cohesion and collision avoidance, a consensus algorithm for velocity matching, and a destination-seeking method for guidance. The main analytic results in this chapter examine the formation properties of agents and provide sufficient conditions for agents to converge to their destinations. Flocking and destination seeking is also considered in [30]; however, the analysis in [30] considers only a single destination and does not examine formation properties.

The flocking-and-destination-seeking algorithm that we present is completely decentralized, namely, each agent’s controller does not incorporate a centralized leader and relies on only local sensing to determine the relative positions and velocities of nearby agents. Each agent has knowledge of its own destination but does not require knowledge of other agents’ destinations. The controller in this chapter achieves multiple objectives, that is, flocking and destination seeking, and thus, extends the work of [1, 9, 18–30, 63–65].

The combined flocking-and-destination-seeking problem has applications such as point-to-point passenger transport and point-to-point mail delivery. For example, consider a group of autonomous ground vehicles on a highway, where each vehicle has a unique destination that it needs to reach. While traveling to the destination, it is beneficial for a vehicle to reduce wind resistance and energy expenditure by drafting off neighboring vehicles. When a vehicle gets close to its destination, it leaves the flock and approaches the destination. The remaining vehicles then form a new flock and repeat the process until all vehicles reach their destinations. Example 5 in Section 2.7 applies the flocking-and-destination-seeking algorithm to a vehicles-on-a-highway problem.

2.2 Problem Formulation

Let the positive integer n be the number of agents, and define $\mathcal{I} \triangleq \{1, 2, \dots, n\}$, which is the agent index set. For each $i \in \mathcal{I}$, consider the double-integrator dynamics

$$\dot{q}_i(t) = p_i(t), \quad (2.1)$$

$$\dot{p}_i(t) = u_i(t), \quad (2.2)$$

where $t \geq 0$; $q_i(0)$ and $p_i(0)$ are the initial conditions; and $q_i(t) \in \mathbb{R}^m$, $p_i(t) \in \mathbb{R}^m$, and $u_i(t) \in \mathbb{R}^m$ are the position, velocity, and control of the i th agent, respectively. Define $\mathcal{P} \triangleq \{(i, j) \in \mathcal{I} \times \mathcal{I} : i \neq j\}$, which is the set of ordered pairs, and let $\|\cdot\|$ denote the Euclidean norm.

Let $\delta_c \geq 0$ be the collision radius, which is the desired minimum separation distance between agents. The rules for flocking are that agents stay close to one another, avoid collisions, and match velocities [16]. We use these rules to define flocking. Let T be a connected subset of $[0, \infty)$. Then, the agents in \mathcal{I} *flock with radius $d > \delta_c$ over the interval T* if the following conditions hold:

(F1) For all $(i, j) \in \mathcal{P}$ and all $t \in T$,

$$\|q_i(t) - q_j(t)\| > \delta_c.$$

(F2) For all $(i, j) \in \mathcal{P}$ and all $t \in T$,

$$\|p_j(t) - p_i(t)\| \approx 0.$$

(F3) For all $i \in \mathcal{I}$ and all $t \in T$,

$$\max_{j \in \mathcal{I} \setminus \{i\}} \|q_j(t) - q_i(t)\| \leq d(n-1).$$

(F4) For all $i \in \mathcal{I}$ and all $t \in T$,

$$\min_{j \in \mathcal{I} \setminus \{i\}} \|q_j(t) - q_i(t)\| \approx d.$$

Condition (F1) states that there are no collisions. Condition (F2) states that all agents have approximately the same velocity. Condition (F3) states that each agent is at most a distance $d(n-1)$ away from its farthest neighbor. Condition (F4) states that each agent maintains a distance of approximately d from its nearest neighbor.

We address not only flocking but also destination seeking. For all $i \in \mathcal{I}$ let $\xi_i \in \mathbb{R}^m$ be the i th agent's destination. Let $r_\beta \geq 0$, and for each $i \in \mathcal{I}$ and each $t \geq 0$ we say the i th agent is far from its destination if $\|\xi_i - q_i(t)\| > r_\beta$. Assume there exists $t_f > 0$ such that for all $t \in [0, t_f)$ the agents in \mathcal{I} are far from their destinations. In this case, we consider 2 objectives:

(O1) *Flocking*: The agents in \mathcal{I} flock with radius $d > 0$ over a connected subset of $[0, t_f)$.

(O2) *Destination seeking*: For all $i \in \mathcal{I}$, $\lim_{t \rightarrow \infty} q_i(t) = \xi_i$ and $\lim_{t \rightarrow \infty} p_i(t) = 0$.

Objective (O1) states that if agents are far from their destinations, then they flock. Objective (O2) states that each agent approaches its destination asymptotically. Unless otherwise stated, all statements in this chapter that involve the subscript i are for all $i \in \mathcal{I}$.

2.3 Review of Algorithm 1 from [1]

We review Algorithm 1 from [1], which is a flocking method for agents with double-integrator dynamics. Let $\epsilon > 0$, and consider $\|\cdot\|_\epsilon: \mathbb{R}^m \rightarrow [0, \infty)$ defined by

$$\|x\|_\epsilon \triangleq \frac{1}{\epsilon} \left(\sqrt{1 + \epsilon \|x\|^2} - 1 \right). \quad (2.3)$$

Note that $\|\cdot\|_\epsilon$ is continuously differentiable on \mathbb{R}^m , but $\|\cdot\|_\epsilon$ is not a norm on \mathbb{R}^m . Define $\sigma_\epsilon: \mathbb{R}^m \rightarrow \mathbb{R}^m$ by

$$\sigma_\epsilon(x) \triangleq \left(\frac{\partial}{\partial x} [\|x\|_\epsilon] \right)^\top = \frac{x}{1 + \epsilon \|x\|_\epsilon}. \quad (2.4)$$

Next, let $h \in (0, 1)$, and define $\rho_h: [0, \infty) \rightarrow [0, 1]$ by

$$\rho_h(\eta) \triangleq \begin{cases} 1, & \text{if } \eta \in [0, h), \\ \frac{1}{2} + \frac{1}{2} \cos \pi \frac{\eta - h}{1 - h}, & \text{if } \eta \in [h, 1], \\ 0, & \text{if } \eta \in (1, \infty), \end{cases} \quad (2.5)$$

which decreases from 1 to 0 as η increases from 0 to ∞ , and the rate of change of ρ_h depends on h . Let $b \geq a > 0$, define $c \triangleq (b - a)/\sqrt{4ab}$, and consider $\phi: \mathbb{R} \rightarrow (-b, a)$ defined by

$$\phi(\eta) \triangleq \frac{1}{2} \left[\frac{(a + b)(\eta + c)}{\sqrt{1 + (\eta + c)^2}} + (a - b) \right], \quad (2.6)$$

which is a sigmoidal function.

Next, let $r_c > 0$ be the *communication radius*, which is the maximum distance at which an agent can sense another agent's relative position and relative velocity. For all $t \geq 0$, define the *neighbor set* $\mathcal{N}_i(t) \triangleq \{j \in \mathcal{I} \setminus \{i\} : \|q_j(t) - q_i(t)\| < r_c\}$, which is the set of agents whose distance to the i th agent is no greater than the communication radius r_c at time t . Let $d \in (\delta_c, r_c]$ be the *flock radius*, which is the desired distance between agents in the flock.

For all $t \geq 0$, define

$$q(t) \triangleq \begin{bmatrix} q_1(t) \\ \vdots \\ q_n(t) \end{bmatrix}, \quad p(t) \triangleq \begin{bmatrix} p_1(t) \\ \vdots \\ p_n(t) \end{bmatrix}.$$

Then, [1, Algorithm 1] considers the control $u_i(t) \equiv v_i(q(t), p(t))$, where

$$\begin{aligned}
v_i(q, p) \triangleq & \underbrace{\sum_{j \in \mathcal{N}_i} \rho_h \left(\frac{\|q_j - q_i\|_\epsilon}{\|r_c\|_\epsilon} \right) \phi(\|q_j - q_i\|_\epsilon - \|d\|_\epsilon) \sigma_\epsilon(q_j - q_i)}_{\text{Flock attraction and repulsion}} \\
& + \underbrace{\sum_{j \in \mathcal{N}_i} \rho_h \left(\frac{\|q_j - q_i\|_\epsilon}{\|r_c\|_\epsilon} \right) [p_j - p_i]}_{\text{Velocity consensus}}. \tag{2.7}
\end{aligned}$$

For each $t \geq 0$ and each $j \in \mathcal{N}_i(t)$, the flock-attraction-and-repulsion term in (2.7) is such that the i th agent is attracted to the j th agent if $\|q_j(t) - q_i(t)\| > d$, and repelled from the j th agent if $\|q_j(t) - q_i(t)\| < d$. The velocity-consensus term in (2.7) attempts to match the i th agent's velocity with a weighted average of the velocities of all agents in the neighbor set.

The parameters in the control (2.7) are ϵ , h , a , and b . Increasing ϵ decreases the strength of the flock-attraction-and-repulsion term relative to the strength of the velocity-consensus term. Increasing h increases the rate of change of ρ_h . Increasing a increases the strength of attraction relative to the strength of repulsion and velocity consensus. Increasing b increases the strength of repulsion relative to the strength of attraction and velocity consensus.

Theorem 1 of [1] provides conditions such that the agents with dynamics (2.1), (2.2) and control $u_i = v_i$ form at least one flock. However, the control $u_i = v_i$ can cause fragmentation, that is, $u_i = v_i$ can result in multiple flocks rather than a single flock. Thus, the control $u_i = v_i$ may violate (F3). In contrast, [1, Algorithm 2] is shown to force the agents in \mathcal{I} to flock without fragmentation. However, [1, Algorithm 2] relies on a centralized flock leader whose position and velocity are known by each agent and is used in each agent's control. Neither [1, Algorithm 1] nor [1, Algorithm 2] address destination seeking and thus cannot be used to achieve (O2).

2.4 Flocking and Destination Seeking

We present a control that combines flock-attraction-and-repulsion and velocity-consensus terms with additional terms to achieve (O1) and (O2). For all $t \geq 0$, define the *attraction set*

$$\mathcal{A}_i(t) \triangleq \{j \in \mathcal{I} \setminus \{i\} : d \leq \|q_j(t) - q_i(t)\| < r_c\} \subseteq \mathcal{N}_i(t),$$

which is the set of agents whose distances from the i th agent are between the flock and communication radii. Define

$$A_i(q) \triangleq \sum_{j \in \mathcal{A}_i} \rho_h \left(\frac{\|q_j - q_i\|_\epsilon}{\|r_c\|_\epsilon} \right) \phi(\|q_j - q_i\|_\epsilon - \|d\|_\epsilon) \sigma_\epsilon(q_j - q_i), \tag{2.8}$$

which has the same form as the flock-attraction-and-repulsion term in (2.7) except that the neighbor set \mathcal{N}_i is replaced by the attraction set \mathcal{A}_i . Next, for all $t \geq 0$,

define the *repulsion set*

$$\mathcal{R}_i(t) \triangleq \{j \in \mathcal{I} \setminus \{i\} : \|q_j(t) - q_i(t)\| < d\} \subseteq \mathcal{N}_i(t),$$

which is the set of agents whose distances to the i th agent are less than the flock radius. Define

$$R_i(q) \triangleq \sum_{j \in \mathcal{R}_i} \rho_h \left(\frac{\|q_j - q_i\|_\epsilon}{\|r_c\|_\epsilon} \right) \phi(\|q_j - q_i\|_\epsilon - \|d\|_\epsilon) \sigma_\epsilon(q_j - q_i), \quad (2.9)$$

which has the same form as the flock-attraction-and-repulsion term in (2.7) except that the neighbor set \mathcal{N}_i is replaced by the repulsion set \mathcal{R}_i . For all $t \geq 0$, $\mathcal{A}_i(t) \cup \mathcal{R}_i(t) = \mathcal{N}_i(t)$, and $A_i(q) + R_i(q)$ is equal to the flock-attraction-and-repulsion term in (2.7). Next, define

$$C_i(q, p) \triangleq \sum_{j \in \mathcal{N}_i} \rho_h \left(\frac{\|q_j - q_i\|_\epsilon}{\|r_c\|_\epsilon} \right) [p_j - p_i], \quad (2.10)$$

which is the velocity-consensus term in (2.7). Therefore, $v_i(q, p) = A_i(q) + R_i(q) + C_i(q, p)$.

Let $r_\alpha \in [0, r_\beta]$, and for all $t \geq 0$, we say that the i th agent is close to its destination if $\|\xi_i - q_i(t)\| \leq r_\alpha$. Let $\mu: [0, \infty) \rightarrow [0, 1]$ be a continuous function that satisfies the following properties:

- (M1) If $\eta \geq r_\beta$, then $\mu(\eta) = 1$.
- (M2) If $\eta < r_\alpha$, then $\mu(\eta) = 0$.
- (M3) $\partial\mu(\|x\|)/\partial x$ is continuous on \mathbb{R}^m .

If $r_\beta > r_\alpha \geq 0$, then an example μ that satisfies (M1)–(M3) is

$$\mu(\eta) = \begin{cases} 0, & \text{if } \eta \leq r_\alpha, \\ \frac{1}{2} + \frac{1}{2} \cos \pi \frac{r_\beta^2 - \eta^2}{r_\beta^2 - r_\alpha^2}, & \text{if } r_\alpha < \eta < r_\beta, \\ 1, & \text{if } \eta \geq r_\beta, \end{cases} \quad (2.11)$$

which is shown in Figure 2.1. Note that if $r_\alpha = r_\beta = 0$, then (M1) implies that $\mu = 1$.

For all $t \geq 0$, define $z_i(t) \triangleq \xi_i - q_i(t)$, which is the vector from the i th agent to its destination. If the i th agent is far from its destination, then the i th agent's objective is to flock with nearby agents. In contrast, if the i th agent is close to its destination, then the i th agent's objective is not to flock but rather to reach its destination.

The following result considers a control that consists of the flock attraction $\mu(\|z_i\|)A_i(q)$, flock repulsion $R_i(q)$, and velocity consensus $\mu(\|z_i\|)C_i(q, p)$. The result is confirmed by direct calculation.

Proposition 1. Consider (2.1) and (2.2), where for all $t \geq 0$,

$$u_i(q(t), p(t), z_i(t)) = \mu(\|z_i(t)\|)A_i(q(t)) + R_i(q(t)) + \mu(\|z_i(t)\|)C_i(q(t), p(t)). \quad (2.12)$$

Then, the following statements hold:

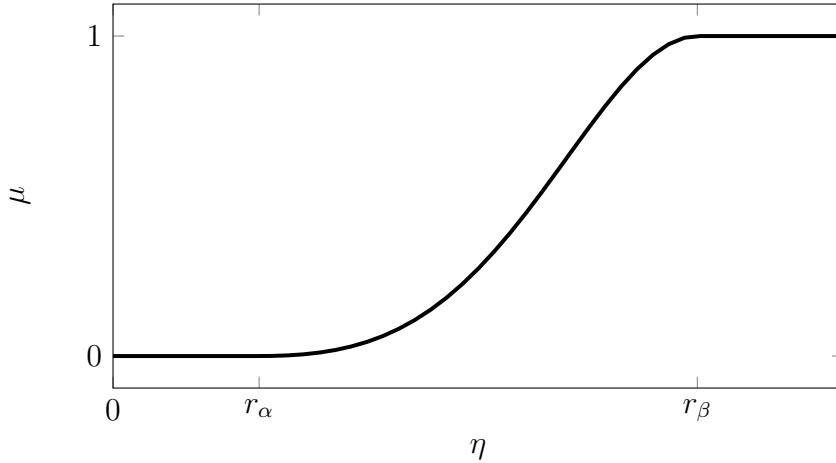


Figure 2.1: An example $\mu : [0, \infty) \rightarrow [0, 1]$ that satisfies (M1)–(M3).

- (a) If $\|z_i(t)\| \geq r_\beta$, then $u_i(q(t), p(t), z_i(t)) = v_i(q(t), p(t))$.
- (b) If $\|z_i(t)\| < r_\alpha$, then $u_i(q(t), p(t), z_i(t)) = R_i(q(t))$.
- (c) $u_i(q, p, z_i)$ is continuously differentiable on $\mathbb{R}^{mn} \times \mathbb{R}^{mn} \times \mathbb{R}^m$.

Part (a) states that if the i th agent is far from its destination, then (2.12) is equivalent to (2.7). Part (b) states that if the i th agent is close to its destination, then (2.12) consists of only flock repulsion. Thus, if $\|z_i(t)\| < r_\alpha$, then the i th agent is neither attracted to nor matches velocities with nearby agents.

We now describe two additional desired properties for the agents in \mathcal{I} . Let $r_2 > r_1 > 0$. If $\|z_i(t)\| > r_2$, then we want the i th agent's speed $\|p_i(t)\|$ to tend to the *flocking speed* $p_f > 0$. In contrast, if $\|z_i(t)\| \leq r_1$, then we want the i th agent to approach its destination. Specifically, if $\|z_i(t)\| \leq r_1$, then we want q_i to satisfy the differential equation

$$\ddot{y}_i(t) + 2\zeta\omega_n\dot{y}_i(t) + \omega_n^2 y_i(t) = \omega_n^2 \xi_i, \quad (2.13)$$

where $y_i(t) \in \mathbb{R}^m$, $\omega_n > 0$, and $\zeta > 0$.

To achieve these properties, we consider a control that includes destination-seeking and damping terms. Let $\gamma \in (0, \omega_n^2 r_1)$, and consider $\nu: [0, \infty) \rightarrow (0, \omega_n^2]$ defined by

$$\nu(\eta) \triangleq \begin{cases} \omega_n^2, & \text{if } \eta \leq r_1, \\ \frac{1}{2} \left(\omega_n^2 + \frac{\gamma}{\eta} \right) - \frac{1}{2} \left(\omega_n^2 - \frac{\gamma}{\eta} \right) \cos \pi \frac{r_2^2 - \eta^2}{r_2^2 - r_1^2}, & \text{if } r_1 < \eta < r_2, \\ \frac{\gamma}{\eta}, & \text{if } \eta \geq r_2, \end{cases} \quad (2.14)$$

which is continuously differentiable on $[0, \infty)$ and shown in Figure 2.2. We use the *destination-seeking control* $\nu(\|z_i\|)z_i$ to attract the i th agent to its destination.

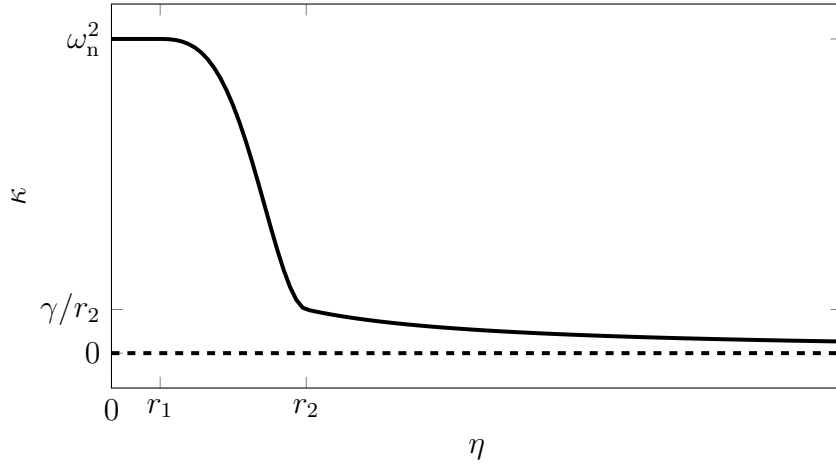


Figure 2.2: A plot of $\nu : [0, \infty) \rightarrow (0, \omega_n^2]$, which is continuously differentiable on $[0, \infty)$. For all $\eta \leq r_1$, $\nu(\eta) = \omega_n^2$, and for all $\eta \geq r_2$, $\nu(\eta) = \gamma/\eta$.

Next, consider $\kappa : [0, \infty) \rightarrow (-\infty, 0)$ defined by

$$\kappa(\eta) \triangleq \begin{cases} -2\zeta\omega_n, & \text{if } \eta \leq r_1, \\ -\frac{1}{2} \left(2\zeta\omega_n + \frac{\gamma}{p_f} \right) - \frac{1}{2} \left(2\zeta\omega_n - \frac{\gamma}{p_f} \right) \cos \pi \frac{r_2^2 - \eta^2}{r_2^2 - r_1^2}, & \text{if } r_1 < \eta < r_2, \\ -\frac{\gamma}{p_f}, & \text{if } \eta \geq r_2, \end{cases} \quad (2.15)$$

which is continuously differentiable on $[0, \infty)$ and shown in Figure 2.3. We use the *damping control* $\kappa(\|z_i\|)p_i$ to oppose the velocity p_i .

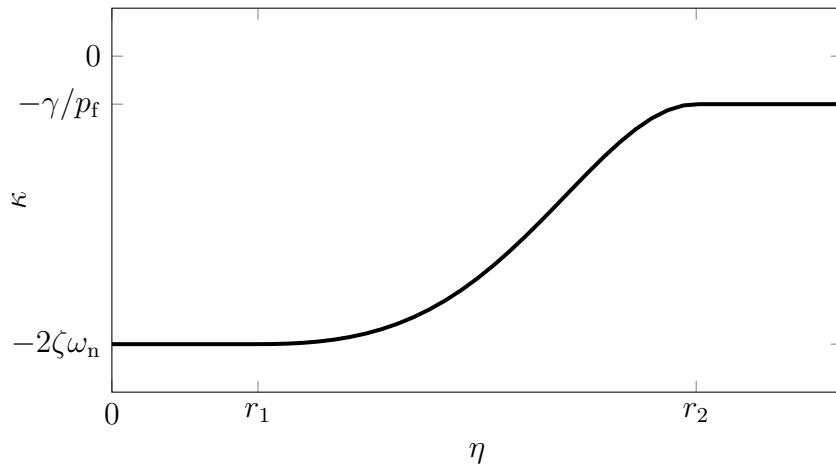


Figure 2.3: A plot of $\kappa : [0, \infty) \rightarrow (-\infty, 0)$, which is continuously differentiable on $[0, \infty)$. For all $\eta \leq r_1$, $\kappa(\eta) = -2\zeta\omega_n$, and for all $\eta \geq r_2$, $\kappa(\eta) = -\gamma/p_f$.

Define

$$\xi \triangleq \begin{bmatrix} \xi_1 \\ \vdots \\ \xi_n \end{bmatrix}.$$

The following result demonstrates that a control composed of destination seeking $\nu(\|z_i\|)z_i$ and damping $\kappa(\|z_i\|)p_i$ forces the i th agent's position q_i to converge asymptotically to its destination ξ_i .

Proposition 2. Consider (2.1) and (2.2), where for all $t \geq 0$,

$$u_i(z_i(t), p_i(t)) = \nu(\|z_i(t)\|)z_i(t) + \kappa(\|z_i(t)\|)p_i(t). \quad (2.16)$$

Then, the following statements hold:

- (a) $(q(t), p(t)) \equiv (\xi, 0)$ is a globally asymptotically stable equilibrium of (2.1), (2.2), and (2.16).
- (b) There exists $t_1 > 0$ such that for all $t \geq t_1$, $\|z_i(t)\| \leq r_1$ and $q_i(t)$ satisfies

$$\ddot{q}_i(t) + 2\zeta\omega_n\dot{q}_i(t) + \omega_n^2q_i(t) = \omega_n^2\xi_i.$$

- (c) Assume $\|z_i(0)\| > r_2$. Then, there exists $t_0 > 0$ such that for all $t \in [0, t_0)$,

$$u_i(z_i(t), p_i(t)) = \frac{\gamma}{\|z_i(t)\|}z_i(t) - \frac{\gamma}{p_f}p_i(t).$$

- (d) $u_i(z_i, p_i)$ is continuously differentiable on $\mathbb{R}^m \times \mathbb{R}^m$.

Part (b) states that there exists a time after which an agent approaches its destination with the dynamics (2.13) of a damped oscillator. If an agent's initial position is greater than r_2 from its destination, then part (c) provides an expression for the destination-seeking-and-damping control.

If $\|z_i(t)\| > r_2$, then (2.14) and (2.15) imply that (2.16) is equivalent to $u_i(z_i(t), p_i(t)) = \gamma z_i(t)/\|z_i(t)\| - \gamma p_i(t)/p_f$. In this case, it follows from (2.2) that $p_i(t)$ satisfies

$$\dot{p}_i(t) = -\frac{\gamma}{p_f}p_i(t) + \frac{\gamma}{\|z_i(t)\|}z_i(t), \quad (2.17)$$

which can be viewed as a linear time-invariant differential equation with the bounded input $\gamma z_i(t)/\|z_i(t)\|$. If the destination ξ_i is infinitely far from the position q_i (i.e., $\|z_i\| = \infty$), then $z_i/\|z_i\|$ is a constant unit vector. In this case, (2.17) implies that $p_i(t)$ tends toward $p_f z_i(t)/\|z_i(t)\|$, and the speed $\|p_i(t)\|$ tends toward p_f . Thus, if $\|z_i(t)\|$ is sufficiently large, then the i th agent has forces that drive its speed $\|p_i(t)\|$ toward p_f .

We now combine the flock-attraction, flock-repulsion, velocity-consensus, destination-seeking, and damping terms to form the control

$$u_i(q, p, z_i) = \underbrace{\mu(\|z_i\|)A_i(q)}_{\text{Flock attraction}} + \underbrace{R_i(q)}_{\text{Flock repulsion}} + \underbrace{\mu(\|z_i\|)C_i(q, p)}_{\text{Velocity consensus}}$$

$$+ \underbrace{\nu(\|z_i\|)z_i}_{\text{Destination seeking}} + \underbrace{\kappa(\|z_i\|)p_i}_{\text{Damping}}. \quad (2.18)$$

Since (2.18) is the sum of the controllers in Propositions 1 and 2, it follows that (2.18) is continuously differentiable on $\mathbb{R}^{mn} \times \mathbb{R}^{mn} \times \mathbb{R}^m$. In addition, we note that flock attraction, flock repulsion, and destination seeking are bounded.

The parameters of u_i are $\epsilon, h, a, b, r_\alpha, r_\beta, \mu, r_1, r_2, \gamma, p_f, \zeta$, and ω_n , where the first 6 parameters and the function μ apply to the flock-attraction, flock-repulsion, and velocity-consensus terms, and the latter 6 parameters apply to the destination-seeking and damping terms. Note that ϵ, h, a , and b are discussed in Section 2.3. We now discuss $r_\alpha, r_\beta, \mu, r_1, r_2, \gamma, p_f, \zeta$, and ω_n .

The radii r_α, r_β, r_1 , and r_2 determine the i th agent's control behavior for specific distances from its destination ξ_i . If $\|z_i(t)\| > r_\beta$, then the i th agent and nearby agents attempt to flock. If $\|z_i(t)\| \leq r_\alpha$, then the i th agent is repelled from nearby agents but does not attempt to flock. If $\|z_i(t)\| > r_2$, then the i th agent has forces that drive its speed $\|p_i(t)\|$ toward p_f . If $\|z_i(t)\| \leq r_1$, then the i th agent has forces that make it behave like the damped oscillator. While $r_1 = r_\alpha$ and $r_2 = r_\beta$ is an intuitive choice, this is not required.

The function μ determines the strength of flock attraction and velocity consensus relative to flock repulsion, destination seeking, and damping. If $\mu(\|z_i(t)\|) = 1$, then the combination of flock-attraction, flock-repulsion, and velocity-consensus terms in (2.18) is equal to the combination of flock-attraction-and-repulsion and velocity-consensus terms in (2.7). As $\mu(\|z_i(t)\|)$ decreases, the strength of flock attraction and velocity consensus decreases relative to flock repulsion, destination seeking, and damping. If $\mu(\|z_i(t)\|) = 0$, then the flock-attraction and velocity-consensus terms are zero.

For $\|z_i(t)\| \geq r_2$, γ is the magnitude of the destination-seeking term $\nu(\|z_i(t)\|)z_i(t)$. In this case, increasing γ increases the i th agent's attraction to its destination. For $\|z_i(t)\| \geq r_2$, increasing γ also increases the rate at which the i th agent's speed $\|p_i(t)\|$ tends to p_f . The flocking speed p_f , which is the desired speed of agents, can be chosen for a variety of reasons such as fuel or time constraints.

Finally, ζ and ω_n are the damping ratio and natural frequency of the dynamics (2.13) that govern the desired behavior of an agent when it's near its destination.

2.5 Flocking Analysis

In this section, we analyze the flocking behavior of agents with control (2.18). Since (2.18) is designed to drive each agent to its destination, the agents flock over at most a finite time interval before approaching their destinations. To analyze flocking, we impose assumptions on the destinations so that we can use asymptotic analysis to examine flocking. In particular, we impose assumptions that preclude agents from reaching their destinations, and thus allow us to demonstrate flocking with asymptotic analysis.

To analyze asymptotic flocking, we could consider destinations ξ_1, \dots, ξ_n that are infinitely far from the initial positions $q_1(0), \dots, q_n(0)$. However, in this case, $z_i = \xi_i - q_i$ is not well defined. Instead, we impose the following assumptions regarding the agents' destinations:

- (A1) All agents have the same destination, and this destination moves with constant velocity $\chi \in \mathbb{R}^m$, where $\|\chi\| = p_f$.
- (A2) For all $t \geq 0$, $\|z_i(t)\| > \max\{r_\beta, r_2\}$.

These assumptions are used for flocking analysis only and apply only to this section of the chapter. We refer to (A1) as the *moving-destination assumption*. Assumption (A2) combined with (M1), (2.14), and (2.15) implies that $\mu(\|z_i(t)\|) = 1$, $\nu(\|z_i(t)\|)z_i(t) = \gamma z_i(t)/\|z_i(t)\|$, and $\kappa(\|z_i(t)\|) = -\gamma/p_f$. Thus, (A2) implies that the control (2.18) depends on the direction $z_i(t)/\|z_i(t)\|$ but not the distance $\|z_i(t)\|$. Therefore, the control (2.18) with the moving-destination assumption (A1) is equivalent to the control (2.18) with a non-moving destination that is infinitely far from the initial positions. Thus, (A1) and (A2) are in some sense equivalent to an infinitely far non-moving destination. Asymptotic flocking under (A1) and (A2) suggests that if the initial positions $q_1(0), \dots, q_n(0)$ are sufficiently far from the destinations ξ_1, \dots, ξ_n , and the destinations are sufficiently close together relative to the distances $\|z_1\|, \dots, \|z_n\|$, then the agents flock over a finite time interval.

It follows from (A1) that the destination dynamics are $\dot{\xi}_i(t) = \chi$, where $\xi_i(t) \in \mathbb{R}^m$ is the i th agent's destination, $\xi_i(0) \in \mathbb{R}^m$ is the initial position, and $\xi_1(0) = \dots = \xi_n(0)$. For all $t \geq 0$, define $w_i(t) \triangleq \dot{z}_i(t) = \chi - p_i(t)$. Thus, (2.1) and (2.2) imply that for all $t \geq 0$,

$$\dot{z}_i(t) = w_i(t), \tag{2.19}$$

$$\dot{w}_i(t) = -u_i(t). \tag{2.20}$$

For all $t \geq 0$, define

$$z(t) \triangleq \begin{bmatrix} z_1(t) \\ \vdots \\ z_n(t) \end{bmatrix}, \quad w(t) \triangleq \begin{bmatrix} w_1(t) \\ \vdots \\ w_n(t) \end{bmatrix}.$$

We use Lyapunov-like analysis to examine the asymptotic properties of (2.1), (2.2), and (2.18) under (A1) and (A2). Consider $\psi: [0, \infty) \rightarrow [0, \infty)$ defined by

$$\psi(\eta) \triangleq \int_{\|d\|_\epsilon}^{\eta} \rho_h \left(\frac{s}{\|r_c\|_\epsilon} \right) \phi(s - \|d\|_\epsilon) ds. \tag{2.21}$$

If $\eta = \|d\|_\epsilon$, then $\psi(\eta) = 0$; otherwise, $\psi(\eta) > 0$. Furthermore, consider $\psi_s: \mathbb{R}^{mn} \rightarrow [0, \infty)$ defined by

$$\psi_s(q) \triangleq \frac{1}{2} \sum_{(i,j) \in \mathcal{P}} \psi(\|q_j - q_i\|_\epsilon). \tag{2.22}$$

If for all $(i, j) \in \mathcal{P}$, $\|q_j - q_i\| = d$, then $\psi_s(q) = 0$; otherwise, $\psi_s(q) > 0$. Consider the Lyapunov-like function $W: \mathbb{R}^{mn} \times \mathbb{R}^{mn} \rightarrow [0, \infty)$ defined by

$$W(z, w) \triangleq \psi_s(z) + \left[\sum_{i \in \mathcal{I}} \gamma \|z_i\| - \frac{\gamma}{p_f} \chi^T z_i \right] + \frac{1}{2} \|w\|^2. \quad (2.23)$$

Since $\|\chi\| = p_f$, it follows that

$$\sum_{i \in \mathcal{I}} \gamma \|z_i\| - \frac{\gamma}{p_f} \chi^T z_i \geq \sum_{i \in \mathcal{I}} \gamma \|z_i\| - \frac{\gamma}{p_f} \|\chi\| \|z_i\| = 0.$$

Since, in addition, $\psi_s \geq 0$, it follows that for all $(z, w) \in \mathbb{R}^{mn} \times \mathbb{R}^{mn}$, $W(z, w) \geq 0$. If for all $(i, j) \in \mathcal{P}$, $\|z_j - z_i\| = d$, $\chi^T z_i = p_f \|z_i\|$, and $w_i = 0$, then $W(z, w) = 0$; otherwise, $W(z, w) > 0$.

The following result provides sufficient conditions such that the agents do not collide; all agents match velocity; the maximum distance between any 2 agents is asymptotically bounded by $d(n-1)$; and the derivative of ψ_s along the trajectories of (2.18)–(2.20) tends to 0. The proof is in Section 2.10.

Theorem 1. Consider the closed-loop system (2.18)–(2.20), where the initial conditions are $z_i(0) \in \mathbb{R}^m$ and $w_i(0) \in \mathbb{R}^m$. Assume (A1) and (A2) hold. Then, the following statements hold:

- (a) If $W(z(0), w(0)) < \psi(\|\delta_c\|_\epsilon)$, then for all $(i, j) \in \mathcal{P}$ and all $t \geq 0$, $\|q_j(t) - q_i(t)\| > \delta_c$.
- (b) $\lim_{t \rightarrow \infty} p_i(t) = \chi$.
- (c) Assume r_c is such that for all $(i, j) \in \mathcal{P}$ and all $t \geq 0$, $\|r_c\|_\epsilon > \|q_j(t) - q_i(t)\|_\epsilon/h$. Then, for all $\delta > 0$ there exists $t_1 \geq 0$ such that for all $t \geq t_1$, $\max_{(i,j) \in \mathcal{P}} \|q_j(t) - q_i(t)\| \leq d(n-1) + \delta$.
- (d) $\lim_{t \rightarrow \infty} \left. \frac{\partial \psi_s(z)}{\partial z} \right|_{z=z(t)} = 0$.
- (e) $\lim_{t \rightarrow \infty} u_i(q(t), p(t), z_i(t)) = 0$.
- (f) $\lim_{t \rightarrow \infty} [A_i(q(t)) + R_i(q(t))] = 0$.
- (g) $\lim_{t \rightarrow \infty} \frac{z_i(t)}{\|z_i(t)\|} = \frac{\chi}{p_f}$.

Part (a) states that if $W(z(0), w(0)) < \psi(\|\delta_c\|_\epsilon)$, then there are no collisions, which implies (F1). Part (b) states that every agent's velocity tends to χ . Therefore, the difference in velocity between any 2 agents tends to zero, which implies (F2). Part (c) states that if the communication radius r_c is sufficiently large, then the maximum distance between any 2 agents is asymptotically bounded by $d(n-1)$, which implies (F3). Part (d) states that the derivative of ψ_s along the trajectories of (2.18)–(2.20)

tends to 0. Thus, the asymptotic configuration of agents is a critical point of ψ_s . Furthermore, [1, Lemma 3] shows that if r_c/d is sufficiently small and the asymptotic configuration of the agents in \mathcal{I} minimizes ψ_s , then that configuration satisfies (F4). Part (e) states that the control tends to 0. Part (f) states that the sum of flock attraction and flock repulsion of each agent tends to 0. Part (g) states that the direction of $z_i(t)$ tends to the direction of the destination velocity χ .

Part (a) of Theorem 1 provides a sufficient condition on $z(0)$ and $w(0)$ such that there are no collisions. If $q(0)$ is close to a flocking formation (i.e., a minimum of ψ_s), $p(0)$ is close to the destination velocity χ (i.e., $w(0) \approx 0$), and $\chi^T z_i \approx p_f \|z_i\|$, then $W(z(0), w(0))$ is close to its minimum. In this case, $W(z(0), w(0))$ tends to satisfy $W(z(0), w(0)) < \psi(\|\delta_c\|_\epsilon)$, and part (a) of Theorem 1 implies that there are no collisions. We note that the upper bound $\psi(\|\delta_c\|_\epsilon)$ in part (a) tends to increase as the repulsion parameter b increases. Numerical testing suggests that for initial conditions $z(0)$ and $w(0)$, where $W(z(0), w(0))$ is not near its minimum, selecting the repulsion parameter b sufficiently large tends to result in $W(z(0), w(0))$ and $\psi(\|\delta_c\|_\epsilon)$ that satisfy $W(z(0), w(0)) < \psi(\|\delta_c\|_\epsilon)$; in this case, part (a) implies that there are no collisions. We also note that $W(z(0), w(0)) < \psi(\|\delta_c\|_\epsilon)$ is a sufficient-but-not-necessary condition such that there are no collisions. In fact, numerical testing suggests that for many initial conditions $z(0)$ and $w(0)$, where $W(z(0), w(0)) \geq \psi(\|\delta_c\|_\epsilon)$, there are no collisions.

2.6 Destination-Seeking Analysis

In this section, we analyze the asymptotic properties of (2.1), (2.2), and (2.18) without (A1) and (A2). We provide a sufficient condition such that agents approach a subset of the closed-loop equilibria of (2.1), (2.2), and (2.18). We also provide a sufficient condition such that agents approach their destinations asymptotically. Define

$$u(q, p) \triangleq \begin{bmatrix} u_1(q, p, \xi_1 - q_1) \\ \vdots \\ u_n(q, p, \xi_n - q_i) \end{bmatrix},$$

where u_i is given by (2.18).

The set of closed-loop equilibria of (2.1), (2.2), and (2.18) is

$$\mathcal{E} \triangleq \{(q_e, p_e) \in \mathbb{R}^{mn} \times \mathbb{R}^{mn} : p_e = 0 \text{ and } u(q_e, 0) = 0\}.$$

Figure 2.4 shows 4 types of equilibria for $n = 2$. In Figure 2.4(a), $q(t) \equiv \xi$, and all terms in u are zero. In Figure 2.4(b), the sum of flock attraction and destination seeking is zero, that is, $\mu(\|z_i\|)A_i(q) + \nu(\|z_i\|)z_i = 0$, and all other terms in u are zero. In Figure 2.4(c) and 2.4(d), the sum of flock repulsion and destination seeking is zero, that is, $R_i(q) + \nu(\|z_i\|)z_i = 0$, and all other terms in u are zero. For $n \geq 2$, the closed-loop system (2.1), (2.2), and (2.18) has equilibria that consist of combinations of the 4 types shown in Figure 2.4.

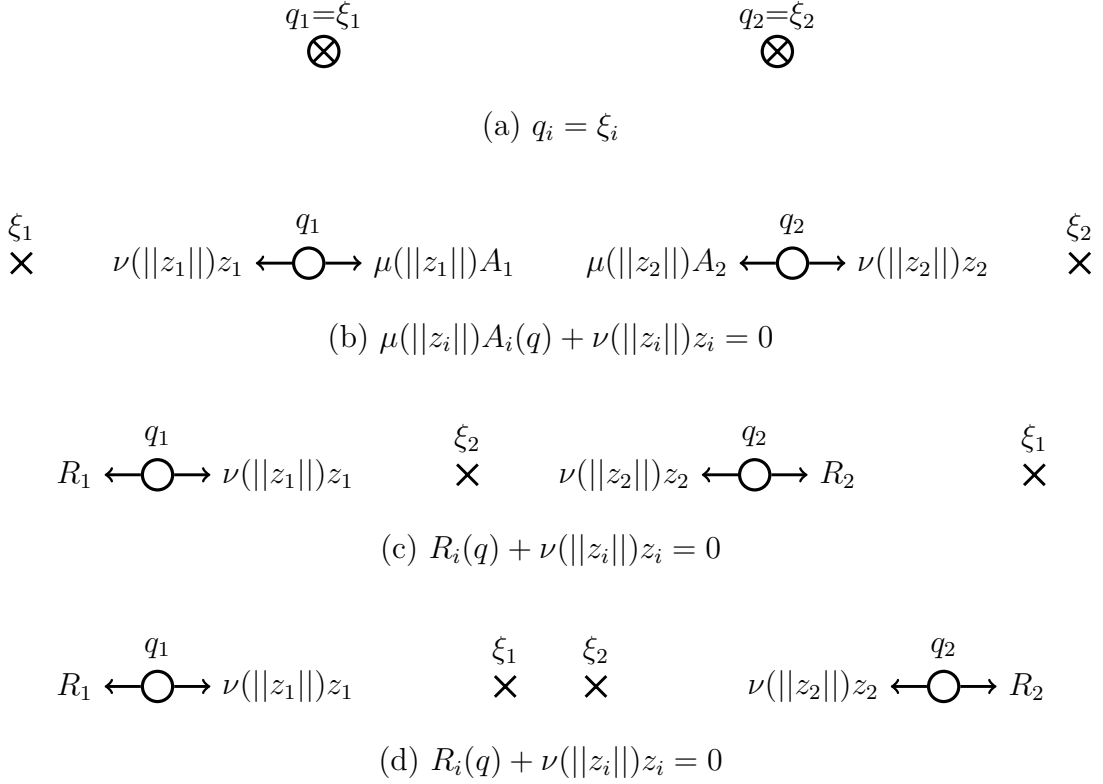


Figure 2.4: Four types of equilibria for $n = 2$. Agents are shown by O s, and destinations are shown by \times s. In (a), $q(t) \equiv \xi$, and all terms in u are zero. In (b), the sum of flock attraction and destination seeking is zero, and all other terms in u are zero. In (c) and (d), the sum of flock repulsion and destination seeking is zero, and all other terms in u are zero.

Figure 2.4 shows that $(\xi, 0)$ is not the only closed-loop equilibria of (2.1), (2.2), and (2.18). In fact, $(\xi, 0)$ may not be in \mathcal{E} . Define

$$r_\gamma \triangleq \begin{cases} d, & \text{if } r_\alpha \in (0, d], \\ r_\alpha, & \text{if } r_\alpha \in (d, r_c), \\ r_c, & \text{if } r_\alpha \in \{0\} \cup [r_c, \infty). \end{cases} \quad (2.24)$$

The radius r_γ is such that if all agents are at their destinations and the destinations are at least r_γ apart, then flock attraction, flock repulsion, and velocity consensus are 0. The following result provides a sufficient condition such that $(\xi, 0) \in \mathcal{E}$. The proof is in Section 2.11.

Lemma 1. If for all $(i, j) \in \mathcal{P}$, $\|\xi_j - \xi_i\| \in \{d\} \cup [r_\gamma, \infty)$, then $(\xi, 0) \in \mathcal{E}$.

The following result provides a sufficient condition such that all agents asymptotically approach their destinations. This result is a consequence of Proposition 2, and the proof is in Section 2.12.

Theorem 2. Consider the closed-loop system (2.1), (2.2), and (2.18), where for all $(i, j) \in \mathcal{P}$, $\|\xi_j - \xi_i\| \geq r_\gamma$, and define $r_\delta \triangleq \frac{1}{2}(\min_{(i,j) \in \mathcal{P}} \|\xi_j - \xi_i\| - d) \geq 0$. Assume there exists $t_0 \geq 0$ such that for all $t \geq t_0$ and all $i \in \mathcal{I}$, at least one of the following conditions holds:

- (a) For all $j \in \mathcal{I} \setminus \{i\}$, $\|q_j(t) - q_i(t)\| > r_c$.
- (b) $\|z_i(t)\| < \min\{r_\alpha, r_\delta\}$.

Then, $\lim_{t \rightarrow \infty} q(t) = \xi$ and $\lim_{t \rightarrow \infty} p(t) = 0$.

Theorem 2 states that if there exists a time after which all agents are greater than r_c apart from other agents or less than $\min\{r_\alpha, r_\delta\}$ from their destinations, then all agents asymptotically approach their destinations. The assumption that there exists a time such that all agents are sufficiently far from other agents or sufficiently close to their destinations precludes agents from converging to equilibria, where nonzero flock attraction or repulsion cancel nonzero destination seeking. Examples of these types of equilibria are shown in Figure 2.4(b)–(d). If flock attraction is sufficiently small relative to destination seeking, then numerical simulations suggest that the assumption of Theorem 2 holds. To decrease flock attraction relative to destination seeking, we decrease a or increase γ and ω_n .

We now use Lyapunov-like analysis to examine the asymptotic properties of (2.1), (2.2), and (2.18) without the assumption that for sufficiently large $t \geq 0$ all agents are greater than r_c apart from other agents or less than $\min\{r_\alpha, r_\beta\}$ from their destinations. Consider the Lyapunov-like function $V: \mathbb{R}^{mn} \times \mathbb{R}^{mn} \rightarrow [0, \infty)$ defined by

$$V(q, p) \triangleq \psi_s(q) + \sum_{i \in \mathcal{I}} \int_0^{\|\xi_i - q_i\|} \lambda \nu(\lambda) d\lambda + \frac{1}{2} \|p\|^2. \quad (2.25)$$

If for all $(i, j) \in \mathcal{P}$, $\|\xi_j - \xi_i\| = d$, $q_i = \xi_i$, and $p_i = 0$, then $V(q, p) = 0$; otherwise, $V(q, p) > 0$. Note that $V(q, p)$ has multiple minimizers.

The following result provides a sufficient condition such that $(q(t), p(t)) \equiv (\xi, 0)$ is a locally asymptotically equilibrium of (2.1), (2.2), and (2.18), and the agents do not collide. This result also shows that $(q(t), p(t))$ converges to a subset of \mathcal{E} . The proof is in Section 2.12.

Theorem 3. Consider the closed-loop system (2.1), (2.2), and (2.18), and let $r_\alpha = r_\beta = 0$. Then, the following statements hold:

- (a) Assume that for all $(i, j) \in \mathcal{P}$, $\|\xi_j - \xi_i\| > r_c$. Then, $(q(t), p(t)) \equiv (\xi, 0)$ is a locally asymptotically stable equilibrium of (2.1), (2.2), and (2.18).
- (b) For all $q(0) \in \mathbb{R}^{mn}$ and all $p(0) \in \mathbb{R}^{mn}$, $(q(t), p(t))$ converges to the set $\mathcal{M} \triangleq \{(q, p) \in \mathcal{E} : V(q, p) \leq V(q(0), p(0))\}$.
- (c) If $V(q(0), p(0)) < \psi(\|\delta_c\|_\epsilon)$, then for all $(i, j) \in \mathcal{P}$ and all $t \geq 0$, $\|q_j(t) - q_i(t)\| > \delta_c$.

Part (a) states that if all destinations are at least r_c apart from one another, then $(q(t), p(t)) \equiv (\xi, 0)$ is a locally asymptotically stable equilibrium of (2.1), (2.2), and (2.18). Part (b) states that, for all initial conditions, (q, p) converges to \mathcal{M} , which is a subset of \mathcal{E} . Therefore, all agents tend to zero velocity and zero control. Part (c) states that if $V(q(0), p(0)) < \psi(\|\delta_c\|_\epsilon)$, then there are no collisions. Part (c) provides a sufficient condition such that there are no collisions. The condition in part (c) is not necessary.

2.7 Numerical Examples

In this section, we present examples that demonstrate the control (2.18). Unless otherwise stated, $\delta_c = 0.5$ m, $d = 15$ m, $r_c = 30$ m, $r_\alpha = r_1 = 25$ m, $r_\beta = r_2 = 50$ m, $a = 0.33$, $b = 3.5$, $h = 0.2$, $\epsilon = 0.1$, $\omega_n = 0.5$ rad/s, $p_f = 20$ m/s, $\gamma = 5$ m/s², and μ is given by (2.11). Let $\hat{e}_k \in \mathbb{R}^{1 \times m}$ be the k th row of the $m \times m$ identity matrix.

Example 4. This example shows the effect of γ . Consider $n = 3$ agents, where $m = 2$, $q_1(0) = [0 \ 8]^\text{T}$ m, $\xi_1 = [1500 \ 50]^\text{T}$ m, $q_2(0) = [0 \ 0]^\text{T}$ m, $\xi_2 = [2600 \ 20]^\text{T}$ m, $q_3(0) = [0 \ -24]^\text{T}$ m, $\xi_3 = [2700 \ -55]^\text{T}$ m, and $p_1(0) = p_2(0) = p_3(0) = [0 \ 0]^\text{T}$ m/s. We consider 2 cases: $\gamma = 2$ m/s² and $\gamma = 9$ m/s². Figures 2.5 and 2.6 show that as γ decreases from 9 m/s² to 2 m/s², the agents are close together over a longer distance, take longer to approach their destinations, and tend to $p_f = 20$ m/s more slowly. In both cases, for all time the minimum interagent distance is above the collision threshold, that is, for all $t \geq 0$, $\min_{(i,j) \in \mathcal{P}} \|q_j(t) - q_i(t)\| > \delta_c = 0.5$ m. Thus, the agents achieve (O1) and (O2). \triangle

Example 5. This example considers a group of autonomous vehicles on a highway. Consider $n = 6$ agents, where $m = 2$, $r_c = 70$ m, and $a = 0.8$. Each agent starts with 0 velocity, and the control (2.18) is turned on once another agent is less than $0.75r_c$ away. Figure 2.7 shows the trajectories of each agent, where the time next to each agent's initial position indicates the time at which it starts moving. While agents are far from their destinations, they flock with neighboring agents. As agents approach their destinations, they leave the flock, and the remaining agents form a new flock. Figure 2.8 shows the minimum interagent distance $\min_{(i,j) \in \mathcal{P}} \|q_j - q_i\|$ and the maximum control magnitude $\max_{i \in \mathcal{I}} \|u_i\|$. The minimum interagent distance is always greater than the collision radius δ_c and reaches a minimum of approximately $d = 15$ m. The maximum control magnitude reaches a maximum of approximately 6 m/s² at $t = 40$ s. \triangle

Example 6. Consider $n = 20$ agents, where $m = 2$, the initial velocities are all 0, and 10 agents are distributed near $[0 \ 300]^\text{T}$ m, while the other 10 agents are distributed near $[0 \ -300]^\text{T}$ m. Figure 2.9 shows that initially 2 flocks are formed. Then, each flock splits into 2 flocks based on agents' destinations. Next, 2 of the flocks cross without collisions or fragmentation. Finally, all agents exit the flocks and approach their destinations. Figure 2.10 shows that the minimum interagent distance

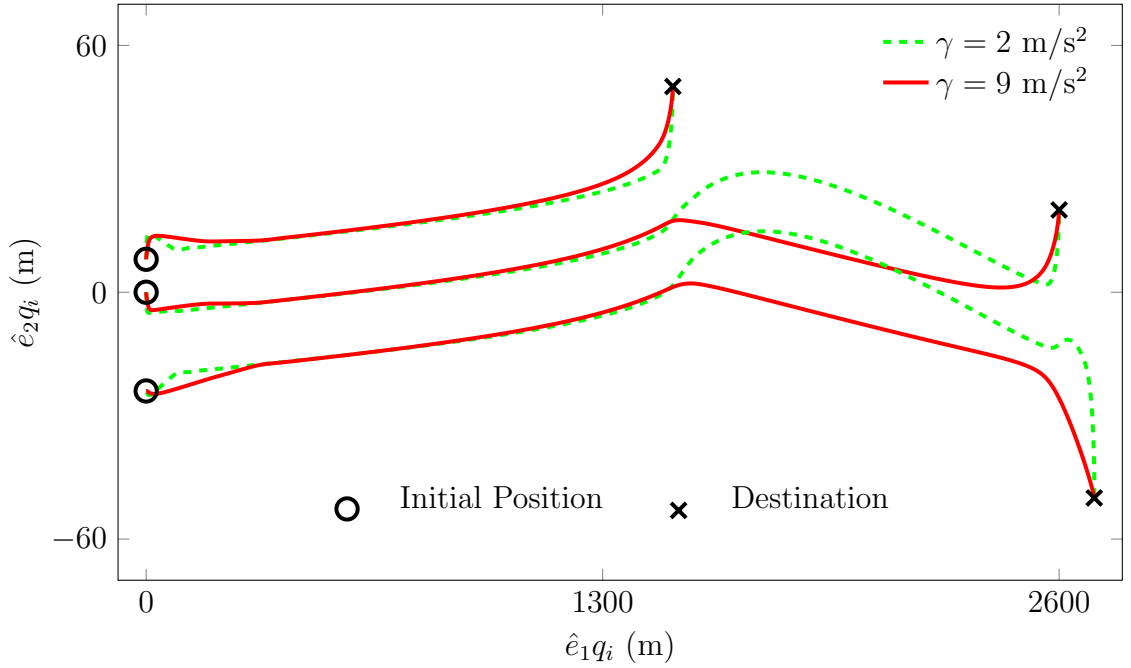


Figure 2.5: Trajectories of $n = 3$ agents for $\gamma = 2 \text{ m/s}^2$ and 9 m/s^2 . As γ decreases from 9 m/s^2 to 2 m/s^2 , agents are close together over a longer distance. The agents achieve (O1) and (O2).

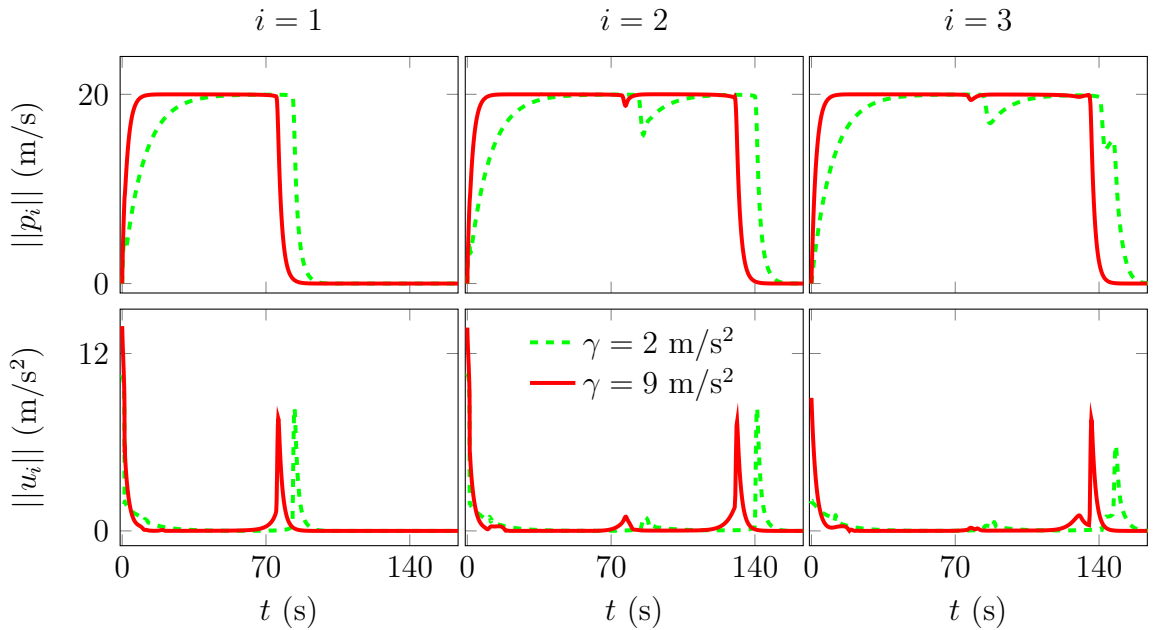


Figure 2.6: Speed and magnitude of control of $n = 3$ agents for $\gamma = 2 \text{ m/s}^2$ and 9 m/s^2 . As γ decreases from 9 m/s^2 to 2 m/s^2 , agents takes longer to approach their destinations and tend to $p_f = 20 \text{ m/s}$ more slowly. The agents achieve (O1) and (O2).

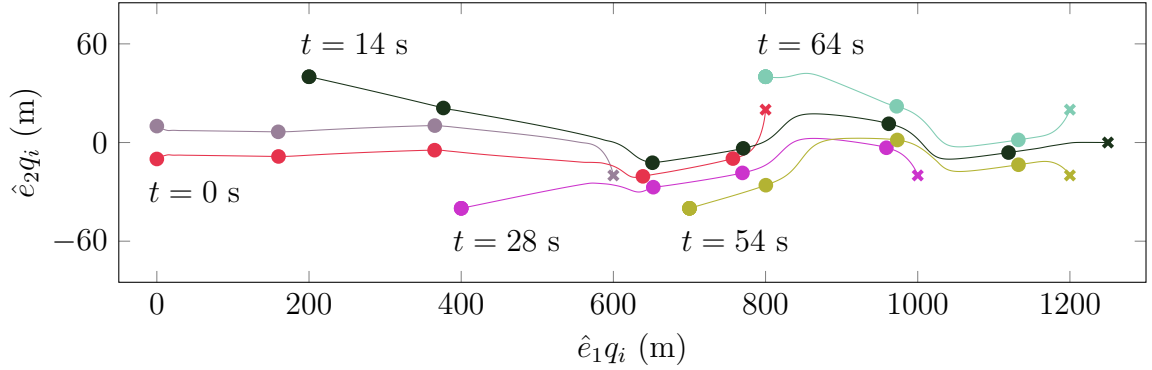


Figure 2.7: A group of $n = 6$ agents that flock before they reach their destinations. Each agent starts with 0 velocity, and the control (2.18) is applied once another agent is less than $0.75r_c$ away. The time next to each agent's initial position indicates the time at which it starts moving. While agents are far from their destinations, they flock with neighboring agents. As agents approach their destinations, they leave the flock, and the remaining agents form a new flock.

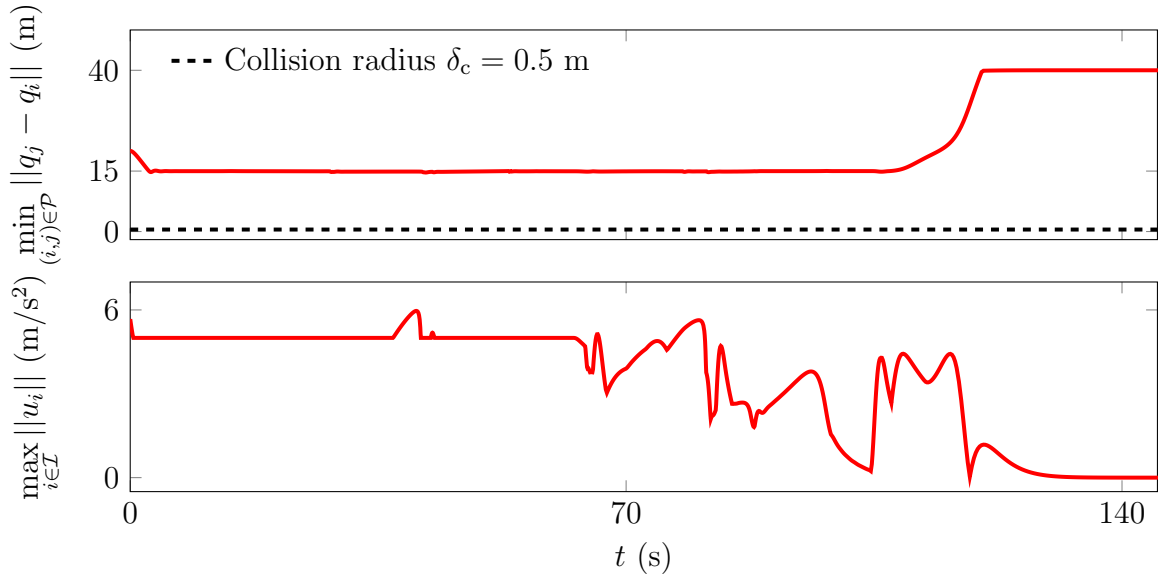


Figure 2.8: For the trajectory shown in Figure 2.7, the minimum interagent distance $\min_{(i,j) \in \mathcal{P}} \|q_j - q_i\|$ is always greater than the collision radius δ_c and reaches a minimum of approximately $d = 15$ m, and the maximum control magnitude $\max_{i \in \mathcal{I}} \|u_i\|$ reaches a maximum of approximately 6 m/s^2 at $t = 40$ s.

is always greater than the collision radius δ_c and is at a minimum of approximately 1 m at $t = 0$ s, and the maximum control magnitude is at a maximum of approximately of 44 m/s² at $t = 0$ s. Thus, the agents achieve (O1) and (O2). \triangle

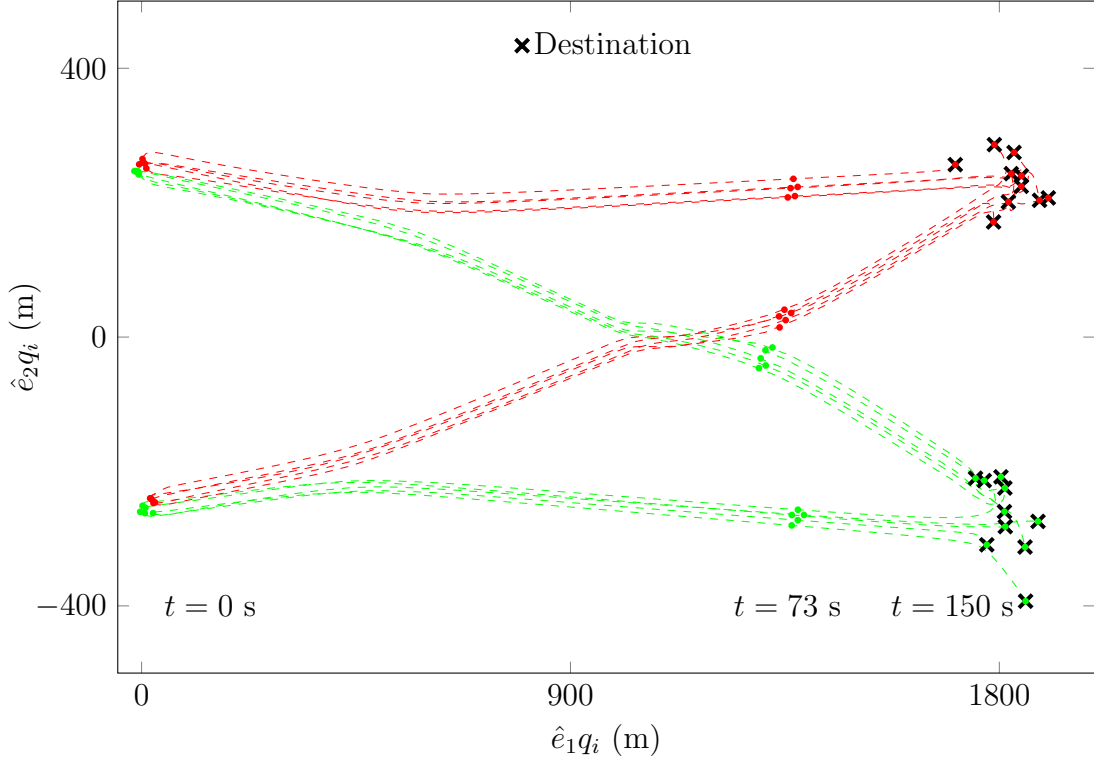


Figure 2.9: A group of $n = 20$ agents that flock before they reach their destinations. Initially 2 flocks are formed. Then, each of those flocks splits into 2 flocks based on the agents' destinations. Next, 2 of the flocks cross without collisions or fragmentation. Finally, all agents exit the flocks and approach their destinations. Thus, the agents achieve (O1) and (O2).

Example 7. Consider $n = 20$ agents, where $m = 3$, all agents are distributed near $[0 \ 0 \ 200]^T$ m, and the initial velocities are distributed near 0 m/s. Figure 2.11 shows that the agents flock by $t = 26$ s. Then, the agents exit the flock and approach their destinations. Figure 2.12 shows that the minimum interagent distance is always greater than the collision radius δ_c and is at a minimum of approximately 4.4 m at $t = 0$ s, and the maximum control magnitude reaches a maximum of approximately 46 m/s² at $t = 0.6$ s. Thus, the agents achieve (O1) and (O2). \triangle

2.8 Conclusions

We presented the flocking-and-destination-seeking control (2.18) for a set of n agents with double-integrator dynamics and potentially unique destinations. The control

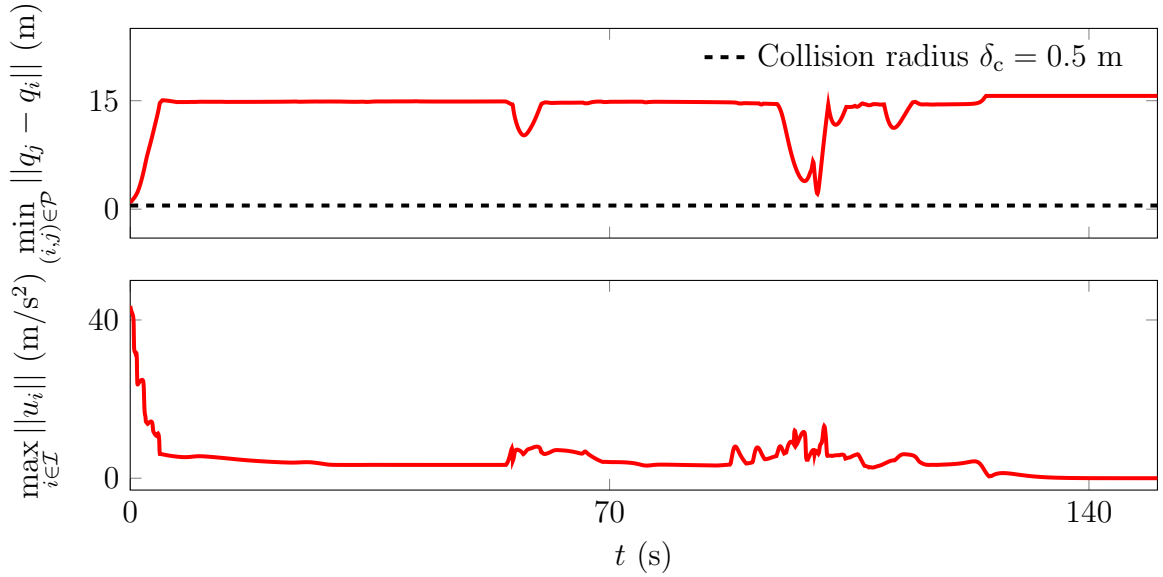


Figure 2.10: For the trajectory shown in Figure 2.9, the minimum interagent distance is always greater than the collision radius δ_c and is at a minimum of approximately 1 m at $t = 0$ s, and the maximum control magnitude is at a maximum of approximately 44 m/s² at $t = 0$ s.

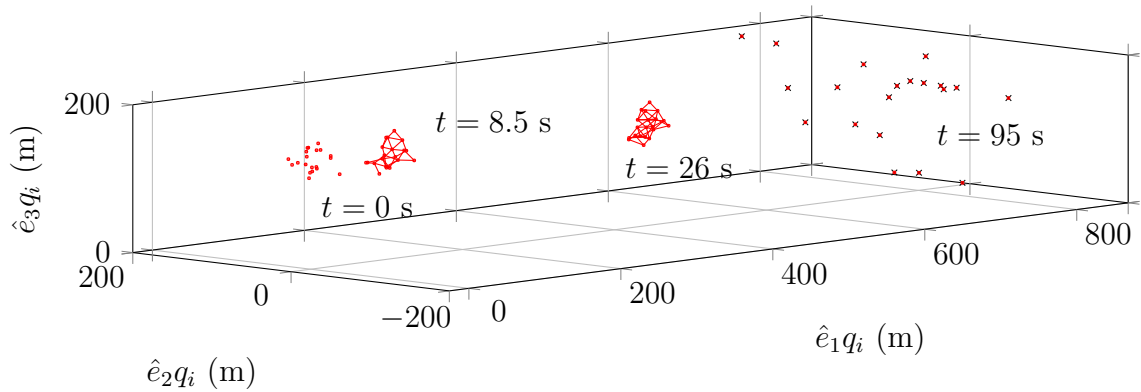


Figure 2.11: A group of $n = 20$ agents that flock before they reach their destinations. The agents flock by $t = 26$ s. Then, the agents exit the flock and approach their destinations. The agents achieve (O1) and (O2). The dots indicate agent positions, while the lines connecting dots indicate that the 2 agents are approximately $d = 15$ m apart.

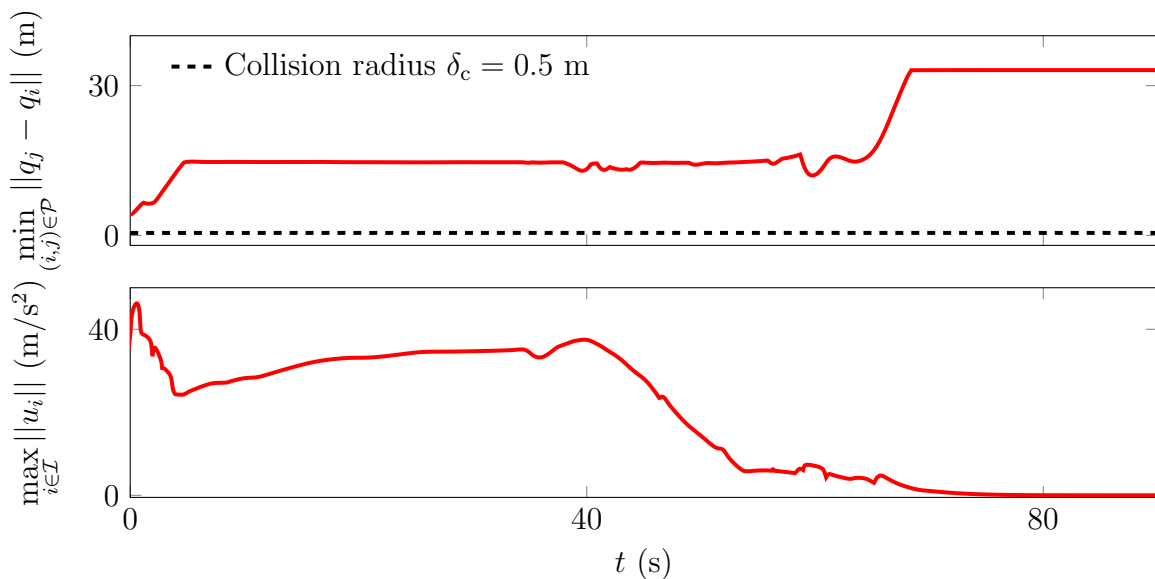


Figure 2.12: For the trajectory shown in Figure 2.11, the minimum interagent distance is always greater than the collision radius δ_c and is at a minimum of approximately 4.4 m at $t = 0$ s, and the maximum control magnitude reaches a maximum of approximately 46 m/s² at $t = 0.6$ s.

(2.18) includes terms that induce flocking as well as terms that drive each agent towards its destination. The control is decentralized and does not require a centralized flock leader. The control accomplishes 2 objectives: (i) if an agent is far from its destination, then that agent flocks with nearby agents, and (ii) if an agent is close to its destination, then that agent approaches its destination.

2.9 Proof of Proposition 2

Proof of Proposition 2. To show (a), consider the Lyapunov function $V_1: \mathbb{R}^{mn} \times \mathbb{R}^{mn} \rightarrow [0, \infty)$ defined by

$$V_1(q, p) \triangleq \sum_{i \in \mathcal{I}} \int_0^{\|\xi_i - q_i\|} \lambda \nu(\lambda) d\lambda + \frac{1}{2} \|p\|^2,$$

which is radially unbounded in q and p . If $q = \xi$ and $p = 0$, then $V_1(q, p) = 0$; otherwise, $V_1(q, p) > 0$. The derivative of $V_1(q, p)$ along the trajectories of (2.1), (2.2), and (2.16) is

$$\begin{aligned} \dot{V}_1(q, p) &\triangleq \sum_{i \in \mathcal{I}} \frac{\partial V_1(q, p)}{\partial q_i} p_i + \frac{\partial V_1(q, p)}{\partial p_i} u_i(z_i, p_i) \\ &= \sum_{i \in \mathcal{I}} \left(\frac{\partial}{\partial q_i} \left[\int_0^{\|\xi_i - q_i\|} \lambda \nu(\lambda) d\lambda \right] + \nu(\|z_i\|) z_i^T + \kappa(\|z_i\|) p_i^T \right) p_i. \end{aligned}$$

Define $\nu'(\eta) \triangleq \nu(\sqrt{\eta})$, and it follows that

$$\int_0^{||\xi_i - q_i||} \lambda \nu(\lambda) d\lambda = \frac{1}{2} \int_0^{||\xi_i - q_i||^2} \nu'(\tau) d\tau,$$

where $\tau = \lambda^2$ and $d\tau = 2\lambda d\lambda$. Thus,

$$\begin{aligned} \frac{\partial}{\partial q_i} \left[\int_0^{||\xi_i - q_i||} \lambda \nu(\lambda) d\lambda \right] &= \frac{\partial}{\partial q_i} \left[\frac{1}{2} \int_0^{||\xi_i - q_i||^2} \nu'(\tau) d\tau \right] \\ &= -\nu(||\xi_i - q_i||) [\xi_i - q_i]^T \\ &= -\nu(||z_i||) z_i^T. \end{aligned}$$

Therefore, $\dot{V}_1(q, p) = \sum_{i \in \mathcal{I}} \kappa(||z_i||) p_i^T p_i$, which is nonpositive because $\kappa < 0$.

Define $\mathcal{S} \triangleq \{(q_s, p_s) \in \mathbb{R}^{mn} \times \mathbb{R}^{mn} : \dot{V}_1(q_s, p_s) = 0\}$. Since $\dot{V}_1(q, p) = 0$ implies that $p = 0$, it follows that $\mathcal{S} = \{(q_s, p_s) \in \mathbb{R}^{mn} \times \mathbb{R}^{mn} : p_s = 0\}$. Define $E_i \triangleq [0_{m \times m(i-1)} \quad I_m \quad 0_{m \times m(n-i)}] \in \mathbb{R}^{m \times mn}$, where $0_{l_1 \times l_2}$ is the $l_1 \times l_2$ matrix of zeros, and I_m is the $m \times m$ identity matrix. Let $\tilde{q}: [0, \infty) \rightarrow \mathbb{R}^{mn}$ and $\tilde{p}: [0, \infty) \rightarrow \mathbb{R}^{mn}$ be such that for all $t \geq 0$, $(\tilde{q}(t), \tilde{p}(t)) \in \mathcal{S}$, and $\tilde{q}_i(t) \triangleq E_i \tilde{q}(t)$ and $\tilde{p}_i(t) \triangleq E_i \tilde{p}(t)$ satisfy (2.1), (2.2), and (2.16). Since for all $t \geq 0$, $(\tilde{q}(t), \tilde{p}(t)) \in \mathcal{S}$, it follows that $\tilde{p}(t) \equiv 0$. Furthermore, since $z_i = \xi_i - q_i$, it follows from (2.2) and (2.16) that

$$0 \equiv \dot{\tilde{p}}_i(t) \equiv \tilde{p}_i(t) + u_i(\xi_i - \tilde{q}_i(t), \tilde{p}_i(t)) \equiv \nu(||\xi_i - \tilde{q}_i(t)||) [\xi_i - \tilde{q}_i(t)],$$

which implies that $\tilde{q}_i(t) \equiv \xi_i$ because $\nu > 0$. Thus, $(\tilde{q}(t), \tilde{p}(t)) \equiv (\xi, 0)$ is the only solution of (2.1), (2.2), and (2.16) such that for all $t \geq 0$, $(\tilde{q}(t), \tilde{p}(t)) \in \mathcal{S}$. Therefore, [84, Corollary 4.2] implies that $(q(t), p(t)) \equiv (\xi, 0)$ is a globally asymptotically stable equilibrium of (2.1), (2.2), and (2.16), which confirms (a).

To show (b), since $(q(t), p(t)) \equiv (\xi, 0)$ is a globally asymptotically stable equilibrium of (2.1), (2.2), and (2.16), it follows that there exists $t_1 > 0$ such that for all $t \geq t_1$, $||z_i(t)|| \leq r_1$. Thus, (2.1), (2.2), and (2.14)–(2.16) imply that for all $t \geq t_1$, $q_i(t)$ satisfies $\ddot{q}_i(t) + 2\zeta\omega_n \dot{q}_i(t) + \omega_n^2 q_i(t) = \omega_n^2 \xi_i$, which confirms (b).

To show (c), assume $||z_i(0)|| > r_2$. Therefore, there exists $t_0 > 0$ such that for all $t \in [0, t_0)$, $||z_i(t)|| > r_2$, and it follows from (2.14)–(2.16) that for all $t \in [0, t_0)$, $u_i(q_i(t), p_i(t)) = \gamma z_i(t)/||z_i(t)|| - \gamma p_i(t)/p_f$, which confirms (c).

Part (d) follows from direct calculation. \square

2.10 Proof of Theorem 1

Proof of Theorem 1. Since (A2) holds, it follows from (M1) that for all $t \geq 0$, $\mu(||z_i(t)||) = 1$, which implies that the derivative of $W(z, w)$ along the trajectories of (2.18)–(2.20) is

$$\begin{aligned} \dot{W}(z, w) &\triangleq \frac{\partial W(z, w)}{\partial z} w - \frac{\partial W(z, w)}{\partial w} g(q, p, z) \\ &= \sum_{i \in \mathcal{I}} \left(\frac{\partial}{\partial z_i} \left[\sum_{k \in \mathcal{I}} \gamma ||z_k|| - \frac{\gamma}{p_f} \chi^T z_k \right] + \frac{\partial \psi_s(z)}{\partial z_i} - A_i^T(q) - R_i^T(q) \right) \end{aligned}$$

$$- C_i^T(q, p) - \nu(\|z_i\|)z_i^T - \kappa(\|z_i\|)p_i^T \Big) w_i, \quad (2.26)$$

where $g(q, p, z) \triangleq [u_1^T(q, p, z_1) \ \cdots \ u_n^T(q, p, z_n)]^T$, where u_i is given by (2.18).

Since (A1) holds, it follows that for all $(i, j) \in \mathcal{P}$, $q_j - q_i = z_i - z_j$, which implies that $\psi(\|q_j - q_i\|_\epsilon) = \psi(\|z_i - z_j\|_\epsilon)$ and hence, $\psi_s(q) = \psi_s(z)$. Thus, using (2.4), (2.8), (2.9), (2.21), and (2.22), we obtain that for all $i \in \mathcal{I}$,

$$\begin{aligned} \frac{\partial \psi_s(z)}{\partial z_i} &= -\frac{\partial \psi_s(q)}{\partial q_i} = -\frac{\partial}{\partial q_i} \left[\sum_{k=1}^{n-1} \sum_{j=k+1}^n \psi(\|q_j - q_k\|_\epsilon) \right] \\ &= -\sum_{j \in \mathcal{I} \setminus \{i\}} \frac{\partial \psi(\|q_j - q_i\|_\epsilon)}{\partial q_i} \\ &= \sum_{j \in \mathcal{I} \setminus \{i\}} \rho_h \left(\frac{\|q_j - q_i\|_\epsilon}{\|r_c\|_\epsilon} \right) \phi(\|q_j - q_i\|_\epsilon - \|d\|_\epsilon) \sigma_\epsilon(q_j - q_i) \\ &= A_i^T(q) + R_i^T(q). \end{aligned} \quad (2.27)$$

Define

$$\mathcal{D} \triangleq \{(z, w) \in \mathbb{R}^{mn} \times \mathbb{R}^{mn} : \text{for all } i \in \mathcal{I}, \|z_i\| > r_2, \text{ where } z = [z_1^T \ \cdots \ z_n^T]^T\},$$

and it follows from (2.14) and (2.15) that for all $(z, w) \in \mathcal{D}$ and all $i \in \mathcal{I}$,

$$\begin{aligned} &\left(\frac{\partial}{\partial z_i} \left[\sum_{k \in \mathcal{I}} \gamma \|z_k\| - \frac{\gamma}{p_f} \chi^T z_k \right] - \nu(\|z_i\|)z_i^T - \kappa(\|z_i\|)p_i^T \right) w_i \\ &= \left[\frac{\gamma}{\|z_i\|} z_i - \frac{\gamma}{p_f} \chi \right]^T w_i - \frac{\gamma}{\|z_i\|} z_i^T w_i + \frac{\gamma}{p_f} p_i^T w_i \\ &= -\frac{\gamma}{p_f} \|w_i\|^2. \end{aligned} \quad (2.28)$$

Since for all $(i, j) \in \mathcal{P}$, $z_i - z_j = q_j - q_i$ and $w_i - w_j = p_j - p_i$, it follows from (2.10) that for all $(z, w) \in \mathcal{D}$,

$$\begin{aligned} \sum_{i \in \mathcal{I}} C_i^T(q, p) w_i &= \sum_{i \in \mathcal{I}} \sum_{j \in \mathcal{I} \setminus \{i\}} \rho_h \left(\frac{\|q_j - q_i\|_\epsilon}{\|r_c\|_\epsilon} \right) [w_i^T w_i - w_j^T w_i] \\ &= \sum_{i \in \mathcal{I}} \sum_{j=i+1}^n \rho_h \left(\frac{\|q_j - q_i\|_\epsilon}{\|r_c\|_\epsilon} \right) [w_i^T w_i - w_j^T w_i + w_j^T w_j - w_i^T w_j] \\ &= \frac{1}{2} \sum_{(i,j) \in \mathcal{P}} \rho_h \left(\frac{\|z_i - z_j\|_\epsilon}{\|r_c\|_\epsilon} \right) \|w_j - w_i\|^2. \end{aligned} \quad (2.29)$$

Substituting (2.27)–(2.29) into (2.26) yields that for all $(z, w) \in \mathcal{D}$,

$$\dot{W}(z, w) = -\frac{\gamma}{p_f} \|w\|^2 - \frac{1}{2} \sum_{(i,j) \in \mathcal{P}} \rho_h \left(\frac{\|z_i - z_j\|_\epsilon}{\|r_c\|_\epsilon} \right) \|w_j - w_i\|^2, \quad (2.30)$$

which is nonpositive.

To show (b), note that for all $t \geq 0$, $(z(t), w(t)) \in \mathcal{D}$. Therefore, (2.23) and (2.30) imply that for all $t \geq 0$, $W(z(t), w(t)) \geq 0$ and $\dot{W}(z(t), w(t)) \leq 0$. Thus, $\lim_{t \rightarrow \infty} W(z(t), w(t))$ exists. Since for all $(i, j) \in \mathcal{P}$, $\psi(\|z_j - z_i\|_\epsilon) \leq \psi_s(z)$, it follows from (2.23) that for all $(z, w) \in \mathcal{D}$ and all $(i, j) \in \mathcal{P}$, $W(z, w) \geq \psi(\|z_j - z_i\|_\epsilon) + \|w\|^2/2 \geq 0$. Since for all $t \geq 0$, $W(z(t), w(t))$ is bounded, it follows that for all $(i, j) \in \mathcal{P}$ and all $t \geq 0$, $z_j(t) - z_i(t)$ and $w(t)$ are bounded, which implies that $q_j(t) - q_i(t)$ and $p_i(t)$ are bounded. Therefore, (2.8)–(2.10), (2.14), (2.15), and (2.18) imply that for all $t \geq 0$, $g(q(t), p(t), z(t))$ is bounded. Note that for all $(z, w) \in \mathcal{D}$,

$$\begin{aligned} \ddot{W}(z, w) &\triangleq \frac{\partial \dot{W}(z, w)}{\partial z} w - \frac{\partial \dot{W}(z, w)}{\partial w} g(q, p, z) \\ &= -\frac{1}{4\|r_c\|_\epsilon} \sum_{(i,j) \in \mathcal{P}} \left. \frac{d\rho_h(\eta)}{d\eta} \right|_{\eta=\|z_j-z_i\|_\epsilon/\|r_c\|_\epsilon} \|w_j - w_i\|^2 \sigma_\epsilon^T(z_i - z_j) [w_i - w_j] \\ &\quad + \sum_{(i,j) \in \mathcal{P}} [u_j(q, p, z_j) - u_i(q, p, z_i)]^T [w_j - w_i] + \frac{2\gamma}{p_f} g^T(q, p, z) w. \end{aligned}$$

Since $d\rho_h(\eta)/d\eta$ and σ_ϵ are bounded and for all $t \geq 0$, $g(q(t), p(t), z(t))$ and $w(t)$ are bounded, it follows that for all $t \geq 0$, $\ddot{W}(z(t), w(t))$ is bounded, which implies that $\dot{W}(z(t), w(t))$ is uniformly continuous. Since $\lim_{t \rightarrow \infty} W(z(t), w(t))$ exists and $\dot{W}(z(t), w(t))$ is uniformly continuous, Barbalat's lemma [84, Lemma 8.2] implies that $\lim_{t \rightarrow \infty} \dot{W}(z(t), w(t)) = 0$. Thus, (2.30) implies that $\lim_{t \rightarrow \infty} w(t) = 0$, or equivalently, $\lim_{t \rightarrow \infty} p_i(t) = \chi$, which confirms (b).

To show (e), note that for all $(z, w) \in \mathcal{D}$ and all $(i, j) \in \mathcal{P}$, $\rho_h(\|z_j - z_i\|_\epsilon/\|r_c\|_\epsilon) = 1$ and $d\rho_h(\eta)/d\eta|_{\eta=\|z_j-z_i\|_\epsilon/\|r_c\|_\epsilon} = 0$. Since, in addition, $\mu = 1$, it follows from (2.18) that for all $(z, w) \in \mathcal{D}$,

$$\begin{aligned} \dot{u}_i(q, p, z_i) &\triangleq \frac{\partial u_i(q, p, z_i)}{\partial q} p + \frac{\partial u_i(q, p, z_i)}{\partial p} g(q, p, z) + \frac{\partial u_i(q, p, z_i)}{\partial z_i} w_i \\ &= \sum_{j \in \mathcal{I} \setminus \{i\}} \left(\left. \frac{d\phi(\eta)}{d\eta} \right|_{\eta=\|q_j-q_i\|_\epsilon-\|d\|_\epsilon} \sigma_\epsilon(q_j - q_i) \sigma_\epsilon^T(q_j - q_i) + \frac{\phi(\|q_j - q_i\|_\epsilon - \|d\|_\epsilon)}{1 + \epsilon\|q_j - q_i\|_\epsilon} I_m \right. \\ &\quad \left. - \frac{\epsilon\phi(\|q_j - q_i\|_\epsilon - \|d\|_\epsilon)}{(1 + \epsilon\|q_j - q_i\|_\epsilon)^3} [q_j - q_i][q_j - q_i]^T \right) [p_j - p_i] + u_j(q, p, z_j) \\ &\quad - \frac{\gamma}{\|z_i\|^3} (z_i z_i^T) w_i + \frac{\gamma}{\|z_i\|} w_i - \left(n - 1 + \frac{\gamma}{p_f} \right) u_i(q, p, z_i). \end{aligned} \quad (2.31)$$

Since for all $t \geq 0$, $\|z_i(t)\| > r_2$; and $p_i(t)$, $u_i(t)$, $w_i(t)$, and $q_j(t) - q_i(t)$ are bounded, it follows from (2.3) and (2.4) that for all $t \geq 0$, $\|q_j(t) - q_i(t)\|_\epsilon$, $\sigma_\epsilon(q_j(t) - q_i(t))$, and $-(\gamma/\|z_i(t)\|^3)[(z_i(t)z_i^T(t))w_i(t)] + (\gamma/\|z_i(t)\|)w_i(t)$ are bounded. Since, in addition, ϕ and $d\phi(\eta)/d\eta$ are bounded, (2.31) implies that for all $t \geq 0$, $\dot{u}_i(q(t), p(t), z_i(t))$ is bounded. Therefore, $u_i(q(t), p(t), z_i(t))$ is uniformly continuous. Since $\lim_{t \rightarrow \infty} p_i(t)$ exists and $\dot{p}_i(t) = u_i(q(t), p(t), z_i(t))$ is uniformly continuous, [84, Lemma 8.2] implies that $\lim_{t \rightarrow \infty} u_i(q(t), p(t), z_i(t)) = 0$, which confirms (e).

To show (g), note that for all $(i, j) \in \mathcal{P}$, $\|q_j - q_i\|_\epsilon = \|q_i - q_j\|_\epsilon$ and $\sigma_\epsilon(q_j - q_i) = -\sigma_\epsilon(q_i - q_j)$; and (2.8)–(2.10) imply that for all $(q, p) \in \mathbb{R}^{mn} \times \mathbb{R}^{mn}$, $\sum_{i \in \mathcal{I}} A_i(q) + R_i(q) + C_i(q, p) = 0$. Since, in addition, for all $t \geq 0$, $\|z_i(t)\| > r_2$, $\lim_{t \rightarrow \infty} u_i(q(t), p(t), z_i(t)) = 0$, and $\lim_{t \rightarrow \infty} p_i(t) = \chi$, it follows from (2.14), (2.15), and (2.18) that

$$\begin{aligned} 0 &= \lim_{t \rightarrow \infty} \left(\sum_{i \in \mathcal{I}} u_i(q(t), p(t), z_i(t)) + \kappa(\|z_i(t)\|)[\chi - p_i(t)] \right) \\ &= \lim_{t \rightarrow \infty} \sum_{i \in \mathcal{I}} \left[\frac{\gamma}{\|z_i(t)\|} z_i(t) - \frac{\gamma}{p_f} \chi \right], \end{aligned}$$

which implies that $\lim_{t \rightarrow \infty} \sum_{i \in \mathcal{I}} z_i(t)/\|z_i(t)\| = n\chi/p_f$. Since $\|\chi\| = p_f$, it follows that $\lim_{t \rightarrow \infty} \sum_{i \in \mathcal{I}} z_i^T(t)\chi/(\|z_i(t)\|p_f) = n$. Assume for contradiction that there exists $k \in \mathcal{I}$ such that $\lim_{t \rightarrow \infty} z_k^T(t)\chi/(\|z_k(t)\|p_f) \neq 1$. Let $\delta_1 > 0$ be such that for all $t \geq 0$, there exists $t_1 \geq t$ such that $|z_k^T(t_1)\chi/(\|z_k(t_1)\|p_f) - 1| > \delta_1$. Since $\lim_{t \rightarrow \infty} \sum_{i \in \mathcal{I}} z_i^T(t)\chi/(\|z_i(t)\|p_f) = n$, it follows that there exists $t_2 \geq 0$ such that for all $t \geq t_2$, $|\sum_{i \in \mathcal{I}} z_i^T(t)\chi/(\|z_i(t)\|p_f) - n| < \delta_1$. Since $\lim_{t \rightarrow \infty} z_k^T(t)\chi/(\|z_k(t)\|p_f) \neq 1$, it follows that there exists $t_3 \geq t_2$ such that $|z_k^T(t_3)\chi/(\|z_k(t_3)\|p_f) - 1| > \delta_1$, which implies that $z_k^T(t_3)\chi/(\|z_k(t_3)\|p_f) < 1 - \delta_1$ because $z_k^T\chi/(\|z_k\|p_f) \leq 1$. Since for all $i \in \mathcal{I} \setminus \{k\}$, $z_i^T(t_3)\chi/(\|z_i(t_3)\|p_f) \leq 1$ and $z_k^T(t_3)\chi/(\|z_k(t_3)\|p_f) < 1 - \delta_1$, it follows that

$$\sum_{i \in \mathcal{I}} \frac{z_i^T(t_3)\chi}{\|z_i(t_3)\|p_f} = \frac{z_k^T(t_3)\chi}{\|z_k(t_3)\|p_f} + \sum_{i \in \mathcal{I} \setminus \{k\}} \frac{z_i^T(t_3)\chi}{\|z_i(t_3)\|p_f} < 1 - \delta_1 + n - 1 = n - \delta_1,$$

or equivalently, $|\sum_{i \in \mathcal{I}} z_i^T(t_3)\chi/(\|z_i(t_3)\|p_f) - n| > \delta_1$, which is a contradiction. Thus, for all $i \in \mathcal{I}$, $\lim_{t \rightarrow \infty} z_i^T(t)\chi/(\|z_i(t)\|p_f) = 1$, which implies that

$$\lim_{t \rightarrow \infty} \left\| \frac{1}{\|z_i(t)\|} z_i(t) - \frac{1}{p_f} \chi \right\|^2 = 2 - 2 \lim_{t \rightarrow \infty} \frac{z_i^T(t)\chi}{\|z_i(t)\|p_f} = 0.$$

Therefore, $\lim_{t \rightarrow \infty} z_i(t)/\|z_i(t)\| = \chi/p_f$, which confirms (g).

To show (f), since for all $t \geq 0$, $\|z_i(t)\| > r_2$, $\lim_{t \rightarrow \infty} p_i(t) = \chi$, and $\lim_{t \rightarrow \infty} z_i(t)/\|z_i(t)\| = \chi/p_f$, it follows from (2.10), (2.14), and (2.15) that $\lim_{t \rightarrow \infty} C_i(q(t), p(t)) = 0$ and $\lim_{t \rightarrow \infty} [\nu(\|z_i(t)\|)z_i(t) + \kappa(\|z_i(t)\|)p_i(t)] = 0$. Since, in addition, $\lim_{t \rightarrow \infty} u_i(q(t), p(t), z_i(t)) = 0$, it follows from (2.18) that

$$\begin{aligned} 0 &= \lim_{t \rightarrow \infty} [u_i(q(t), p(t), z(t)) - C_i(q(t), p(t)) - \nu(\|z_i(t)\|)z_i(t) - \kappa(\|z_i(t)\|)p_i(t)] \\ &= \lim_{t \rightarrow \infty} [A_i(q(t)) + R_i(q(t))], \end{aligned}$$

which confirms (f).

To show (d), it follows from (2.27) that $\partial\psi_s(z)/\partial z_i = A_i^T(q) + R_i^T(q)$, which implies $\lim_{t \rightarrow \infty} \partial\psi_s(z)/\partial z_i|_{z=z(t)} = \lim_{t \rightarrow \infty} [A_i^T(q(t)) + R_i^T(q(t))] = 0$, which confirms (d).

To show (c), assume r_c is such that for all $(i, j) \in \mathcal{P}$ and all $t \geq 0$, $\|r_c\|_\epsilon > \|q_j(t) - q_i(t)\|_\epsilon/h$. Define $f: (d, \infty) \rightarrow (0, \infty)$ by $f(\eta) \triangleq \phi(\|\eta\|_\epsilon - \|d\|_\epsilon)\sigma_\epsilon(\eta) =$

$\phi(\|\eta\|_\epsilon - \|d\|_\epsilon)\eta/(1 + \epsilon\|\eta\|_\epsilon)$. For all $\eta \in (d, \infty)$, $\phi(\|\eta\|_\epsilon - \|d\|_\epsilon) > 0$, which implies that for all $\eta \in (d, \infty)$,

$$\begin{aligned} \frac{df(\eta)}{d\eta} &= \frac{d\phi(\eta_1)}{d\eta_1} \Big|_{\eta_1 = \|\eta\|_\epsilon - \|d\|_\epsilon} \frac{d\|\eta\|_\epsilon}{d\eta} \frac{\eta}{1 + \epsilon\|\eta\|_\epsilon} + \phi(\|\eta\|_\epsilon - \|d\|_\epsilon) \frac{d}{d\eta} \left(\frac{\eta}{1 + \epsilon\|\eta\|_\epsilon} \right) \\ &= \frac{a + b}{2(1 + (\|\eta\|_\epsilon - \|d\|_\epsilon + c)^2)^{3/2}} \left(\frac{\eta}{1 + \epsilon\|\eta\|_\epsilon} \right)^2 + \frac{\phi(\|\eta\|_\epsilon - \|d\|_\epsilon)}{(1 + \epsilon\|\eta\|_\epsilon)^3} \\ &> 0. \end{aligned}$$

Let $\delta > 0$, and define $v_\delta \triangleq f(d(n-1) + \delta)$. Let $t_1 \geq 0$ be such that for all $t \geq t_1$, $\|A_i(q(t)) + R_i(q(t))\| \leq v_\delta/n$, which exists because $\lim_{t \rightarrow \infty} [A_i(q(t)) + R_i(q(t))] = 0$. Let $t_2 \geq t_1$, and it follows that

$$\|A_i(q(t_2)) + R_i(q(t_2))\| \leq \frac{v_\delta}{n}. \quad (2.32)$$

For all $(i, j) \in \mathcal{P}$, define $Q(i, j) \triangleq q_j(t_2) - q_i(t_2)$. Assume for contradiction that there exists $(i, j) \in \mathcal{P}$ such that $\|Q(i, j)\| > d(n-1) + \delta$. Let $(\alpha, \beta) \in \mathcal{P}$ be such that $\|Q(\alpha, \beta)\| = \max_{(i, j) \in \mathcal{P}} \|Q(i, j)\|$. Since $\|Q(\alpha, \beta)\| > d(n-1) + \delta$ and for all $\eta \in (d, \infty)$, $df(\eta)/d\eta > 0$, it follows that

$$v_\delta = f(d(n-1) + \delta) < f(\|Q(\alpha, \beta)\|). \quad (2.33)$$

Let $l_1, l_2, \dots, l_n \in \mathcal{I}$ be such that: (i) $l_1 = \alpha$ and $l_n = \beta$; (ii) for all $(i, j) \in \mathcal{P}$, $l_i \neq l_j$; and (iii) for all $i \in \mathcal{I} \setminus \{n\}$, $Q^\top(l_i, l_{i+1})Q(\alpha, \beta) \geq 0$. Since $\|Q(\alpha, \beta)\| > d(n-1) + \delta$, it follows from (iii) that

$$\begin{aligned} (d(n-1) + \delta) \|Q(\alpha, \beta)\| &< \|Q(\alpha, \beta)\|^2 \\ &= \sum_{i=1}^{n-1} Q^\top(l_i, l_{i+1})Q(\alpha, \beta) \\ &\leq (n-1) \max_{i \in \mathcal{I} \setminus \{n\}} Q^\top(l_i, l_{i+1})Q(\alpha, \beta), \end{aligned}$$

which implies that there exists $\omega \in \mathcal{I} \setminus \{n\}$ such that

$$\left(d + \frac{\delta}{n-1} \right) \|Q(\alpha, \beta)\| < Q^\top(l_\omega, l_{\omega+1})Q(\alpha, \beta). \quad (2.34)$$

Define $\mathcal{I}_1 \triangleq \{l_1, \dots, l_\omega\}$ and $\mathcal{I}_2 \triangleq \{l_{\omega+1}, \dots, l_n\}$, which are nonempty. It follows from (iii) that for all $(i, j) \in \mathcal{P}$ such that $i < j$,

$$Q^\top(l_i, l_j)Q(\alpha, \beta) = \sum_{k=i}^{j-1} Q^\top(l_k, l_{k+1})Q(\alpha, \beta) \geq 0.$$

Thus, for all $i \in \mathcal{I}_1$, $Q^\top(i, l_\omega)Q(\alpha, \beta) \geq 0$, and for all $j \in \mathcal{I}_2$, $Q^\top(l_{\omega+1}, j)Q(\alpha, \beta) \geq 0$. Therefore, for all $(i, j) \in \mathcal{I}_1 \times \mathcal{I}_2$,

$$0 \leq Q^\top(i, l_\omega)Q(\alpha, \beta) + Q^\top(l_{\omega+1}, j)Q(\alpha, \beta) = Q^\top(i, j)Q(\alpha, \beta) - Q^\top(l_\omega, l_{\omega+1})Q(\alpha, \beta),$$

which implies that $Q^T(l_\omega, l_{\omega+1})Q(\alpha, \beta) \leq Q^T(i, j)Q(\alpha, \beta)$. Thus, it follows from (2.34) that for all $(i, j) \in \mathcal{I}_1 \times \mathcal{I}_2$,

$$\left(d + \frac{\delta}{n-1}\right) \|Q(\alpha, \beta)\| < Q^T(i, j)Q(\alpha, \beta) \leq \|Q(i, j)\| \|Q(\alpha, \beta)\|,$$

which implies that $Q^T(i, j)Q(\alpha, \beta) > 0$ and $\|Q(i, j)\| > d$. Therefore, (2.4) and (2.6) imply that for all $(i, j) \in \mathcal{I}_1 \times \mathcal{I}_2$, $\phi(\|Q(i, j)\|_\epsilon - \|d\|_\delta) > 0$ and $\sigma_\epsilon^T(Q(i, j))Q(\alpha, \beta) > 0$, which implies that

$$\phi(\|Q(i, j)\|_\epsilon - \|d\|_\delta)\sigma_\epsilon^T(Q(i, j))Q(\alpha, \beta) > 0. \quad (2.35)$$

Since for all $(i, j) \in \mathcal{P}$ and all $t \geq 0$, $\|r_c\|_\epsilon > \|q_j(t) - q_i(t)\|_\epsilon/h$, or equivalently, $\|q_j(t) - q_i(t)\|_\epsilon/\|r_c\|_\epsilon < h$, it follows from (2.5) that for all $(z(t_2), w(t_2)) \in \mathcal{D}$ and all $(i, j) \in \mathcal{P}$, $\rho_h(\|Q(i, j)\|_\epsilon/\|r_c\|_\epsilon) = 1$. Since, in addition, for all $(i, j) \in \mathcal{P}$, $\|Q(i, j)\|_\epsilon = \|Q(j, i)\|_\epsilon$ and $\sigma_\epsilon(Q(i, j)) = -\sigma_\epsilon(Q(j, i))$, it follows from (2.8) and (2.9) that

$$\begin{aligned} \sum_{i \in \mathcal{I}_1} A_i(q(t_2)) + R_i(q(t_2)) &= \sum_{i \in \mathcal{I}_1} \sum_{j \in \mathcal{I} \setminus \{i\}} \phi(\|Q(i, j)\|_\epsilon - \|d\|_\delta)\sigma_\epsilon(Q(i, j)) \\ &= \sum_{i \in \mathcal{I}_1} \sum_{j \in \mathcal{I}_2} \phi(\|Q(i, j)\|_\epsilon - \|d\|_\delta)\sigma_\epsilon(Q(i, j)). \end{aligned}$$

Furthermore, since $\alpha = l_1 \in \mathcal{I}_1$ and $\beta = l_n \in \mathcal{I}_2$, it follows from (2.32), (2.33), and (2.35) that

$$\begin{aligned} v_\delta \|Q(\alpha, \beta)\| &< f(\|Q(\alpha, \beta)\|) \|Q(\alpha, \beta)\| \\ &= \phi(\|Q(i, j)\|_\epsilon - \|d\|_\delta)\sigma_\epsilon^T(Q(i, j))Q(\alpha, \beta) \\ &\leq \sum_{i \in \mathcal{I}_1} \sum_{j \in \mathcal{I}_2} \phi(\|Q(i, j)\|_\epsilon - \|d\|_\delta)\sigma_\epsilon^T(Q(i, j))Q(\alpha, \beta) \\ &= \sum_{i \in \mathcal{I}_1} [A_i(q(t_2)) + R_i(q(t_2))]^T Q(\alpha, \beta) \\ &\leq \sum_{i \in \mathcal{I}_1} \|A_i(q(t_2)) + R_i(q(t_2))\| \|Q(\alpha, \beta)\| \\ &\leq \sum_{i \in \mathcal{I}_1} \frac{v_\delta}{n} \|Q(\alpha, \beta)\| \\ &< v_\delta \|Q(\alpha, \beta)\|, \end{aligned}$$

which is a contradiction. Thus, for all $t \geq t_1$, $\max_{(i, j) \in \mathcal{P}} \|q_j(t) - q_i(t)\| \leq d(n-1) + \delta$, which confirms (c).

To show (a), assume $W(z(0), w(0)) < \psi(\|\delta_c\|_\epsilon)$. Let $(i, j) \in \mathcal{P}$. Since for all $t \geq 0$, $\psi(\|z_j(t) - z_i(t)\|_\epsilon) \leq \psi_s(z(t)) \leq W(z(t), w(t))$ and $\dot{W}(z(t), w(t)) \leq 0$, it follows that for all $t \geq 0$,

$$\psi(\|z_j(t) - z_i(t)\|_\epsilon) \leq W(z(t), w(t)) \leq W(z(0), w(0)) < \psi(\|\delta_c\|_\epsilon).$$

Therefore, for all $t \geq 0$, $\|z_i(t) - z_j(t)\|_\epsilon > \delta_c$, which implies $\|q_j(t) - q_i(t)\|_\epsilon > \delta_c$, which confirms (a). \square

2.11 Proof of Lemma 1

Proof of Lemma 1. Assume that for all $(i, j) \in \mathcal{P}$, $\|\xi_j - \xi_i\| \in \{d\} \cup [r_\gamma, \infty)$. Let $t_0 \geq 0$, and assume $q(t_0) = \xi$ and $p(t_0) = 0$. Since $q_i(t_0) = \xi_i$, it follows that for all $(i, j) \in \mathcal{P}$, $\|q_j(t_0) - q_i(t_0)\| \in \{d\} \cup [r_\gamma, \infty)$. We consider 2 cases: $r_\alpha = 0$ and $r_\alpha > 0$. First, assume $r_\alpha = 0$, and it follows from (2.24) that $r_\gamma = r_c$. Thus, for all $(i, j) \in \mathcal{P}$, $\|q_j(t_0) - q_i(t_0)\| \in \{d\} \cup [r_c, \infty)$, which implies that $\mathcal{A}_i(q(t_0)) = \{j \in \mathcal{I} \setminus \{i\} : \|q_j(t_0) - q_i(t_0)\| = d\}$. Therefore, (2.6) and (2.8) imply that $A_i(q(t_0)) = 0$. Next, assume $r_\alpha > 0$, and since $z_i(t_0) = 0$, (M2) implies that $\mu(\|z_i(t_0)\|) = 0$. Thus, for $r_\alpha \geq 0$, it follows that $\mu(\|z_i(t_0)\|)A_i(q(t_0)) = 0$. Since for all $(i, j) \in \mathcal{P}$, $\|q_j(t_0) - q_i(t_0)\| \geq \min\{d, r_\gamma\} = d$, it follows that $\mathcal{R}_i(t_0) = \emptyset$, which implies from (2.9) that $R_i(q(t_0)) = 0$. In addition, since $q(t_0) = \xi$ and $p(t_0) = 0$, it follows that $C_i(q(t_0), p(t_0)) = 0$, $\nu(\|z_i(t_0)\|)z_i(t_0) = 0$, and $\kappa(\|z_i(t_0)\|)p_i(t_0) = 0$. Therefore, $u(q(t_0), 0) = 0$, which implies that $(\xi, 0) = (q(t_0), p(t_0)) \in \mathcal{E}$. \square

2.12 Proof of Theorems 2 and 3

Proof of Theorem 2. Let $i \in \mathcal{I}$, and assume that for all $t \geq t_0$ (a) or (b) hold. Let $t_1 \geq t_0$, and it follows that for $t = t_1$, (a) or (b) hold.

First, assume that for $t = t_1$ (a) holds, and it follows that $\mathcal{A}_i(t_1) = \mathcal{R}_i(t_1) = \mathcal{N}_i(t_1) = \emptyset$, which implies from (2.8)–(2.10) that $A_i(q(t_1)) = R_i(q(t_1)) = C_i(q(t_1), p(t_1)) = 0$.

Next, assume that for $t = t_1$, (b) holds and (a) does not hold. Thus, $\|z_i(t_1)\| < \min\{r_\alpha, r_\delta\} \leq r_\delta$. Let $j \in \mathcal{N}_i(t_1)$, which exists because (a) does not hold. Since $\|q_j(t_1) - q_i(t_1)\| < r_c$, it follows from the assumption of Theorem 2 that $\|z_j(t_1)\| < \min\{r_\alpha, r_\delta\} \leq r_\delta$. Since $\|z_i(t_1)\| < r_\delta$ and $\|z_j(t_1)\| < r_\delta$, it follows that

$$\begin{aligned} d &= \min_{(k,l) \in \mathcal{P}} \|\xi_l - \xi_k\| - 2r_\delta \\ &\leq \|\xi_j - \xi_i\| - 2r_\delta \\ &= \|z_j(t_1) - z_i(t_1) + q_j(t_1) - q_i(t_1)\| - 2r_\delta \\ &\leq \|z_j(t_1)\| + \|z_i(t_1)\| + \|q_j(t_1) - q_i(t_1)\| - 2r_\delta \\ &< \|q_j(t_1) - q_i(t_1)\|. \end{aligned}$$

Therefore, $\mathcal{R}_i(t_1) = \emptyset$, which implies from (2.9) that $R_i(q(t_1)) = 0$. Since, in addition, $\|z_i(t_1)\| < \min\{r_\alpha, r_\delta\} \leq r_\alpha$, it follows from (M2) that $\mu(\|z_i(t_1)\|) = 0$, which implies that $\mu(\|z_i(t_1)\|)A_i(q(t_1)) = \mu(\|z_i(t_1)\|)C_i(q(t_1), p(t_1)) = 0$.

Thus, combining cases yields that

$$\mu(\|z_i(t_1)\|)A_i(q(t_1)) + R_i(q(t_1)) + \mu(\|z_i(t_1)\|)C_i(q(t_1), p(t_1)) = 0.$$

Therefore, for all $t \geq t_0$, $u_i(q(t), p(t), z_i(t)) = \nu(\|z_i(t)\|)z_i(t) + \kappa(\|z_i(t)\|)p_i(t)$. Thus, part (b) of Proposition 2 implies that there exists $t_2 \geq t_0$ such that for all $t \geq t_2$, $\ddot{q}_i(t) + 2\zeta\omega_n\dot{q}_i(t) + \omega_n^2q_i(t) = \omega_n^2\xi_i$, which implies that $\lim_{t \rightarrow \infty} q_i(t) = \xi_i$ and $\lim_{t \rightarrow \infty} p_i(t) = 0$. \square

Proof of Theorem 3. Since $r_\alpha = r_\beta = 0$, it follows from (M1) that $\mu = 1$, which implies that the derivative of $V(q, p)$ along the trajectories of (2.1), (2.2), and (2.18)

is

$$\begin{aligned}
\dot{V}(q, p) &\triangleq \frac{\partial V(q, p)}{\partial q} p + \frac{\partial V(q, p)}{\partial p} u(q, p) \\
&= \sum_{i \in \mathcal{I}} \left(\frac{\partial \psi_s(q)}{\partial q_i} + \frac{\partial}{\partial q_i} \left[\int_0^{\|\xi_i - q_i\|} \lambda \nu(\lambda) d\lambda \right] + A_i^T(q) \right. \\
&\quad \left. + R_i^T(q) + C_i^T(q, p) + \nu(\|z_i\|) z_i^T + \kappa(\|z_i\|) p_i^T \right) p_i. \tag{2.36}
\end{aligned}$$

Since for all $(k, j) \in \mathcal{P}$, $\|q_j - q_k\|_\epsilon = \|q_k - q_j\|_\epsilon$, it follows that $\psi(\|q_j - q_k\|_\epsilon) = \psi(\|q_k - q_j\|_\epsilon)$. Therefore, (2.4), (2.8), (2.9), (2.21), and (2.22) imply that for all $i \in \mathcal{I}$,

$$\begin{aligned}
\frac{\partial \psi_s(q)}{\partial q_i} &= \frac{\partial}{\partial q_i} \left[\sum_{k=1}^{n-1} \sum_{j=k+1}^n \psi(\|q_j - q_k\|_\epsilon) \right] \\
&= \sum_{j \in \mathcal{I} \setminus \{i\}} \frac{\partial \psi(\|q_j - q_i\|_\epsilon)}{\partial q_i} \\
&= - \sum_{j \in \mathcal{I} \setminus \{i\}} \rho_h \left(\frac{\|q_j - q_i\|_\epsilon}{\|r_c\|_\epsilon} \right) \phi(\|q_j - q_i\|_\epsilon - \|d\|_\epsilon) \sigma_\epsilon^T(q_j - q_i) \\
&= -A_i^T(q) - R_i^T(q). \tag{2.37}
\end{aligned}$$

Define $\nu'(\eta) \triangleq \nu(\sqrt{\eta})$, and it follows that

$$\int_0^{\|\xi_i - q_i\|} \lambda \nu(\lambda) d\lambda = \frac{1}{2} \int_0^{\|\xi_i - q_i\|^2} \nu'(\tau) d\tau,$$

where $\tau = \lambda^2$ and $d\tau = 2\lambda d\lambda$. Thus,

$$\begin{aligned}
\frac{\partial}{\partial q_i} \left[\int_0^{\|\xi_i - q_i\|} \lambda \nu(\lambda) d\lambda \right] &= \frac{\partial}{\partial q_i} \left[\frac{1}{2} \int_0^{\|\xi_i - q_i\|^2} \nu'(\tau) d\tau \right] \\
&= -\nu(\|\xi_i - q_i\|) [\xi_i - q_i]^T \\
&= -\nu(\|z_i\|) z_i^T. \tag{2.38}
\end{aligned}$$

For all $(i, j) \in \mathcal{P}$ such that $\|q_j - q_i\| < r_c$, it follows that $j \in \mathcal{N}_i$. Furthermore, it follows from (2.5) that for all $(i, j) \in \mathcal{P}$ such that $\|q_j - q_i\| \geq r_c$, $\rho_h(\|q_j - q_i\|_\epsilon / \|r_c\|_\epsilon) = 0$. Therefore, (2.10) implies that

$$\begin{aligned}
\sum_{i \in \mathcal{I}} C_i^T(q, p) p_i &= \frac{1}{2} \sum_{i \in \mathcal{I}} \sum_{j \in \mathcal{I} \setminus \{i\}} \rho_h \left(\frac{\|q_j - q_i\|_\epsilon}{\|r_c\|_\epsilon} \right) [-p_i^T p_i + p_j^T p_i] \\
&= -\frac{1}{2} \sum_{(i, j) \in \mathcal{P}} \rho_h \left(\frac{\|q_j - q_i\|_\epsilon}{\|r_c\|_\epsilon} \right) \|p_j - p_i\|^2. \tag{2.39}
\end{aligned}$$

Substituting (2.37)–(2.39) into (2.36) yields

$$\dot{V}(q, p) = -\frac{1}{2} \sum_{(i,j) \in \mathcal{P}} \rho_h \left(\frac{\|q_j - q_i\|_\epsilon}{\|r_c\|_\epsilon} \right) \|p_j - p_i\|^2 + \sum_{i \in \mathcal{I}} \kappa(\|z_i\|) \|p_i\|^2, \quad (2.40)$$

and since $\kappa < 0$, it follows that $\dot{V}(q, p) \leq 0$.

To show (b), it can be shown that $\int_0^{\|\xi_i - q_i\|} \lambda \nu(\lambda) d\lambda$ is radially unbounded in q_i , which implies that $V(q, p)$ is radially unbounded. Since for all $(q, p) \in \mathbb{R}^m \times \mathbb{R}^m$, $\dot{V}(q, p) \leq 0$, it follows that for all $t \geq 0$, $\dot{V}(q(t), p(t)) \leq 0$, which implies that

$$V(q(t), p(t)) = V(q(0), p(0)) + \int_0^t \dot{V}(q(\tau), p(\tau)) d\tau \leq V(q(0), p(0)).$$

Since $V(q, p)$ is positive semidefinite, radially unbounded, and for all $t \geq 0$, $V(q(t), p(t)) \leq V(q(0), p(0))$, it follows that q and p are bounded.

Define

$$\Omega \triangleq \{(q, p) \in \mathbb{R}^{mn} \times \mathbb{R}^{mn} : V(q, p) \leq V(q(0), p(0))\},$$

which is compact and positively invariant with respect to (2.1), (2.2), and (2.18). Furthermore, define

$$\Omega_1 \triangleq \{(q, p) \in \Omega : \dot{V}(q, p) = 0\} = \{(q, p) \in \Omega : p = 0\}.$$

Since $p = 0$ implies that $\dot{p} = u(q, p) = 0$, it follows that \mathcal{M} is the largest set contained in Ω_1 that is invariant with respect to (2.1), (2.2), and (2.18). Thus, LaSalle's invariance theorem [84, Theorem 4.4] implies that, for all $q(0) \in \mathbb{R}^{mn}$ and $p(0) \in \mathbb{R}^{mn}$, $(q(t), p(t))$ converges to \mathcal{M} , which confirms (b).

To show (a), assume that for all $(i, j) \in \mathcal{P}$, $\|\xi_j - \xi_i\| > r_c$. Therefore, there exists $\delta > 0$ such that for all $(i, j) \in \mathcal{P}$, $\|\xi_j - \xi_i\| > r_c + \delta$. Define

$$\mathcal{D} \triangleq \left\{ (q, p) \in \mathbb{R}^{mn} \times \mathbb{R}^{mn} : \|\xi - q\| < \frac{\delta}{2} \right\},$$

which implies that for all $(q, p) \in \mathcal{D}$,

$$\|z_i\| \leq \left(\sum_{i \in \mathcal{I}} \|z_i\|^2 \right)^{1/2} = \|\xi - q\| < \frac{\delta}{2}.$$

Thus, for all $(q, p) \in \mathcal{D}$ and all $(i, j) \in \mathcal{P}$,

$$\begin{aligned} r_c &< \|\xi_j - \xi_i\| - \delta \\ &= \|z_j - z_i + q_j - q_i\| - \delta \\ &\leq \|z_j\| + \|z_i\| + \|q_j - q_i\| - \delta \\ &< \frac{\delta}{2} + \frac{\delta}{2} + \|q_j - q_i\| - \delta \\ &= \|q_j - q_i\|, \end{aligned}$$

which implies that $\|q_j - q_i\|_\epsilon / \|r_c\|_\epsilon > 1$. Hence, it follows from (2.5) and (2.21) that

$$\psi(\|q_j - q_i\|_\epsilon) = \int_{\|d\|_\epsilon}^{\|r_c\|_\epsilon} \rho_h \left(\frac{s}{\|r_c\|_\epsilon} \right) \phi(s - \|d\|_\epsilon) ds,$$

which combined with (2.22) implies that

$$\psi_s(q) = \frac{n(n-1)}{2} \int_{\|d\|_\epsilon}^{\|r_c\|_\epsilon} \rho_h \left(\frac{s}{\|r_c\|_\epsilon} \right) \phi(s - \|d\|_\epsilon) ds.$$

Consider the candidate Lyapunov function $V_1: \mathcal{D} \rightarrow \mathbb{R}$ defined by

$$V_1(q, p) \triangleq V(q, p) - \frac{n(n-1)}{2} \int_{\|d\|_\epsilon}^{\|r_c\|_\epsilon} \rho_h \left(\frac{s}{\|r_c\|_\epsilon} \right) \phi(s - \|d\|_\epsilon) ds.$$

It follows from (2.25) that $V_1(\xi, 0) = 0$. Since $\nu > 0$, it follows that for all $q_i \in \mathbb{R}^m \setminus \{\xi_i\}$, $\int_0^{\|\xi_i - q_i\|} \lambda \nu(\lambda) d\lambda > 0$. Therefore, (2.25) implies that for all $(q, p) \in \mathcal{D} \setminus \{(\xi, 0)\}$, $V_1(q, p) > 0$.

The derivative of $V_1(q, p)$ along the trajectories of (2.1), (2.2), and (2.18) is

$$\dot{V}_1(q, p) \triangleq \frac{\partial V_1(q, p)}{\partial q} p + \frac{\partial V_1(q, p)}{\partial p} u(q, p) = \dot{V}(q, p).$$

Define

$$\begin{aligned} \mathcal{S} &\triangleq \{(q, p) \in \mathcal{D} : \dot{V}_1(q, p) = 0\} = \{(q, p) \in \mathcal{D} : p = 0\}, \\ E_i &\triangleq [0_{m \times m(i-1)} \quad I_m \quad 0_{m \times m(n-i)}] \in \mathbb{R}^{m \times mn}, \end{aligned}$$

where $0_{l_1 \times l_2}$ is the $l_1 \times l_2$ matrix of zeros, and I_m is the $m \times m$ identity matrix. Let $\tilde{q}: [0, \infty) \rightarrow \mathbb{R}^{mn}$ and $\tilde{p}: [0, \infty) \rightarrow \mathbb{R}^{mn}$ be such that for all $t \geq 0$, $(\tilde{q}(t), \tilde{p}(t)) \in \mathcal{S}$ and for all $i \in \mathcal{I}$, $\tilde{q}_i(t) \triangleq E_i \tilde{q}(t)$ and $\tilde{p}_i(t) \triangleq E_i \tilde{p}(t)$ satisfy (2.1), (2.2), and (2.18). Thus, $\tilde{p}(t) \equiv 0$. Since $\mathcal{S} \subset \mathcal{D}$, it follows that for all $(i, j) \in \mathcal{P}$ and all $t \geq 0$, $\|\tilde{q}_j(t) - \tilde{q}_i(t)\| > r_c$, which implies that $\rho_h(\|\tilde{q}_j(t) - \tilde{q}_i(t)\|_\epsilon / \|r_c\|_\epsilon) \equiv 0$. Therefore, (2.8)–(2.10) imply that $A_i(\tilde{q}(t)) \equiv R_i(\tilde{q}(t)) \equiv C_i(\tilde{q}(t), \tilde{p}(t)) \equiv 0$. Since, in addition, $\tilde{p}(t) \equiv 0$, it follows from (2.2) and (2.18) that

$$0 \equiv \dot{\tilde{p}}_i(t) \equiv u_i(\tilde{q}(t), \tilde{p}(t), \xi_i - \tilde{q}_i(t)) \equiv \nu(\|\xi_i - \tilde{q}_i(t)\|) [\xi_i - \tilde{q}_i(t)],$$

which implies that $\tilde{q}_i(t) \equiv \xi_i$ because $\nu > 0$. Thus, $(\tilde{q}(t), \tilde{p}(t)) \equiv (\xi, 0)$ is the only solution to (2.1), (2.2), and (2.18) such that for all $t \geq 0$, $(\tilde{q}(t), \tilde{p}(t)) \in \mathcal{S}$. Therefore, [84, Corollary 4.1] implies that $(q(t), p(t)) \equiv (\xi, 0)$ is a locally asymptotically equilibrium of (2.1), (2.2), and (2.18), which confirms (a).

Finally, to show (c), assume $V(q(0), p(0)) < \psi(\|\delta_c\|_\epsilon)$. Since for all $(i, j) \in \mathcal{P}$, $\psi(\|q_j - q_i\|_\epsilon) \leq \psi_s(q) \leq V(q, p)$ and $\dot{V}(q, p) \leq 0$, it follows that for all $t \geq 0$, $\psi(\|q_j(t) - q_i(t)\|_\epsilon) \leq V(q(t), p(t)) \leq V(q(0), p(0)) < \psi(\|\delta_c\|_\epsilon)$. Thus, for all $(i, j) \in \mathcal{P}$ and all $t \geq 0$, $\|q_i(t) - q_j(t)\|_\epsilon > \|\delta_c\|_\epsilon$, which implies $\|q_j(t) - q_i(t)\| > \delta_c$, which confirms (c). \square

Chapter 3 Discrete-Time Flocking

We present a multi-agent control method that addresses flocking in discrete time. The method is decentralized, that is, each agent’s controller relies on local sensing to determine the relative positions and velocities of nearby agents. Each agent has the discrete-time double-integrator dynamics obtained by sampling the continuous-time double integrator and applying a zero-order hold on the control input. The method can use a centralized flock leader for guidance. We use a novel flock-correction-to-guidance term that prevents formations from collapsing around the leader. We demonstrate with analysis that agents using the discrete-time flocking method converge to a set of flocking formations. Notably, the flocking analysis relies on logarithmic potential functions. We also provide simulations demonstrating that agents using the discrete-time flocking method converge to a set of flocking formations and follow the centralized leader (if applicable).

3.1 Introduction

Multi-agent systems have many exciting applications such as distributed sensing, formation flying, and cooperative surveillance. For example, autonomous aircraft or spacecraft can fly in formations for distributed sensing [8, 9]. These applications require decentralized methods for coordinating and controlling groups of autonomous agents [11].

For coordinated control, each agent relies on sensing to determine the relative positions and velocities of nearby agents. Then, each agent uses these measurements combined with other information such as mission objectives to accomplish tasks, which can include: guidance, velocity matching, collision avoidance, and cohesion. Guidance causes an agent or agents to follow a leader agent or leader trajectory, or approach a desired destination. Velocity matching causes nearby agents to approach a consensus velocity; collision avoidance repels an agent from nearby agents (or obstacles); and cohesion attracts an agent to nearby agents.

Agent guidance is often achieved using leader-follower methods [1, 9, 19, 21–26, 58, 60, 62], which rely on a centralized leader, who can be an actual or virtual member of the formation and whose real-time relative position and relative velocity are known by all agents [1, 22–26] or at least by some [9, 19, 21]. Consensus algorithms [17, 34–53, 53–56, 85] are used to achieve velocity matching.

Some consensus algorithms can be extended to address formation control [46–48, 57, 58, 60]. These approaches are position-formation methods that force agents into a configuration using desired relative-position vectors between pairs of agents. In

contrast, distance-formation methods induce a configuration using only a desired relative distance between adjacent agents. In this case, the agents autonomously determine their configuration based on the desired interagent distance and initial conditions. One approach for distance formation is to use potential functions that create attractive forces when nearby agents are too far away and repulsive forces when nearby agents are too close [1, 21–27, 61]. Flocking methods such as [1, 21–27, 61] use distance-formation algorithms for cohesion and collision avoidance, and consensus algorithms for velocity matching. A survey of multi-agent formation methods is presented in [29]. In addition, many flocking methods include a centralized leader for flock guidance.

The majority of the formation-control literature focuses on algorithms for agents with continuous-time dynamics (e.g., [1, 8, 9, 11, 19, 21–27, 61]). However, a controller that stabilizes a continuous-time dynamic system may not stabilize the discrete-time dynamic system obtained from sampling and holding the continuous system because of sampled-data effects [77]. To address sampled-data effects, formation-control approaches for agents with discrete-time dynamics are given in [46, 47, 57, 58, 60, 83]. These methods include velocity consensus as well as cohesion and collision avoidance, but only [83] is a distance-formation algorithm.

In this chapter, we present a discrete-time distance-formation flocking algorithm. This distance-formation algorithm is decentralized, but it can also incorporate a centralized leader. We use a discrete-time flocking algorithm, where the parameters of the algorithm depend on the number of agents and the sample time. The algorithm contains a novel flock-correction-to-guidance term that prevents formations from collapsing around the leader. The objective of this flocking algorithm is to induce a formation of agents, where all agents have the same velocity, do not collide with one another, and form a single group of agents, that is, the flock is not fragmented. Our analysis uses a logarithmic potential function, which is similar to a logarithmic Lyapunov-like function [86–91].

This chapter has several contributions that extend the current literature. In contrast to [83], we provide sufficient conditions such that the agent-averaged position and velocity converge to the leader’s position and velocity. In addition, we demonstrate with an example that if agents follow a leader and use flock correction to guidance, then the agents converge to the same flocking configuration as without flock correction to guidance; and if agents follow a leader and do not use flock correction to guidance, then the flocking configuration collapses around the leader.

The discrete-time distance-formation algorithm has applications in distributed sensing, formation flying, and cooperative surveillance. This discrete-time algorithm is beneficial for applications with slow sampling rates. As shown in Sections 3.3 and 3.6, the discrete-time flocking algorithm can yield improved performance relative to continuous-time algorithms when implemented with sampled-data systems.

3.2 Problem Formulation

Let the positive integer n be the number of agents, and define $\mathcal{I} \triangleq \{1, 2, \dots, n\}$, which is the agent index set. For each $i \in \mathcal{I}$, consider the discrete-time dynamics

$$q_i(k+1) = q_i(k) + T_s p_i(k) + \frac{1}{2} T_s^2 u_i(k), \quad (3.1)$$

$$p_i(k+1) = p_i(k) + T_s u_i(k), \quad (3.2)$$

where $k \in \mathbb{N} \triangleq \{0, 1, 2, \dots\}$; $T_s > 0$ is the sample time; $q_i(k) \in \mathbb{R}^m$, $p_i(k) \in \mathbb{R}^m$, and $u_i(k) \in \mathbb{R}^m$ are the position, velocity, and control of the i th agent; and $q_i(0)$ and $p_i(0)$ are the initial conditions. Note that (3.1) and (3.2) are the discrete-time double-integrator dynamics obtained by sampling the continuous-time double integrator with sample time T_s and applying a zero-order hold on the control input. Define $\mathcal{P} \triangleq \{(i, j) \in \mathcal{I} \times \mathcal{I} : i \neq j\}$, which is the set of ordered pairs, and let $\|\cdot\|$ denote the Euclidean norm.

Let $\delta_c \geq 0$ be the *collision radius*, which is the minimum acceptable distance between agents. The rules for flocking are that agents stay close to one another, avoid collisions, and match velocities [16]. We use these rules to define asymptotic flocking. The agents in \mathcal{I} *flock with interagent distance* $d > 0$ if the following conditions hold:

(F1) For all $(i, j) \in \mathcal{P}$ and all $k \in \mathbb{N}$, $\|q_j(k) - q_i(k)\| > \delta_c$.

(F2) For all $(i, j) \in \mathcal{P}$, $\lim_{k \rightarrow \infty} [p_j(k) - p_i(k)] = 0$.

(F3) There exists $k_0 \in \mathbb{N}$ such that for all $k \geq k_0$, $\max_{(i,j) \in \mathcal{P}} \|q_j(k) - q_i(k)\| \leq d(n-1)$.

Condition (F1) states that there are no collisions. Condition (F2) states that all agents approach the same velocity. Condition (F3) states that asymptotically each agent is at most a distance $d(n-1)$ away from its farthest neighbor; this condition is flock cohesion.

We present a discrete-time flocking algorithm that accomplishes (F1)–(F3). In addition, this algorithm can force the flock to follow a virtual leader, whose dynamics are

$$q_g(k+1) = q_g(k) + T_s p_g(k) + \frac{1}{2} T_s^2 u_g(k), \quad (3.3)$$

$$p_g(k+1) = p_g(k) + T_s u_g(k), \quad (3.4)$$

where $q_g(k) \in \mathbb{R}^m$ and $p_g(k) \in \mathbb{R}^m$ are the position and velocity of the leader; $q_g(0)$ and $p_g(0)$ are the initial conditions; and $u_g: \mathbb{N} \rightarrow \mathbb{R}^m$ is an external forcing signal. The leader dynamics (3.3) and (3.4) take the form of a discrete-time double integrator and thus match the agent dynamics (3.1) and (3.2).

Unless otherwise stated, all statements in this chapter that involve the subscript i are for all $i \in \mathcal{I}$, and all statements that involve the subscripts i and j are for all $(i, j) \in \mathcal{P}$. Also, for $\ell = 1, \dots, m$, we let $e_\ell \in \mathbb{R}^{1 \times m}$ denote the ℓ th row of I_m .

3.3 Motivation

To motivate discrete-time flocking, we examine the effect of discretization (i.e., sample and zero-order hold) on a continuous-time flocking controller, specifically, [1, Alg. 1]. We consider the discrete-time double-integrator dynamics (3.1) and (3.2), where u_i is determined by discretizing the continuous-time controller [1, Alg. 1] with sample time T_s and applying a zero-order hold. In this section, we adopt the notation of [1]. Unless otherwise stated, the notation from this section is not used in other sections of this chapter. In this section, we focus on flocking without a leader.

Let $d > 0$ be the desired distance between agents. The attraction parameter is $a > 0$, and the repulsion parameter is $b \geq a$. Let $\epsilon > 0$, and define $\|\cdot\|_\sigma: \mathbb{R}^m \rightarrow [0, \infty)$ and $\sigma_\epsilon: \mathbb{R}^m \rightarrow \mathbb{R}^m$ by $\|x\|_\sigma \triangleq (\sqrt{1 + \epsilon\|x\|^2} - 1)/\epsilon$ and $\sigma_\epsilon(x) \triangleq (1/(1 + \epsilon\|x\|_\sigma))x$.

In this section, we assume that the communication radius $r > d$ is sufficiently large such that for all $k \in \mathbb{N}$, $\rho_h(\|q_j(k) - q_i(k)\|_\sigma / \|r\|_\sigma) = 1$, where $\rho_h: [0, \infty) \rightarrow [0, 1]$ be given by [1, Eq. (9)]. We also assume $a = b$. Then, [1, Algorithm 1] is

$$u_i(k) \triangleq \sum_{j \in \mathcal{I} \setminus \{i\}} \phi(\|q_j(k) - q_i(k)\|_\sigma - \|d\|_\sigma) \sigma_\epsilon(q_j(k) - q_i(k)) + p_j(k) - p_i(k), \quad (3.5)$$

where $\phi: \mathbb{R} \rightarrow \mathbb{R}$ is given by $\phi(\eta) = a\eta / \sqrt{1 + \eta^2}$.

First, we consider the case with $n = 2$ agents. In this case, it follows from (3.1), (3.2), and (3.5) that for all $k \in \mathbb{N}$,

$$\delta q(k+1) \triangleq q_2(k+1) - q_1(k+1) = f_1(\delta q(k), \delta p(k)), \quad (3.6)$$

$$\delta p(k+1) \triangleq p_2(k+1) - p_1(k+1) = f_2(\delta q(k), \delta p(k)), \quad (3.7)$$

where

$$f_1(\delta q, \delta p) \triangleq \left(1 - \frac{T_s^2 \phi(\|\delta q\|_\sigma - \|d\|_\sigma)}{1 + \epsilon \|\delta q\|_\sigma}\right) \delta q + T_s(1 - T_s) \delta p, \quad (3.8)$$

$$f_2(\delta q, \delta p) \triangleq \frac{-2T_s \phi(\|\delta q\|_\sigma - \|d\|_\sigma)}{1 + \epsilon \|\delta q\|_\sigma} \delta q + (1 - 2T_s) \delta p. \quad (3.9)$$

Define

$$\delta \mathcal{E} \triangleq \{(\delta q_e, \delta p_e) \in \mathbb{R}^m \times \mathbb{R}^m: \|\delta q_e\| = d \text{ and } \delta p_e = 0\},$$

which is the set of equilibria of the closed-loop system (3.6)–(3.9) such that the agents are d apart and have the same velocity. Note that $(\delta q(k), \delta p(k)) \equiv (0, 0)$ is an equilibrium of (3.6)–(3.9), but $(0, 0) \notin \delta \mathcal{E}$.

Let $(\delta q_e, \delta p_e) \in \delta \mathcal{E}$, and it follows from (3.8) and (3.9) that

$$A \triangleq \begin{bmatrix} \frac{\partial f_1(\delta q, \delta p)}{\partial \delta q} & \frac{\partial f_1(\delta q, \delta p)}{\partial \delta p} \\ \frac{\partial f_2(\delta q, \delta p)}{\partial \delta q} & \frac{\partial f_2(\delta q, \delta p)}{\partial \delta p} \end{bmatrix}_{(\delta q, \delta p) = (\delta q_e, \delta p_e)} = \begin{bmatrix} I_m - \frac{T_s^2 a}{1 + \epsilon d^2} \delta q_e \delta q_e^T & T_s(1 - T_s) I_m \\ -\frac{2T_s a}{1 + \epsilon d^2} \delta q_e \delta q_e^T & (1 - 2T_s) I_m \end{bmatrix}. \quad (3.10)$$

The following result describes the locations of the eigenvalues of A . The proof is in Section 3.9.

Proposition 3. The matrix A given by (3.10) has $m - 1$ eigenvalues at 1 and $m - 1$ eigenvalues at $1 - 2T_s$. Furthermore, the following statements hold:

- (a) Both of the remaining eigenvalues are inside the open unit disk if and only if $T_s < \min \{1, 2(1 + \epsilon d^2)/(ad^2)\}$.
- (b) At least one of the remaining eigenvalues is outside the closed unit disk if and only if $T_s > \min \{1, 2(1 + \epsilon d^2)/(ad^2)\}$.

The following results describe the stability properties of the equilibria of (3.6)–(3.9). These results are an immediate consequence of Proposition 3 and Lyapunov’s indirect method.

Corollary 1. If $m = 1$ and $T_s < \min \{1, 2(1 + \epsilon d^2)/(ad^2)\}$, then every element of $\delta\mathcal{E}$ is a locally asymptotically stable equilibrium of (3.6)–(3.9).

Corollary 2. If $T_s > \min \{1, 2(1 + \epsilon d^2)/(ad^2)\}$, then every element of $\delta\mathcal{E}$ is an unstable equilibrium of (3.6)–(3.9).

Corollary 2 implies that if the continuous-time flocking controller [1, Alg. 1] is discretized with a sample time T_s that is not sufficiently small, then the closed-loop system (3.6)–(3.9) is unstable. The following example demonstrates that the instability described in Corollary 2 is such that the agents approach a limit cycle, where they oscillate about the desired flocking distance d .

Example 8. Let $m = 2$, $a = b = 5$, $\epsilon = 0.1$, $d = 12$, and $T_s = 0.05$ s. Thus, $T_s = 0.05$ s $>$ 0.04 s $= \min \{1, 2(1 + \epsilon d^2)/(ad^2)\}$, and Corollary 2 implies that every element of $\delta\mathcal{E}$ is an unstable equilibrium of (3.6)–(3.9). The initial positions $q_1(0)$ and $q_2(0)$ are randomly distributed about 0. The initial velocity $p_1(0)$ is randomly distributed about 0, and $p_2(0) = [20 \ 0]^T - p_1(0)$, which makes the average initial velocity $[10 \ 0]^T$. Figure 3.1 shows the trajectory of the closed-loop dynamics (3.1), (3.2), and (3.5), and Figure 3.2 shows the time histories of $\|q_2 - q_1\|$ and $\|p_2 - p_1\|$. The agents asymptotically oscillate towards and away from one another. The relative distance asymptotically oscillates about d , and the relative velocity asymptotically oscillates. Thus, neither (F2) nor (F3) are satisfied. \triangle

Corollary 1 states that if $m = 1$ and T_s is sufficiently small, then every element of $\delta\mathcal{E}$ is a locally asymptotically stable equilibrium of (3.6)–(3.9). For $m > 1$ and T_s sufficiently small, Proposition 3 implies that A has at least one eigenvalue at 1. In this case, Lyapunov’s indirect method cannot be applied to determine local stability. Numerical simulations suggest that for $n = 2$ and $m > 1$, the condition $T_s < \min \{1, 2(1 + \epsilon d^2)/(ad^2)\}$ may be sufficient to ensure that every element of $\delta\mathcal{E}$ is a locally semistable equilibrium. However, a proof of this conjecture is open. See [92, pp. 194–195] for the definition of discrete-time local semistability.

The above analysis and example are for $n = 2$ agents. For $n > 2$ agents, the condition $T_s < \min \{1, 2(1 + \epsilon d^2)/(ad^2)\}$ is not sufficient to achieve (F1)–(F3). For $n > 2$, numerical testing suggests that the bound on T_s depends not only on a , b , ϵ , and d , but also n . The following example for $n = 3$ agents shows a trajectory of (3.1),

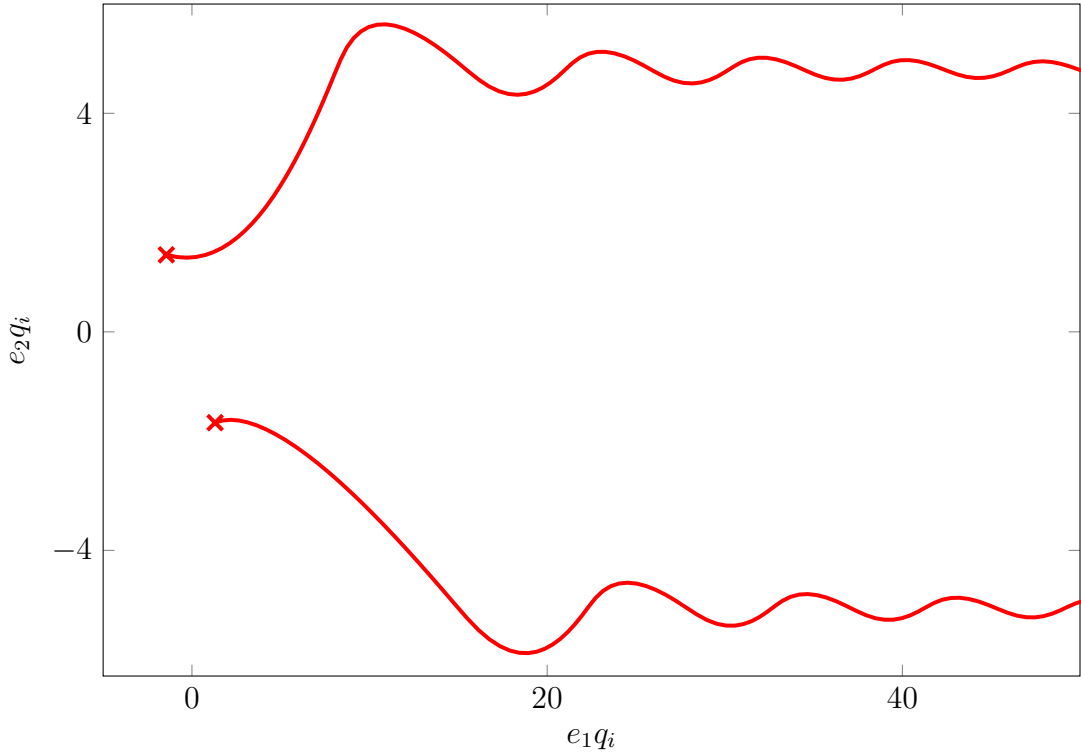


Figure 3.1: A trajectory of the closed-loop dynamics (3.1), (3.2), and (3.5). The agents asymptotically oscillate towards and away from each other.

(3.2), and (3.5), where $T_s < \min \{1, 2(1 + \epsilon d^2)/(ad^2)\}$. In this example, the agents start near a flocking configuration but diverge from this configuration.

Example 9. Let $n = 3$, $m = 2$, $a = b = 0.2$, $\epsilon = 0.1$, $d = 12$, and $T_s = 0.7$ s. Thus, $T_s = 0.7$ s < 1 s = $\min \{1, 2(1 + \epsilon d^2)/(ad^2)\}$. The initial positions are $q_1(0) = [0 \ 0]^T$, $q_2(0) = [d \ 0]^T$, and $q_3(0) = [0.5d \ 0.865d]^T$, which implies that all pairs of agents are approximately d apart. The initial velocities are $p_i(0) = 0$. Thus, the agents start near a flocking configuration. Figure 3.3 shows the distance $\|q_2 - q_1\|$ between agents and the magnitude of the relative velocity $\|p_2 - p_1\|$. The agents do not stay in a flocking configuration. In fact, $\|q_2 - q_1\|$ and $\|p_2 - p_1\|$ grow without bound. Neither (F2) nor (F3) are satisfied. \triangle

The analysis and examples in this section demonstrate that continuous-time flocking algorithms may not perform well in sampled-data settings particularly for large sample times or for a large number of agents. Discretizing these algorithms with sufficiently small sample times may yield the desired flocking formations. However, for $n > 2$ agents, it is unclear how to determine an upper bound on the sample time required to obtain stable formations. In this chapter, we present a new discrete-time flocking algorithm that is designed to guarantee stability properties for arbitrary sample time T_s , number of agents n , and spatial dimension m .

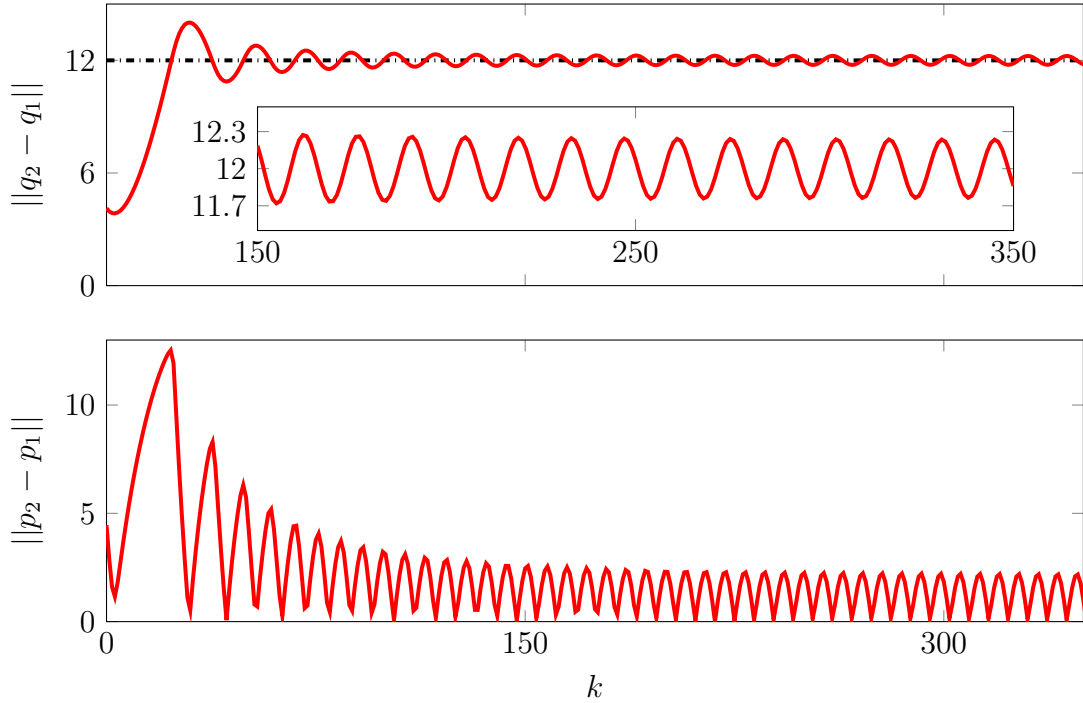


Figure 3.2: The distance $\|q_2 - q_1\|$ between agents and the magnitude of the relative velocity $\|p_2 - p_1\|$ for a trajectory of the closed-loop dynamics (3.1), (3.2), and (3.5). The distance between agents oscillates about d asymptotically, and the relative velocity oscillates asymptotically.

3.4 Discrete-Time Flocking

Let $r_c > \delta_c$ be the *communication radius*, which is the maximum distance at which an agent can sense another agent's relative position and relative velocity. For all $k \in \mathbb{N}$, define the *neighbor set* $\mathcal{N}_i(k) \triangleq \{j \in \mathcal{I} \setminus \{i\} : \|q_j(k) - q_i(k)\| < r_c\}$, which is the set of agents whose distance to the i th agent is less than the communication radius r_c . Let $d \in (\delta_c, r_c)$ be the *flock radius*, which is the desired distance between adjacent agents in the flock. For all $k \in \mathbb{N}$, define the *attraction set* $\mathcal{A}_i(k) \triangleq \{j \in \mathcal{I} \setminus \{i\} : d \leq \|q_j(k) - q_i(k)\| < r_c\} \subseteq \mathcal{N}_i(k)$, which is the set of agents whose distances from the i th agent are between the flock and communication radii, and define the *repulsion set* $\mathcal{R}_i(k) \triangleq \{j \in \mathcal{I} \setminus \{i\} : \|q_j(k) - q_i(k)\| < d\} \subseteq \mathcal{N}_i(k)$, which is the set of agents whose distances to the i th agent are less than the flock radius. Note that for all $k \in \mathbb{N}$, $\mathcal{N}_i(k) = \mathcal{A}_i(k) \cup \mathcal{R}_i(k)$.

For each $k \in \mathbb{N}$, let $\hat{q}_i(k) \in \mathbb{R}^m$ be an estimate of $q_i(k+1)$, that is, $\hat{q}_i(k)$ is an estimate of the i th agent's position at step $k+1$. We discuss how to design $\hat{q}_i(k)$ later in this section. Let $\bar{n} \geq n$ and $\bar{T}_s \geq T_s$. We assume \bar{n} and \bar{T}_s are known; however, n and T_s need not be known. If n and T_s are known, then $\bar{n} = n$ and $\bar{T}_s = T_s$ are appropriate choices.

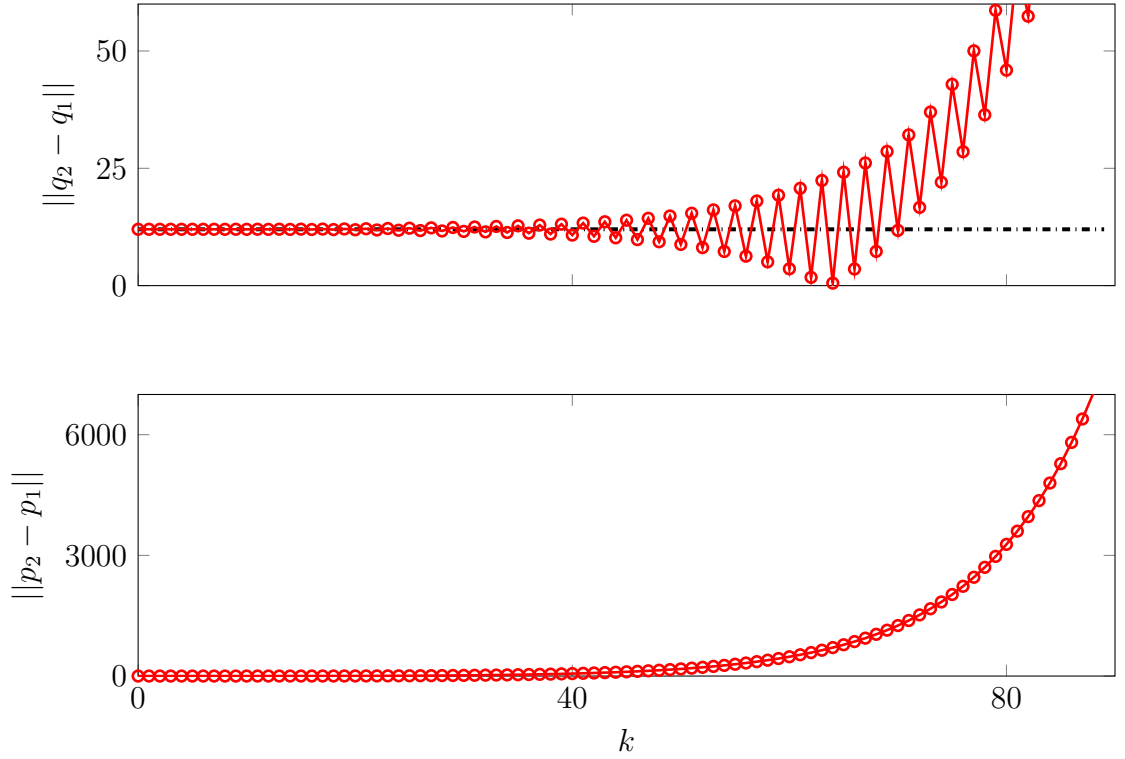


Figure 3.3: The distance $\|q_2 - q_1\|$ between agents and the magnitude of the relative velocity $\|p_2 - p_1\|$ for a trajectory of the closed-loop dynamics (3.1), (3.2), and (3.5). The agents start near a flocking configuration; however, the agents do not stay in a flocking configuration.

To develop the flocking controller, let

$$\alpha_1 \in (0, \infty), \quad \alpha_2 \in \left(0, \frac{4(\alpha_1 + 1)}{\bar{n}\bar{T}_s^2}\right), \quad (3.11)$$

and consider $\phi: [0, \infty) \rightarrow [\alpha_2/(\alpha_1 + 1) - \alpha_2/\alpha_1, \alpha_2/(\alpha_1 + 1)]$ defined by

$$\phi(\eta) \triangleq \frac{\alpha_2}{\alpha_1 + 1} - \frac{\alpha_2}{\alpha_1 + \eta^2/d^2}. \quad (3.12)$$

Note that $\phi(d) = 0$; for all $\eta \in [0, d)$, $\phi(\eta) < 0$; and, for all $\eta \in (d, \infty)$, $\phi(\eta) > 0$. Next, let

$$\beta \in \left[\frac{\alpha_2\bar{T}_s}{2(\alpha_1 + 1)}, \frac{2}{\bar{n}\bar{T}_s}\right), \quad (3.13)$$

where this interval exists because $\alpha_2 < 4(\alpha_1 + 1)/(\bar{n}\bar{T}_s^2)$.

Let

$$\gamma_1 \in \left[0, \frac{2}{\bar{T}_s^2}\right), \quad \gamma_2 \in \left[\frac{\bar{T}_s\gamma_1}{2}, \frac{1}{\bar{T}_s}\right), \quad (3.14)$$

where the interval for γ_2 exists because $\gamma_1 < 2/\bar{T}_s^2$. For all $k \in \mathbb{N}$, define

$$q(k) \triangleq \begin{bmatrix} q_1(k) \\ \vdots \\ q_n(k) \end{bmatrix}, \quad p(k) \triangleq \begin{bmatrix} p_1(k) \\ \vdots \\ p_n(k) \end{bmatrix}, \quad \hat{q}(k) \triangleq \begin{bmatrix} \hat{q}_1(k) \\ \vdots \\ \hat{q}_n(k) \end{bmatrix}.$$

Thus, we consider the discrete-time flocking control $u_i: \mathbb{R}^{mn} \times \mathbb{R}^{mn} \times \mathbb{R}^{mn} \times \mathbb{R}^m \times \mathbb{R}^m \rightarrow \mathbb{R}^m$ defined by

$$\begin{aligned} u_i(q, p, \hat{q}, q_g, p_g) = & \underbrace{\sum_{j \in \mathcal{A}_i} \phi(\|\hat{q}_j - \hat{q}_i\|)[q_j - q_i]}_{\text{Flock attraction}} \\ & + \underbrace{\sum_{j \in \mathcal{R}_i} \phi(\|\hat{q}_j - \hat{q}_i\|)[q_j - q_i]}_{\text{Flock repulsion}} \\ & + \underbrace{\sum_{j \in \mathcal{N}_i} \beta[p_j - p_i]}_{\text{Velocity consensus}} \\ & + \underbrace{\gamma_1[q_g - q_i] + \gamma_2[p_g - p_i]}_{\text{Guidance}} \\ & - \underbrace{\left(\sum_{j \in \mathcal{N}_i} \frac{\gamma_1}{\text{card}(\mathcal{N}_i) + 1} [q_j - q_i] + \frac{\gamma_2}{\text{card}(\mathcal{N}_i) + 1} [p_j - p_i] \right)}_{\text{Flock correction to guidance}}, \quad (3.15) \end{aligned}$$

where $\text{card}(\mathcal{N}_i)$ is the cardinality of \mathcal{N}_i .

The flock-attraction term in (3.15) is such that for all $j \in \mathcal{A}_i$, the i th agent is attracted to the j th agent. The flock-repulsion term is such that for all $j \in \mathcal{R}_i$, the i th agent is repelled from the j th agent. The velocity-consensus term attempts to match the i th agent's velocity with the average velocity of all agents in the neighbor set \mathcal{N}_i . The guidance terms cause the i th agent to be attracted to the leader's position and attempt to match its velocity. The flock-correction-to-guidance term is such that for all $j \in \mathcal{N}_i$, the i th agent experiences corrective forces that repel it from the j th agent and prevents configurations from collapsing around the leader for a large number n of agents. This collapsing effect has been noted as an issue in [29].

The parameters in the control (3.15) are α_1 , α_2 , β , γ_1 , and γ_2 . Decreasing α_1 increases flock repulsion relative to flock attraction, which helps prevent collisions. Increasing α_2 increases the magnitude of ϕ and thus, the flock-attraction and flock-repulsion forces. Increasing β increases the magnitude of the velocity-consensus force. Numerical simulations suggest that choosing β closer to its upper bound $2/(\bar{n}\bar{T}_s)$ tends to yield better performance. Positive γ_1 causes the i th agent to be attracted to the leader's position, whereas positive γ_2 causes the i th agent to attempt to match the leader's velocity.

The estimate \hat{q}_i can be chosen in multiple ways. The analysis in the next section uses the estimate $\hat{q}_i(k) \equiv q_i(k) + T_s p_i(k) + (T_s^2/2)u_i(k) \equiv q_i(k+1)$. This choice of the

estimate $\hat{q}_i(k)$ depends on $u_i(k)$, which can make this estimate difficult to implement. However, we present an iterative algorithm for implementing $\hat{q}_i(k) \equiv q_i(k+1)$ at the end of the next section. In contrast, the estimate $\hat{q}_i(k) \equiv q_i(k) + T_s p_i(k)$ is easy to implement. In addition, for bounded u_i and sufficiently small T_s , the estimate $\hat{q}_i(k) \equiv q_i(k) + T_s p_i(k)$ is approximately equal to $q_i(k+1)$. The simulations in Section 3.7 use the estimate $\hat{q}_i(k) \equiv q_i(k) + T_s p_i(k)$.

3.5 Flocking Analysis

In this section, we analyze the closed-loop dynamics (3.1)–(3.4) and (3.15). Let

$$E_i \triangleq \begin{bmatrix} 0_{m \times m(i-1)} & I_m & 0_{m \times m(n-i)} \end{bmatrix} \in \mathbb{R}^{m \times mn},$$

and define $\mathcal{Q} \triangleq \{q \in \mathbb{R}^{mn} : \text{for all } (i, j) \in \mathcal{P}, \|[E_j - E_i]q\| < r_c\}$, which is the set of agent positions such that all agents can communicate with one another. The flocking analysis in this section relies on the following assumptions:

(A1) $\hat{q}(k) \equiv q(k+1)$.

(A2) r_c is sufficiently large such that for all $k \in \mathbb{N}$, $q(k) \in \mathcal{Q}$.

At the end of this section, we present an iterative numerical approach for implementing $\hat{q}(k) \equiv q(k+1)$ and thus satisfying (A1). Assumption (A2) states that the communication radius is sufficiently large such that all agents communicate with one another. Theorem 5 in this section provides a sufficient condition such that (A2) is satisfied.

Define $q_a \triangleq -q_g + \sum_{i \in \mathcal{I}} q_i/n$ and $p_a \triangleq -p_g + \sum_{i \in \mathcal{I}} p_i/n$, which are the agent-averaged position and velocity relative to the leader's position and velocity. Then, it follows from (3.1)–(3.4) and (3.15) that for all $k \in \mathbb{N}$,

$$q_a(k+1) = q_a(k) + T_s p_a(k) + \frac{1}{2} T_s^2 u_a(q(k), p(k), q_g(k), p_g(k), u_g(k)), \quad (3.16)$$

$$p_a(k+1) = p_a(k) + T_s u_a(q(k), p(k), q_g(k), p_g(k), u_g(k)), \quad (3.17)$$

where $u_a: \mathbb{R}^{mn} \times \mathbb{R}^{mn} \times \mathbb{R}^m \times \mathbb{R}^m \times \mathbb{R}^m \rightarrow \mathbb{R}^m$ is defined by

$$u_a(q, p, q_g, p_g, u_g) \triangleq -u_g + \frac{1}{n} \sum_{i \in \mathcal{I}} u_i(q, p, \hat{q}, q_g, p_g), \quad (3.18)$$

which is the agent-averaged control relative to u_g . We call (3.16)–(3.18) the *agent-averaged dynamics*.

Next, define $q_{ji} \triangleq q_j - q_i$ and $p_{ji} \triangleq p_j - p_i$. Then, it follows from (3.1), (3.2), and (3.15) that for all $k \in \mathbb{N}$,

$$q_{ji}(k+1) = q_{ji}(k) + T_s p_{ji}(k) + \frac{1}{2} T_s^2 u_{ji}(q(k), p(k), \hat{q}(k)), \quad (3.19)$$

$$p_{ji}(k+1) = p_{ji}(k) + T_s u_{ji}(q(k), p(k), \hat{q}(k)), \quad (3.20)$$

where $u_{ji} : \mathbb{R}^{mn} \times \mathbb{R}^{mn} \times \mathbb{R}^{mn} \rightarrow \mathbb{R}^m$ is defined by

$$u_{ji}(q, p, \hat{q}) \triangleq u_j(q, p, \hat{q}, q_g, p_g) - u_i(q, p, \hat{q}, q_g, p_g). \quad (3.21)$$

We call (3.19)–(3.21) the *interagent dynamics*. Note that the interagent dynamics do not depend on the leader's position q_g or velocity p_g . Thus, (3.1)–(3.4) and (3.15) can be decomposed into 2 parts: the agent-averaged dynamics (3.16)–(3.18) and the interagent dynamics (3.19)–(3.21).

The following result provides sufficient conditions such that the agent-averaged position and velocity converge to the leader's position and velocity. The proof is in Section 3.10. We let \otimes denote the Kronecker product.

Lemma 2. Consider the closed-loop dynamics (3.1)–(3.4) and (3.15), and the associated agent-averaged dynamics (3.16)–(3.18), where (A1) and (A2) are satisfied and $u_g(k) \equiv 0$. Then, for all $q(0) \in \mathcal{Q}$, $p(0) \in \mathbb{R}^{mn}$, $q_g(0) \in \mathbb{R}^m$, and $p_g(0) \in \mathbb{R}^m$, the following statements hold:

(a) If $\gamma_1 = 0$ and $\gamma_2 \in (0, 1/\bar{T}_s)$, then p_a satisfies

$$p_a(k+1) = (1 - T_s \gamma_2) p_a(k), \quad (3.22)$$

and $\lim_{k \rightarrow \infty} p_a(k) = 0$.

(b) If $\gamma_1 \in (0, 2/\bar{T}_s^2)$ and $\gamma_2 \in (\bar{T}_s \gamma_1/2, 1/\bar{T}_s)$, then q_a and p_a satisfy

$$\begin{bmatrix} q_a(k+1) \\ p_a(k+1) \end{bmatrix} = \left(\begin{bmatrix} 1 - \frac{1}{2} T_s^2 \gamma_1 & T_s(1 - \frac{1}{2} T_s \gamma_2) \\ -T_s \gamma_1 & 1 - T_s \gamma_2 \end{bmatrix} \otimes I_m \right) \begin{bmatrix} q_a(k) \\ p_a(k) \end{bmatrix}, \quad (3.23)$$

and $\lim_{k \rightarrow \infty} q_a(k) = 0$ and $\lim_{k \rightarrow \infty} p_a(k) = 0$.

To analyze the combined agent-averaged dynamics (3.16)–(3.18) and the interagent dynamics (3.19)–(3.21), consider $\psi : [0, \infty) \rightarrow [0, \infty)$ defined by

$$\begin{aligned} \psi(\eta) &\triangleq 2\alpha_2 \int_d^\eta \frac{\sigma}{\alpha_1 + 1} - \frac{\sigma}{\alpha_1 + \sigma^2/d^2} d\sigma \\ &= \alpha_2 \left[\frac{\eta^2 - d^2}{\alpha_1 + 1} + d^2 \ln \frac{\alpha_1 + 1}{\alpha_1 + \eta^2/d^2} \right]. \end{aligned} \quad (3.24)$$

Note that $\psi(d) = 0$ and for all $\eta \in [0, \infty) \setminus \{d\}$, $\psi(\eta) > 0$. Consider the logarithmic potential function $V : \mathcal{Q} \times \mathbb{R}^{mn} \rightarrow [0, \infty)$ defined by

$$V(q, p) \triangleq \sum_{(i,j) \in \mathcal{P}} \psi(\| [E_j - E_i]q \|) + \lambda \| [E_j - E_i]p \|^2, \quad (3.25)$$

where $\lambda \triangleq 1/n - T_s \beta/2$, which is positive because $\beta < 2/(\bar{n}\bar{T}_s) \leq 2/(nT_s)$. If $\| [E_j - E_i]q \| = d$ and $[E_j - E_i]p = 0$, then $V(q, p) = 0$; otherwise, $V(q, p) > 0$.

Define the Lyapunov-like difference $\Delta V(k) \triangleq V(q(k+1), p(k+1)) - V(q(k), p(k))$. The following result shows that $V(q(k), p(k))$ is nonincreasing along the trajectories of (3.1), (3.2), and (3.15). The proof is in Section 3.10.

Lemma 3. Consider the closed-loop dynamics (3.1)–(3.4), and (3.15), where (A1) is satisfied. Let $k_0 \in \mathbb{N}$, and assume $q(k_0) \in \mathcal{Q}$. Then, $\Delta V(k_0) \leq 0$. Furthermore, $\Delta V(k_0) = 0$ if and only if $q_{ji}(k_0 + 1) = q_{ji}(k_0)$.

Define

$$\begin{aligned} \mathcal{E} &\triangleq \{(q_e, p_e) \in \mathcal{Q} \times \mathbb{R}^{mn} : \text{for all } (i, j) \in \mathcal{P}, u_{ji}(q_e, p_e, q_e) = 0 \text{ and } [E_j - E_i]p_e = 0\} \\ &= \{(q_e, p_e) \in \mathcal{Q} \times \mathbb{R}^{mn} : \text{for all } (i, j) \in \mathcal{P}, u_{ji}(q_e, 0, q_e) = 0 \text{ and } [E_j - E_i]p_e = 0\}, \end{aligned} \quad (3.26)$$

which is the set of agent positions and velocities such that all agents communicate with one another and have the same velocity and control.

The following result provides sufficient conditions for flocking and is the main result of this chapter. The proof is in Section 3.11.

Theorem 4. Consider the closed-loop dynamics (3.1)–(3.4) and (3.15), where (A1) and (A2) are satisfied. Then, for all $q(0) \in \mathcal{Q}$, $p(0) \in \mathbb{R}^{mn}$, $q_g(0) \in \mathbb{R}^m$, and $p_g(0) \in \mathbb{R}^m$, the following statements hold:

- (a) If $V(q(0), p(0)) < 2\psi(\delta_c)$, then for all $k \in \mathbb{N}$, $\|q_{ji}(k)\| > \delta_c$.
- (b) $\lim_{k \rightarrow \infty} p_{ji}(k) = 0$.
- (c) For all $\delta > 0$ there exists $k_\delta \in \mathbb{N}$ such that for all $k \geq k_\delta$, $\max_{(i,j) \in \mathcal{P}} \|q_{ji}(k)\| \leq d(n-1) + \delta$.
- (d) $(q(k), p(k))$ converges to the set $\{(q_e, p_e) \in \mathcal{E} : V(q_e, p_e) \leq V(q(0), p(0))\}$.
- (e) For all $i \in \mathcal{I}$, $\lim_{k \rightarrow \infty} \sum_{j \in \mathcal{N}_i(k)} \phi(\|\hat{q}_j(k) - \hat{q}_i(k)\|) q_{ji}(k) = 0$.
- (f) If $\gamma_1 = \gamma_2 = 0$, then $\sum_{j \in \mathcal{I}} p_j(k) \equiv \sum_{j \in \mathcal{I}} p_j(0)$ and $\lim_{k \rightarrow \infty} p_i(k) = \sum_{j \in \mathcal{I}} p_j(0)/n$.
- (g) If $\gamma_1 \in [0, 2/\bar{T}_s^2)$, $\gamma_2 \in (\bar{T}_s \gamma_1/2, 1/\bar{T}_s)$, and $u_g(k) \equiv 0$, then $\lim_{k \rightarrow \infty} p_i(k) = p_g(0)$.
- (h) If $\gamma_1 \in (0, 2/\bar{T}_s^2)$, $\gamma_2 \in (\bar{T}_s \gamma_1/2, 1/\bar{T}_s)$, and $u_g(k) \equiv 0$, then $\lim_{k \rightarrow \infty} q_a(k) = 0$.

Part (a) states that if $V(q(0), p(0)) < 2\psi(\delta_c)$, then there are no collisions, which implies (F1). Part (b) states that all agents converge to the same velocity, which implies (F2). Part (c) states that the relative position between agents is asymptotically bounded by $d(n-1)$, which implies (F3). Thus, parts (a)–(c) imply that the agents in \mathcal{I} achieve (F1)–(F3), and thus flock with radius $d > 0$.

Part (d) states that agents converge to a subset of \mathcal{E} , which implies that agents converge to the same velocity and control. Part (e) states the sum of attraction and repulsion of the i th agent converges to 0. Part (f) states that if $\gamma_1 = \gamma_2 = 0$, then the i th agent's velocity converges to the agent-averaged initial velocity. Part (g) states that if $\gamma_1 \in [0, 2/\bar{T}_s^2)$, $\gamma_2 \in (\bar{T}_s \gamma_1/2, 1/\bar{T}_s)$, and $u_g(k) \equiv 0$, then the i th agent's velocity converges to the leader's initial velocity. Part (h) states that if $\gamma_1 \in (0, 2/\bar{T}_s^2)$, $\gamma_2 \in (\bar{T}_s \gamma_1/2, 1/\bar{T}_s)$, and $u_g(k) \equiv 0$, then the agent-averaged position converges to the leader's position.

Assumption (A2) requires that r_c is sufficiently large such that for all $k \in \mathbb{N}$, $q(k) \in \mathcal{Q}$. The following result provides a sufficient condition for (A2). The proof is in Section 3.11.

Theorem 5. Consider the closed-loop dynamics (3.1)–(3.4) and (3.15), where (A1) is satisfied. Assume $q(0) \in \mathbb{R}^{mn}$ and $p(0) \in \mathbb{R}^{mn}$ are such that $V(q(0), p(0)) < 2\psi(r_c)$. Then, for all $k \in \mathbb{N}$, $q(k) \in \mathcal{Q}$, and parts (a)–(h) of Theorem 4 hold.

The analyses in this section use the estimate $\hat{q}(k) \equiv q(k+1)$, which can be difficult to implement because $\hat{q}(k)$ depends on $u(k)$. The following iterative algorithm provides a process to compute an estimate $\hat{q}(k)$ on each step k such that $\|\hat{q}(k) - q(k+1)\| < \epsilon$ for an arbitrarily small $\epsilon > 0$.

Algorithm 1. Consider the closed-loop dynamics (3.1)–(3.4) and (3.15), where (A2) is satisfied. Let $\epsilon > 0$ be the required accuracy of the estimate $\hat{q}(k)$ of $q(k+1)$. For each step $k \in \mathbb{N}$, consider the estimator of $q(k+1)$ given by the difference equation

$$z_k(l+1) = q(k) + T_s p(k) + \frac{1}{2} T_s^2 u(q(k), p(k), z_k(l), q_g(k), p_g(k)), \quad (3.27)$$

where $l \in \mathbb{N}$, $z_k(l) \in \mathbb{R}^{mn}$, and $z_k(0)$ is the initial estimate of $q(k+1)$. For each step $k \in \mathbb{N}$, the estimate $\hat{q}(k)$ is obtained using the following algorithm:

Step 1: Initialize l to 0, and select $z_k(0) \in \mathbb{R}^{mn}$, which is the initial estimate of $q(k+1)$.

Step 2: Compute $z_k(l+1)$ using (3.27). If $\|z_k(l+1) - z_k(l)\| < \epsilon$, then go to Step 3; otherwise, increment l by 1 and repeat this step.

Step 3: The estimate of $q(k+1)$ is $\hat{q}(k) = z_k(l)$. △

For each $k \in \mathbb{N}$, one possible choice for the initial estimate is $z_k(0) = q(k) + T_s p(k)$. Note that Algorithm 1 can be implemented decentrally for each agent using feedback $q(k)$ and $p(k)$. In numerical testing with $\epsilon = 10^{-13}$ and different values of $q(k)$, $p(k)$, $q_g(k)$, $p_g(k)$, α_1 , α_2 , β , γ_1 , γ_2 , n , m , T_s , and d , we observed that after a sufficient number of iterations $\|z_k(l+1) - z_k(l)\| < \epsilon$. In practice, the tolerance $\epsilon > 0$ would be selected based on the computational resources and the acceptable amount of time to iterate on each step k . In fact, Algorithm 1 can be easily modified to impose a maximum number of iterations, which would be determined based on practical constraints.

3.6 Motivating Example Revisited

We now reconsider Example 8 in Section 3.3, where instead of using the control given by [1, Alg. 1], we use the control (3.15). Let T_s , d , and $r_c = r$ be the same as in Section 3.3. The initial positions $q_1(0)$ and $q_2(0)$, and initial velocities $p_1(0)$ and $p_2(0)$ are the same as in Example 8. Let $\alpha_1 = 0.01$, $\alpha_2 = 3$, $\beta = 3.3$, and $\gamma_1 = \gamma_2 = 0$, which are the parameters of (3.15) and are selected to satisfy (3.11), (3.13), and

(3.14). We use the estimate $\hat{q}(k)$ obtained from Algorithm 1, where $\epsilon = 10^{-13}$ and $z_k(0) = q(k) + T_s p(k)$.

Figure 3.4 shows the trajectory of the closed-loop dynamics (3.1), (3.2), and (3.15) overlaid on Figure 3.1, and Figure 3.5 shows the time histories of $\|q_2 - q_1\|$ and $\|p_2 - p_1\|$ overlaid on Figure 3.2. Using the control (3.15), the distance between agents converges to d without oscillations and the agents approach the same velocity. Thus, the agents flock asymptotically, and this flocking behavior contrasts the asymptotic oscillations observed in Figures 3.1 and 3.2, where the control is given by [1, Alg. 1].

If, in the above example, we use the control (3.15) with the estimate $\hat{q}(k) \equiv q(k) + T_s p(k)$ instead of the estimate obtained from Algorithm 1, then the response (solid lines) is indistinguishable from the response shown in Figures 3.4 and 3.5.

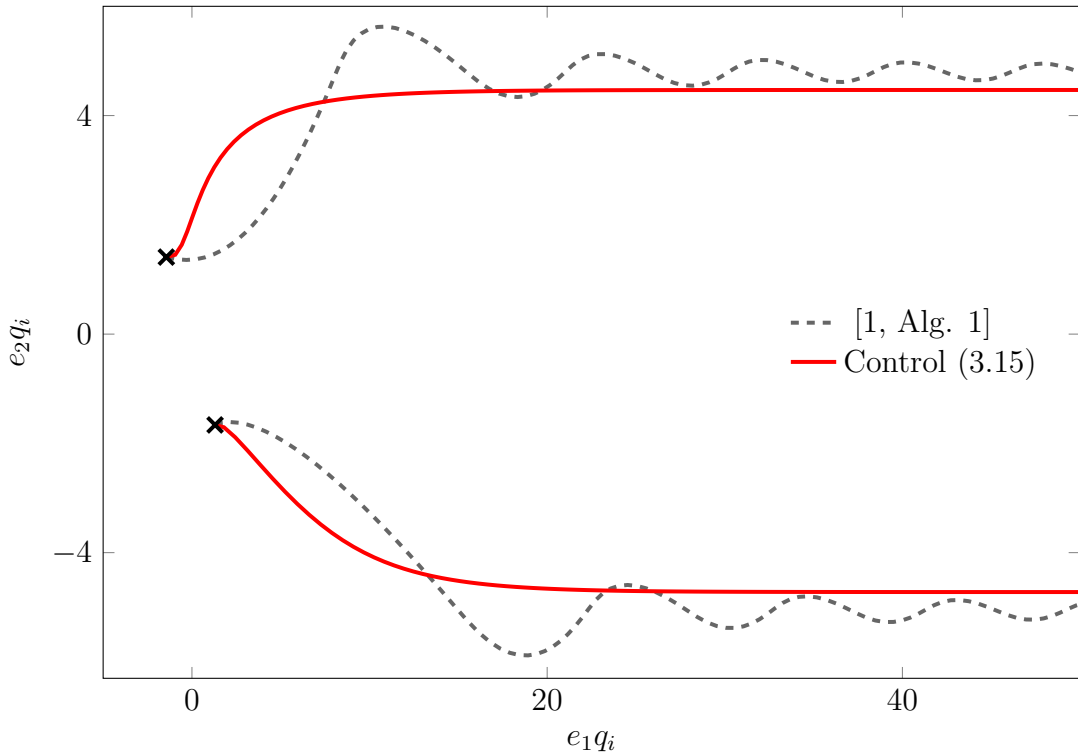


Figure 3.4: A trajectory of the closed-loop system (3.1), (3.2), and (3.15) overlaid on the trajectory from Figure 3.1, which uses the control [1, Alg. 1]. The agents using (3.15) flock asymptotically.

3.7 Numerical Examples

In this section, we present examples that demonstrate the discrete-time flocking control (3.15). For all examples, we let $T_s = 0.05$ s, $\delta_c = 2$ m, $d = 12$ m, $\alpha_1 = 0.01$, $\alpha_2 = 3$, and $\beta = 3.3$. We use the estimate $\hat{q}(k) \equiv q(k) + T_s p(k)$.

The following example demonstrates that the flock-correction-to-guidance (FCTG) term helps prevent the agents' configuration from collapsing around the leader, which

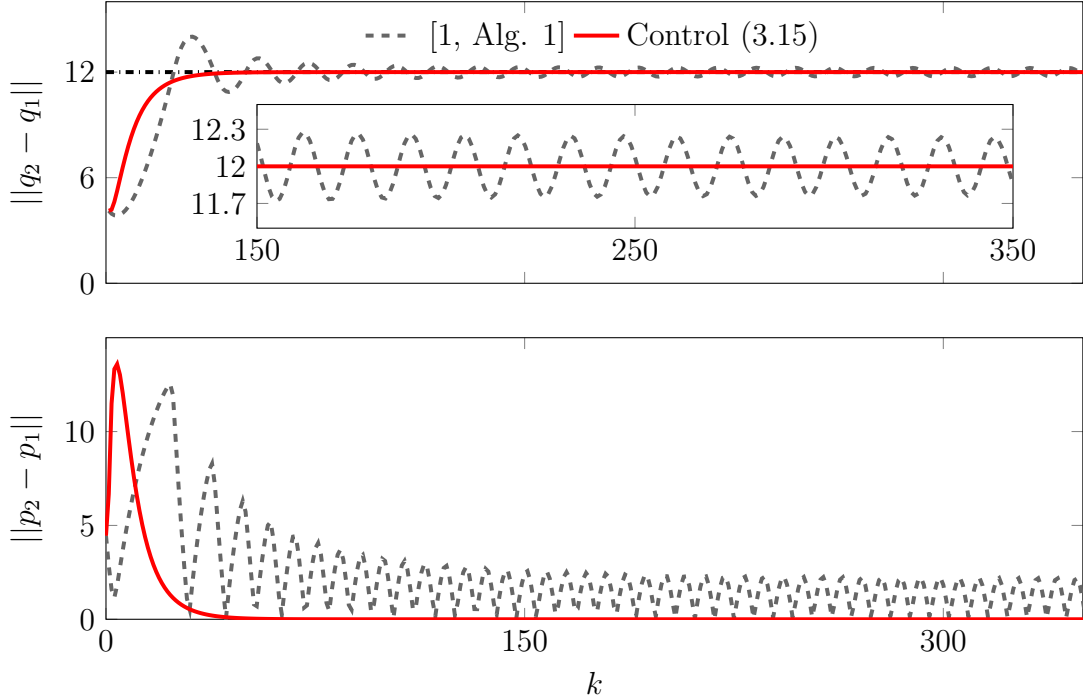


Figure 3.5: The distance $\|q_2 - q_1\|$ between agents and the magnitude of the relative velocity $\|p_2 - p_1\|$ for a trajectory of the closed-loop system (3.1), (3.2), and (3.15) overlaid on the plot from Figure 3.2, which uses the control [1, Alg. 1]. Using (3.15), the distance between the agents converges to d , and the relative velocity converges to 0.

in turn helps prevent collisions.

Example 10. Let $n = 3$ agents, $m = 2$, and $r_c = 100$ m. The initial positions are $q_1(0) = [9 \ 0]^T$, $q_2(0) = [-2 \ 7]^T$, and $q_3(0) = [-5 \ -3]^T$; and the initial velocities are $p_1(0) = p_2(0) = p_3(0) = 0$. In addition, let $\gamma_1 = 50$ and $\gamma_2 = 10$, and consider the leader dynamics (3.3) and (3.4), where $q_g(k) \equiv 0$, $p_g(k) \equiv 0$, and $u_g(k) \equiv 0$. Thus, the leader agent is stationary. Figure 3.6 shows the trajectory of agents using the control (3.15), which includes the FCTG term, and the control (3.15), where the FCTG term is omitted. Figure 3.7 shows that the distances between agents using the control (3.15) with FCTG converges to d , whereas the agents whose controls do not contain the FCTG term converge to a distance less than d apart. \triangle

The remaining numerical examples demonstrate formations of agents with and without a leader.

Example 11. Let $n = 3$ agents, $m = 2$, and $r_c = 100$ m. Assume there is no leader (i.e., $\gamma_1 = \gamma_2 = 0$). The initial positions $q_1(0)$, $q_2(0)$, and $q_3(0)$ are randomly distributed about 0; and the initial velocities $p_1(0)$ and $p_2(0)$ are randomly distributed about 0, and $p_3(0) = [30 \ 0]^T - p_1(0) - p_2(0)$, which makes the average initial velocity $[10 \ 0]^T$. Figure 3.8 shows that the agents form a flock, where all agents have the

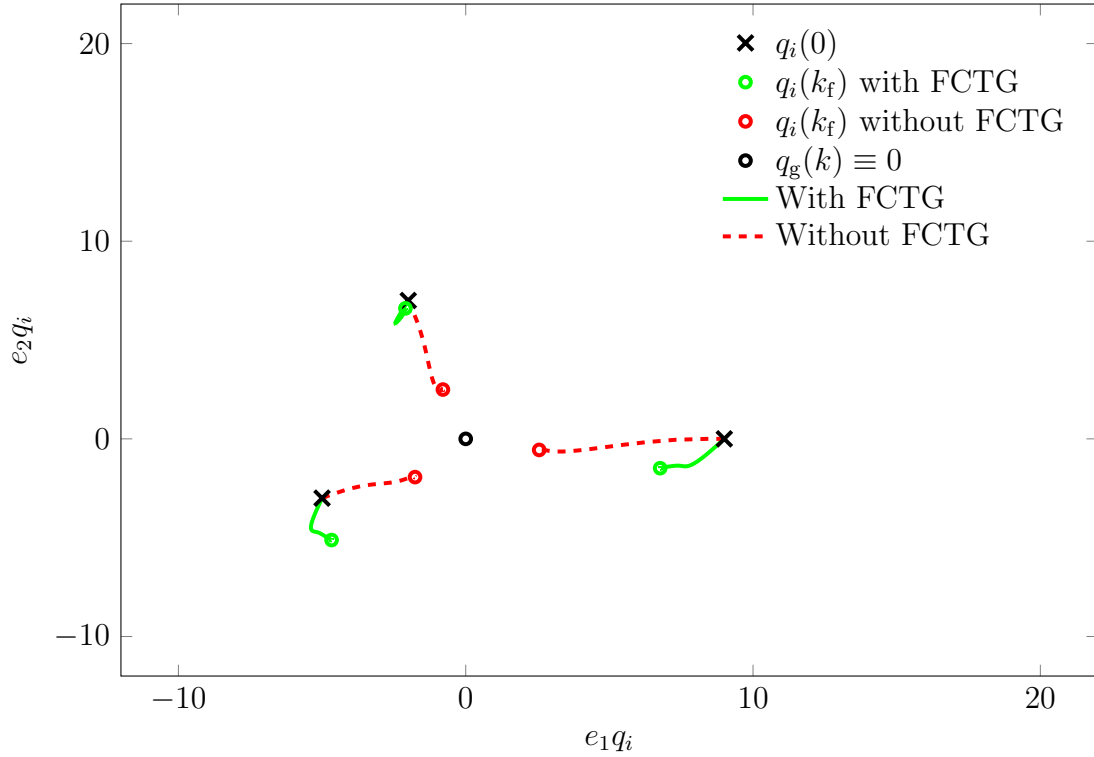


Figure 3.6: Trajectories of $n = 3$ agents that follow a leader whose position and velocity are $q_g(k) \equiv 0$ and $p_g(k) \equiv 0$. In one trajectory, agents use the control (3.15), which contains the FCTG term; in the other, agents use the control (3.15), where the FCTG term is omitted. The step $k_f \in \mathbb{N}$ is such that $q_i(k_f + 1) \approx q_i(k_f)$.

same velocity and are d apart from all other agents. Furthermore, for all $k \in \mathbb{N}$, $\|q_j(k) - q_i(k)\| > \delta_c$, which implies that there are no collisions. In this example, we use the estimate $\hat{q}(k) \equiv q(k) + T_s p(k) \approx q(k+1)$, whereas Theorem 4 uses the estimate $\hat{q}(k) \equiv q(k+1)$. Figure 3.8 shows that with this approximation, the agents in \mathcal{I} flock with radius d . \triangle

The asymptotic configurations in Example 10 (with FCTG) and Example 11 are both such that $\lim_{k \rightarrow \infty} \|q_j(k) - q_i(k)\| = d$. Therefore, in these cases, agents converge to this d -apart configuration independent of whether or not there is a leader.

Example 12. Let $n = 3$ agents, $m = 2$, and $r_c = 100$ m. Let $\gamma_1 = 3$ and $\gamma_2 = 6$, and consider the leader dynamics (3.3) and (3.4), where $q_g(0) = 0$, $p_g(0) = [10 \ 0]^T$, and

$$u_g(k) = \begin{bmatrix} 0 \\ -e_2 q_g(k) + 50 \sin \theta k - 2e_2 p_g(k) + 100\theta \cos \theta k \end{bmatrix},$$

and $\omega = 0.025$ rad. Thus, the leader has a constant velocity in the e_1 direction and a sinusoidal velocity in the e_2 direction. The initial conditions $q(0)$ and $p(0)$ are randomly distributed about 0. Figure 3.9 shows that the agents flock and follow the leader. \triangle

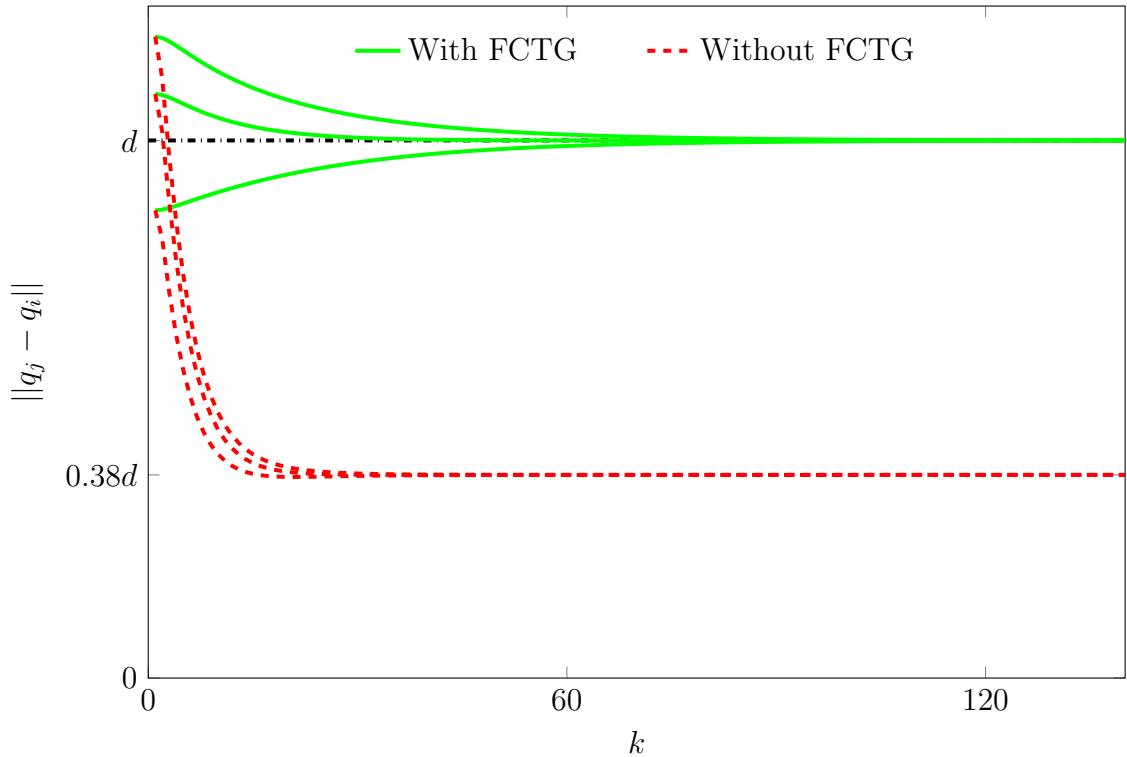


Figure 3.7: The distances between $n = 3$ agents that follow the leader agent whose position is $q_g(k) \equiv 0$ and whose velocity is $p_g(k) \equiv 0$. In one trajectory, agents use the control (3.15), which contains the FCTG term; in the other, agents use the control (3.15), where the FCTG term is omitted. The agents using the FCTG term converge to d apart, whereas the agents that do not use the FCTG term converge to a distance less than d apart.

Example 13. Let $n = 10$ agents, $m = 3$, and $r_c = 100$ m. Let $\gamma_1 = 3$ and $\gamma_2 = 6$, and consider the leader dynamics (3.3) and (3.4), where $q_g(0) = 0$, $p_g(0) = [5 \ 0 \ 0]^T$, and

$$u_g(k) = \begin{bmatrix} 0 \\ 0 \\ -e_3 q_g(k) + 50 \sin \theta k - 2e_3 p_g(k) + 100\theta \cos \theta k \end{bmatrix},$$

where $\omega = 0.025$ rad. Thus, the leader has a constant velocity in the e_1 and e_2 directions and a sinusoidal velocity in the e_3 direction. The initial conditions $q(0)$ and $p(0)$ are randomly distributed about 0. Figure 3.10 shows that the agents flock and follow the leader. \triangle

3.8 Conclusions

We presented a discrete-time distance-formation control (3.15) that addresses flocking for agents with the sampled-data double-integrator dynamics, which are obtained by sampling the continuous-time double integrator and applying a zero-order hold

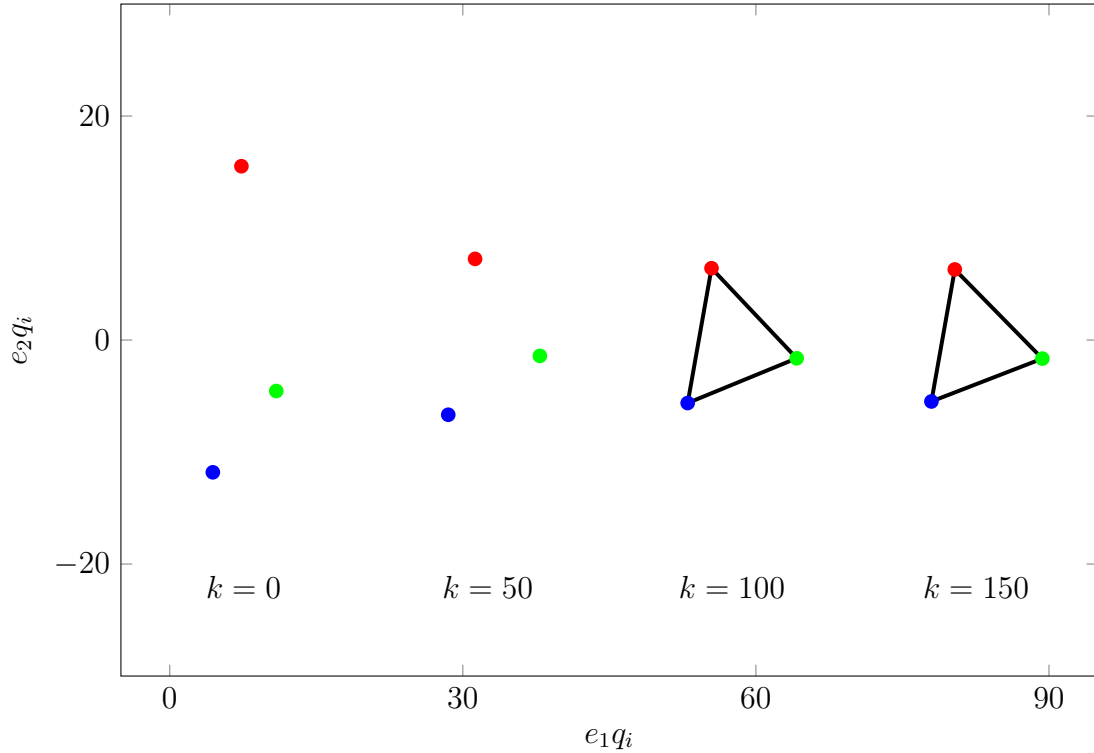


Figure 3.8: A group of $n = 3$ agents with no leader that flock. The agents form a flock, where all agents have the same velocity and are d apart from one another. The line between agents shows that agents are approximately d apart.

on the control input. The control (3.15) includes flock-attraction, flock-repulsion, velocity-consensus, guidance, and flock-correction-to-guidance terms. We demonstrated with analysis and simulation that discretizing (i.e., sample and zero-order hold) a continuous-time flocking algorithm (specifically [1]) can lead to instabilities. In contrast, we demonstrated with analysis and simulation that the discrete-time flocking method in this chapter causes agents to flock, that is, avoid collisions, match velocities, and achieve a cohesive formation.

3.9 Proof of Proposition 3

Proof of Proposition 3. Let $S \in \mathbb{R}^{m \times m}$ be an orthogonal matrix such that $S\delta q_e = de_1^T$, which exists because $\|\delta q_e\| = d$. Let $P \in \mathbb{R}^{2m \times 2m}$ be the permutation of the $2m \times 2m$ identity matrix, where the second and $(m + 1)$ th columns are switched. Define

$$\begin{aligned} \tilde{A} &\triangleq P \begin{bmatrix} S & 0_{m \times m} \\ 0_{m \times m} & S \end{bmatrix} A \begin{bmatrix} S^T & 0_{m \times m} \\ 0_{m \times m} & S^T \end{bmatrix} P^{-1} \\ &= \begin{bmatrix} M & 0_{2 \times (m-1)} & 0_{2 \times (m-1)} \\ 0_{(m-1) \times 2} & I_{m-1} & T_s(1 - T_s)N \\ 0_{(m-1) \times 2} & 0_{(m-1) \times (m-1)} & (1 - 2T_s)I_{m-1} \end{bmatrix}, \end{aligned} \quad (3.28)$$

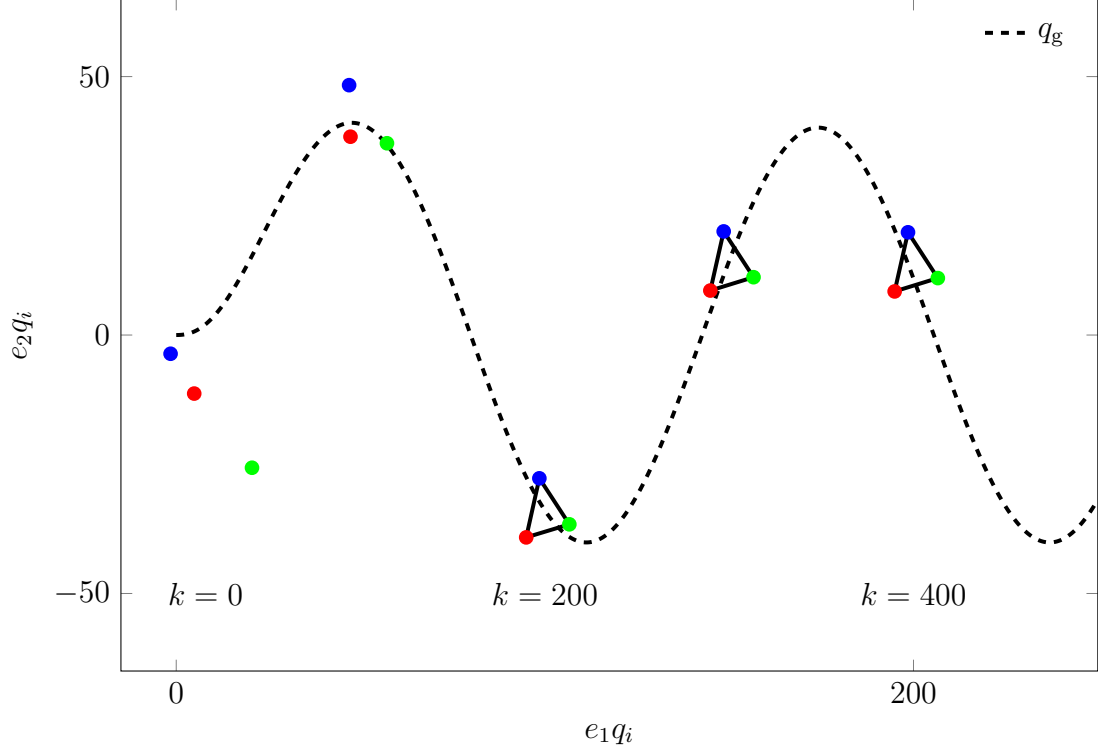


Figure 3.9: A group of $n = 3$ agents that flock and follow a leader. The line between agents shows that agents are approximately d apart.

where

$$M \triangleq \begin{bmatrix} 1 - \frac{T_s^2 ad^2}{1 + \epsilon d^2} & T_s(1 - T_s) \\ -\frac{2T_s ad^2}{1 + \epsilon d^2} & 1 - 2T_s \end{bmatrix} \in \mathbb{R}^{2 \times 2},$$

$$N \triangleq \begin{bmatrix} 0_{(m-2) \times 1} & I_{m-2} \\ 1 & 0_{1 \times (m-2)} \end{bmatrix} \in \mathbb{R}^{(m-1) \times (m-1)}.$$

Since the eigenvalues of A coincide with those of \tilde{A} , and \tilde{A} is upper block triangular, it follows from (3.28) that A has $m - 1$ eigenvalues at 1 and $m - 1$ eigenvalues at $1 - 2T_s$, and the 2 remaining eigenvalues of A are the eigenvalues of M .

It follows from Proposition 4 in Section 3.12 that the eigenvalues of M are in the open unit disk if and only if $T_s = f < \min\{1, 2/g\} = \min\{1, 2(1 + \epsilon d^2)/(ad^2)\}$, which confirms (a). Similarly, it follows from Proposition 5 in Section 3.12 that at least one of the eigenvalues of M is outside the closed unit disk if and only if $T_s = f > \min\{1, 2/g\} = \min\{1, 2(1 + \epsilon d^2)/(ad^2)\}$, which confirms (b). \square

3.10 Proof of Lemmas 2 and 3

Proof of Lemma 2. Assumption (A2) implies that for all $k \in \mathbb{N}$, $\|q_{ji}(k)\| < r_c$. Since, in addition, $u_g(k) \equiv 0$, it follows from (3.18) that for all $k \in \mathbb{N}$,

$$u_a(q(k), p(k), q_g(k), p_g(k), u_g(k)) = -\gamma_1 q_a(k) - \gamma_2 p_a(k),$$

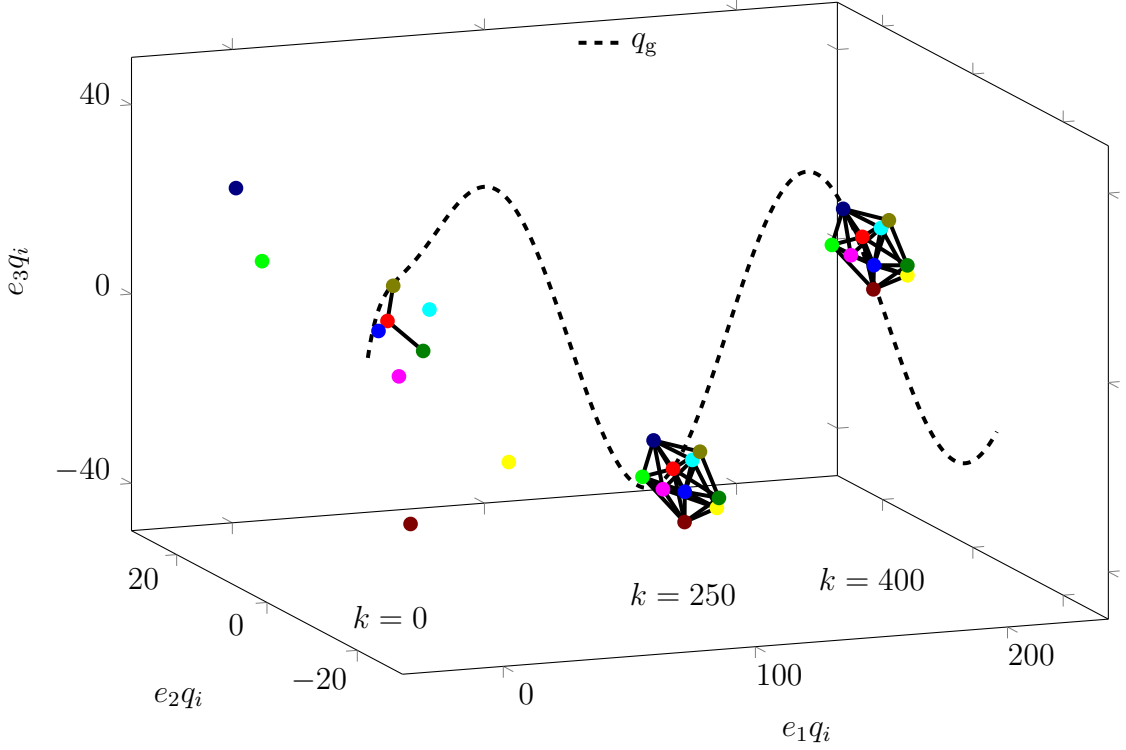


Figure 3.10: A group of $n = 10$ agents that flock and follow a leader. The line between agents shows that agents are approximately d apart.

which substituted into (3.16) and (3.17) yields (3.23).

To show (a), assume that $\gamma_1 = 0$ and $\gamma_2 \in (0, 1/\bar{T}_s)$, and it follows from (3.23) that for all $k \in \mathbb{N}$, $p_a(k)$ satisfies (3.22). Since $\gamma_2 \in (0, 1/\bar{T}_s) \subseteq (0, 1/T_s)$, it follows that all the eigenvalues of $(1 - T_s\gamma_2)I_m$ are inside the open unit disk. Therefore, $\lim_{k \rightarrow \infty} p_a(k) = 0$, which confirms (a).

To show (b), assume $\gamma_1 \in (0, 2/\bar{T}_s^2)$ and $\gamma_2 \in (\bar{T}_s\gamma_1/2, 1/\bar{T}_s)$, and define

$$B \triangleq \begin{bmatrix} 1 - \frac{1}{2}T_s^2\gamma_1 & T_s(1 - \frac{1}{2}T_s\gamma_2) \\ -T_s\gamma_1 & 1 - T_s\gamma_2 \end{bmatrix}.$$

Since $\gamma_1 > 0$ and $\gamma_2 \in (\bar{T}_s\gamma_1/2, 1/\bar{T}_s) \subseteq (T_s\gamma_1/2, 1/T_s)$, it follows that $\det B = 1 + T_s^2\gamma_1/2 - T_s\gamma_2 > T_s^2\gamma_1/2 > 0$ and $\det B < 1$. Thus, $0 < \det B < 1$.

Since $\gamma_1 > 0$, it follows that $\text{tr } B = 2 - T_s\gamma_2 - T_s^2\gamma_1/2 = 1 + \det B - T_s\gamma_1^2 < 1 + \det B$. Since $\det B > 0$, it follows that $|\text{tr } B| < |1 + \det B| = 1 + \det B$.

Finally, since $|\det B| < 1$ and $|\text{tr } B| < 1 + \det B$, it follows from [93, Fact 11.21.1] that the eigenvalues of B are in the open unit disk. Thus, the eigenvalues of $B \otimes I_m$ are in the open unit disk, and it follows from (3.23) that $\lim_{k \rightarrow \infty} q_a(k) = 0$ and $\lim_{k \rightarrow \infty} p_a(k) = 0$, which confirms (b). \square

Proof of Lemma 3. It follows from (3.24) and (3.25) that

$$\begin{aligned}
\Delta V(k_0) &= \sum_{(i,j) \in \mathcal{P}} \alpha_2 \frac{\|q_{ji}(k_0+1)\|^2 - \|q_{ji}(k_0)\|^2}{\alpha_1 + 1} \\
&\quad + \alpha_2 d^2 \ln \left(\frac{\alpha_1 + \|q_{ji}(k_0)\|^2/d^2}{\alpha_1 + \|q_{ji}(k_0+1)\|^2/d^2} \right) \\
&\quad + \lambda \|p_{ji}(k_0+1)\|^2 - \lambda \|p_{ji}(k_0)\|^2 \\
&= \sum_{(i,j) \in \mathcal{P}} \alpha_2 \frac{\|q_{ji}(k_0+1)\|^2 - \|q_{ji}(k_0)\|^2}{\alpha_1 + 1} \\
&\quad + \alpha_2 d^2 \ln \left(1 + \frac{(\|q_{ji}(k_0)\|^2 - \|q_{ji}(k_0+1)\|^2)/d^2}{\alpha_1 + \|q_{ji}(k_0+1)\|^2/d^2} \right) \\
&\quad + \lambda \|p_{ji}(k_0+1)\|^2 - \lambda \|p_{ji}(k_0)\|^2. \tag{3.29}
\end{aligned}$$

Since for all $\eta > 0$, $\ln \eta \leq \eta - 1$, it follows from (3.12) and (3.29) that $\Delta V(k_0) \leq W_1$, where

$$\begin{aligned}
W_1 &\triangleq \sum_{(i,j) \in \mathcal{P}} \alpha_2 \frac{\|q_{ji}(k_0+1)\|^2 - \|q_{ji}(k_0)\|^2}{\alpha_1 + 1} \\
&\quad + \alpha_2 \frac{\|q_{ji}(k_0)\|^2 - \|q_{ji}(k_0+1)\|^2}{\alpha_1 + \|q_{ji}(k_0+1)\|^2/d^2} \\
&\quad + \lambda \|p_{ji}(k_0+1)\|^2 - \lambda \|p_{ji}(k_0)\|^2 \\
&= \sum_{(i,j) \in \mathcal{P}} \phi(\|q_{ji}(k_0+1)\|) (\|q_{ji}(k_0+1)\|^2 - \|q_{ji}(k_0)\|^2) \\
&\quad + \lambda \|p_{ji}(k_0+1)\|^2 - \lambda \|p_{ji}(k_0)\|^2. \tag{3.30}
\end{aligned}$$

Define $\hat{q}_{ji}(k_0) \triangleq \hat{q}_j(k_0) - \hat{q}_i(k_0)$, and it follows from (A1), (3.19), and (3.20) that

$$\begin{aligned}
W_1 &= T_s \left[\sum_{(i,j) \in \mathcal{P}} 2\phi(\|\hat{q}_{ji}(k_0)\|) q_{ji}^T(k_0) p_{ji}(k_0) \right. \\
&\quad + T_s \phi(\|\hat{q}_{ji}(k_0)\|) q_{ji}^T(k_0) u_{ji}(q(k_0), p(k_0), \hat{q}(k_0)) \\
&\quad + 2\lambda p_{ji}^T(k_0) u_{ji}(q(k_0), p(k_0), \hat{q}(k_0)) \\
&\quad + T_s \phi(\|\hat{q}_{ji}(k_0)\|) \left\| p_{ji}(k_0) + \frac{1}{2} T_s u_{ji}(q(k_0), p(k_0), \hat{q}(k_0)) \right\|^2 \\
&\quad \left. + T_s \lambda \|u_{ji}(q(k_0), p(k_0), \hat{q}(k_0))\|^2 \right]. \tag{3.31}
\end{aligned}$$

Note that all terms in (3.31) are at time step k_0 . For notational convenience, we omit the argument k_0 from this point forward. Since (3.12) and (3.13) imply that $\sup_{\eta \geq 0} \phi(\eta) = \alpha_2/(\alpha_1 + 1) \leq 2\beta/T_s$, it follows from (3.31) that $W_1 \leq W_2$, where

$$W_2 \triangleq T_s \left[\sum_{(i,j) \in \mathcal{P}} 2\phi(\|\hat{q}_{ji}\|) q_{ji}^T p_{ji} \right.$$

$$\begin{aligned}
& + T_s \phi(\|\hat{q}_{ji}\|) q_{ji}^T u_{ji}(q, p, \hat{q}) \\
& + 2\lambda p_{ji}^T u_{ji}(q, p, \hat{q}) \\
& + 2\beta \left\| p_{ji} + \frac{1}{2} T_s u_{ji}(q, p, \hat{q}) \right\|^2 \\
& + T_s \lambda \|u_{ji}(q, p, \hat{q})\|^2.
\end{aligned} \tag{3.32}$$

Next, define

$$L_1 \triangleq \begin{bmatrix} n-1 & -1 & \cdots & -1 \\ -1 & n-1 & & \vdots \\ \vdots & & \ddots & -1 \\ -1 & \cdots & -1 & n-1 \end{bmatrix} \otimes I_m \in \mathbb{R}^{mn \times mn},$$

and

$$L_\phi \triangleq \begin{bmatrix} \sum_{j \in \mathcal{N}_1} \phi(\|\hat{q}_{j1}(k_0)\|) & -\phi(\|\hat{q}_{21}(k_0)\|) & \cdots & -\phi(\|\hat{q}_{n1}(k_0)\|) \\ -\phi(\|\hat{q}_{12}(k_0)\|) & \sum_{j \in \mathcal{N}_2} \phi(\|\hat{q}_{j2}(k_0)\|) & & \vdots \\ \vdots & & \ddots & -\phi(\|\hat{q}_{n(n-1)}(k_0)\|) \\ -\phi(\|\hat{q}_{1n}(k_0)\|) & \cdots & -\phi(\|\hat{q}_{(n-1)n}(k_0)\|) & \sum_{j \in \mathcal{N}_n} \phi(\|\hat{q}_{jn}(k_0)\|) \end{bmatrix} \otimes I_m \in \mathbb{R}^{mn \times mn},$$

and note that

$$\begin{aligned}
\sum_{(i,j) \in \mathcal{P}} \phi(\|\hat{q}_{ji}\|) q_{ji}^T p_{ji} & = 2q^T L_\phi p, \\
\sum_{(i,j) \in \mathcal{P}} \phi(\|\hat{q}_{ji}\|) q_{ji}^T u_{ji}(q, p, \hat{q}) & = 2q^T L_\phi u(q, p, \hat{q}), \\
\sum_{(i,j) \in \mathcal{P}} p_{ji}^T u_{ji}(q, p, \hat{q}) & = 2p^T L_1 u(q, p, \hat{q}), \\
\sum_{(i,j) \in \mathcal{P}} \left\| p_{ji} + \frac{1}{2} T_s u_{ji}(q, p, \hat{q}) \right\|^2 & = 2 \left[p + \frac{1}{2} T_s u(q, p, \hat{q}) \right]^T L_1 \left[p + \frac{1}{2} T_s u(q, p, \hat{q}) \right], \\
\sum_{(i,j) \in \mathcal{P}} \|u_{ji}(q, p, \hat{q})\|^2 & = 2u^T(q, p, \hat{q}) L_1 u(q, p, \hat{q}),
\end{aligned}$$

where

$$u(q, p, \hat{q}) \triangleq \begin{bmatrix} u_1(q, p, \hat{q}, 0, 0) \\ \vdots \\ u_n(q, p, \hat{q}, 0, 0) \end{bmatrix}.$$

Thus, it follows from (3.32) that

$$W_2 = 4T_s q^T L_\phi p + 2T_s^2 q^T L_\phi u(q, p, \hat{q})$$

$$\begin{aligned}
& + 4T_s \lambda p^T L_1 u(q, p, \hat{q}) \\
& + 4T_s \beta \left[p + \frac{1}{2} T_s u(q, p, \hat{q}) \right]^T L_1 \left[p + \frac{1}{2} T_s u(q, p, \hat{q}) \right] \\
& + 2T_s^2 \lambda u^T(q, p, \hat{q}) L_1 u(q, p, \hat{q}).
\end{aligned} \tag{3.33}$$

Next, let $\mathbf{1}_{n \times n} \in \mathbb{R}^{n \times n}$ denote the $n \times n$ matrix of ones, and define $\hat{\mathbf{1}} \triangleq \mathbf{1}_{n \times n} \otimes I_m \in \mathbb{R}^{mn \times mn}$. Since $(1/n)L_1 - I_{mn} = -(1/n)\hat{\mathbf{1}}$, it follows from (3.15) and (A2) that

$$\begin{aligned}
u(q, p, \hat{q}) &= -L_\phi q - \beta L_1 p + \frac{\gamma_1}{n} L_1 q + \frac{\gamma_2}{n} L_1 p - \gamma_1 q - \gamma_2 p \\
&= -L_\phi q - \beta L_1 p - \frac{\gamma_1}{n} \hat{\mathbf{1}} q - \frac{\gamma_2}{n} \hat{\mathbf{1}} p.
\end{aligned} \tag{3.34}$$

Since $L_1 \hat{\mathbf{1}} = 0_{mn \times mn}$ and $L_\phi \hat{\mathbf{1}} = 0_{mn \times mn}$, it follows from (3.33) and (3.34) that

$$\begin{aligned}
W_2 &= 2T_s^2 q^T L_\phi \left[-I_{mn} + \frac{1}{n} L_1 \right] L_\phi q \\
&+ 2T_s q^T L_\phi \left[2I_{mn} - 2 \left(T_s \beta + \frac{2}{n} \right) L_1 + \frac{2T_s \beta}{n} L_1^2 \right] p \\
&+ 2T_s \beta p^T \left[2L_1 - \left(T_s \beta + \frac{2}{n} \right) L_1^2 + \frac{T_s \beta}{n} L_1^3 \right] p.
\end{aligned}$$

Furthermore, since $(1/n)L_1 - I_{mn} = -(1/n)\hat{\mathbf{1}}$ and $L_1^2 = nL_1$, it follows that

$$\begin{aligned}
L_\phi \left[-I_{mn} + \frac{1}{n} L_1 \right] &= -\frac{1}{n} L_\phi \hat{\mathbf{1}} = 0_{mn \times mn}, \\
L_\phi \left[2I_{mn} - 2 \left(T_s \beta + \frac{1}{n} \right) L_1 + \frac{2T_s \beta}{n} L_1^2 \right] &= \frac{2}{n} L_\phi \hat{\mathbf{1}} = 0_{mn \times mn}, \\
2L_1 - \left(T_s \beta + \frac{2}{n} \right) L_1^2 + \frac{T_s \beta}{n} L_1^3 &= 0_{mn \times mn},
\end{aligned}$$

which implies that $W_2 = 0$. Therefore, $\Delta V(k_0) \leq W_1 \leq W_2 = 0$.

To prove that $\Delta V(k_0) = 0$ if and only if $q_{ji}(k_0 + 1) = q_{ji}(k_0)$, first assume that $q_{ji}(k_0 + 1) = q_{ji}(k_0)$. Thus, it follows from (3.29) and (3.30) that $\Delta V(k_0) = W_1$. Furthermore, it follows from (3.19) that $p_{ji}(k_0) + (T_s/2)u_{ji}(q(k_0), p(k_0), \hat{q}(k_0)) = 0$, and (3.31) and (3.32) imply that $W_1 = W_2$. Thus, $\Delta V(k_0) = W_1 = W_2 = 0$.

Conversely, assume that $\Delta V(k_0) = 0$. Since $0 = \Delta V(k_0) \leq W_1 \leq W_2 = 0$, it follows that $W_1 = W_2$. Therefore, (3.31) and (3.32) imply that

$$\sum_{(i,j) \in \mathcal{P}} (2\beta - T_s \phi(\|\hat{q}_{ji}(k_0)\|)) \left\| p_{ji}(k_0) + \frac{1}{2} T_s u_{ji}(q(k_0), p(k_0), \hat{q}(k_0)) \right\|^2 = 0.$$

Since (3.12) and (3.13) imply that for all $\eta \geq 0$, $T_s \phi(\eta) < T_s \alpha_2 / (\alpha_1 + 1) \leq 2\beta$, it follows that $2\beta - T_s \phi(\|\hat{q}_{ji}(k_0)\|) > 0$. Therefore, $p_{ji}(k_0) + (T_s/2)u_{ji}(q(k_0), p(k_0), \hat{q}(k_0)) = 0$, and (3.19) implies that $q_{ji}(k_0 + 1) = q_{ji}(k_0)$. \square

3.11 Proof of Theorems 4 and 5

Proof of Theorem 4. To show (a), assume $q(0)$ and $p(0)$ are such that $V(q(0), p(0)) < 2\psi(\delta_c)$. It follows from (A1) and Lemma 3 that for all $k \in \mathbb{N}$, $\Delta V(k) \leq 0$. Thus, (3.25) implies that for all $k \in \mathbb{N}$,

$$2\psi(\|q_{ji}(k)\|) \leq V(q(k), p(k)) \leq V(q(0), p(0)) < 2\psi(\delta_c).$$

Since $\psi(\|q_{ji}(k)\|) < \psi(\delta_c)$ and ψ is strictly decreasing on $[0, \delta_c]$, it follows that for all $k \in \mathbb{N}$, $\|q_{ji}(k)\| > \delta_c$, which confirms (a).

To show (d), let $\hat{q}_*: \mathcal{Q} \times \mathbb{R}^{mn} \times \mathbb{R}^m \times \mathbb{R}^m \rightarrow \mathbb{R}^{mn}$ satisfy

$$\hat{q}_*(q, p, q_g, p_g) = q + T_s p + \frac{1}{2} T_s^2 u(q, p, \hat{q}_*(q, p, q_g, p_g), q_g, p_g),$$

where

$$u(q, p, \hat{q}, q_g, p_g) \triangleq \begin{bmatrix} u_1(q, p, \hat{q}, q_g, p_g) \\ \vdots \\ u_n(q, p, \hat{q}, q_g, p_g) \end{bmatrix}.$$

Note that (3.1) and (A1) imply that for all $k \in \mathbb{N}$,

$$\hat{q}_*(q(k), p(k), q_g(k), p_g(k)) = q(k+1) = \hat{q}(k). \quad (3.35)$$

Also note that (3.15) implies that for all $(q, p, q_g, p_g) \in \mathbb{R}^{mn} \times \mathbb{R}^{mn} \times \mathbb{R}^m \times \mathbb{R}^m$,

$$[E_j - E_i] \hat{q}_*(q, p, q_g, p_g) = [E_j - E_i] \hat{q}_*(q, p, 0, 0). \quad (3.36)$$

Next, consider $D_V: \mathbb{R}^{mn} \times \mathbb{R}^{mn} \rightarrow \mathbb{R}$ defined by

$$D_V(q, p) \triangleq V(\hat{q}_*(q, p, 0, 0), p + T_s u(q, p, \hat{q}_*(q, p, 0, 0), 0, 0)) - V(q, p),$$

and define

$$\mathcal{R}_c \triangleq \{(q, p) \in \mathcal{Q} \times \mathbb{R}^{mn} : V(q, p) \leq V(q(0), p(0)) \text{ and } D_V(q, p) = 0\}.$$

It follows from (3.19), (3.20), (3.35), and (3.36) that $D_V(q(k), p(k)) = \Delta V(k)$. Thus, it follows from (3.35), (3.36), and Lemma 3 that

$$\mathcal{R}_c = \{(q, p) \in \mathcal{Q} \times \mathbb{R}^{mn} : V(q, p) \leq V(q(0), p(0)) \text{ and } [E_j - E_i][\hat{q}_*(q, p, 0, 0) - q] = 0\}. \quad (3.37)$$

Let $\mathcal{M}_c \subseteq \mathcal{R}_c$ be the largest invariant set with respect to (3.19)–(3.21) that is contained in \mathcal{R}_c . Let $\tilde{q}: \mathbb{N} \rightarrow \mathcal{Q}$ and $\tilde{p}: \mathbb{N} \rightarrow \mathbb{R}^{mn}$ be such that $(\tilde{q}(0), \tilde{p}(0)) \in \mathcal{M}_c$, and $q_{ji}(k) \equiv [E_j - E_i] \tilde{q}(k)$ and $p_{ji}(k) \equiv [E_j - E_i] \tilde{p}(k)$ satisfy the difference equations (3.19)–(3.21). Thus, for all $k \in \mathbb{N}$, $(\tilde{q}(k), \tilde{p}(k)) \in \mathcal{M}_c \subseteq \mathcal{R}_c$. For all $k \in \mathbb{N}$, define $\tilde{q}_{ji}(k) \triangleq [E_j - E_i] \tilde{q}(k)$ and $\tilde{p}_{ji}(k) \triangleq [E_j - E_i] \tilde{p}(k)$, and it follows from (3.35)–(3.37) that $\tilde{q}_{ji}(k+1) \equiv \tilde{q}_{ji}(k)$. Thus, (3.20) and (3.19) imply that for all $k \in \mathbb{N}$,

$$\tilde{p}_{ji}(k+1) = \tilde{p}_{ji}(k) + T_s u_{ji}(\tilde{q}(k), \tilde{p}(k), \tilde{q}(k+1))$$

$$\begin{aligned}
&= \tilde{p}_{ji}(k) + \frac{2}{T_s} [\tilde{q}_{ji}(k+1) - \tilde{q}_{ji}(k) - T_s \tilde{p}_{ji}(k)] \\
&= -\tilde{p}_{ji}(k).
\end{aligned} \tag{3.38}$$

Next, (3.15) and (3.21) imply that for all $k \in \mathbb{N}$,

$$u_{ji}(\tilde{q}(k), 0, \tilde{q}(k+1)) = u_{ji}(\tilde{q}(k+1), 0, \tilde{q}(k+2)). \tag{3.39}$$

Furthermore, (3.19) implies that for all $k \in \mathbb{N}$, $\tilde{p}_{ji}(k) = -(T_s/2)u_{ji}(\tilde{q}(k), \tilde{p}(k), \tilde{q}(k+1))$, which combined with (A2), (3.15), and (3.21) implies that for all $k \in \mathbb{N}$,

$$\tilde{p}_{ji}(k) = -\frac{1}{2}T_s u_{ji}(\tilde{q}(k), 0, \tilde{q}(k+1)) + \frac{1}{2}T_s n\beta \tilde{p}_{ji}(k). \tag{3.40}$$

Therefore, using (3.40) followed by (3.39), (3.40), and (3.38) yields that for all $k \in \mathbb{N}$,

$$\begin{aligned}
\left(1 - \frac{1}{2}T_s n\beta\right) \tilde{p}_{ji}(k) &= -\frac{1}{2}T_s u_{ji}(\tilde{q}(k), 0, \tilde{q}(k+1)) \\
&= -\frac{1}{2}T_s u_{ji}(\tilde{q}(k+1), 0, \tilde{q}(k+2)) \\
&= \left(1 - \frac{1}{2}T_s n\beta\right) \tilde{p}_{ji}(k+1) \\
&= -\left(1 - \frac{1}{2}T_s n\beta\right) \tilde{p}_{ji}(k),
\end{aligned}$$

which implies that $\tilde{p}_{ji}(k) = 0$ because $\beta < 2/(\bar{n}T_s) \leq 2/(nT_s)$. Since $\tilde{q}_{ji}(k+1) \equiv \tilde{q}_{ji}(k)$ and $\tilde{p}_{ji}(k) \equiv 0$, it follows from (3.19) that $u_{ji}(\tilde{q}(k), \tilde{p}(k), \tilde{q}(k+1)) \equiv 0$. Next, since $\tilde{q}_{ji}(k+1) \equiv \tilde{q}_{ji}(k)$, it follows from (3.15) and (3.21) that $u_{ji}(\tilde{q}(k), \tilde{p}(k), \tilde{q}(k)) \equiv u_{ji}(\tilde{q}(k), \tilde{p}(k), \tilde{q}(k+1)) \equiv 0$. Therefore, $\mathcal{M}_c \subseteq \mathcal{E}_c \triangleq \{(q_e, p_e) \in \mathcal{E} : V(q_e, p_e) \leq V(q(0), p(0))\}$.

Finally, it follows from Lemma 3 that for all $(q, p) \in \mathcal{Q} \times \mathbb{R}^{mn}$, $D_V(q, p) \leq 0$. Since, in addition, $\mathcal{M}_c \subseteq \mathcal{E}_c$ is the largest invariant set contained in \mathcal{R}_c , it follows from [92, Theorem 13.3] that $(q(k), p(k))$ converges to $\mathcal{M}_c \subseteq \mathcal{E}_c$. Thus, $(q(k), p(k))$ converges to \mathcal{E}_c , which confirms (d).

To show (b), let $\epsilon > 0$. Since $(q(k), p(k))$ converges to \mathcal{E}_c , let $k_\epsilon \in \mathbb{N}$ be such that for all $k \geq k_\epsilon$,

$$\inf_{(q_e, p_e) \in \mathcal{E}_c} \|p(k) - p_e\| < \frac{\epsilon}{\sqrt{n}}.$$

Since, in addition, for all $(q_e, p_e) \in \mathcal{E}_c$, $[E_j - E_i]p_e = 0$, it follows that for all $k \geq k_\epsilon$,

$$\begin{aligned}
\|p_{ji}(k)\| &= \|[E_j - E_i]p(k)\| \\
&= \inf_{(q_e, p_e) \in \mathcal{E}_c} \|E_j[p(k) - p_e] - E_i[p(k) - p_e]\| \\
&\leq \inf_{(q_e, p_e) \in \mathcal{E}_c} \|E_j[p(k) - p_e]\| + \|E_i[p(k) - p_e]\| \\
&\leq \inf_{(q_e, p_e) \in \mathcal{E}_c} \sum_{l \in \mathcal{I}} \|E_l[p(k) - p_e]\|
\end{aligned}$$

$$\begin{aligned}
&\leq \sqrt{n} \inf_{(q_e, p_e) \in \mathcal{E}_c} \sqrt{\sum_{l \in \mathcal{I}} \|E_l[p(k) - p_e]\|^2} \\
&= \sqrt{n} \inf_{(q_e, p_e) \in \mathcal{E}_c} \|p(k) - p_e\| \\
&< \epsilon.
\end{aligned}$$

Therefore, $\lim_{k \rightarrow \infty} p_{ji}(k) = 0$, which confirms (b).

To show (e), it follows from (3.20) that $T_s u_{ji}(q(k), p(k), q(k+1)) \equiv p_{ji}(k+1) - p_{ji}(k)$, and since $\lim_{k \rightarrow \infty} p_{ji}(k) = 0$, it follows that $\lim_{k \rightarrow \infty} u_{ji}(q(k), p(k), q(k+1)) = 0$. Next, note that (A2) implies that $u_{ji}(q(k), 0, q(k+1)) \equiv u_{ji}(q(k), p(k), q(k+1)) + n\beta p_{ji}(k)$. Since, in addition, $\lim_{k \rightarrow \infty} p_{ji}(k) = 0$ and $\lim_{k \rightarrow \infty} u_{ji}(q(k), p(k), q(k+1)) = 0$, it follows that $\lim_{k \rightarrow \infty} u_{ji}(q(k), 0, q(k+1)) = 0$. Consider $F_i: \mathbb{N} \rightarrow \mathbb{R}^m$ defined by $F_i(k) \triangleq \sum_{j \in \mathcal{N}_i(k)} \phi(\|q_{ji}(k+1)\|) q_{ji}(k)$, and note that $\sum_{j \in \mathcal{I}} F_j(k) \equiv 0$. Thus, $F_i(k) \equiv F_i(k) - \sum_{j \in \mathcal{I}} F_j(k) \equiv \sum_{j \in \mathcal{I} \setminus \{i\}} u_{ij}(q(k), 0, q(k+1))$. Since, in addition, $\lim_{k \rightarrow \infty} u_{ij}(q(k), 0, q(k+1)) = 0$, it follows that $\lim_{k \rightarrow \infty} F_i(k) = 0$, which confirms (e).

To show (c), let $\delta > 0$, and let $\delta_1 \in (0, \delta)$. Since $\lim_{k \rightarrow \infty} F_i(k) = 0$, let $k_1 \in \mathbb{N}$ be such that for all $k \geq k_1$,

$$\|F_i(k)\| \leq \frac{\phi(d + \delta_1/(n-1))(d + \delta_1/(n-1))}{n}. \quad (3.41)$$

Next, let $\delta_2 \triangleq \delta - \delta_1$. Since $\lim_{k \rightarrow \infty} p_{ji}(k) = 0$ and $\lim_{k \rightarrow \infty} u_{ji}(q(k), p(k), q(k+1)) = 0$, let $k_2 \geq k_1$ be such that for all $k \geq k_2$,

$$\max_{(i,j) \in \mathcal{P}} \left\| T_s p_{ji}(k) + \frac{1}{2} T_s^2 u_{ji}(q(k), p(k), q(k+1)) \right\| \leq \frac{\delta_2}{n-1}. \quad (3.42)$$

Assume for contradiction that there exists $k_\delta \geq k_2$ such that $\max_{(i,j) \in \mathcal{P}} \|q_{ji}(k_\delta)\| > d(n-1) + \delta$. Define $Q(j, i) \triangleq q_{ji}(k_\delta)$, $P(j, i) \triangleq p_{ji}(k_\delta)$, $\hat{Q}(j, i) \triangleq q_{ji}(k_\delta + 1)$, and $U(j, i) \triangleq u_{ji}(q(k_\delta), p(k_\delta), q(k_\delta + 1))$. Let $(l_1, l_n) \in \mathcal{P}$ be such that $\|Q(l_n, l_1)\| = \max_{(i,j) \in \mathcal{P}} \|Q(j, i)\|$, and let $l_2, \dots, l_{n-1} \in \mathcal{I}$ be such that: for all $(i, j) \in \mathcal{P}$, $l_i \neq l_j$; and for all $j \in \mathcal{I} \setminus \{n\}$,

$$Q^\top(l_{j+1}, l_j) Q(l_n, l_1) \geq 0. \quad (3.43)$$

To show that l_2, \dots, l_{n-1} exist, we consider 2 cases. First, assume for contradiction that there exists $l_0 \in \mathcal{I} \setminus \{l_1, l_n\}$ such that $Q^\top(l_0, l_1) Q(l_n, l_1) < 0$. Since $\|Q(l_n, l_1)\| = \max_{(i,j) \in \mathcal{P}} \|Q(j, i)\|$, it follows that

$$\begin{aligned}
\|Q(l_n, l_1)\|^2 &= Q^\top(l_n, l_0) Q(l_n, l_1) + Q^\top(l_0, l_1) Q(l_n, l_1) \\
&\leq \|Q(l_n, l_1)\|^2 + Q^\top(l_0, l_1) Q(l_n, l_1) \\
&< \|Q(l_n, l_1)\|^2,
\end{aligned}$$

which is a contradiction. Therefore, l_0 does not exist. Second, assume for contradiction that there exists $l_{n+1} \in \mathcal{I} \setminus \{l_1, l_n\}$ such that $Q^\top(l_{n+1}, l_n) Q(l_n, l_1) > 0$. Since $\|Q(l_n, l_1)\| = \max_{(i,j) \in \mathcal{P}} \|Q(j, i)\|$, it follows that

$$0 < Q^\top(l_{n+1}, l_n) Q(l_n, l_1) + \|Q(l_n, l_1)\|^2 - \|Q(l_n, l_1)\|^2$$

$$\begin{aligned}
&= Q^T(l_{n+1}, l_1)Q(l_n, l_1) - \|Q(l_n, l_1)\|^2 \\
&\leq \|Q(l_n, l_1)\|^2 - \|Q(l_n, l_1)\|^2 \\
&= 0,
\end{aligned}$$

which is a contradiction. Therefore, l_{n+1} does not exist. Thus, l_2, \dots, l_{n-1} exist.

Next, it follows from (3.43) that for all $(l_i, l_j) \in \mathcal{P}$ such that $l_i < l_j$,

$$Q^T(l_j, l_i)Q(l_n, l_1) = \sum_{o=i}^{j-1} Q^T(l_{o+1}, l_o)Q(l_n, l_1) \geq 0. \quad (3.44)$$

Since $\|Q(l_n, l_1)\| > d(n-1) + \delta$, it follows from (3.44) that

$$\begin{aligned}
(d(n-1) + \delta)\|Q(l_n, l_1)\| &< \|Q(l_n, l_1)\|^2 \\
&= \sum_{j=1}^{n-1} Q^T(l_{j+1}, l_j)Q(l_n, l_1) \\
&\leq (n-1) \max_{j \in \mathcal{I} \setminus \{n\}} Q^T(l_{j+1}, l_j)Q(l_n, l_1),
\end{aligned}$$

which implies that there exists $\omega \in \mathcal{I} \setminus \{n\}$ such that

$$\left(d + \frac{\delta}{n-1}\right) \|Q(l_n, l_1)\| < Q^T(l_{\omega+1}, l_\omega)Q(l_n, l_1). \quad (3.45)$$

Define $\mathcal{I}_1 \triangleq \{l_1, \dots, l_\omega\}$ and $\mathcal{I}_2 \triangleq \{l_{\omega+1}, \dots, l_n\}$. Since for all $(i, j) \in \mathcal{I}_1 \times \mathcal{I}_2$, $i \leq l_\omega < l_{\omega+1} \leq j$, it follows from (3.44) that $Q^T(l_{\omega+1}, l_\omega)Q(l_n, l_1) \leq Q^T(j, i)Q(l_n, l_1)$. Thus, (3.45) implies that for all $(i, j) \in \mathcal{I}_1 \times \mathcal{I}_2$,

$$d + \frac{\delta}{n-1} < \frac{Q^T(j, i)Q(l_n, l_1)}{\|Q(l_n, l_1)\|} \leq \|Q(j, i)\|. \quad (3.46)$$

Since $\delta = \delta_1 + \delta_2$, using (3.42) followed by (3.46) yields that for all $(i, j) \in \mathcal{I}_1 \times \mathcal{I}_2$,

$$\begin{aligned}
\|Q(j, i)\| - \left\|T_s P(j, i) + \frac{1}{2}T_s^2 U(j, i)\right\| &\geq \|Q(j, i)\| - \frac{\delta_2}{n-1} \\
&> d + \frac{\delta_1}{n-1},
\end{aligned}$$

which implies from (3.19) that for all $(i, j) \in \mathcal{I}_1 \times \mathcal{I}_2$,

$$\begin{aligned}
\|\hat{Q}(j, i)\| &= \left\|Q(j, i) + T_s P(j, i) + \frac{1}{2}T_s^2 U(j, i)\right\| \\
&\geq \left|\|Q(j, i)\| - \left\|T_s P(j, i) + \frac{1}{2}T_s^2 U(j, i)\right\|\right| \\
&> d + \frac{\delta_1}{n-1}.
\end{aligned}$$

Furthermore, since $\phi(d) = 0$ and ϕ is a strictly increasing function, it follows that for all $(i, j) \in \mathcal{I}_1 \times \mathcal{I}_2$, $0 < \phi(d + \delta_1/(n-1)) < \phi(\|\hat{Q}(j, i)\|)$. Since, in addition, for all $(i, j) \in \mathcal{I}_1 \times \mathcal{I}_2$, $i < j$, it follows from (3.44) that for all $(i, j) \in \mathcal{I}_1 \times \mathcal{I}_2$,

$$\phi(\|\hat{Q}(j, i)\|)Q^T(j, i)Q(l_n, l_1) > 0. \quad (3.47)$$

Finally, it follows from (3.46) followed by (3.47) that

$$\begin{aligned} \phi\left(d + \frac{\delta_1}{n-1}\right) \left(d + \frac{\delta_1}{n-1}\right) \|Q(l_n, l_1)\| &< \phi(\|\hat{Q}(l_n, l_1)\|) \|Q(l_n, l_1)\|^2 \\ &\leq \sum_{i \in \mathcal{I}_1} \sum_{j \in \mathcal{I}_2} \phi(\|\hat{Q}(j, i)\|) Q^T(j, i) Q(l_n, l_1). \end{aligned} \quad (3.48)$$

Since $\sum_{i \in \mathcal{I}_1} \sum_{j \in \mathcal{I}_1 \setminus \{i\}} \phi(\|\hat{Q}(j, i)\|) Q(j, i) = 0$, it follows from (A2) that

$$\sum_{i \in \mathcal{I}_1} \sum_{j \in \mathcal{I}_2} \phi(\|\hat{Q}(j, i)\|) Q(j, i) = \sum_{i \in \mathcal{I}_1} F_i(k_\delta).$$

Thus, it follows from (3.48) followed by (3.41) that

$$\begin{aligned} \phi\left(d + \frac{\delta_1}{n-1}\right) \left(d + \frac{\delta_1}{n-1}\right) \|Q(l_n, l_1)\| &< \sum_{i \in \mathcal{I}_1} F_i^T(k_\delta) Q(l_n, l_1) \\ &\leq \sum_{i \in \mathcal{I}_1} \|F_i(k_\delta)\| \|Q(l_n, l_1)\| \\ &\leq \sum_{i \in \mathcal{I}_1} \frac{1}{n} \phi\left(d + \frac{\delta_1}{n-1}\right) \left(d + \frac{\delta_1}{n-1}\right) \|Q(l_n, l_1)\| \\ &< \phi\left(d + \frac{\delta_1}{n-1}\right) \left(d + \frac{\delta_1}{n-1}\right) \|Q(l_n, l_1)\|, \end{aligned}$$

which is a contradiction. Therefore, for all $k \geq k_2$, $\max_{(i,j) \in \mathcal{P}} \|q_{ji}(k)\| \leq d(n-1) + \delta$, which confirms (c).

To show (f), assume $\gamma_1 = \gamma_2 = 0$, and it follows from (3.15) that $\sum_{j \in \mathcal{I}} u_j(q, p, \hat{q}, q_g, p_g) = 0$. Therefore, (3.2) implies that

$$\sum_{j \in \mathcal{I}} p_j(k+1) \equiv \sum_{j \in \mathcal{I}} p_j(k) + T_s u_j(q(k), p(k), \hat{q}(k), q_g(k), p_g(k)) \equiv \sum_{j \in \mathcal{I}} p_j(k).$$

Thus, $\sum_{j \in \mathcal{I}} p_j(k) \equiv \sum_{j \in \mathcal{I}} p_j(0)$. Moreover, $p_i(k) \equiv \sum_{j \in \mathcal{I}} [p_j(k) - p_{ji}(k)]/n \equiv \sum_{j \in \mathcal{I}} [p_j(0) - p_{ji}(k)]/n$, and since $\lim_{k \rightarrow \infty} p_{ji}(k) = 0$, it follows that $\lim_{k \rightarrow \infty} p_i(k) = \sum_{j \in \mathcal{I}} p_j(0)/n$, which confirms (f).

To show (g), assume $\gamma_1 \in [0, 2/T_s^2]$, $\gamma_2 \in (T_s \gamma_1/2, 1/T_s)$, and $u_g(k) \equiv 0$. Therefore, Lemma 2 implies that $\lim_{k \rightarrow \infty} p_a(k) = 0$. Since $u_g(k) \equiv 0$, it follows from (3.4) that $p_g(k) \equiv p_g(0)$. Since $p_a(k) + \sum_{j \in \mathcal{I}} p_{ji}(k)/n \equiv p_g(k) - p_i(k) \equiv p_g(0) - p_i(k)$, $\lim_{k \rightarrow \infty} p_a(k) = 0$, and $\lim_{k \rightarrow \infty} p_{ji}(k) = 0$, it follows that $p_g(0) - \lim_{k \rightarrow \infty} p_i(k) = 0$, which confirms (g).

To show (h), assume $\gamma_1 \in (0, 2/T_s^2)$, $\gamma_2 \in (T_s \gamma_1/2, 1/T_s)$, and $u_g(k) \equiv 0$. Therefore, part (b) of Lemma 2 implies that $\lim_{k \rightarrow \infty} q_a(k) = 0$, which confirms (h). \square

Proof of Theorem 5. To show that for all $k \in \mathbb{N}$, $V(q(k), p(k)) < 2\psi(r_c)$, we use induction on k . First, since $V(q(0), p(0)) < 2\psi(r_c)$, it follows that for $k = 0$, $V(q(k), p(k)) < 2\psi(r_c)$. Next, let $k_1 \in \mathbb{N}$, and assume that $V(q(k_1), p(k_1)) < 2\psi(r_c)$. It follows from (3.24) and (3.25) that $\psi(\|q_{ji}(k_1)\|) \leq V(q(k_1), p(k_1))$, which implies that $\psi(\|q_{ji}(k_1)\|) < \psi(r_c)$. Since, in addition ψ is strictly increasing on $[r_c, \infty)$, it follows that $\|q_{ji}(k_1)\| < r_c$, which implies that $q(k_1) \in \mathcal{Q}$. Thus, Lemma 3 implies that $\Delta V(k_1) \leq 0$, which implies that $V(q(k_1 + 1), p(k_1 + 1)) \leq V(q(k_1), p(k_1)) < 2\psi(r_c)$. Therefore, for all $k \in \mathbb{N}$, $V(q(k), p(k)) < 2\psi(r_c)$.

Since for all $k \in \mathbb{N}$, $V(q(k), p(k)) < 2\psi(r_c)$, it follows from (3.24) and (3.25) that for all $k \in \mathbb{N}$, $\psi(\|q_{ji}(k_1)\|) \leq V(q(k), p(k))/2 < \psi(r_c)$. Thus, for all $k \in \mathbb{N}$, $\|q_{ji}(k)\| < r_c$, which implies that $q(k) \in \mathcal{Q}$. Therefore, the assumptions of Theorem 4 are satisfied, which implies that parts (a)–(h) of Theorem 4 hold. \square

3.12 Propositions 4 and 5 used in the proof of Proposition 3

The following section is independent of the rest of the chapter. The proofs of the following 2 results are after the statement of the second result.

Proposition 4. Let $f > 0$ and $g > 0$, and define

$$M \triangleq \begin{bmatrix} 1 - f^2g & f - f^2 \\ -2fg & 1 - 2f \end{bmatrix} \in \mathbb{R}^{2 \times 2}.$$

Then, both eigenvalues of M are in the open disk if only if $f < \min\{1, 2/g\}$.

Proposition 5. Let $f > 0$ and $g > 0$, and define

$$M \triangleq \begin{bmatrix} 1 - f^2g & f - f^2 \\ -2fg & 1 - 2f \end{bmatrix} \in \mathbb{R}^{2 \times 2}.$$

Then, at least 1 of the eigenvalues of M is outside the closed unit disk if and only if $f > \min\{1, 2/g\}$.

Proof of Proposition 4. Define

$$r_1 \triangleq 1 - f - \frac{1}{2}f^2g - f\sqrt{\left(1 + \frac{1}{2}fg\right)^2 - 2g} \in \mathbb{C}, \quad (3.49)$$

$$r_2 \triangleq 1 - f - \frac{1}{2}f^2g + f\sqrt{\left(1 + \frac{1}{2}fg\right)^2 - 2g} \in \mathbb{C}, \quad (3.50)$$

which are the eigenvalues of A , and note that

$$\left(1 + \frac{1}{2}fg\right)^2 - 2g = \frac{g^2}{4} \left(f + \frac{2}{g} - \sqrt{\frac{8}{g}}\right) \left(f + \frac{2}{g} + \sqrt{\frac{8}{g}}\right). \quad (3.51)$$

Assume $f < \min\{1, 2/g\}$. We consider 3 cases: (i) $g \leq 2$ and $f \geq \sqrt{8/g} - 2/g$; (ii) $g \leq 2$ and $f < \sqrt{8/g} - 2/g$; and (iii) $g > 2$. Assume (i) $g \leq 2$ and $f \geq \sqrt{8/g} - 2/g$.

Since $g \leq 2$, it follows that $f < \min\{1, 2/g\} = 1$. Since $f \geq \sqrt{8/g} - 2/g$, it follows from (3.49)–(3.51) that r_1 and r_2 have 0 imaginary parts and $r_1 \leq r_2$. Since $f\sqrt{(1 + fg/2)^2 - 2g} < f(1 + fg/2)$, it follows from (3.50) that $r_2 < 1$. Since $f < 1$, it follows that

$$\begin{aligned}
\left(f\sqrt{\left(1 + \frac{1}{2}fg\right)^2 - 2g}\right)^2 &= f^2\left(1 + fg + \frac{1}{4}f^2g^2 - 2g\right) \\
&= \frac{1}{4}f^4g^2 + f^3g + f^2 - 2f^2g \\
&< \frac{1}{4}f^4g^2 + f^3g + f^2 - 2f^2g - 4f + 4 \\
&= \left(2 - \frac{1}{2}f^2g - f\right)^2.
\end{aligned} \tag{3.52}$$

Since $a < 1$ and $g \leq 2$, it follows that $2 - f^2g/2 - f > 0$. Therefore, (3.52) implies that

$$f\sqrt{\left(1 + \frac{1}{2}fg\right)^2 - 2g} < 2 - \frac{1}{2}f^2g - f,$$

which implies from (3.49) that

$$r_1 = 1 - f - \frac{1}{2}f^2g - f\sqrt{\left(1 + \frac{1}{2}fg\right)^2 - 2g} > -1.$$

Thus, $-1 < r_1 \leq r_2 < 1$, which implies that both eigenvalues of M are in the open unit disk.

Next, assume (ii) $g \leq 2$ and $f < \sqrt{8/g} - 2/g$. Since $g \leq 2$, it follows that $f < \min\{1, 2/g\} = 1$. Since $f < \sqrt{8/g} - 2/g$, it follows from (3.49)–(3.51) that r_1 and r_2 have nonzero imaginary parts and $|(1 + fg/2)^2 - 2g| = 2g - (1 + fg/2)^2$. Therefore, (3.49) and (3.50) imply that

$$\begin{aligned}
|r_1|^2 &= |r_2|^2 \\
&= \left(1 - f - \frac{1}{2}f^2g\right)^2 + f^2\left|\left(1 + \frac{1}{2}fg\right)^2 - 2g\right| \\
&= 1 + f^2 + \frac{1}{4}f^4g^2 - 2f - f^2g + f^3g + 2f^2g - f^2 - f^3g - \frac{1}{4}f^4g^2 \\
&= 1 - 2f + f^2g.
\end{aligned} \tag{3.53}$$

Since, in addition, $f < 1$ and $g \leq 2$, it follows from (3.53) that $|r_1| = |r_2| < 1$. Thus, both eigenvalues of M are in the open unit disk.

Next, assume (iii) $g > 2$, which implies that $f < \min\{1, 2/g\} = 2/g$. Since $f < 2/g$ and $2 < g$, it follows that $(1 + fg/2)^2 < 4 < 2g$, which implies from (3.49) and (3.50) that r_1 and r_2 have nonzero imaginary parts. Since, in addition, $f < 2/g$, it follows

from (3.53) that $|r_1| = |r_2| < 1$. Therefore, the eigenvalues of M are in the open unit disk.

Conversely, assume both eigenvalues of M are in the open unit disk. We consider 3 cases: (iv) $g < 2$ and $f < \sqrt{8/g} - 2/g$; (v) $g < 2$ and $f \geq \sqrt{8/g} - 2/g$; and (vi) $g \geq 2$. Assume (iv) $g < 2$ and $f < \sqrt{8/g} - 2/g$. Thus, $f < \sup_{g \in (0,2)} \sqrt{8/g} - 2/g = 1 = \min\{1, 2/g\}$.

Next, assume (v) $g < 2$ and $f \geq \sqrt{8/g} - 2/g$. Since $f \geq \sqrt{8/g} - 2/g$, it follows from (3.49) and (3.51) that r_1 has 0 imaginary part. Since, in addition, both eigenvalues of M are in the open unit disk, it follows that $-1 < r_1$. Thus, it follows from (3.49) that

$$\begin{aligned} \frac{1}{4}f^4g^2 + f^3g + f^2 - 2f^2g &= \left(f \sqrt{\left(1 + \frac{1}{2}fg\right)^2 - 2g} \right)^2 \\ &< \left(2 - \frac{1}{2}f^2g - f \right)^2 \\ &= \frac{1}{4}f^4g^2 + f^3g + f^2 - 2f^2g - 4f + 4, \end{aligned}$$

which implies that $f < 1$. Since $g < 2$, it follows that $1 = \min\{1, 2/g\}$. Therefore, $f < \min\{1, 2/g\}$.

Finally, assume (vi) $g \geq 2$. Assume for contradiction that $f \geq \sqrt{8/g} - 2/g$. Thus, (3.49) and (3.51) imply that r_1 has 0 imaginary part. Since, in addition, both eigenvalues of M are in the open unit disk, it follows that $r_1 > -1$. Therefore, it follows from (3.49) that

$$\begin{aligned} 0 &\leq f \sqrt{\left(1 + \frac{1}{2}fg\right)^2 - 2g} \\ &< -\frac{1}{2}f^2g - f + 2 \\ &= -\frac{g}{2} \left(f - \frac{1 + \sqrt{1+4g}}{g} \right) \left(f - \frac{1 - \sqrt{1+4g}}{g} \right), \end{aligned}$$

and thus, $f < (\sqrt{1+4g} - 1)/g$. Since $\sqrt{8/g} - 2/g \leq f < (\sqrt{1+4g} - 1)/g$, it follows that $\sqrt{8g} < 1 + \sqrt{1+4g}$. Squaring both sides yields that $8g < 2 + 4g + 2\sqrt{1+4g}$, or equivalently, $2g - 1 < \sqrt{1+4g}$. Squaring both sides again yields that $4g^2 - 4g + 1 < 1 + 4g$, or equivalently, $g < 2$, which is a contradiction because $g \geq 2$. Thus, $f < \sqrt{8/g} - 2/g$. Therefore, it follows from (3.49)–(3.51) that r_1 and r_2 have nonzero imaginary parts. Since, in addition, both eigenvalues of M are in the open unit disk, it follows from (3.53) that $1 - 2f + f^2g = |r_1|^2 = |r_2|^2 < 1$, which implies that $f < 2/g = \min\{1, 2/g\}$ because $g \geq 2$. \square

Proof of Proposition 5. Define

$$r_1 \triangleq 1 - f - \frac{1}{2}f^2g - f \sqrt{\left(1 + \frac{1}{2}fg\right)^2 - 2g} \in \mathbb{C}, \quad (3.54)$$

$$r_2 \triangleq 1 - f - \frac{1}{2}f^2g + f\sqrt{\left(1 + \frac{1}{2}fg\right)^2 - 2g} \in \mathbb{C}, \quad (3.55)$$

which are the eigenvalues of M , and note that

$$\left(1 + \frac{1}{2}fg\right)^2 - 2g = \frac{g^2}{4} \left(f + \frac{2}{g} - \sqrt{\frac{8}{g}}\right) \left(f + \frac{2}{g} + \sqrt{\frac{8}{g}}\right). \quad (3.56)$$

Assume $f > \min\{1, 2/g\}$. We consider 2 cases: (i) $f \geq \sqrt{8/g} - 2/g$, and (ii) $f < \sqrt{8/g} - 2/g$. First, assume (i) $f \geq \sqrt{8/g} - 2/g$, and it follows from (3.56) that r_1 and r_2 have 0 imaginary parts. Since, in addition, $f > 1$, it follows that

$$\begin{aligned} \left(f\sqrt{\left(1 + \frac{1}{2}fg\right)^2 - 2g}\right)^2 &= f^2 \left(1 + fg + \frac{1}{4}f^2g^2 - 2g\right) \\ &= \frac{1}{4}f^4g^2 + f^3g + f^2 - 2f^2g \\ &> \frac{1}{4}f^4g^2 + f^3g + f^2 - 2f^2g - 4f + 4 \\ &= \left(2 - \frac{1}{2}f^2g - f\right)^2, \end{aligned}$$

which implies from (3.54) that

$$r_1 = 1 - f - \frac{1}{2}f^2g - f\sqrt{\left(1 + \frac{1}{2}fg\right)^2 - 2g} < -1.$$

Thus, an eigenvalue of M is outside the closed unit disk.

Next, assume (ii) $f < \sqrt{8/g} - 2/g$, and it follows from (3.56) that r_1 and r_2 have nonzero imaginary parts. Therefore, it follows from (3.54) and (3.55) that

$$\begin{aligned} |r_1|^2 &= |r_2|^2 \\ &= \left(1 - f - \frac{1}{2}f^2g\right)^2 + f^2 \left|\left(1 + \frac{1}{2}fg\right)^2 - 2g\right| \\ &= 1 + f^2 + \frac{1}{4}f^4g^2 - 2f - f^2g + f^3g + 2f^2g - f^2 - f^3g - \frac{1}{4}f^4g^2 \\ &= 1 - 2f + f^2g. \end{aligned} \quad (3.57)$$

Since $f > 2/g$, it follows that $f^2g - 2f > 0$, which implies that $|r_1| = |r_2| > 1$. Thus, an eigenvalue of M is outside the closed unit disk.

Conversely, assume at least 1 eigenvalue of M is outside the closed unit disk. We consider 2 cases: (iii) $f \geq \sqrt{8/g} - 2g$, and (iv) $f < \sqrt{8/g} - 2g$. Assume (iii) $f \geq \sqrt{8/g} - 2g$, and it follows from (3.54)–(3.56) that r_1 and r_2 have 0 imaginary parts and $r_1 \leq r_2$. Since $\sqrt{(1 + fg/2)^2 - 2g} < 1 + fg/2$, it follows from (3.55) that

$r_2 \leq 1$. Since, in addition, at least 1 eigenvalue of M is outside the closed unit disk, it follows that $r_1 < -1$, which implies from (3.54) that

$$\begin{aligned} \frac{1}{4}f^4g^2 + f^3g + f^2 - 2f^2g &= \left(f\sqrt{\left(1 + \frac{1}{2}fg\right)^2 - 2g} \right)^2 \\ &> \left(2 - \frac{1}{2}f^2g - f \right)^2 \\ &= \frac{1}{4}f^4g^2 + f^3g + f^2 - 2f^2g - 4f + 4. \end{aligned}$$

Thus, $f > 1$. Assume for contradiction that $g \geq 2$, and, since $f > 1$ it follows that

$$-\frac{g}{2} \left(f - \frac{1 + \sqrt{1 + 4g}}{g} \right) \left(f - \frac{1 - \sqrt{1 + 4g}}{g} \right) = -\frac{1}{2}f^2g - f + 2 < 0,$$

which implies that $f < (\sqrt{1 + 4g} - 1)/g$. Since $\sqrt{8/g} - 2/g \leq f < (\sqrt{1 + 4g} - 1)/g$, it follows that $\sqrt{8g} < \sqrt{1 + 4g} + 1$. Squaring both sides yields that $8g < 2 + 4g + 2\sqrt{1 + 4g}$, which implies that $2g - 1 < \sqrt{1 + 4g}$. Squaring both sides again yields that $4g^2 - 4g + 1 = (2g - 1)^2 < 1 + 4g$, which implies that $g < 2$, which is a contradiction. Therefore, $g < 2$, which implies that $f > 1 = \min\{1, 2/g\}$.

Finally, assume (iv) $f < \sqrt{8/g} - 2/g$, and it follows from (3.54)–(3.56) that r_1 and r_2 have nonzero imaginary parts. Since, in addition, at least 1 eigenvalue of M is outside the closed unit disk, it follows from (3.57) that $1 < |r_1|^2 = |r_2|^2 = 1 - 2f + f^2g$, which implies that $f > 2/g$. Since $2/g < f < \sqrt{8/g} - 2/g$, it follows that $16/g^2 = (4/g)^2 < (\sqrt{8/g})^2 = 8/g$ or equivalently, $g > 2$. Therefore, $f > 2/g = \min\{1, 2/g\}$. \square

Chapter 4 Experimental Demonstrations of Discrete-Time Flocking Using Rotorcraft

We present results from experiments that use a group of three rotorcraft and the discrete-time flocking control in Chapter 3. We use a motion-capture system to sense each rotorcraft’s position. In addition, we use a centralized computer to calculate each rotorcraft’s control and transmit the control to the rotorcraft. The centralized computer is not required by the discrete-time flocking control but is used to simplify implementation. These experiments show that the rotorcraft tend to a flocking configuration both with and without a centralized leader. Furthermore, these experiments show that the rotorcraft approximately follow a leader (if applicable).

4.1 Introduction

Chapter 3 provides discrete-time flocking results and simulations showing that agents converge to a flocking configuration whether or not a leader agent is present. However, the results presented in Chapter 3 are based on simplified agent dynamics (i.e., discrete-time double-integrator dynamics) and do not account for real-world challenges such as sensor noise and time delay.

In this chapter, we examine the performance of the discrete-time flocking control in experiments with three rotorcraft. Implementing the discrete-time flocking control on rotorcraft allows us to analyze aspects of the control that are harder to analyze mathematically such as asynchronous sampling, measurement noise, and communication delays and dropouts.

Experimental demonstrations of formation-control algorithms are in [22, 23, 78–80]. Of these, [79, 80] consider quadcopters, but [79, 80] use a position-formation algorithm for cohesion, whereas this chapter uses a distance-formation approach.

In this chapter, we implement the discrete-time flocking control presented in Chapter 3. In order to implement the discrete-time flocking control in Chapter 3, we review pertinent aspects of the algorithm, and we describe the experimental setup. We present results of experiments where rotorcraft flock with and without a virtual leader agent.

4.2 Approximate Dynamics for an Attitude-Stabilized Quadcopter

Let the positive integer n be the number of rotorcraft, and define $\mathcal{I} \triangleq \{1, 2, \dots, n\}$, which is the rotorcraft index set. Unless otherwise stated, all statements that involve the subscript i are for all $i \in \mathcal{I}$.

Let F_E be the Earth frame, which is assumed to be an inertia frame and has orthogonal unit vectors \hat{i}_E , \hat{j}_E , and \hat{k}_E . The origin o_E of F_E is any point on the Earth's surface, and the \hat{i}_E - \hat{j}_E plane is parallel to the Earth's surface, which is assumed to be flat. Let F_i be a frame whose origin o_i is fixed to the quadcopter's center of mass and has orthogonal unit vectors \hat{i}_i , \hat{j}_i , and \hat{k}_i , where \hat{i}_i is directed through the nose (i.e., front) of the i th quadcopter and where $\hat{k}_i = \hat{k}_E$. Let $\psi_i \in (-\pi, \pi]$ be the angle from \hat{i}_E to \hat{i}_i as shown in Figure 4.1. Note that ψ_i is the yaw angle of the i th quadcopter. Thus, the direction cosine matrix of F_i relative to F_E is

$$\mathcal{O}(\psi_i) \triangleq \begin{bmatrix} \cos \psi_i & \sin \psi_i & 0 \\ -\sin \psi_i & \cos \psi_i & 0 \\ 0 & 0 & 1 \end{bmatrix}.$$

The position of o_i relative to o_E is denoted by \vec{r}_i as shown in Figure 4.1. The velocity of o_i relative to o_E with respect to F_E is denoted by $\dot{\vec{r}}_i^E$. The position and velocity are resolved in the Earth frame as $q_{c,i} \triangleq \vec{r}_i|_E$ and $p_{c,i} \triangleq \dot{\vec{r}}_i|_E$.

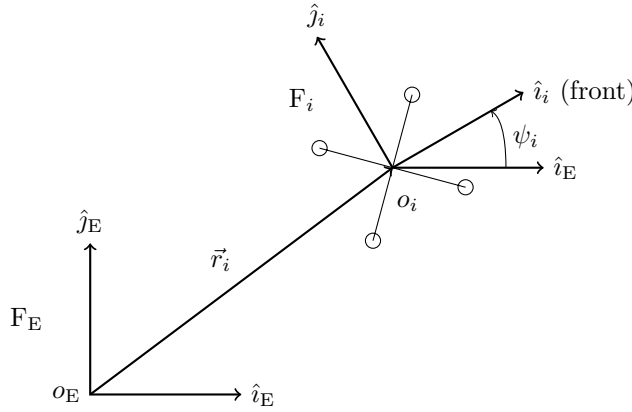


Figure 4.1: The position of the i th quadcopter's center of mass o_i relative to o_E is \vec{r}_i . The orientation of F_i relative to F_E is $\mathcal{O}(\psi_i)$, where ψ_i is the yaw angle, which is the angle from \hat{i}_E to \hat{i}_i . Note that $\hat{k}_E = \hat{k}_i$ is directed out of the page.

The rotorcraft used in our experiments are Parrot Rolling Spider quadcopters, and each one is attitude-stabilized by Parrot's proprietary inner-loop controller, which is implemented on each quadcopter's onboard processor. Note that we do not alter this inner-loop controller in any way. This inner-loop controller accepts an external force command $v_{c,i}(t) \in \mathbb{R}^3$, where the 3 elements of v_i are directed in the \hat{i}_i -, \hat{j}_i -, and \hat{k}_i -direction, respectively. The inner-loop controller also accepts an external yaw command; however, the yaw command is constant in all experiments in this chapter. These external commands can be provided a user operating a smartphone-simulated joystick or by an outer-loop controller, which is the method used in our experiments. Thus, the dynamics of each attitude-stabilized quadcopter are approximated by the double integrator

$$\dot{q}_{c,i}(t) = p_{c,i}(t), \quad (4.1)$$

$$\dot{p}_{c,i}(t) = u_{c,i}(t), \quad (4.2)$$

where $u_{c,i} \in \mathbb{R}^3$ is the external force command resolved in the Earth frame, which is determined from an outer-loop flocking controller; and $q_{c,i}(0)$ and $p_{c,i}(0)$ are the initial conditions. Thus,

$$v_{c,i}(t) = \mathcal{O}(\psi_i(t))u_{c,i}(t)$$

is the force command for the inner-loop controller as shown in Figure 4.2.

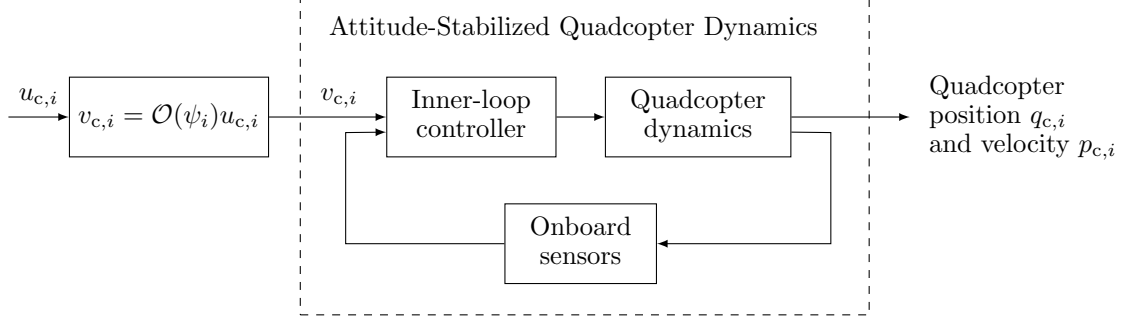


Figure 4.2: The Parrot Rolling Spider quadcopter is attitude-stabilized by Parrot’s proprietary inner-loop controller. The attitude-stabilized quadcopter dynamics are approximated by the double integrator (4.1) and (4.2).

In this chapter, we implement a modified version of the discrete-time flocking control from Chapter 3 in experiments with $n = 3$ rotorcraft. To implement the sampled-data controller, we sample the position $q_{c,i}(t)$ and velocity $p_{c,i}(t)$ with sample time $T_s > 0$ and apply a zero-order hold on the control input $u_{c,i}(t)$. Thus, for all $k \in \mathbb{N}$, the sampled position and velocity are $q_i(k) \triangleq q_{c,i}(kT_s)$ and $p_i(k) \triangleq p_{c,i}(kT_s)$. Furthermore, for all $k \in \mathbb{N}$ and all $t \in [kT_s, (k+1)T_s)$, $u_{c,i}(t) = u_i(k)$, where $u_i: \mathbb{N} \rightarrow \mathbb{R}^m$ is the control and $m = 3$ is the spatial dimension. In this case, we obtain the discrete-time dynamics

$$q_i(k+1) = q_i(k) + T_s p_i(k) + \frac{1}{2} T_s^2 u_i(k), \quad (4.3)$$

$$p_i(k+1) = p_i(k) + T_s u_i(k), \quad (4.4)$$

where $k \in \mathbb{N}$, and $q_i(0) = q_{c,i}(0)$ and $p_i(0) = p_{c,i}(0)$ are the initial conditions.

We also consider a flock leader, which is a virtual member of the flock, whose discrete-time dynamics are

$$q_g(k+1) = q_g(k) + T_s p_g(k) + \frac{1}{2} T_s^2 u_g(k), \quad (4.5)$$

$$p_g(k+1) = p_g(k) + T_s u_g(k), \quad (4.6)$$

where $k \in \mathbb{N}$; $q_g(k) \in \mathbb{R}^m$ and $p_g(k) \in \mathbb{R}^m$ are the position and velocity of the leader; $q_g(0)$ and $p_g(0)$ are the initial conditions; and $u_g: \mathbb{N} \rightarrow \mathbb{R}^m$ is an external forcing signal. The leader dynamics (4.5) and (4.6) take the form of a sampled-data double integrator and thus match the sampled-data dynamics (4.3) and (4.4).

4.3 Discrete-Time Flocking

Define $\mathcal{P} \triangleq \{(i, j) \in \mathcal{I} \times \mathcal{I} : i \neq j\}$, which is the set of ordered pairs, and let $\|\cdot\|$ denote the Euclidean norm. Let $\delta_c \geq 0$ be the *collision radius*, which is the desired minimum separation distance between rotorcraft. The rules for flocking are that rotorcraft stay close to one another, avoid collisions, and match velocities [16]. We use these rules to define asymptotic flocking. The rotorcraft in \mathcal{I} *flock with radius* $d > 0$ if the following conditions hold:

(F1) For all $(i, j) \in \mathcal{P}$ and all $k \in \mathbb{N}$,

$$\|q_j(k) - q_i(k)\| > \delta_c.$$

(F2) For all $(i, j) \in \mathcal{P}$,

$$\lim_{k \rightarrow \infty} [p_j(k) - p_i(k)] = 0.$$

(F3) There exists $k_1 \geq 0$ such that for all $k \geq k_1$ and all $i \in \mathcal{I}$,

$$\max_{j \in \mathcal{I} \setminus \{i\}} \|q_j(k) - q_i(k)\| \leq d(n-1).$$

Condition (F1) states that there are no collisions. Condition (F2) states that all rotorcraft approach the same velocity. Condition (F3) states that asymptotically each rotorcraft is at most a distance $d(n-1)$ away from its farthest neighbor.

In these experiments, we use $n = 3$ rotorcraft. In this case, it is possible to achieve a formation where each rotorcraft is d apart from all other rotorcraft. So, we also consider the condition:

(F4) For all $(i, j) \in \mathcal{P}$,

$$\lim_{k \rightarrow \infty} \|q_j(k) - q_i(k)\| = d.$$

Condition (F4) states that the distance between pairs of rotorcraft tends to d . For $n > 4$ rotorcraft, (F4) is not possible.

Next, we describe a modified version of the discrete-time flocking algorithm presented in Chapter 3. Let $r_c > \delta_c$ be the *communication radius*, which is the maximum distance at which a rotorcraft can sense another rotorcraft's relative position and relative velocity. For all $k \in \mathbb{N}$, define the *neighbor set*

$$\mathcal{N}_i(k) \triangleq \{j \in \mathcal{I} \setminus \{i\} : \|q_j(k) - q_i(k)\| < r_c\},$$

which is the set of rotorcraft whose distance to the i th rotorcraft is less than the communication radius r_c . Let $d \in (\delta_c, r_c)$ be the *flock radius*, which is the desired distance between adjacent rotorcraft in the flock. For all $k \in \mathbb{N}$, define the *attraction set*

$$\mathcal{A}_i(k) \triangleq \{j \in \mathcal{I} \setminus \{i\} : d \leq \|q_j(k) - q_i(k)\| < r_c\} \subseteq \mathcal{N}_i(k),$$

which is the set of rotorcraft whose distances from the i th rotorcraft are between the flock and communication radii, and define the *repulsion set*

$$\mathcal{R}_i(k) \triangleq \{j \in \mathcal{I} \setminus \{i\} : \|q_j(k) - q_i(k)\| < d\} \subseteq \mathcal{N}_i(k),$$

which is the set of rotorcraft whose distances to the i th rotorcraft are less than the flock radius. Note that for all $k \in \mathbb{N}$, $\mathcal{N}_i(k) = \mathcal{A}_i(k) \cup \mathcal{R}_i(k)$.

For each $k \in \mathbb{N}$, let $\hat{q}_i(k) \in \mathbb{R}^m$ be an estimate of $q_i(k+1)$, that is, $\hat{q}_i(k)$ is an estimate of the i th rotorcraft's position at the next sample time. Let $\bar{n} \geq n$ and $\bar{T}_s \geq T_s$. We assume \bar{n} and \bar{T}_s are known; however, n and T_s need not be known. For the experiments in this chapter, both n and T_s are known. Thus, we let $\bar{n} = n$ and $\bar{T}_s = T_s$.

To develop the flocking controller, let

$$\alpha_1 \in (0, \infty), \quad \alpha_2 \in \left(0, \frac{4(\alpha_1 + 1)}{\bar{n}\bar{T}_s^2}\right), \quad (4.7)$$

and consider $\phi: [0, \infty) \rightarrow [\alpha_2/(\alpha_1 + 1) - \alpha_2/\alpha_1, \alpha_2/(\alpha_1 + 1)]$ defined by

$$\phi(\eta) \triangleq \frac{\alpha_2}{\alpha_1 + 1} - \frac{\alpha_2}{\alpha_1 + \eta^2/d^2} = \frac{\alpha_2(\eta^2/d^2 - 1)}{(\alpha_1 + 1)(\alpha_1 + \eta^2/d^2)}. \quad (4.8)$$

Note that $\phi(d) = 0$; for all $\eta \in [0, d)$, $\phi(\eta) < 0$; and, for all $\eta \in (d, \infty)$, $\phi(\eta) > 0$. Next, let

$$\beta \in \left[\frac{\alpha_2\bar{T}_s}{2(\alpha_1 + 1)}, \frac{2}{\bar{n}\bar{T}_s}\right), \quad (4.9)$$

where the interval exists because $\alpha_2 < 4(\alpha_1 + 1)/(\bar{n}\bar{T}_s^2)$.

Let

$$\gamma_1 \in \left[0, \frac{2}{\bar{T}_s^2}\right), \quad \gamma_2 \in \left[\frac{\bar{T}_s\gamma_1}{2}, \frac{1}{\bar{T}_s}\right), \quad \gamma_3 \geq 0, \quad \gamma_4 \geq 0, \quad (4.10)$$

where the interval for γ_2 exists because $\gamma_1 < 2/\bar{T}_s^2$.

For all $k \in \mathbb{N}$, define

$$q(k) \triangleq \begin{bmatrix} q_1(k) \\ \vdots \\ q_n(k) \end{bmatrix}, \quad p(k) \triangleq \begin{bmatrix} p_1(k) \\ \vdots \\ p_n(k) \end{bmatrix}, \quad \hat{q}(k) \triangleq \begin{bmatrix} \hat{q}_1(k) \\ \vdots \\ \hat{q}_n(k) \end{bmatrix}.$$

Let $e_\ell \in \mathbb{R}^{1 \times 3}$ be the ℓ th row of 3×3 identity matrix. Consider the discrete-time flocking control with additional altitude guidance $u_i: \mathbb{R}^{mn} \times \mathbb{R}^{mn} \times \mathbb{R}^{mn} \times \mathbb{R}^m \times \mathbb{R}^m \rightarrow \mathbb{R}^m$ defined by

$$\begin{aligned} u_i(q, p, \hat{q}, q_g, p_g) \triangleq & \underbrace{\sum_{j \in \mathcal{A}_i} \phi(\|\hat{q}_j - \hat{q}_i\|)[q_j - q_i]}_{\text{Flock attraction}} + \underbrace{\sum_{j \in \mathcal{R}_i} \phi(\|\hat{q}_j - \hat{q}_i\|)[q_j - q_i]}_{\text{Flock repulsion}} \\ & + \underbrace{\sum_{j \in \mathcal{N}_i} \beta[p_j - p_i]}_{\text{Velocity consensus}} + \underbrace{\gamma_1[q_g - q_i] + \gamma_2[p_g - p_i]}_{\text{Guidance}} \end{aligned}$$

$$\begin{aligned}
& + \underbrace{\gamma_3 e_3^T e_3 [q_g - q_i] + \gamma_4 e_3^T e_3 [p_g - p_i]}_{\text{Additional altitude guidance}} \\
& - \underbrace{\left(\sum_{j \in \mathcal{N}_i} \frac{\gamma_1}{\text{card}(\mathcal{N}_i) + 1} [q_j - q_i] + \frac{\gamma_2}{\text{card}(\mathcal{N}_i) + 1} [p_j - p_i] \right)}_{\text{Flock correction to guidance}}, \quad (4.11)
\end{aligned}$$

where $\text{card}(\mathcal{N}_i)$ is the cardinality of \mathcal{N}_i . Thus, for all $k \in \mathbb{N}$ and all $t \in [kT_s, (k+1)T_s)$, the command to the quadcopter's inner-loop controller is

$$v_{c,i}(t) = v_i(q(k), p(k), \hat{q}(k), q_g(k), p_g(k), \psi_i(kT_s)),$$

where $v_i: \mathbb{R}^{mn} \times \mathbb{R}^{mn} \times \mathbb{R}^{mn} \times \mathbb{R}^m \times \mathbb{R}^m \times (-\pi, \pi] \rightarrow \mathbb{R}^m$ is defined by

$$v_i(q, p, \hat{q}, q_g, p_g, \psi_i) \triangleq \mathcal{O}(\psi_i) u_i(q, p, \hat{q}, q_g, p_g). \quad (4.12)$$

If $\gamma_3 = 0$ and $\gamma_4 = 0$, then (4.11) is identical to the discrete-time flocking control in Chapter 3. However, if $\gamma_3 = 0$ and $\gamma_4 = 0$, then the rotorcraft may move into a formation, where one rotorcraft is above another. In this case, the downwash from the higher-altitude rotorcraft may cause an undesirable disturbance on the lower-altitude rotorcraft. If $\gamma_3 > 0$ and $\gamma_4 > 0$, then the rotorcraft prioritize matching the leader's altitude more than its lateral position. In this case, the rotorcraft tend to a configuration that is parallel to the ground, that is, in the $\hat{i}_E - \hat{j}_E$ plane.

The estimate \hat{q}_i can be chosen in multiple ways. In this chapter, we use the estimate

$$\hat{q}_i(k) \equiv q_i(k) + T_s p_i(k),$$

which uses the sampled position and velocity of the current step to estimate the position at the next time step. It follows from (4.3) that for bounded u_i and sufficiently small T_s , the estimate $\hat{q}_i(k) \equiv q_i(k) + T_s p_i(k)$ is approximately equal to $q_i(k+1)$.

In this chapter, we compare our experimental results with the theoretical results in Theorem 6. We repeat the main result from Chapter 3 to make this chapter self contained. Consider $\psi: [0, \infty) \rightarrow [0, \infty)$ defined by

$$\psi(\eta) \triangleq 2\alpha_2 \int_d^\eta \frac{\sigma}{\alpha_1 + 1} - \frac{\sigma}{\alpha_1 + \sigma^2/d^2} d\sigma = \alpha_2 \left[\frac{\eta^2 - d^2}{\alpha_1 + 1} + d^2 \ln \frac{\alpha_1 + 1}{\alpha_1 + \eta^2/d^2} \right],$$

and consider the logarithmic potential function $V: \mathcal{Q} \times \mathbb{R}^{mn} \rightarrow [0, \infty)$ defined by

$$V(q, p) \triangleq \sum_{(i,j) \in \mathcal{P}} \psi(\| [E_j - E_i] q \|) + \lambda \| [E_j - E_i] p \|^2,$$

where

$$\lambda \triangleq \frac{1}{n} - \frac{1}{2} T_s \beta.$$

The following contains results related to the asymptotic flock configuration as well as the rotorcraft-averaged position and velocity are related to those of the leader.

Theorem 6. Consider the closed-loop dynamics in (4.3)–(4.6) and (4.11), where $\gamma_3 = \gamma_4 = 0$. Define $\mathcal{Q} \triangleq \{q \in \mathbb{R}^{mn} : \text{for all } (i, j) \in \mathcal{P}, \|q_j - q_i\| < r_c, \text{ where } q = [q_1^\top \dots q_n^\top]^\top\}$. Assume that for all $k \in \mathbb{N}$, $\hat{q}_i(k) = q_i(k+1)$ and $q(k) \in \mathcal{Q}$. Then, for all $q(0) \in \mathcal{Q}$, $p(0) \in \mathbb{R}^{mn}$, $q_g(0) \in \mathbb{R}^m$, and $p_g(0) \in \mathbb{R}^m$, the following statements hold:

(a) If $V(q(0), p(0)) < 2\psi(\delta_c)$, then for all $k \in \mathbb{N}$, $\|q_{ji}(k)\| > \delta_c$.

(b) $\lim_{k \rightarrow \infty} [p_j(k) - p_i(k)] = 0$.

(c) For all $\delta > 0$ there exists $k_\delta \in \mathbb{N}$ such that for all $k \geq k_\delta$,

$$\max_{(i,j) \in \mathcal{P}} \|q_j(k) - q_i(k)\| \leq d(n-1) + \delta.$$

(d) For all $i \in \mathcal{I}$, $\lim_{k \rightarrow \infty} \sum_{j \in \mathcal{A}_i(k) \cup \mathcal{R}_i(k)} \phi(\|\hat{q}_j(k) - \hat{q}_i(k)\|)[q_j(k) - q_i(k)] = 0$.

(e) If $\gamma_1 = \gamma_2 = 0$, then for all $k \in \mathbb{N}$,

$$\sum_{i \in \mathcal{I}} p_i(k) = \sum_{i \in \mathcal{I}} p_i(0),$$

and

$$\lim_{k \rightarrow \infty} p_i(k) = \frac{1}{n} \sum_{j \in \mathcal{I}} p_j(0).$$

(f) If $\gamma_2 \in (\bar{T}_s \gamma_1 / 2, 1 / \bar{T}_s)$, and $u_g(k) \equiv 0$, then $\lim_{k \rightarrow \infty} p_i(k) = p_g(0)$.

(g) If $\gamma_1 \in (0, 2 / \bar{T}_s^2)$, $\gamma_2 \in (\bar{T}_s \gamma_1 / 2, 1 / \bar{T}_s)$, and $u_g(k) \equiv 0$, then

$$\lim_{k \rightarrow \infty} \left[-q_g(k) + \frac{1}{n} \sum_{i \in \mathcal{I}} q_i(k) \right] = 0.$$

Note that Theorem 6 invokes 2 key assumptions: the estimate $\hat{q}_i(k)$ of the position at step $k+1$ equals the position $q_i(k+1)$, and the communication radius r_c is sufficiently large such that all agents communicate with each other at all times.

Part (a) implies that if $V(q(0), p(0)) < 2\psi(\delta_c)$, then there are no collisions, which implies (F1). Part (b) implies that the rotorcraft converge to the same velocity, which implies (F2). Part (c) implies that the relative position between agents is asymptotically bounded by $d(n-1)$, which implies (F3). Thus, parts (a)–(c) imply that the rotorcraft flock with radius d .

Part (d) implies that the sum of flock attraction and repulsion of each rotorcraft tends to 0. Numerical simulations suggest that for $n = 3$ and $m = 3$, if the sum of flock attraction and repulsion of each rotorcraft tends to 0, then the agents tend to a configuration, where each agent is d apart from other agents, which implies (F4).

Part (e) implies that if there is no leader, then the sum of velocities is constant. Furthermore, all rotorcraft tend to the average initial velocity. Part (f) implies that if the rotorcraft follow a leader and the leader has constant velocity, then each rotorcraft's velocity tends to the leader's velocity. Part (g) implies that if the rotorcraft follow and leader and the leader has constant velocity, then the rotorcraft-averaged position tends to the leader's position.

4.4 Description of Experimental Setup

In this section, we describe the hardware setup for implementing the discrete-time flocking control (4.11). The experimental hardware includes: rotorcraft, a motion-capture system, a desktop computer, and Android devices.

We use $n = 3$ Parrot Rolling Spider quadcopters. These quadcopters have 4 propellers whose thrust vectors point downward. By increasing or decreasing the thrust of all propellers, the quadcopter can move up and down. By increasing or decreasing the thrust of some propellers relative to the others, the quadcopter changes its orientation, which causes it to move laterally. Thus, quadcopters may move in approximately any direction.

Each Rolling Spider has a removable axle that we attach. The axle attaches to wheels, which serve as propeller guards, but we do not attach the wheels because they reduce mobility and battery life. We tape 4 infrared-reflective markers (specifically, Optitrack’s 6.9 mm markers with M3 base) to each Rolling Spider—one on the nose, one near the tail above the battery, and one on each end of the axle. All 4 markers are visible from the top of the Rolling Spider but not the bottom. The markers form a planar diamond configuration on the Rolling Spider as shown in Figure 4.3. The marker placement on each Rolling Spider is unique so that the motion-capture system can identify the Rolling Spiders based solely on the marker placement.



Figure 4.3: A picture of the Rolling Spider quadcopter with 4 attached markers for motion capture. The markers are arranged in a planar diamond configuration.

The quadcopters’ positions are tracked using an Optitrack motion-capture system that uses a combination of cameras, markers, and software to determine rigid-body positions and attitude. We use 6 OptiTrack Prime 13 cameras, which emit and receive infrared light to track objects. The cameras are arranged in a circular configuration,

pointed towards the test-flight volume, and angled slightly downward, as shown in Figure 4.4. The cameras are mounted on tripods and are approximately 3 m off the ground, and the collective tracking volume of the cameras is approximately 3 m by 4 m by 3 m. The cameras emit infrared light towards the infrared-reflective markers on the Rolling Spider quadcopters. Then, the cameras sense the light reflected from the infrared-reflect markers and send the pixel coordinates of all reflected light to the desktop computer for processing. All the cameras are connected to a switch using CAT6 cables, and the switch is connected to a desktop computer using a CAT6 cable.



Figure 4.4: The 6 OptiTrack Prime 13 cameras are mounted on tripods, arranged in a circular configuration, pointed towards the test-flight volume, and angled slightly downward.

The attached desktop computer runs Motive:Tracker, which is proprietary software developed by Optitrack for the motion-capture system. We use Motive:Tracker to build rigid bodies composed of the 4 markers on each Rolling Spider. Motive:Tracker tracks and streams position and attitude for each rigid body, but it does not calculate translational or angular velocity estimates. For each $k \in \mathbb{N} \setminus \{0\}$, we define the translational velocity estimate

$$\hat{p}_i(k) = \frac{1}{T_s} [q_i(k) - q_i(k-1)], \quad (4.13)$$

where $\hat{p}_i(0) = 0$ is the initial estimate. The velocity estimator (4.13) uses the backward-Euler rule. Thus, the control is $v_i(q(k), \hat{p}(k), \hat{q}(k), q_g(k), p_g(k), \psi_i(kT_s))$, where $\hat{p}(k) \triangleq [\hat{p}_1^T(k) \dots \hat{p}_n^T(k)]^T$ and v_i is defined by (4.12).

The discrete-time flocking control (4.11) allows each rotorcraft to compute its control independently; however, we use a centralized implementation for simplicity. In a centralized setting, computing each rotorcraft's control independently is computationally

inefficient. We can reduce the number of redundant calculations by computing every agent's control simultaneously. Consider the graph $\mathcal{G} = (\mathcal{I}, \mathcal{D})$, where \mathcal{I} is the vertex set and $\mathcal{D} \triangleq \{\{i, j\} \in \mathcal{I} \times \mathcal{I} : i \neq j\}$ is the set of unordered edges [94]. Define the unweighted Laplacian matrix associated with \mathcal{G}

$$L_1(\mathcal{G}) \triangleq \begin{bmatrix} n-1 & -1 & \dots & -1 \\ -1 & n-1 & & \vdots \\ \vdots & & \ddots & -1 \\ -1 & \dots & -1 & n-1 \end{bmatrix} \in \mathbb{R}^{n \times n},$$

and the weighted Laplacian matrix associated with \mathcal{G}

$$L_\phi(\mathcal{G}) \triangleq \begin{bmatrix} \sum_{j \in \mathcal{N}_1} \phi(\|\hat{q}_j - \hat{q}_1\|) & -\phi(\|\hat{q}_2 - \hat{q}_1\|) & \dots & -\phi(\|\hat{q}_n - \hat{q}_1\|) \\ -\phi(\|\hat{q}_1 - \hat{q}_2\|) & \sum_{j \in \mathcal{N}_2} \phi(\|\hat{q}_j - \hat{q}_2\|) & & \vdots \\ \vdots & & \ddots & -\phi(\|\hat{q}_n - \hat{q}_{(n-1)}\|) \\ -\phi(\|\hat{q}_1 - \hat{q}_n\|) & \dots & -\phi(\|\hat{q}_{(n-1)} - \hat{q}_n\|) & \sum_{j \in \mathcal{N}_n} \phi(\|\hat{q}_j - \hat{q}_n\|) \end{bmatrix} \in \mathbb{R}^{n \times n}.$$

The following example shows $L_1(\mathcal{G})$ and $L_\phi(\mathcal{G})$ for $n = 3$ and $\mathcal{N}_i = \mathcal{I} \setminus \{i\}$, which are the values used in the experiments.

Example 14. Let $n = 3$ rotorcraft, and assume $\mathcal{N}_i = \mathcal{I} \setminus \{i\}$, which implies that all rotorcraft communicate with one another. Then,

$$L_1(\mathcal{G}) = \begin{bmatrix} 2 & -1 & -1 \\ -1 & 2 & -1 \\ -1 & -1 & 2 \end{bmatrix},$$

and

$$L_\phi(\mathcal{G}) = \begin{bmatrix} \phi(\|\hat{q}_2 - \hat{q}_1\|) + \phi(\|\hat{q}_3 - \hat{q}_1\|) & -\phi(\|\hat{q}_2 - \hat{q}_1\|) & -\phi(\|\hat{q}_3 - \hat{q}_1\|) \\ -\phi(\|\hat{q}_2 - \hat{q}_1\|) & \phi(\|\hat{q}_2 - \hat{q}_1\|) + \phi(\|\hat{q}_3 - \hat{q}_2\|) & -\phi(\|\hat{q}_3 - \hat{q}_2\|) \\ -\phi(\|\hat{q}_3 - \hat{q}_1\|) & -\phi(\|\hat{q}_3 - \hat{q}_2\|) & \phi(\|\hat{q}_3 - \hat{q}_1\|) + \phi(\|\hat{q}_3 - \hat{q}_2\|) \end{bmatrix}. \quad \Delta$$

Let \otimes denote the Kronecker product, and define $\mathcal{L}_1(\mathcal{G}) \triangleq L_1(\mathcal{G}) \otimes I_m$ and $\mathcal{L}_\phi(\mathcal{G}) \triangleq L_\phi(\mathcal{G}) \otimes I_m$. Thus, the discrete-time flocking control with additional altitude guidance can be written as

$$\begin{bmatrix} u_1(q, \hat{p}, \hat{q}, q_g, p_g) \\ \vdots \\ u_n(q, \hat{p}, \hat{q}, q_g, p_g) \end{bmatrix} = \underbrace{-\mathcal{L}_\phi(\mathcal{G})q}_{\text{Flock attraction and repulsion}} \underbrace{-\beta\mathcal{L}_1(\mathcal{G})\hat{p}}_{\text{Velocity consensus}} + \underbrace{\gamma_1[1_n \otimes q_g - q] + \gamma_2[1_n \otimes p_g - \hat{p}]}_{\text{Guidance}} + \underbrace{\gamma_1[I_n \otimes e_3^T e_3][1_n \otimes q_g - q] + \gamma_2[I_n \otimes e_3^T e_3][1_n \otimes p_g - \hat{p}]}_{\text{Additional altitude guidance}}$$

$$\begin{aligned}
& + \underbrace{\left(\text{diag} \left\{ \frac{1}{\text{card}(\mathcal{N}_1)+1}, \dots, \frac{1}{\text{card}(\mathcal{N}_n)+1} \right\} \otimes I_m \right) \mathcal{L}_1(\mathcal{G})[\gamma_1 q + \gamma_2 \hat{p}]}_{\text{Flock correction to guidance}}, \\
\end{aligned} \tag{4.14}$$

where $1_n \in \mathbb{R}^n$ is the vector of ones. Then, v_i is computed from (4.12) using u_i and ψ_i .

After we compute each Rolling Spider's discrete-time flocking control v_i on the centralized computer, we relay the control v_i to the Rolling Spider. Note that it is possible to send the Rolling Spider control signals directly from the computer, but Android devices send control signals with less lag due to software optimization. Thus, we send the control signals v_i to $n = 3$ Android devices running a custom application that links each Android device to a Rolling Spider. The application receives the control v_i from Matlab and sends it to the linked Rolling Spider.

Figure 4.5 provides a block diagram of the control architecture. The Rolling Spider relies on inner- and outer-loop controllers. The inner-loop controller uses onboard sensing and input v_i . The onboard sensing of the rotorcraft uses sensor fusion of a 3-axis gyroscope, 3-axis accelerometer, vertical camera, and pressure sensor.

The outer-loop control uses the motion-capture cameras, velocity estimator, and inputs q_g and p_g . The motion-capture cameras use marker data to sense the position q_i and yaw angle ψ_i of each rotorcraft. The velocity estimator uses the current position $q_i(k)$ and previous position $q_i(k-1)$ to estimate the velocity at the current step $\hat{p}_i(k)$.

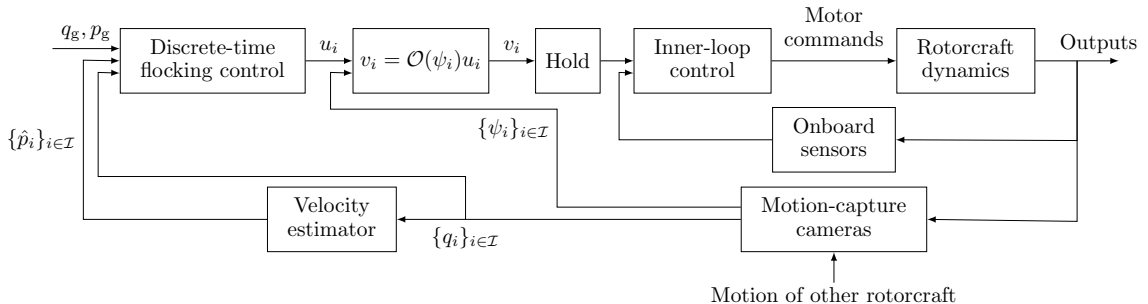


Figure 4.5: The Rolling Spider uses onboard sensing with input v_i for inner-loop control and the motion-capture system's sensing with input q_g and p_g for outer-loop control. The on-board sensing of the rotorcraft uses sensor fusion of a 3-axis gyroscope, 3-axis accelerometer, vertical camera, and pressure sensor. The motion-capture cameras use marker data to sense the position q_i and yaw angle ψ_i of each rotorcraft. The velocity estimator uses the current position $q_i(k)$ and previous position $q_i(k-1)$ to compute the velocity estimate $\hat{p}_i(k)$.

Figure 4.6 provides a data-flow diagram for the experiments. Figure 4.6 shows that there are 4 types of hardware used in the experimental demonstrations.

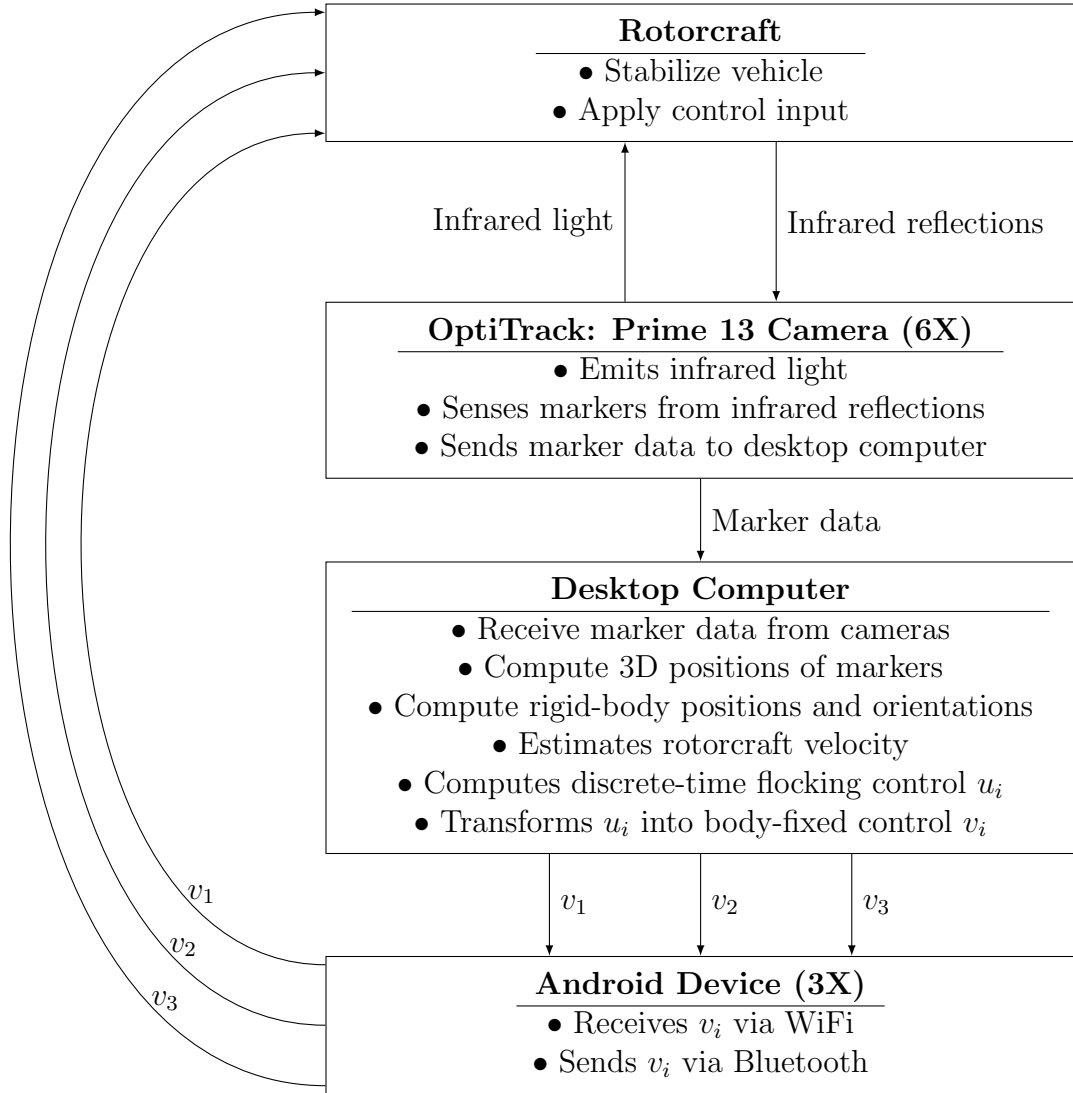


Figure 4.6: Setup of discrete-time flocking control demonstration for $n = 3$ rotorcraft. The boxes represent pieces of hardware, and the arrows denote what is sent from one piece of hardware to the next. The cameras emit infrared light that is reflected by the rotorcraft. The cameras send the marker data to the desktop computer. The computer transforms the marker data into rigid bodies and computes the velocity estimate \hat{p}_i and discrete-time flocking control in the body-fixed frame v_i for each rotorcraft. The Android devices receive the respective controls and send the control to the rotorcraft, which closes the loop.

4.5 Results and Discussion

In this section, we present results from experiments using $n = 3$ rotorcraft, where the discrete-time flocking algorithm (4.11) and (4.12) is implemented in a multi-loop control architecture as described in the previous section. We use $T_s = 0.055$ s for all demonstrations. Unless stated otherwise, the parameters for the discrete-time flocking

control are $\alpha_1 = 0.001$, $\alpha_2 = 0.024$, $\beta = 0.032$, $\gamma_1 = 0.080$, $\gamma_2 = 0.056$, $\gamma_3 = 0.140$, $\gamma_4 = 0.076$, $\delta_c = 200$ mm, $d = 550$ mm, and $r_c = 5000$ mm. We use the estimate $\hat{q}_i(k) \equiv q_i(k) + T_s p_i(k)$.

We developed a series of calibration experiments to determine values for the parameters α_1 , α_2 , β , γ_1 , γ_2 , γ_3 , γ_4 , d , and r_c . First, we determined a safe distance between rotorcraft so that, outside that distance, the rotorcraft do not experience interaction forces from each other's propeller thrust. In order to avoid multiple mid-flight collisions that could damage the rotorcraft, we conducted a grounded experiment with 2 rotorcraft and determined that 200 mm apart is a safe minimum distance. Thus, we let $\delta_c = 200$ mm. We set $r_c = 5000$ mm so that the rotorcraft detect one another in the test-flight volume. To determine d , α_1 , α_2 , β , γ_1 , γ_2 , γ_3 , and γ_4 , we initialized the values to arbitrarily small or large numbers depending on what makes the control gains small and the rotorcraft less like to crash. Specifically, we started with large values of d , β , γ_2 , and γ_4 , and small values of α_1 , α_2 , γ_1 , and γ_3 . After initializing the values, we analyzed the performance of the discrete-time flocking control on the rotorcraft. If the rotorcraft crashed, we decreased α_1 , α_2 , and γ_1 , and increased β , γ_2 , and γ_4 . If the rotorcraft slowly flocked and followed a leader, we increased α_2 , γ_1 , and γ_3 . If the rotorcraft saturated the control, then we decreased parameters. If the rotorcraft flocked well, then we decreased d . The listed set of parameters represents a balance of fast convergence rate to a flocking configuration, fast convergence rate to the leader, small d , and no collisions.

We implement the discrete-time flocking control (4.11) and (4.12) with $\hat{p}_i(k) \equiv p_i(k)$. Note that for all $k \in \mathbb{N}$, $q_{c,i}(kT_s) = q_i(k)$. Thus, we plot sampled-data positions and estimated velocities at times $t = kT_s$, where $k \in \mathbb{N}$.

In the following demonstrations, the rotorcraft start in grounded positions distributed around the motion-capture volume. When the rotorcraft take off, we set $u_i(k) = 0$ for approximately 3 seconds. The space between rotorcraft is chosen so that there are no collisions when the rotorcraft takeoff. Once the rotorcraft take off and are hovering in place, Matlab begins recording the positions and velocities of rotorcraft and computes and sends the control signals. Unless otherwise specified, all positions are measured in millimeters, and all velocities are measured in millimeters per second.

Demonstration 1: Rotorcraft Flock Without a Leader

Let $\gamma_1 = \gamma_2 = \gamma_3 = \gamma_4 = 0$, which implies that the rotorcraft do not try to follow the leader's position or match the leader's velocity. Thus, the rotorcraft do not attempt to go to the same altitude. Figure 4.7 shows the trajectory of the $n = 3$ rotorcraft. Figure 4.7 demonstrates that by $t = 3.5$ s, the rotorcraft are flocking and maintain their configuration for the remainder of the experiment, which lasts for $t = 20$ s. Figure 4.8 shows that the distance between each pair of rotorcraft tends to approximately d , which agrees with parts (c) and (d) of Theorem 6. In addition, Figure 4.8 shows that the velocity difference between each pair of rotorcraft is stays close to 0 in steady state, whereas part (b) of Theorem 6 implies that the velocity difference between each pair of rotorcraft tends to 0.

We examine the last 10 seconds of the experiment to quantify the steady-state

results. Over all pairs of rotorcraft and over the last 10 seconds of the experiment, the average distance between each pair of rotorcraft is 557 mm with standard deviation 52.8 mm, and the average norm of the velocity difference is 185 mm/s with standard deviation 100 mm/s. The standard deviation of the steady-state norm of the velocity difference is approximately double that of the of distance, which we suspect is because the velocity estimate uses 2 sampled positions.

Figure 4.9 shows that the rotorcraft-averaged velocity is approximately constant, which agrees with part (e) of Theorem 6. Because the rotorcraft-averaged velocity is approximately constant, the rotorcraft tend to drift approximately in the direction of the rotorcraft-averaged initial velocity. The standard deviation of the average velocity over all sampled points is $[68.3 \ 62.0 \ 60.7]$ mm/s.

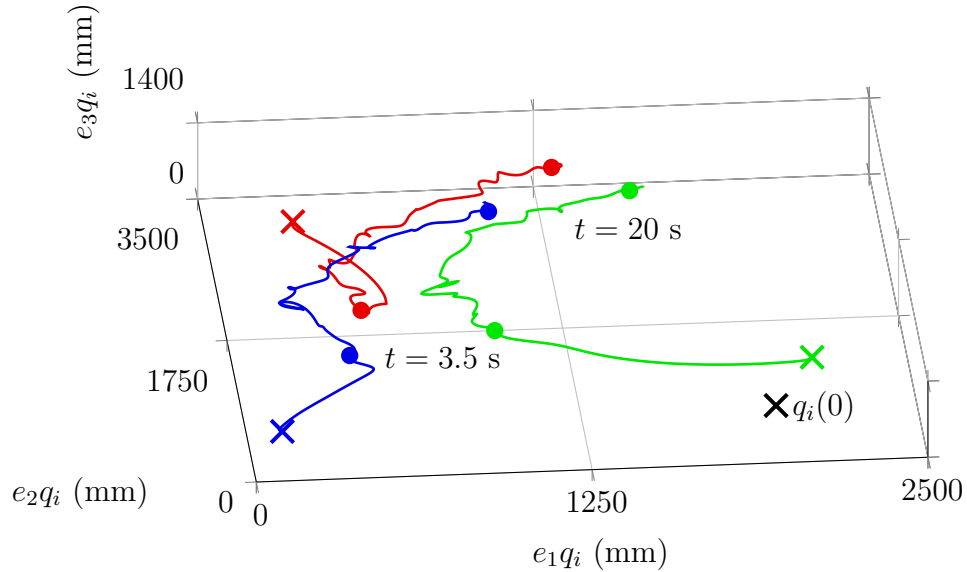


Figure 4.7: The trajectory of $n = 3$ rotorcraft that flock without a leader. The rotorcraft start from random positions in a hover maneuver with approximately 0 velocity. By $t = 3.5$ s, the rotorcraft are flocking and keep their configuration for the remainder of the experiment, which lasts for $t = 20$ s.

Demonstration 2: Rotorcraft Flock and Approach a Stationary Leader

This experiment shows that for a stationary leader, the rotorcraft move into a flocking configuration around the leader. The initial conditions of the leader are

$$q_g(0) = \begin{bmatrix} 200 \\ -1000 \\ 1000 \end{bmatrix}, \quad p_g(0) = \begin{bmatrix} 0 \\ 0 \\ 0 \end{bmatrix}, \quad u_g(k) \equiv \begin{bmatrix} 0 \\ 0 \\ 0 \end{bmatrix}.$$

Since $p_g(0) = 0$ and $u_g(k) \equiv 0$, it follows from (4.5) and (4.6) that $q_g(k) \equiv q_g(0)$. Figure 4.10 shows an abbreviated trajectory of the rotorcraft and leader from $t = 2.4$ s

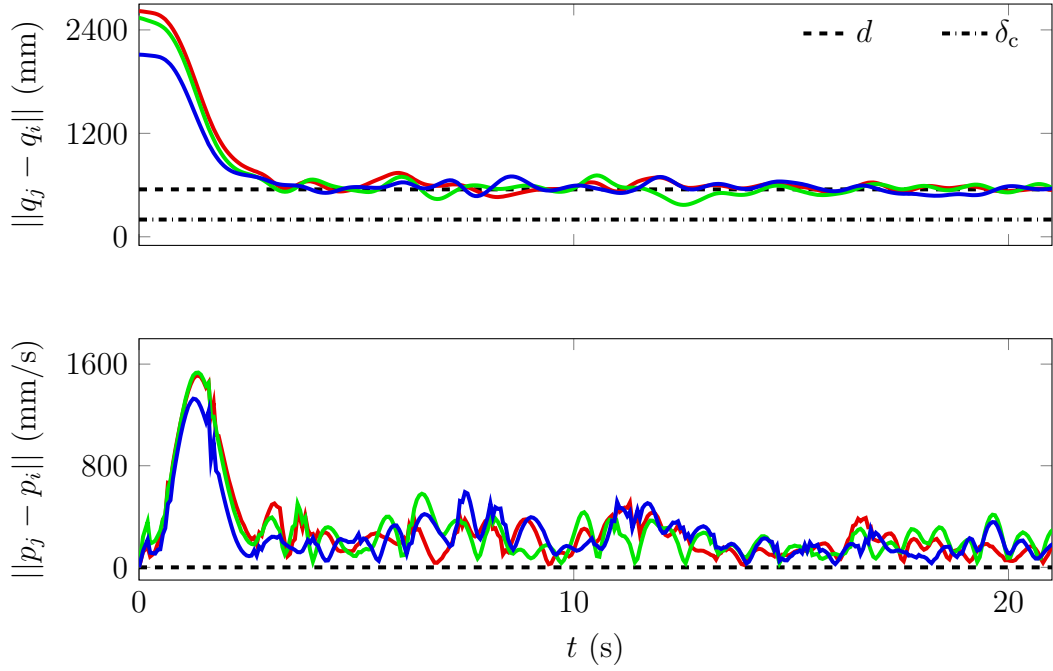


Figure 4.8: The distance and norm of the velocity difference between each pair of rotorcraft. The distance between each pair of rotorcraft tends to approximately d , and the norm of the velocity difference between each pair of rotorcraft stays close to 0 in steady state.

to $t = 20$ s. The first 2.4 s are omitted for clarity of the plot. Figure 4.11 shows that the distance between each pair of rotorcraft tends to approximately d , which agrees with parts (c) and (d) of Theorem 6. Figure 4.12 shows that the rotorcraft-averaged position and velocity tend approximately to the leader's position and velocity, which agrees with parts (f) and (g) of Theorem 6.

We examine the last 10 seconds of the experiment to quantify the steady-state results. Over all pairs of rotorcraft and over the last 10 seconds of the experiment, the average distance between each pair of rotorcraft is 544 mm the average norm of the velocity difference is 191 mm/s, the average norm of the difference between the rotorcraft-averaged position and the leader's position is 40.0 mm, and the average norm of the difference between the rotorcraft-averaged velocity and the leader's velocity is 75.2 mm/s. The standard deviation of the norm of the difference between the rotorcraft-averaged position and the leader's position is 25.4 mm, and the standard deviation of the norm of the difference between the rotorcraft-averaged velocity and the leader's velocity is 32.0 mm/s.

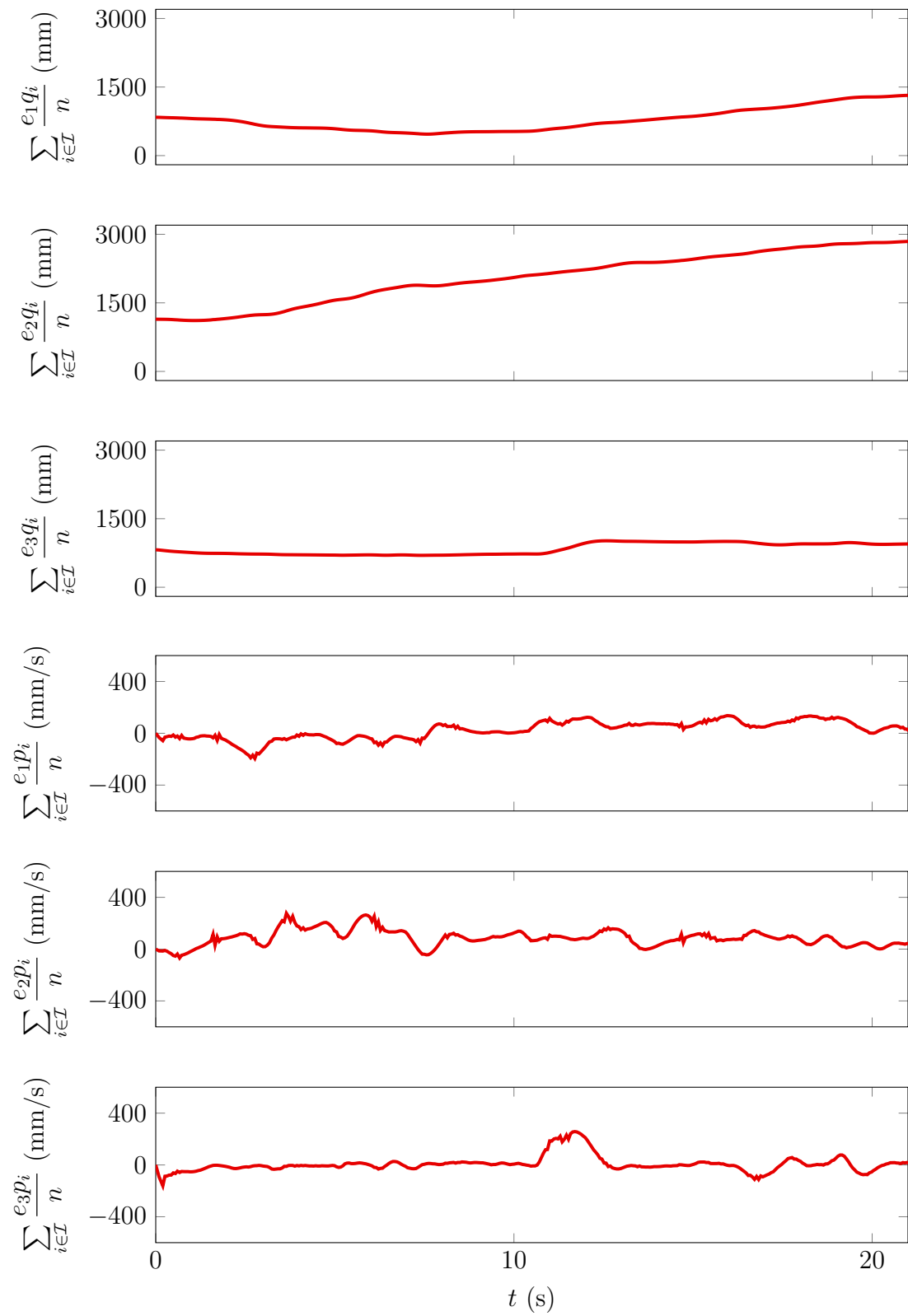


Figure 4.9: The rotorcraft-averaged velocity is approximately constant.

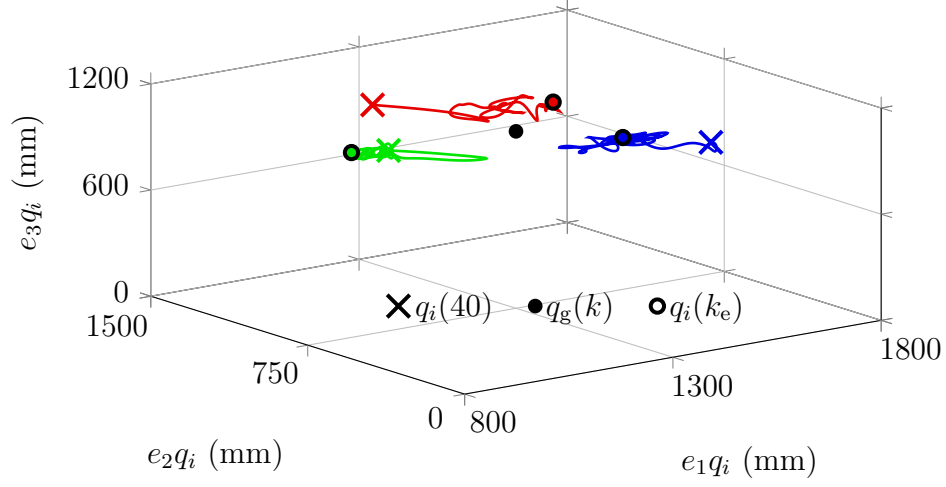


Figure 4.10: The trajectory of $n = 3$ rotorcraft that flock and follow a stationary leader. The plot of the trajectory starts at $t = 2.4$ s ($k = 40$) and shows that the rotorcraft flock around the leader. The time step $k_e \in \mathbb{N}$ is the last measured step in the experiment.

Demonstration 3: Rotorcraft Follow a Leader With a Helical Trajectory

This experiment examines rotorcraft following a leader with a helical trajectory. The initial conditions of the leader are

$$q_g(0) = \begin{bmatrix} 790 \\ -500 \\ 800 \end{bmatrix}, \quad p_g(0) = \begin{bmatrix} 0 \\ 475 \\ 50 \end{bmatrix}.$$

Define

$$A_1 \triangleq \begin{bmatrix} 1 & T_s \\ 0 & 1 \end{bmatrix} \in \mathbb{R}^{2 \times 2}, \quad B_1 \triangleq \begin{bmatrix} \frac{1}{2}T_s^2 \\ T_s \end{bmatrix} \in \mathbb{R}^2,$$

and note that (A_1, B_1) is controllable. Therefore, [95, Theorem 2.17] implies that the eigenvalues of $A_1 + B_1 K_1$, where $K_1 \in \mathbb{R}^{1 \times 2}$, can be arbitrarily assigned. Let \exp be the exponential function and $j \triangleq \sqrt{-1}$. Let $k_1, \dots, k_4 \in \mathbb{R}$ be such that $A_1 + B_1 [k_1 \ k_2]$ has eigenvalues $\pm \exp j/30$ and $A_1 + B_1 [k_3 \ k_4]$ has eigenvalues $\pm \exp j/100$. Let

$$K \triangleq \begin{bmatrix} k_1 & 0 & 0 & k_2 & 0 & 0 \\ 0 & k_1 & 0 & 0 & k_2 & 0 \\ 0 & 0 & k_3 & 0 & 0 & k_4 \end{bmatrix} \in \mathbb{R}^{3 \times 6}, \quad (4.15)$$

and consider the external forcing signal

$$u_g(q_g, p_g) = K \begin{bmatrix} q_g \\ p_g \end{bmatrix}. \quad (4.16)$$

Then, it follows from (4.5), (4.6), and (4.16) that q_g and p_g satisfy the closed-loop dynamics

$$\begin{bmatrix} q_g(k+1) \\ p_g(k+1) \end{bmatrix} = \tilde{A} \begin{bmatrix} q_g(k) \\ p_g(k) \end{bmatrix}, \quad (4.17)$$

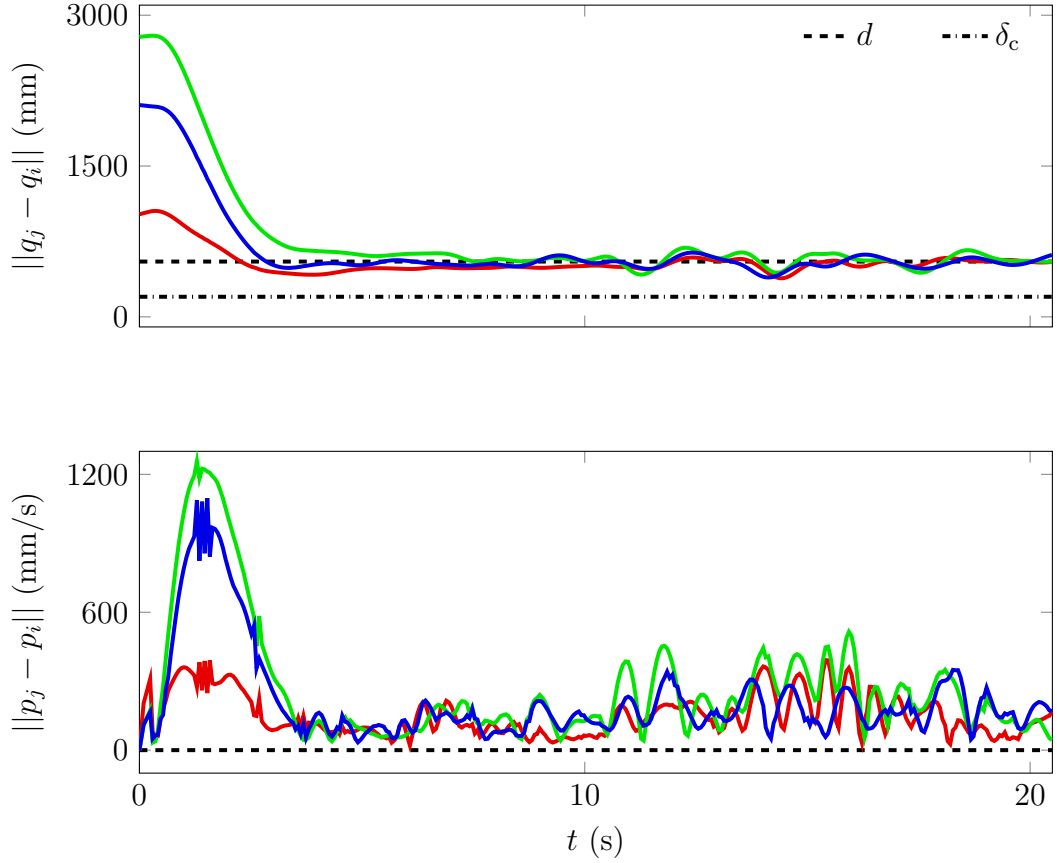


Figure 4.11: The distance and norm of the velocity difference between pairs of rotorcraft. The distance between each pair of rotorcraft tends to approximately d , and the norm of the velocity difference between each pair of rotorcraft is bounded.

where

$$\tilde{A} \triangleq A_1 \otimes I_m + (B_1 \otimes I_m) K. \quad (4.18)$$

The closed-loop leader dynamics (4.17) and (4.18) are linear and time invariant. Moreover, \tilde{A} is similar to

$$\text{diag}\{A_1 + B_1 [k_1 \ k_2], A_1 + B_1 [k_1 \ k_2], A_1 + B_1 [k_3 \ k_4]\}.$$

Thus, all the eigenvalues of \tilde{A} have magnitude 1, and the repeated eigenvalues are semisimple. Therefore, $(q_g(k), p_g(k)) \equiv (0, 0)$ is a Lyapunov stable equilibrium of (4.17). Moreover, the free response of (4.17) to nonzero initial conditions is sinusoidal.

Figure 4.13 shows the trajectory of the rotorcraft and leader. In particular, the top plot displays snapshots of the trajectory from $t = 0$ s to $t = 15$ s and corresponds to the leader ascending the helix. The bottom plot displays snapshots of the trajectory from $t = 18$ s to $t = 45$ s and corresponds to the leader descending the helix. Figure 4.14 shows that the distance between each pair of rotorcraft tends to approximately d , which is the expected result based on parts (c) and (d) of Theorem 6. Figure 4.15

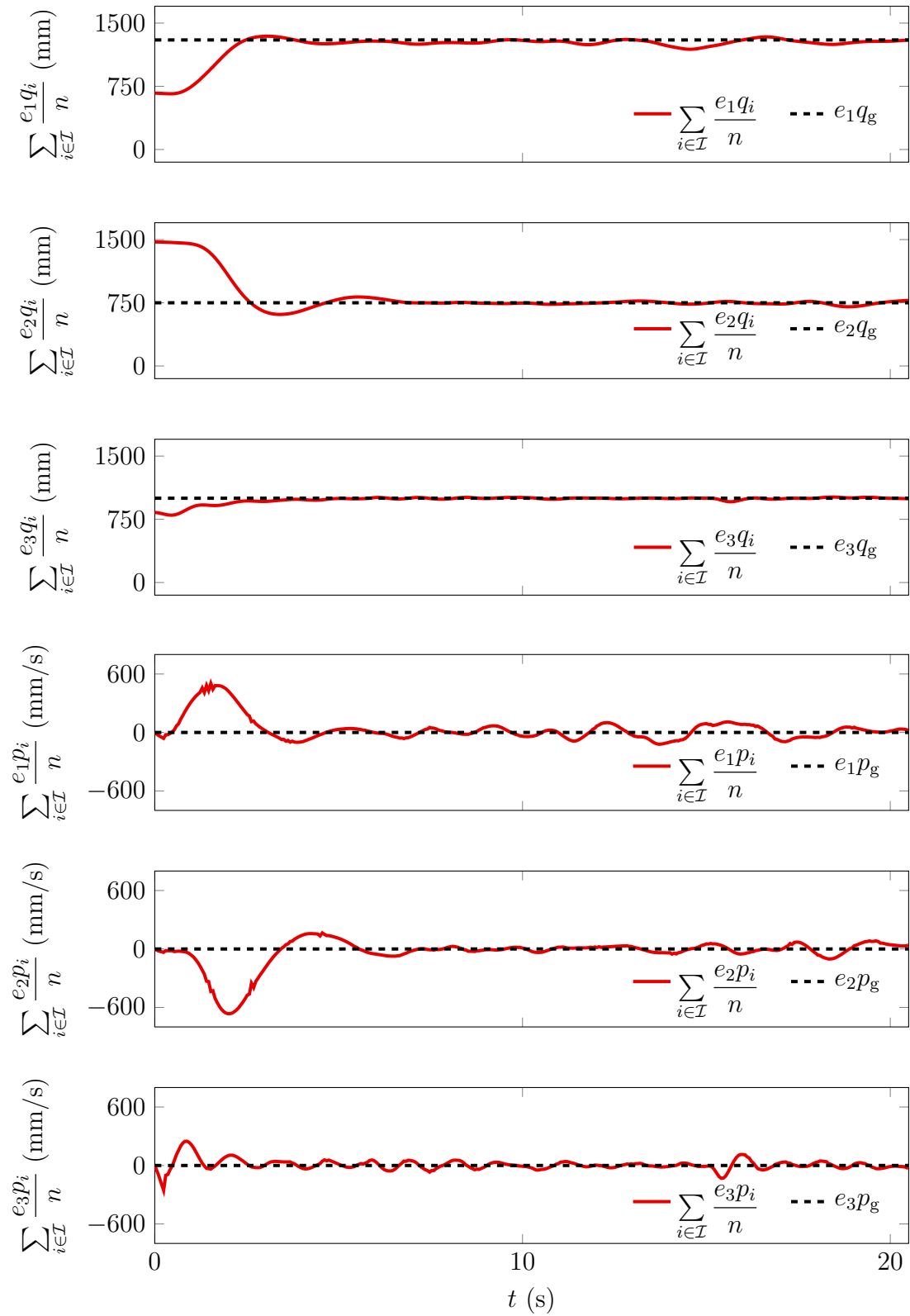


Figure 4.12: The rotorcraft-averaged position and velocity approximately follow the leader's position and velocity.

shows that the rotorcraft-averaged position and velocity approximately follow the leader's position and velocity.

To quantify the steady-state results, we examine the last 10 seconds of the experiment. Over all pairs of rotorcraft and over the last 10 seconds of the experiment, the average distance between each pair of rotorcraft is 549 mm, the average norm of the velocity difference is 103 mm/s, the average norm of the difference between the rotorcraft-averaged position and the leader's position is 116 mm, and the average norm of the difference between the rotorcraft-averaged velocity and the leader's velocity is 88.5 mm/s.

In these experiments, the rotorcraft-averaged position and leader follow the leader with delay. We quantify this delay using a least-squares approach. Let $k_e \in \mathbb{N}$ be the last sample time. Note that there are 182 samples in the last 10 seconds of the experiment (because $T_s = 0.055$ s/sample and $10/T_s \approx 182$ samples). The delay during the last 10 seconds of the experiment is estimated as

$$k_d \triangleq \arg \min_{k_* \in \{0, \dots, k_e - 181\}} \sum_{k=k_*-181}^{k_e} \left\| \begin{bmatrix} -q_g(k - k_*) + \frac{1}{n} \sum_{i \in \mathcal{I}} q_i(k) \\ -p_g(k - k_*) + \frac{1}{n} \sum_{i \in \mathcal{I}} p_i(k) \end{bmatrix} \right\|^2, \quad (4.19)$$

which yields $k_d = 2$ time steps, or equivalently 0.11 s.

Demonstration 4: Rotorcraft Follow a Mouse-Driven Leader

This experiment examines rotorcraft following a leader whose position and velocity are determined by moving a computer mouse. The initial conditions of the leader are

$$q_g(0) = \begin{bmatrix} 486 \\ 2745 \\ 1000 \end{bmatrix}, \quad p_g(0) = \begin{bmatrix} 0 \\ -173 \\ 0 \end{bmatrix}.$$

The leader's position corresponds to the mouse's position, but there is no measurement of velocity. Instead, for all $k \in \mathbb{N}$, we estimate the leader's velocity as

$$p_g(k) = \frac{1}{T_s} [q_g(k) - q_g(k-1)]. \quad (4.20)$$

Since we move the mouse to determine the leader's position and velocity, we do not directly design the external signal u_g .

Figure 4.16 shows the trajectory of the rotorcraft and leader. Figure 4.17 shows that the distance between each pair of rotorcraft tends to approximately d , which agrees with parts (c) and (d) of Theorem 6. Figure 4.18 shows that the rotorcraft-averaged position and velocity approximately follow the leader's position and velocity.

To quantify the steady-state results, we examine the last 10 seconds of the experiment. Over all pairs of rotorcraft and over the last 10 seconds of the experiment, the average distance between each pair of rotorcraft is 543 mm, the average norm of the velocity difference is 113 mm/s, the average norm of the difference between the rotorcraft-averaged position and the leader's position is 164 mm, and the average norm of the difference between the rotorcraft-averaged velocity and the leader's velocity is 306 mm.

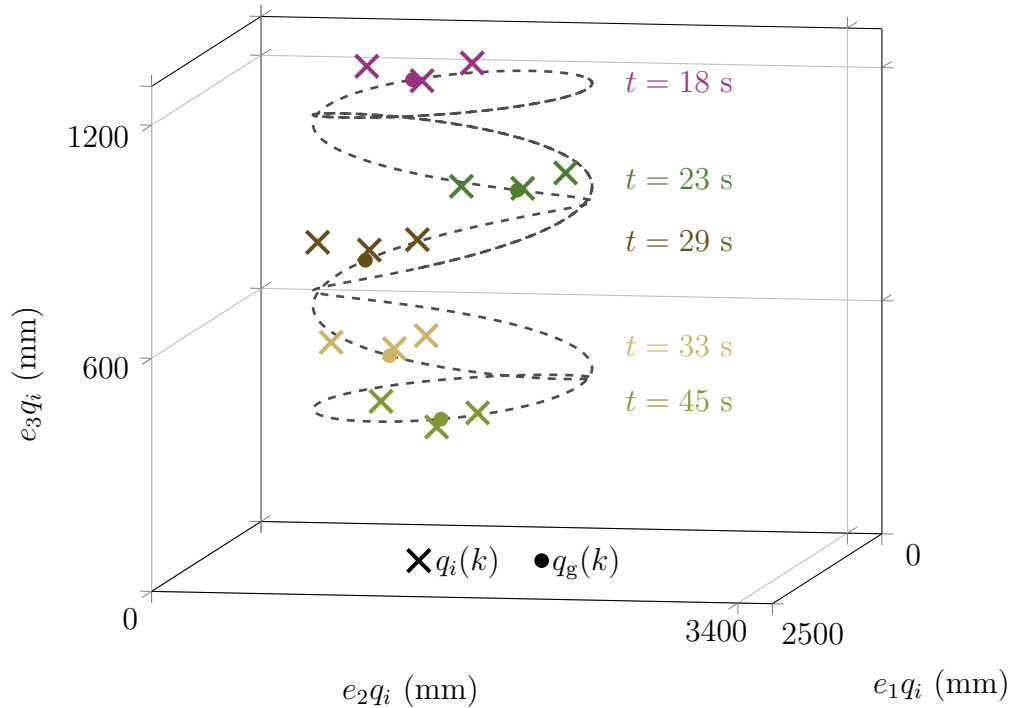
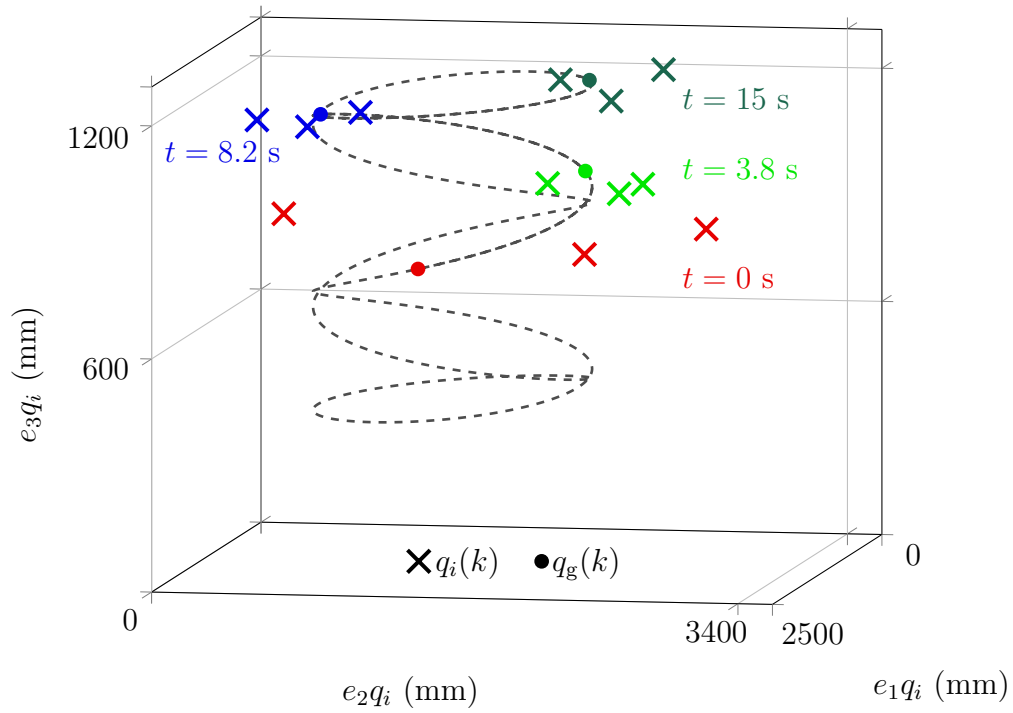


Figure 4.13: The trajectory of $n = 3$ rotorcraft that flock and follow a leader with a helical trajectory. For all times after $t = 3.8$ s, the rotorcraft are in a flocking configuration. The top plot displays snapshots of the trajectory from $t = 0$ s to $t = 15$ s and corresponds to the leader ascending the helix. The bottom plot displays snapshots of the trajectory from $t = 18$ s to $t = 45$ s and corresponds to the leader descending the helix. The dashed line denotes the leader's trajectory.

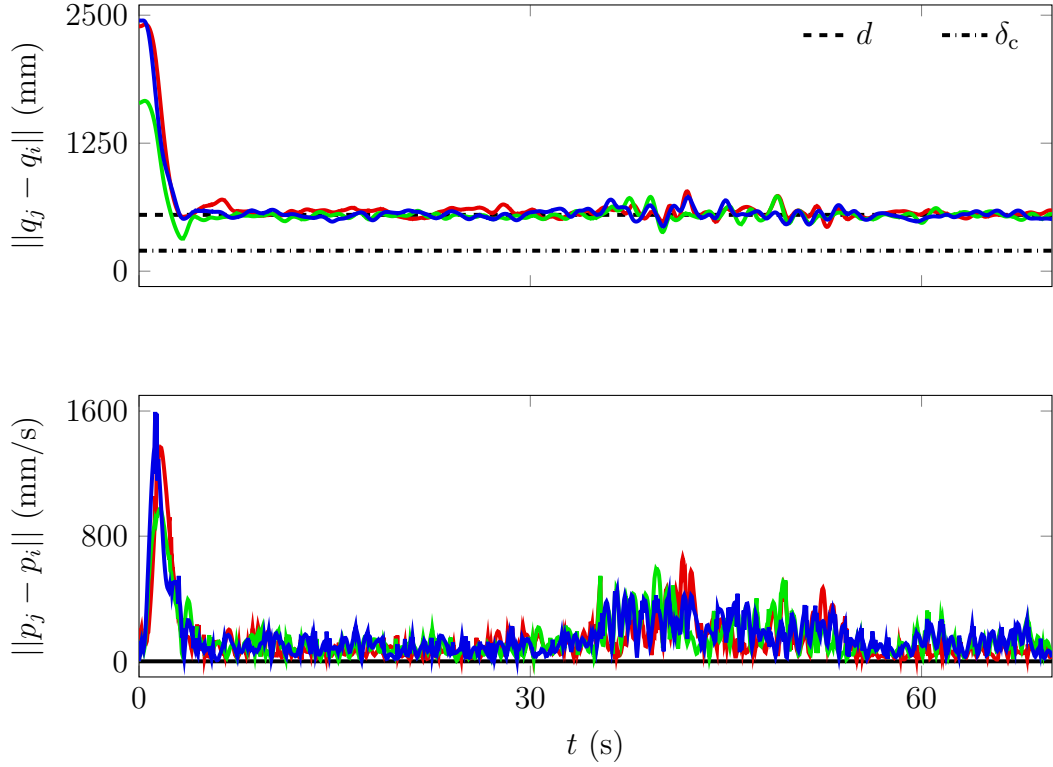


Figure 4.14: The distance and norm of the velocity difference between pairs of rotorcraft. The distance between each pair of rotorcraft tends to approximately d , and the norm of the velocity difference between each pair of rotorcraft is bounded.

In these experiments, the rotorcraft-averaged position and leader follow the leader with delay. Using (4.19), the delay is estimated as $k_d = 10$ time steps, or equivalently 0.55 s.

Summary of Results and Discussion

Table 1 shows that in every demonstration the average inter-rotorcraft distance tends to approximately d . The average inter-rotorcraft speed in every demonstration is greater than 100 mm/s, whereas we expect 0 mm/s based on part (b) of Theorem 6. We suspect that the error in velocity is primarily due to the approximation. To improve inter-rotorcraft velocity matching, we could improve the estimate of the velocity. For example, we could implement a discrete-time low-pass filter into the velocity estimates. In addition, Motive:Tracker samples the rotorcraft’s position at a higher rate than we send control signals. In this case, we could use the extra position measurements, which we ignore in the current implementation, to improve the velocity estimate.

In Demonstration 2, the steady-state rotorcraft-averaged position and velocity relative the leader’s position and velocity are 40.0 mm and 75.2 mm/s, whereas we expect 0 mm and 0 mm/s based on parts (f) and (g) of Theorem 6. The standard deviation of the rotorcraft-averaged position relative to the leader is 25.4 mm, which

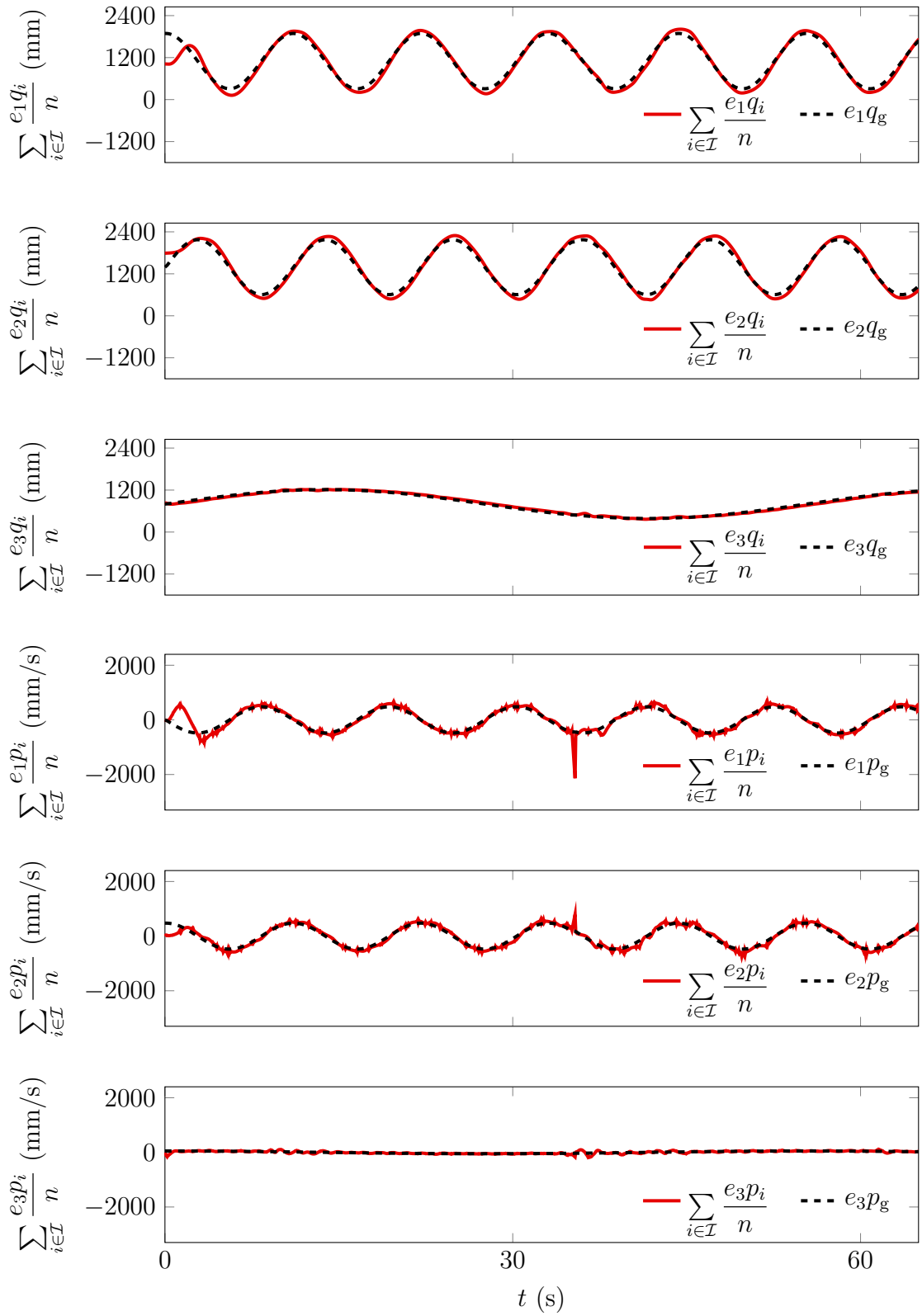


Figure 4.15: The rotorcraft-averaged position and velocity approximately follow the leader's position and velocity.

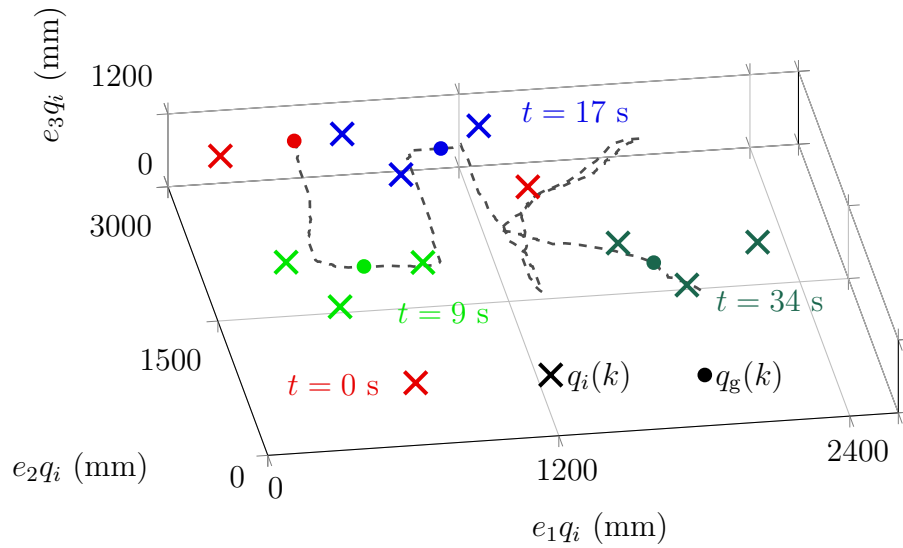


Figure 4.16: The trajectory of $n = 3$ rotorcraft that flock and follow a leader that follows a mouse's position. The rotorcraft tend to a flocking configuration and follow the leader. The dashed line denotes the leader's trajectory.

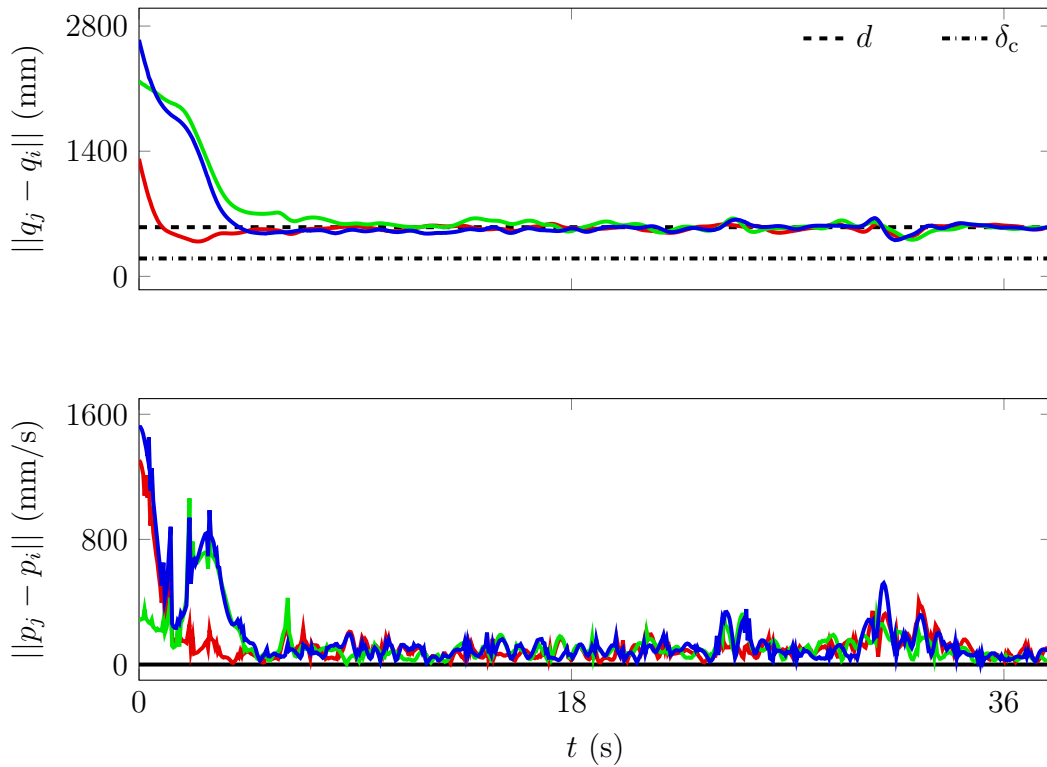


Figure 4.17: The distance and norm of the velocity difference between each pair of rotorcraft. The distance between each pair of rotorcraft tends to approximately d , and the norm of the velocity difference between each pair of rotorcraft is bounded.

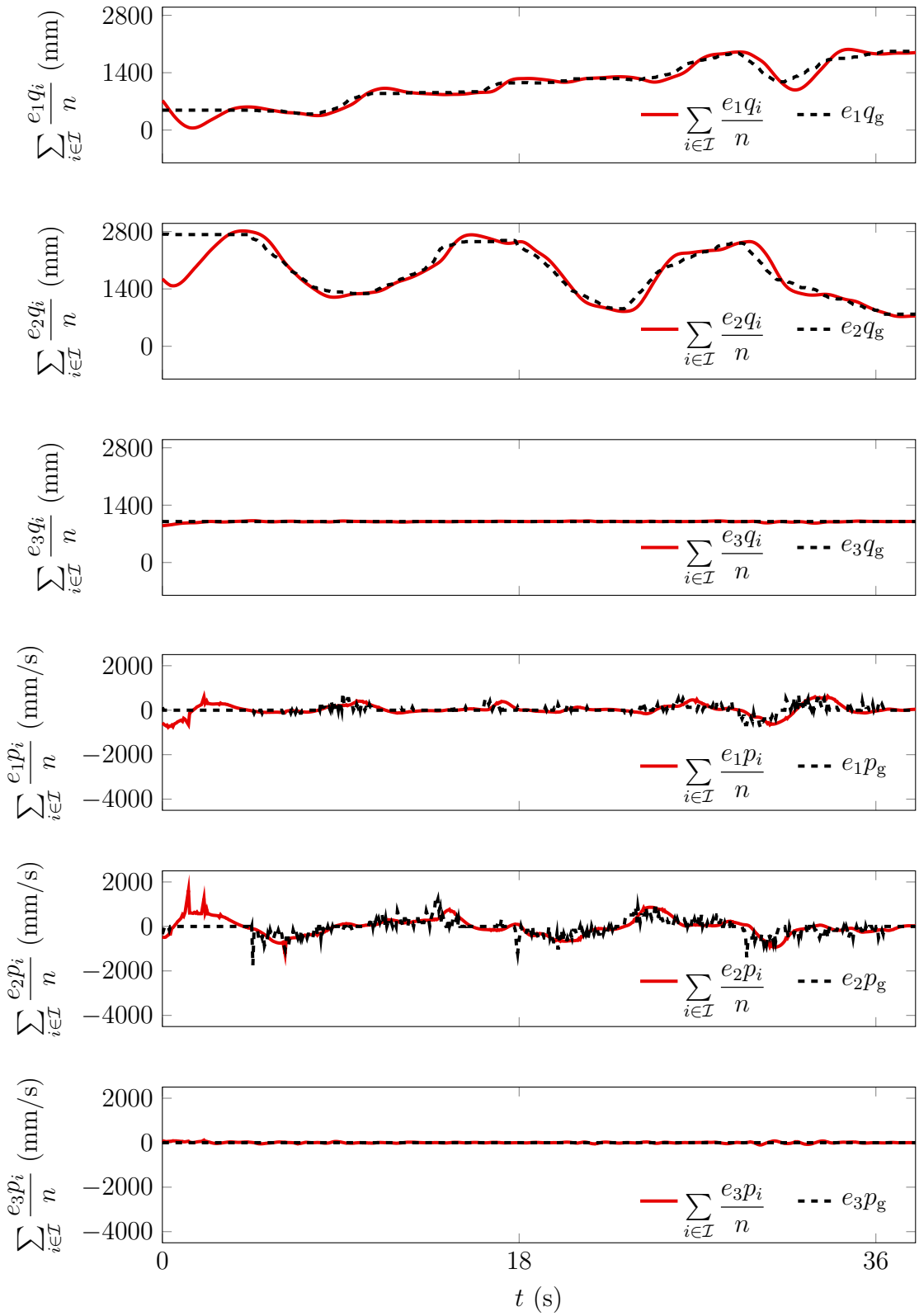


Figure 4.18: The rotorcraft-averaged position and velocity approximately follow the leader's position and velocity.

Table 4.1: Summary of the steady-state results from Demonstrations 1–4 compared to the theoretical results in Chapter 3. The results show that the rotorcraft tend to approximately the same average inter-rotorcraft distance as predicted.

	Demo 1	Demo 2	Demo 3	Demo 4	Theory ^a
Average inter-rotorcraft distance (mm)	557	544	549	543	550
Average inter-rotorcraft relative speed ^b (mm/s)	185	191	103	113	0
Rotorcraft-averaged distance to leader (mm)	—	40.0	116	164	0 ^c
Rotorcraft-averaged speed relative to leader ^b (mm/s)	—	75.2	88.5	306	0 ^c
Delay (time steps)	—	—	2	10	—

^a Chapter 3 with the following assumptions that differ from the experiments:

$$\gamma_3 = \gamma_4 = 0 \text{ and } \hat{q}_i(k) \equiv q_i(k+1)$$

^b That is, the average of the norm of the velocity difference

^c The value 0 additionally assumes $u_g(k) \equiv 0$ in Chapter 3 and thus, only applies to Demonstration 2, where the leader has constant velocity.

implies that the average is within 2 standard deviations from 0. The standard deviation of the rotorcraft-averaged velocity relative to the leader is 32.0 mm/s, which implies that the average is greater than 2 standard deviations from 0. Thus, just as the distance between rotorcraft tends to converge to d better than the inter-rotorcraft velocity tends to 0, the rotorcraft-averaged position tends to converge to the leader’s position better than the rotorcraft-averaged velocity converges to the leader’s velocity.

The discrete-time flocking control (4.11) uses the position and velocity of the leader but does not include a feedforward term that predicts where the leader will be. Thus, if the leader has non-constant velocity as in Demonstrations 3 and 4, then the rotorcraft follow the leader with delay. In Demonstration 4, the leader uses more aggressive maneuvers and thus, has higher delay than Demonstration 3.

In these demonstrations, we use the estimate $\hat{q}_i = q_i + T_s p_i$. However, the results in Theorem 6 rely on the estimate $\hat{q}_i = q_i + T_s p_i + (T_s^2/2)u_i$. The control with the estimate $\hat{q}_i = q_i + T_s p_i + (T_s^2/2)u_i$ has provable stability properties and is implementable; however, it is more difficult to implement because u_i is implicitly defined in this case.

4.6 Conclusion

In this chapter, we implemented the discrete-time flocking control on three rotorcraft and used a motion-capture system to determine rotorcraft positions and attitude. We presented four experimental demonstrations of the discrete-time flocking control. The demonstrations showed that the discrete-time flocking control caused the rotorcraft

to go to a flocking configuration, where the rotorcraft are approximately a desired distance apart from one another, which matches the theoretical results. Moreover, this configuration is independent of the leader's dynamics. We also demonstrated that if a leader is present, then the rotorcraft-averaged position and velocity approximately follow the leader's position and velocity.

Chapter 5 Conclusions and Future Work

We presented multi-agent control methods that address flocking in continuous-time and discrete-time settings. The multi-agent control methods are decentralized and cause agents to work together to accomplish goals that may be difficult or impossible for a single agent to achieve. All the algorithms developed in this dissertation implement a distance-formation method for cohesion that induces configurations based on a desired distance. Distance-formation methods cause an agent to be repelled from all other agents that are too close and thus, prevent collisions. In addition, the configurations induced by distance-formation methods are not labeled, that is, the exact configuration is not specified *a priori*, and can be used for a small or large number of agents.

In the continuous-time setting we presented a flocking-and-destination-seeking algorithm, where each agent has a potentially unique destination that it wants to reach. If the an agent is far from its destination, then it attempts to flock with nearby agents; otherwise, it approaches its destination. We provide analysis that demonstrates if an agent is far from its destination, then it flocks with nearby agents; and if it is close to its destination, then it exits the flock and approaches its destination. The algorithm and analysis techniques in this chapter can be expanded to address the point-to-point passenger and mail transport problems. The techniques developed in this chapter can also be extended to address a broader class of multi-agent, multi-objective problems such as building complex building structures.

In the discrete-time setting we presented a discrete-time flocking control that induces flocking configurations. We demonstrated with analysis and examples that agents implementing the discrete-time flocking control converge to flocking configurations and can follow a leader. The discrete-time flocking algorithm in this dissertation is particularly useful in settings where sampled-data effects are significant. For example, many space applications use slow update rates so the sampled-data effects are significant. In addition, unmanned vehicles with vision-based systems may require computationally heavy image analysis to track objects, which may be computationally intensive. Thus, these vehicles can use the discrete-time flocking algorithm to update the vehicle at a lower sampling rate.

The multi-agent control methods in this dissertation can be extended to address open questions in cooperative control. Some applications of multi-agent control require multiple types of vehicles, such as unmanned aerial vehicles interacting with unmanned ground vehicles. For example, trucks that deliver the mail may drive to a certain location and release unmanned aerial vehicles to deliver mail to the surrounding area. In this case, the multi-agent control method would require agents that have different sets of dynamics. Other applications of multi-agent control require human interaction.

For example, robotic assistants could grab and carry heavy objects for a person. In this case, agents would need to interact with humans to understand what they want as well as interact with objects. Multi-agent control is also useful for distributed sensing. For example, multiple unmanned vehicles can be deployed in the atmosphere to study and predict weather patterns. As humans prepare to colonize Mars, we will likely need multi-vehicle systems to survey terrain and find optimal habitable locations.

Multi-agent systems have numerous applications beyond controlling vehicles. For example, multiple power plants generate electricity and distribute it to multiple locations. These applications require power plants to coordinate with another in order to deliver the optimal amount of power to each location. Mass production of consumable goods such as soft drinks requires large distribution networks to deliver the goods to consumers. By understanding these applications and others as multi-agent systems, we can devise new solutions to improve the world around us.

Bibliography

- [1] R. Olfati-Saber. Flocking for multi-agent dynamic systems: algorithms and theory. *IEEE Trans. Autom. Contr.*, 51(3):401–420, 2006.
- [2] I. D. Couzin, J. Krause, N. R. Franks, and S. A. Levin. Effective leadership and decision-making in animal groups on the move. *Nature*, 433(7025):513–516, 2005.
- [3] T. Lux and M. Marchesi. Scaling and criticality in a stochastic multi-agent model of a financial market. *Nature*, 397(6719):498–500, 1999.
- [4] T. D. Huynh, N. R. Jennings, and N. R. Shadbolt. An integrated trust and reputation model for open multi-agent systems. *Autonomous Agents and Multi-Agent Sys.*, 13(2):119–154, 2006.
- [5] W. Pan, Z. Wang, H. Gao, Y. Li, and M. Du. On multistability of delayed genetic regulatory networks with multivariable regulation functions. *Mathematical Biosciences*, 228(1):100–109, 2010.
- [6] R. Olfati-Saber, J. A. Fax, and R. M. Murray. Consensus and cooperation in networked multi-agent systems. *Proc. IEEE*, 95(1):215–233, 2007.
- [7] L. Xiao and S. Boyd. Fast linear iterations for distributed averaging. *Sys. & Contr. Letters*, 53(1):65–78, 2004.
- [8] G. Punzo, P. Karagiannakis, D. J. Bennet, M. Macdonald, and S. Weiss. Enabling and exploiting self-similar central symmetry formations. *IEEE Trans. Aerosp. Electron. Syst.*, 50(1):689–703, 2014.
- [9] D. M. Stipanović, G. Inalhan, R. Teo, and C. J. Tomlin. Decentralized overlapping control of a formation of unmanned aerial vehicles. *Automatica*, 40(8):1285–1296, 2004.
- [10] C. Sabol, R. Burns, and C. A. McLaughlin. Satellite formation flying design and evolution. *J. Spacecraft and Rockets*, 38(2):270–278, 2001.
- [11] R. M. Murray. Recent research in cooperative control of multivehicle systems. *J. Dynam. Syst., Measure., Contr.*, 129(5):571–583, 2007.
- [12] W. Poundstone. *Prisoner’s Dilemma*. Doubleday, 1992.
- [13] RoboCup Federation. Robocup. <http://www.robocup.org>.

- [14] T. Huntsberger, G. Rodriguez, and P. S. Schenker. Robotics challenges for robotic and human mars exploration. In *Robotics 2000*, pages 340–346, 2000.
- [15] D. Swaroop and J. K. Hedrick. String stability of interconnected systems. *IEEE Trans. Autom. Contr.*, 41(3):349–357, 1996.
- [16] C. W. Reynolds. Flocks, herds, and schools: A distributed behavioral model. *Computer Graphics (SIGGRAPH '87 Conf. Proc.)*, 21(4):25–34, 1987.
- [17] T. Vicsek, A. Czirók, E. Ben-Jacob, I. Cohen, and O. Shochet. Novel type of phase transition in a system of self-driven particles. *Phys. Rev. Lett.*, 75:1226–1229, 1995.
- [18] J. A. Fax and R. M. Murray. Information flow and cooperative control of vehicle formations. *IEEE Trans. Autom. Contr.*, 49(9):1465–1476, 2004.
- [19] G. Lafferriere, A. Williams, J. Caughman, and J. J. P. Veerman. Decentralized control of vehicle formations. *Syst. Contr. Lett.*, 54(9):899–910, 2005.
- [20] M. Guo, M. M. Zavlanos, and D. V. Dimarogonas. Controlling the relative agent motion in multi-agent formation stabilization. *IEEE Trans. Autom. Contr.*, 59(3):820–826, 2014.
- [21] Y. Cao and W. Ren. Distributed coordinated tracking with reduced interaction via a variable structure approach. *IEEE Trans. Autom. Contr.*, 57(1):33–48, 2012.
- [22] R. Vidal, O. Shakernia, and S. Sastry. Following the flock. *IEEE Robot. Automat. Mag.*, 11(4):14–20, 2004.
- [23] D. Gu and Z. Wang. Leader-follower flocking: Algorithms and experiments. *IEEE Trans. Contr. Syst. Tech.*, 17(5):1211–1219, 2009.
- [24] H. Su, X. Wang, and Z. Lin. Flocking of multi-agents with a virtual leader. *IEEE Trans. Autom. Contr.*, 54(2):293–307, 2009.
- [25] H. Shi, L. Wang, and T. Chu. Flocking of multi-agent systems with a dynamic virtual leader. *Int. J. Contr.*, 82(1):43–58, 2009.
- [26] M. M. Zavlanos, M. B. Egerstedt, and G. J. Pappas. Graph-theoretic connectivity control of mobile robot networks. *Proc. IEEE*, 99(9):1525–1540, 2011.
- [27] H. G. Tanner, A. Jadbabaie, and G. J. Pappas. Flocking in fixed and switching networks. *IEEE Trans. Autom. Contr.*, 52(5):863–868, 2007.
- [28] J. Park, H. J. Kim, and S. Ha. Cucker-Smale flocking with inter-particle bonding forces. *IEEE Trans. Autom. Contr.*, 55(11):2617–2623, 2010.
- [29] Y. Cao, W. Yu, W. Ren, and G. Chen. An overview of recent progress in the study of distributed multi-agent coordination. *IEEE Trans. Ind. Informat.*, 9(1):427–438, 2013.

- [30] H. G. Tanner. Flocking with obstacle avoidance in switching networks of interconnected vehicles. In *Proc. IEEE Int. Conf. Robot. Automat.*, pages 3006–3011, 2004.
- [31] Z. Jingyuan and L. Xiang. Flocking of discrete-time multi-agent systems with predictive mechanisms. *Proc. IFAC*, pages 5669–5674, 2011.
- [32] Z. Jingyuan and L. Xiang. Flocking of multi-agent systems via model predictive control based on position-only measurements. *IEEE Trans. Industrial Informatics*, 9(1):377–385, 2013.
- [33] E. Rimon and D. E. Koditschek. Exact robot navigation using artificial potential functions. *IEEE Trans. Robot. Automat.*, 8(5):501–518, 1992.
- [34] K. You and L. Xie. Coordination of discrete-time multi-agent systems via relative output feedback. *Int. J. Robust Nonlinear Contr.*, 21(13):1587–1605, 2011.
- [35] C. Tan and G. Liu. Consensus of discrete-time linear networked multi-agent systems with communication delays. *IEEE Trans. Autom. Contr.*, 58(11):2962–2968, 2013.
- [36] J. Qin and H. Gao. A sufficient condition for convergence of sampled-data consensus for double-integrator dynamics with nonuniform and time-varying communication delays. *IEEE Trans. Autom. Contr.*, 57(9):2417–2422, 2012.
- [37] L. Moreau. Stability of multiagent systems with time-dependent communication links. *IEEE Trans. Autom. Contr.*, 50(2):169–182, 2005.
- [38] S. Martin, A. Girard, A. Fazeli, and A. Jadbabaie. Multiagent flocking under general communication rule. *IEEE Trans. Contr. Networked Syst.*, 1(2):155–166, 2014.
- [39] P. Lin and Y. Jia. Consensus of second-order discrete-time multi-agent systems with nonuniform time-delays and dynamically changing topologies. *Automatica*, 45(9):2154–2158, 2009.
- [40] Z. Li, Z. Duan, and G. Chen. Consensus of discrete-time linear multi-agent systems with observer-type protocols. *CoRR*, 2011.
- [41] G. Gu, L. Marinovici, and F. L. Lewis. Consensusability of discrete-time dynamic multiagent systems. *IEEE Trans. Autom. Contr.*, 57(8):2085–2089, 2012.
- [42] F. Cucker and S. Smale. Emergent behavior in flocks. *IEEE Trans. Autom. Contr.*, 52(5):852–862, 2007.
- [43] E. Canale, F. Dalmao, E. Mordecki, and M. O. Souza. Robustness of Cucker & Smale flocking model. *IET Contr. Theory Applications*, 9(3):346–350, 2015.
- [44] J. Zhou and Q. Wang. Distributed discrete-time nonlinear consensus protocols. In *Proc. IEEE Conf. Decision and Contr.*, pages 4759–4764, 2009.

- [45] T. Okajima, K. Tsumura, T. Hayakawa, and H. Ishii. Adaptive consensus of discrete-time heterogeneous multi-agent systems. In *Proc. SICE Annu. Conf.*, pages 2237–2242, 2011.
- [46] Y. Cao and W. Ren. Sampled-data formation control under dynamic directed interaction. In *Proc. American Contr. Conf.*, pages 5186–5191, 2009.
- [47] T. Hayakawa, T. Matsuzawat, and S. Harat. Formation control of multi-agent systems with sampled information — relationship between information exchange structure and control performance. In *Proc. IEEE Conf. Decision and Contr.*, pages 4333–4338, 2006.
- [48] G. Mohanarajah and T. Hayakawa. Formation stability of multi-agent systems with limited information. In *Proc. IEEE American Contr. Conf.*, pages 704–709, 2008.
- [49] A. Jadbabaie, J. Lin, and A. S. Morse. Coordination of groups of mobile autonomous agents using nearest neighbor rules. *IEEE Trans. Autom. Contr.*, 48(6):988–1001, 2003.
- [50] W. Yu, W. X. Zheng, G. Chen, W. Ren, and J. Cao. Second-order consensus in multi-agent dynamical systems with sampled position data. *Automatica*, 47(7):1496–1503, 2011.
- [51] G. Wen, Z. Duan, W. Yu, and G. Chen. Consensus of multi-agent systems with nonlinear dynamics and sampled-data information: a delayed-input approach. *Int. J. Robust and Nonlinear Contr.*, 23(6):602–619, 2013.
- [52] Z. W. Liu, Z. H. Guan, X. Shen, and G. Feng. Consensus of multi-agent networks with aperiodic sampled communication via impulsive algorithms using position-only measurements. *IEEE Trans. Autom. Contr.*, 57(10):2639–2643, 2012.
- [53] Y. Gao and L. Wang. Sampled-data based consensus of continuous-time multi-agent systems with time-varying topology. *IEEE Trans. Autom. Contr.*, 56(5):1226–1231, 2011.
- [54] Y. Zhang and Y. P. Tian. Consensus of data-sampled multi-agent systems with random communication delay and packet loss. *IEEE Trans. Autom. Contr.*, 55(4):939–943, April 2010.
- [55] G. Xie, H. Liu, L. Wang, and Y. Jia. Consensus in networked multi-agent systems via sampled control: Fixed topology case. In *Proc. IEEE American Contr. Conf.*, pages 3902–3907, 2009.
- [56] G. Xie, H. Liu, L. Wang, and Y. Jia. Consensus in networked multi-agent systems via sampled control: Switching topology case. In *Proc. IEEE American Contr. Conf.*, pages 4525–4530, 2009.

- [57] K. You and L. Xie. Network topology and communication data rate for consensusability of discrete-time multi-agent systems. *IEEE Trans. Autom. Contr.*, 56(10):2262–2275, 2011.
- [58] J. Wang, X.-H. Nian, and H.-B. Wang. Consensus and formation control of discrete-time multi-agent systems. *J. Central South Univ. Tech.*, 18(4):1161–1168, 2011.
- [59] I. Okoloko. Path planning for multiple spacecraft using consensus with LMI avoidance constraints. In *IEEE Aerosp. Conf.*, pages 1–8, 2012.
- [60] Y. Cao and W. Ren. Multi-vehicle coordination for double-integrator dynamics under fixed undirected/directed interaction in a sampled-data setting. *Int. J. Robust Nonlinear Contr.*, 20(9):987–1000, 2010.
- [61] B. J. Wellman and J. B. Hoagg. A flocking algorithm with individual agent destinations and without a centralized leader. *Systems & Control Letters*, 102:57–67, 2017.
- [62] B. Xu, L. Gao, Y. Zhang, and X. Xu. Leader-following consensus stability of discrete-time linear multiagent systems with observer-based protocols. In *Abstr. Applied Anal.*, volume 201. Hindawi Publishing Corporation, 2013.
- [63] D. Panagou, D. M. Stipanović, and P. G. Voulgaris. Distributed coordination control for multi-robot networks using Lyapunov-like barrier functions. *IEEE Trans. Autom. Contr.*, 61(3):617–632, 2016.
- [64] D. V. Dimarogonas, M. M. Zavlanos, S. G. Loizou, and K. J. Kyriakopoulos. Decentralized motion control of multiple holonomic agents under input constraints. In *Proc. IEEE Conf. Decision and Contr.*, volume 4, pages 3390–3395, 2003.
- [65] D. V. Dimarogonas, S. G. Loizou, K. J. Kyriakopoulos, and M. M. Zavlanos. A feedback stabilization and collision avoidance scheme for multiple independent non-point agents. *Automatica*, 42(2):229–243, 2006.
- [66] Y.-K. Zhu, X.-P. Guan, and X.-Y. Luo. Finite-time consensus for multi-agent systems via nonlinear control protocols. *Int. J. of Automation and Computing*, 10(5):455–462, 2014.
- [67] W. Ren, R. W. Beard, and E. M. Atkins. Information consensus in multivehicle cooperative control. *IEEE Contr. Syst.*, 27(2):71–82, 2007.
- [68] W. Ren. On consensus algorithms for double-integrator dynamics. *IEEE Trans. Autom. Contr.*, 53(6):1503–1509, 2008.
- [69] P. Panyakeow and M. Mesbahi. Deconfliction algorithms for a pair of constant speed unmanned aerial vehicles. *IEEE Trans. Aerosp. Electron. Syst.*, 50(1):456–476, 2014.

- [70] W. Wang and J.-J.E. Slotine. Contraction analysis of time-delayed communications and group cooperation. *IEEE Trans. Autom. Contr.*, 51(4):712–717, 2006.
- [71] W. Ni and D. Cheng. Leader-following consensus of multi-agent systems under fixed and switching topologies. *Syst. Contr. Lett.*, 59(3–4):209–217, 2010.
- [72] W. Liu, S. Zhou, S. Yan, and Q. Wu. Lqr-based consensus algorithms of multi-agent systems with a prescribed convergence speed. pages 868–873, 2014.
- [73] A. Chapman and M. Mesbahi. Semi-autonomous consensus: Network measures and adaptive trees. *IEEE Trans. Autom. Contr.*, 58(1):19–31, 2013.
- [74] Y. Liu and Y. Jia. Formation control of discrete-time multi-agent systems by iterative learning approach. *Int. J. Contr., Automat. Syst.*, 10(5):913–919, 2012.
- [75] E. G. Hernandez-Martinez, J. J. Flores-Godoy, and G. Fernandez-Anaya. Decentralized discrete-time formation control for multirobot systems. *Discrete Dynamics in Nature and Society*, 2013:8, 2013.
- [76] D.E. Hernandez-Mendoza, G.R. Pealoza-Mendoza, and E. Aranda-Bricaire. Discrete-time formation and marching control of multi-agent robots systems. In *Electrical Engineering Computing Science and Automatic Control (CCE), 2011 8th International Conference on*, pages 1–6, 2011.
- [77] D. Nesic and A. R. Teel. A framework for stabilization of nonlinear sampled-data systems based on their approximate discrete-time models. *IEEE Trans. Autom. Contr.*, 49(7):1103–1122, 2004.
- [78] Y. Gu, B. Seanor, G. Campa, M. R. Napolitano, L. Rowe, S. Gururajan, and S. Wan. Design and flight testing evaluation of formation control laws. *IEEE Trans. Contr. Sys. Tech.*, 14(6):1105–1112, 2006.
- [79] M. Turpin, N. Michael, and V. Kumar. Trajectory design and control for aggressive formation flight with quadrotors. *Autonomous Robots*, 33(1–2):143–156, 2012.
- [80] S. Mao, W. K. Tan, and K. H. Low. Autonomous formation flight of indoor uavs based on model predictive control. In *AIAA Infotech@ Aerospace*, page 515. 2016.
- [81] R. Merris. Laplacian matrices of graphs: A survey. *Linear Algebra and Its Applications*, 197–198:143–176, 1994.
- [82] R. Olfati-Saber and R.M. Murray. Consensus problems in networks of agents with switching topology and time-delays. *IEEE Trans. Autom. Contr.*, 49(9):1520–1533, 2004.
- [83] B. J. Wellman and J. B. Hoagg. A discrete-time flocking algorithm for agents with sampled-data double-integrator dynamics. In *Proc. IEEE American Contr. Conf.*, 2017.

- [84] H. K. Khalil. *Nonlinear Systems*. Prentice Hall PTR, 2002.
- [85] Y. Joo, R. Harvey, and Z. Qu. Cooperative control of heterogeneous multi-agent systems in a sampled-data setting. In *Proc. IEEE Conf. Decision and Contr.*, pages 2683–2688, 2016.
- [86] J. B. Hoagg, M. A. Santillo, and D. S. Bernstein. Discrete-time adaptive command following and disturbance rejection with unknown exogenous dynamics. *IEEE Trans. Autom. Contr.*, 53:912–928, 2008.
- [87] J. B. Hoagg and D. S. Bernstein. Retrospective cost model reference adaptive control for nonminimum-phase systems. *J. Guid. Contr. Dyn.*, 35(6):1767–1786, 2012.
- [88] T. Hayakawa, W. M. Haddad, and A. Leonessa. A Lyapunov-based adaptive control framework for discrete-time non-linear systems with exogenous disturbances. *Int. J. Contr.*, 77:250–263, 2004.
- [89] S. Akhtar and D. S. Bernstein. Logarithmic Lyapunov functions for direct adaptive stabilization with normalized adaptive laws. *Int. J. Contr.*, 77:630–638, 2004.
- [90] R. Johansson. Lyapunov functions for adaptive systems. In *Proc. IEEE Conf. Decision and Contr.*, pages 449–454, San Antonio, TX, 1983.
- [91] R. Johansson. Global Lyapunov stability and exponential convergence of direct adaptive control. *Int. J. Contr.*, 50:859–869, 1989.
- [92] W. M. Haddad and V. Chellaboina. *Nonlinear dynamical systems and control: a Lyapunov-based approach*. Princeton University Press, 2008.
- [93] D. S. Bernstein. *Matrix Mathematics: Theory, Facts, and Formulas (Second Edition)*. Princeton reference. Princeton University Press, 2009.
- [94] R. Merris. *Algebraic Graph Theory*. Wiley, 2000.
- [95] G. E. Dullerud and F. Paganini. *A course in robust control theory: a convex approach*, volume 36. Springer Science & Business Media, 2013.

Vita

Brandon Wellman studied mechanical engineering at the University of Kentucky, where he received a bachelor's and master's degrees in mechanical engineering in 2011 and 2013 with a focus in mechanical control systems. His current research interest is in the control of multi-agent systems.